DICATIONIC CHELATING PHOSPHINES – SYNTHESIS, STRUCTURE AND REACTIVITY TOWARDS DIENES

Dissertation for
the award of the
degree

"Doctor rerum naturalium" (Dr.rer.nat.)

(alternatively: "Doctor of Philosophy" Ph.D. Division of Mathematics and Natural Sciences)

of the Georg-August-Universität Göttingen

within the doctoral program Chemistry

of the Georg-August University School of Science (GAUSS)

submitted by

Adam Aleksander Zieliński

from Warszawa (Poland)

Göttingen, 2021

Thesis Committee

Prof. Dr. Manuel Alcarazo

(Institute of Organic and Biomolecular Chemistry, Georg-August-University Göttingen)

Prof. Dr. Franc Meyer

(Institute of Inorg. Chem., Georg-August-University Göttingen)

Reviewer: Prof. Dr. Ulf Diederichsen

(Institute of Organic and Biomolecular Chemistry, Georg-August-University Göttingen)

Second Reviewer: Prof. Johannes Walker

(Institute of Organic and Biomolecular Chemistry, Georg-August-University Göttingen)

Further members of the Examination Board:

Dr. Matthias Otte

(Institute of Inorg. Chem., Georg-August-University Göttingen)

Dr. Daniel Janßen-Müller

(Institute of Organic and Biomolecular Chemistry, Georg-August-University Göttingen)

Date of the oral examiniation: 21.06.2021

"To effectively contain a civilization's development and disarm it across such a long span of time, there is only one way: kill its science."

Liu Cixin, The Three-Body Problem

DECLARATION

**Promovierenden-
Erklärung der Georg-August-
Universität Göttingen**

Name: Adam Aleksander Zieliński

Anschrift: Q1 3, 6816, Mannheim

Ich beabsichtige, eine Dissertation zum "Thema Dicationic Chelating Phosphines – Synthesis, Structure And Reactivity Towards Dienes" an der   Georg-August-Universität Göttingen   anzufertigen. Dabei werde ich   von   Prof.   Dr. Manuel Alcarazo betreut.

Ich gebe folgende Erklärung ab:

1.   Die Gelegenheit zum vorliegenden Promotionsvorhaben ist mir nicht kommerziell vermittelt worden. Insbesondere habe ich keine Organisation eingeschaltet, die gegen Entgelt Betreuerinnen und Betreuer für die Anfertigung von Dissertationen sucht oder die mir obliegenden Pflichten hinsichtlich der Prüfungsleistungen für mich ganz oder teilweise erledigt.

2.   Hilfe Dritter wurde bis jetzt und wird auch künftig nur in wissenschaftlich vertretbarem und prüfungsrechtlich zulässigem Ausmaß in Anspruch genommen. Insbesondere werden alle Teile der Dissertation selbst angefertigt; unzulässige

fremde Hilfe habe ich dazu weder unentgeltlich noch entgeltlich entgegengenommen und werde dies auch zukünftig so halten.

3.   Die Ordnung zur Sicherung der guten wissenschaftlichen Praxis an der Universität Göttingen wird von mir beachtet.

4.   Eine entsprechende Promotion wurde an keiner anderen Hochschule im In- oder Ausland beantragt; die eingereichte Dissertation oder Teile von ihr wurden/werden nicht für ein anderes Promotionsvorhaben verwendet.

Mir ist bekannt, dass unrichtige Angaben die Zulassung zur Promotion ausschließen bzw. später zum Verfahrensabbruch oder zur Rücknahme des erlangten Grades führen können.

(Ort), (Datum)

(Unterschrift)

ACKNOWLEDGEMENTS

I would like to offer special thanks to my friends: Michał Chojnowski, Dr. Grzegorz Szczepaniak, Wojciech Kata, Kajetan Dobrenko and Krzysztof Kosiński for their friendship and belief in me.

Finally, I would like to express my gratitude to my parents and grandparents for their love, appreciation, tremendous understanding and encouragement in the past few years. I would like to especially thank my fiancée Dr Elżbieta Gońka for her utmost support, love, optimism and assistance with the preparation of my dissertation.

CONTENTS

LIST OF TABLES

LIST OF FIGURES

LIST OF ABBREVIATIONS AND ACRONYMS

Ac	Acetyl group
Ar	Aromatic (generic) group
B(ArF)$_4$	Tetrakis[3,5-bis(trifluoromethyl)phenyl]borate
Bn	Benzyl group
BuLi	Buthyllithium
COD	Cyclooctadiene
COE	Cyclooctaene
Cy	Cyclohexyl group
dba	Dibenzylideneacetone
DCE	1,2-Dichloroethane
DCM	Dichloromethane
DFT	Density Functional Theory
dppb	1,2-Bis(diphenylphosphino)benzene
Et	Ethyl group
HCTD	Hexacyclotetradecane
*i*Pr	Isopropyl group
IR	Infrared
KHMDS	Potassium bis(trimethylsilyl)amide

Me   Methyl group

Mes   Mesityl (1,3,5-trimethylphenyl) group

NaTPPTS   Tris(sodium-*m*-sulfonatophenyl)phosphane

NHC   N-Heterocyclic Carbene

NMR   Nuclear magnetic resonance

Ph   Phenyl group

PPh$_3$ Triphenylphosphine

*t*Bu   *tert*-Butyl group

TEP   Tolman electronic parameter

TMS   Trimethylsillyl group

1 Introduction

1.1 Catalysis – a brief overview

1.1.1 History of Catalysis

The term catalyst was proposed in 1835 by Jöns Jacob Berzelius and is derived from Greek καταλύειν meaning to loosen, untie.[1] Catalysis was later investigated by Wilhelm Ostwald, from Leipzig University, who described a systematic study of reactions catalyzed by acids and bases. He defined a catalyst as *a substance increasing the rate of the reaction without itself being consumed.*[2] In the aftermath, a modern classification of a catalyst signifies that it is used substoichiometrically in a relation to reagents.[3] It is worth noting that since 1901 Nobel Committee recognized achievements in the field of catalysis 16 times, which corresponds to 19% of overall prize winners (*status quo* 2020), starting with Wilhelm Ostwald in 1909.[4] Up to the date catalytic reactions are one of the main fields of development for organic, organometallic and inorganic chemists, allowing construction of advance systems as well as fine chemicals.[5]

1.1.2 Catalysis classification

Over the years, the exploration of this branch of the chemistry revealed, that catalysis can be divided into different classes, depending on the structure of the catalyst, the source of the energy required for the transformation to occur (photocatalysis) or the phase in which reaction takes place etc. For example, the term: *homogeneous catalysis* is used if the catalyst and substrate are in the same phase, otherwise the term *heterogeneous catalysis* should be applied. Furthermore, depending on the structure of the catalyst: *transition metal catalysis* (where metal atom is present in the catalyst structure) or *organocatalysis* (where as the catalyst serve an organic molecule) classes are derived.[6]

The studies performed in the course of this doctoral dissertation were focused on the synthesis and characterization of the dicationic chelating phosphines together with the investigation of their interactions with the transition metals. Therefore, in

the following chapters of the introduction, only topics connected to the transition metal catalysis, will be addressed.

1.2 Ligands in organometallic chemistry

The term *coordination chemistry* is defined as a discipline studying the chemical compounds consisting of a central metal atom surrounded by complexing agents or ligands. A significant part of coordination complexes are organometallic species, containing at least one metal to carbon bond.[7]

A modern definition of ligands describes them as ions or molecules which form a bond or bonds with the central metal atom or ion of the complex. The majority of the complexes are formed with transition metals, but complexes with f-block metals are also known in the literature.[8] Depending on the nature and amounts of the bond(s) between the ligand and the metal, several ligands classes are distinguished: σ-bonded, π-bonded, polydentate and polyhaptic.

1.2.1 σ-Bonded ligands

σ-Bonded ligands can be categorized into two main groups: covalent or dative ligands, depending on the formal number of electrons involved in the ligand-metal σ-bond (Figure 1). **Covalent ligands** (X-type ligands) form a bond by a donation of one electron to the metal center. Second electron is donated by the transition metal. Examples of such ligands are halogens (F, Cl, Br, I), hydroxide, hydride or cyanide. X-type ligands are usually negatively charged and therefore can be named anionic ligands. **Dative ligands** (L-type ligands) form a bond with a metal by donation of two electrons resulting in coordinate bond. Metal is considered not to contribute any electrons, while bonding with L-type ligands. Common dative ligands include phosphines, carbenes, H_2O and CO. L-type ligands do not possess charge and therefore can be called neutral ligands.
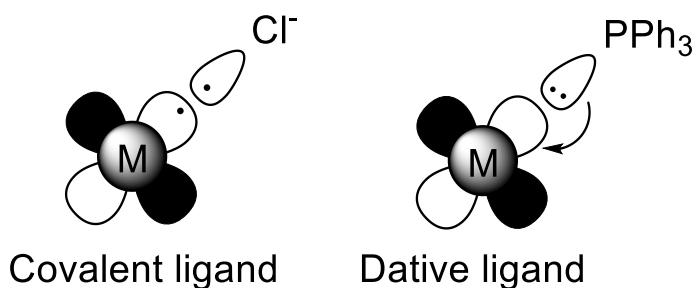
Figure 1. Schematic illustration of the X- and L-type ligands.

1.2.2 π-Bonded ligands

In addition to the systems, where bonds are created due to the Lewis Acid-Base interactions, ligands can form transition metal complexes by bonding of their π-system (Figure 2). Such interaction is explained by Dewar-Chatt-Duncanson model in which organic ligand e.g. ethylene donates electron density originating from π-symmetry bonding orbital of C=C bond.
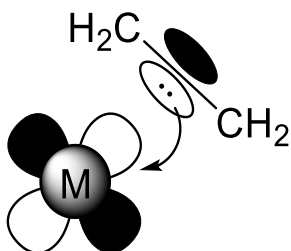
Figure 2. Schematic illustration of π-bonded ligand.

1.2.3 Polydentate ligands

Ligands, which can coordinate metal through more than one site are denoted as polydentate. This is a consequence of having lone electron pairs or multiple atoms in the ligand. A ligand that can coordinate metal with two sites is called bidentate, with three sites tridentate etc. An example of polydentate ligand (commonly used in e.g. cross coupling reactions)[9] is 1,4-bis(diphenylphosphino)butane (dppb) (Figure 3). By the presence of two diphenylphosphine units connected with a rigid butyl linker, this ligand is capable of forming bidentate complexes with transition metals.

κ-Notation is used to describe the number of coordination sites of the ligand in the complex.
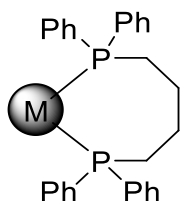
Figure 3. An example of polydentate ligand – dppb.

1.2.4 Polyhaptic ligands

Hapticity describes a number of contiguous atoms, usually in a π-system of the ligand (Figure 4), bonded to a metal.[10] η-Notation is used to describe the number of contiguous atoms coordinated to the central metal atom. Polyhaptic ligands can combine in their structure σ- and π-donor units. Classical examples of polyhaptic ligands are butadiene, benzene and cyclopentadienyl anion. Molecules containing polyhapto ligands are considered to be stereochemically non-rigid.[11]
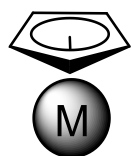
Figure 4. Example of η^6 ligand – cyclopentadienyl anion.

1.3 Organometallic complexes in catalysis

Organometallic complexes can be applied in a numerous catalytic transformations: asymmetric hydrogenation,[12] hydroformylation,[13] cross-coupling reactions,[14] carbon-hydrogen bond activation[15] and metathesis[16] among others.

The principle of catalytic transformations, using organometallic species, resides in the activation of substrates by their coordination to the sphere of the central metal atom. This lowers the activation energy of the reaction between substrates and allows the desired transformation to proceed.[5]

One of the historically prominent examples of transition metal catalyzed reactions is hydrogenation of olefins using rhodium complexes (Figure 5).[17]
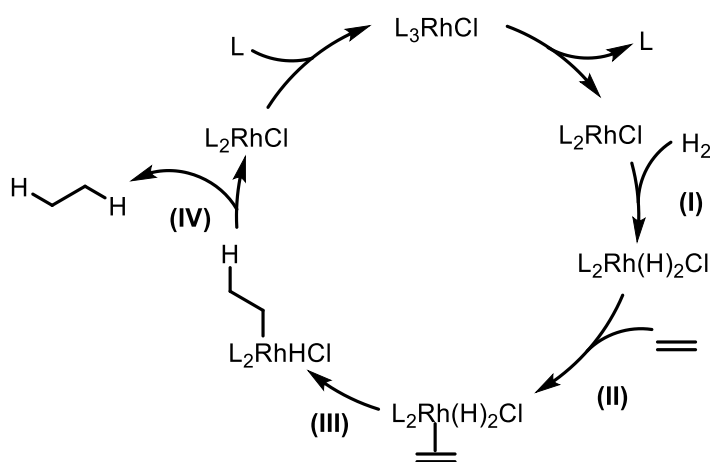
Figure 5. Mechanism of rhodium-catalyzed hydrogenation.

This example demonstrates elementary steps of the simple organometallic reaction: oxidative insertion (I), π-complexation (II), migratory insertion (III) and reductive elimination (IV). The energy of these steps as well as kinetic parameters can be alternated by careful choice of ligands. Throughout the past century many research groups investigated the properties and choice of ligands for this transformation.[18] The significant successes in this field were achieved by the group of Sir Geoffrey Wilkinson. His advances were recognized in 1973 by a Nobel Prize committee, which awarded him, together with Ernst Otto Fischer, for their work on organometallic compounds.[19] His impact is also reflected in the name of the commonly used rhodium complex depicted on Figure 5 (L = PPh3), tris(triphenylphosphine)rhodium(I) chloride, commonly known as Wilkinson's catalyst.

1.3.1 Example of ligand design – olefin metathesis catalysts

One of the most relevant and archetypical examples of ligand design in modern transition metal catalysis is development of ruthenium olefin metathesis catalysts.
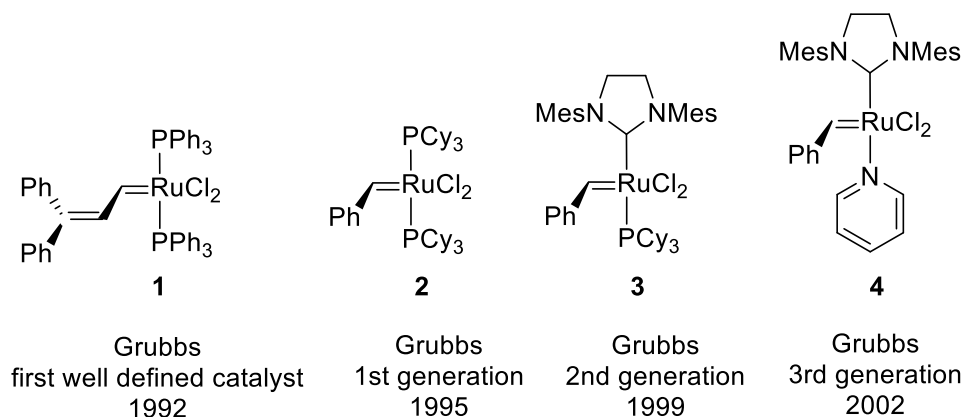
Figure 6. Development of ruthenium-based metathesis catalysts.

First well-defined ruthenium olefin metathesis catalyst was described by Grubbs and co-workers in 1992 (Figure 6).[20] They proposed using ruthenium alkylidene coordinated by two phosphine and two chloride ligand. Although this species was only reactive in metathesis reaction with strained olefins and in polymerization of norbornene, its discovery was significant for the organometallic community as the first olefin metathesis catalyst with well-defined structure. Another difficulties which caused wider exploration of this field, is its sensitivity towards moisture and oxygen which makes it difficult and troublesome to handle.

In 1995 Grubbs published a synthesis of a compound, commercialized and known later as Grubbs 1st generation catalyst (Figure 6).[21] By substituting triphenyl phosphine to more bulky tricyclohexyl phosphine higher catalytic activity was obtained. In addition, changing alkylidene to benzylidene ligand afforded the increase of the stability of this compound.

Next major breakthrough in the design of the olefin metathesis catalysts occurred in 1999, when N-Heterocyclic Carbenes (NHC) coordinated complex was obtained, later known as Grubbs 2nd generation catalyst (Figure 6).[22] NHCs are known to be excellent σ-donors and weak π-acceptors. Those properties influenced lower lability of ancillary ligand if compared with phosphines, resulting in the increased thermal stability. This complex broadened the scope and applications of metathesis

catalysts, in comparison to previously described catalysts, and allowed to perform the reaction with substrates having different functional groups.

Subsequent modifications of this framework resulted in formation of Grubbs 3rd generation catalyst, where both phosphines are replaced, one by NHC ligand and another by labile pyridine ligand (Figure 6).[23] This modification allowed to obtain catalysts which are reactive in challenging cross metathesis reactions and show very high initiation. In 2005 Robert Grubbs (together with Richard Schrock and Yves Chauvin) was awarded a Nobel Prize in Chemistry for his work in the field of olefin metathesis.[24]

1.3.2 π-Acid catalysis

As it was already stated before (Chapter 1.2.2), Dewar-Chatt-Duncanson model describes the bonding situation between transition metals and π-ligands. In addition to σ-bond that is formed by the overlap of π-electrons of the organic ligand, it was postulated that an additional π-bond interaction derived from the back-donation of metal to the ligand is present at such complexes. The back-donation is a manifestation of an interaction of d-orbital electrons of a metal with π*-antibonding orbital of π-ligand. Over the past century chemists investigated the ability of transition metals, mostly Au and Pt, to deprive the carbon-carbon multiple bond from its electron density and involve it in catalytic reactions.[25]

One of the most prominent examples of such reactivity is gold-catalysed hydrofunctionalization of alkynes (Figure 7).[26]
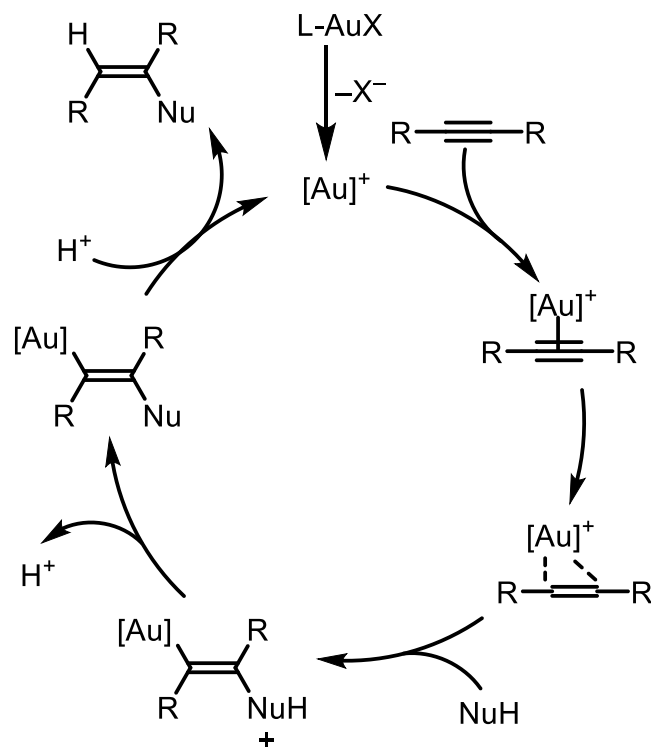
Figure 7. Mechanism of gold-catalyzed hydrofunctionalization.

In this reaction the preactivation of gold atom to form a cationic catalyst occurs. Usually this means the abstraction of (pseudo)halogen by a silver(I) salt. Afterwards a formation of a π-complex with alkyne occurs. Widely accepted postulates states, that after a 'slippage' of Au center at the alkyne a nucleophile attacks the π-ligand. Lastly, protodemetallation occurs to give the final product and regenerate Au species closing the catalytic cycle.[27]

Exploration of this intriguing reactivity enabled chemists to obtain a great number of drug molecules, functional materials and even fine chemicals. The field of π-acid catalysis is intensively investigated and allows researchers to further tune the reactivity of organometallic complexes by using different ligands in this type of transformations.[28,29]

1.3.3 Phosphines as ligands in coordination chemistry

Apart from their stoichiometric uses in various organic transformations phosphines are very well known to be applied as ancillary ligands in different metal catalysts.

Phosphines belong to the group of L-type ligands, where formation of a sigma bond to the metal is a consequence of free electron pair on phosphorus atom. Their σ^* P-R orbital also participates in backbonding with transition metal due to d_π- σ^* interaction. In addition the steric and electronic parameter of phosphines is easy to control and modify, as there is a great variety of tools that enable synthesis of phosphines with different substitution patterns. Because of all these factors phosphines attracted attention of the community, resulting in their libraries and commercial availability.[30]

Apart from Willkinson and Grubbs catalysts discussed above, one of the eminent examples of commercially available metal catalysts with phosphine is tetrakis(triphenylphosphine)palladium(0) – $Pd(PPh_3)_4$. This transition metal complex is widely used as a catalyst for cross-coupling reactions. It is synthetized in a straightforward protocol using $PdCl_2$ and PPh_3 in presence of reducing agent – usually hydrazine. An example of the application of $Pd(PPh_3)_4$ in modern chemistry is Suzuki-Miyaura reaction (Figure 8).[31]
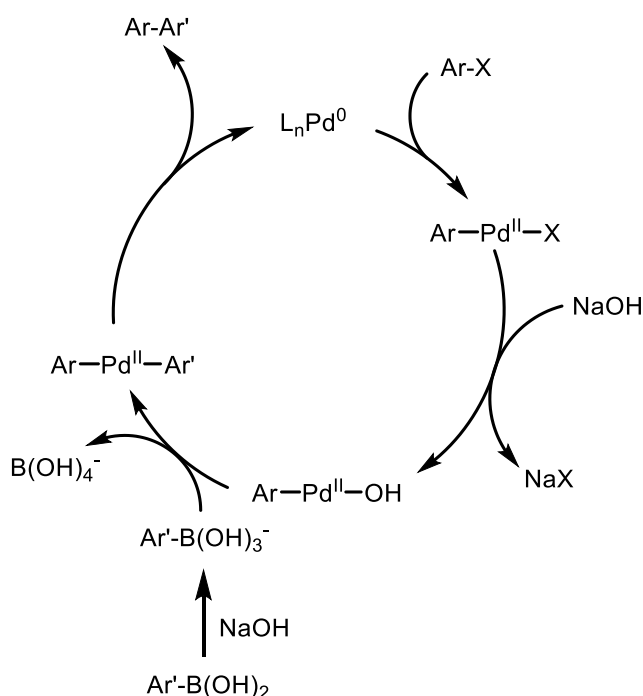
Figure 8. Mechanism of Suzuki-Miyaura cross-coupling.

In the first step of the Suzuki-Miyaura reaction the oxidative addition to palladium takes place. After ligand exchange, transmetallation with borate occurs. Finally bisaryl palladium species reductively eliminates biaryl product and regenerates the catalyst. In 2010 Akira Suzuki (together with Richard Heck and Ei-ichi Negishi) was awarded a Nobel Prize for the contribution in the field of palladium catalyzed cross-coupling reactions.[3,14]

1.3.4 Dialkylbiarylphosphines

Despite the many successful applications of triphenylphosphine as an ancillary ligand in catalysis, cross-coupling of aryl chlorides in good yields was very challenging reaction until late 1990s. In order to address this shortcoming and enable high yielding coupling of aryl chlorides group of Stephen Buchwald introduced a series of dialkylbiarylphosphines (Figure 9).[32] Their catalytic activity with challenging substrates outperforms simple triarylphosphines and is an example of tailored ligand.[33]
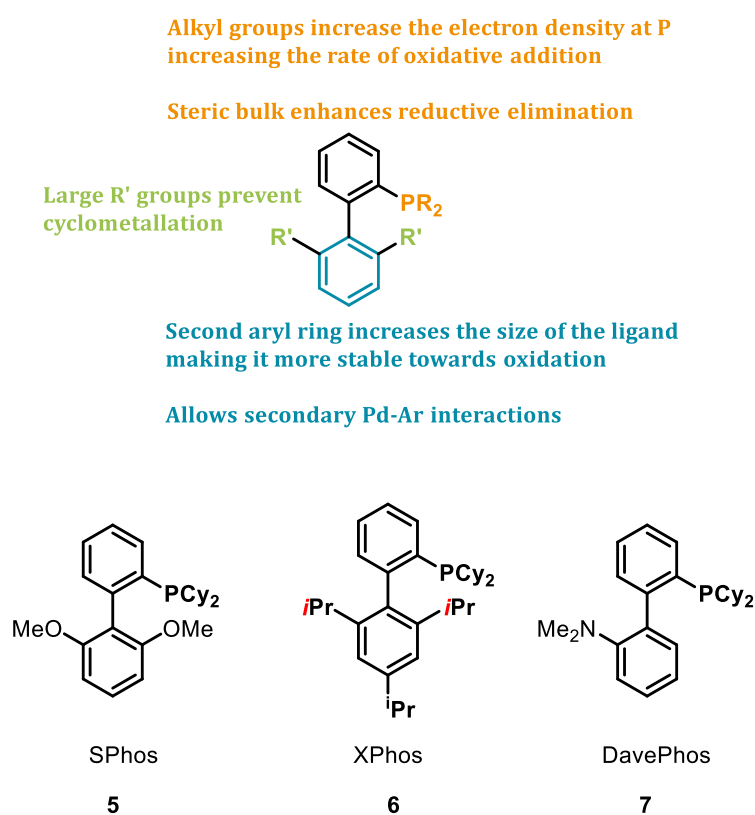
Figure 9. Design and examples of dialkylbiarylphosphines.

1.3.5 Diphosphines

Introduction of the second phosphine atom into the molecule's core allowed to achieve the bidentate, chelating phosphine ligands (Figure 10). By varying the nature of the linker between phosphine atoms and the substituents attached to them the modification of the steric and electronic parameters can be achieved.

An important parameter used to describe the complexes with diphosphine ligands is *bite angle* (β_n), defined as *Ligand-Metal-Ligand* angle (where *Ligand* refers to the chelating diphosphine ligand and *Metal* refers to metal in the complex). It was observed that the regiochemical outcome of the reaction depends on the magnitude of this angle. Its alternation (accomplished by thorough design of the bidentate ligand's structure) allows synthesizing products with the desired configuration. This feature is commonly used in hydroformylation chemistry where phosphines with large bite angle (such as XantPhos) are promoting formation of linear products, whereas phosphines having rather smaller bite angles (such as dppe) produce branched ones.[34]
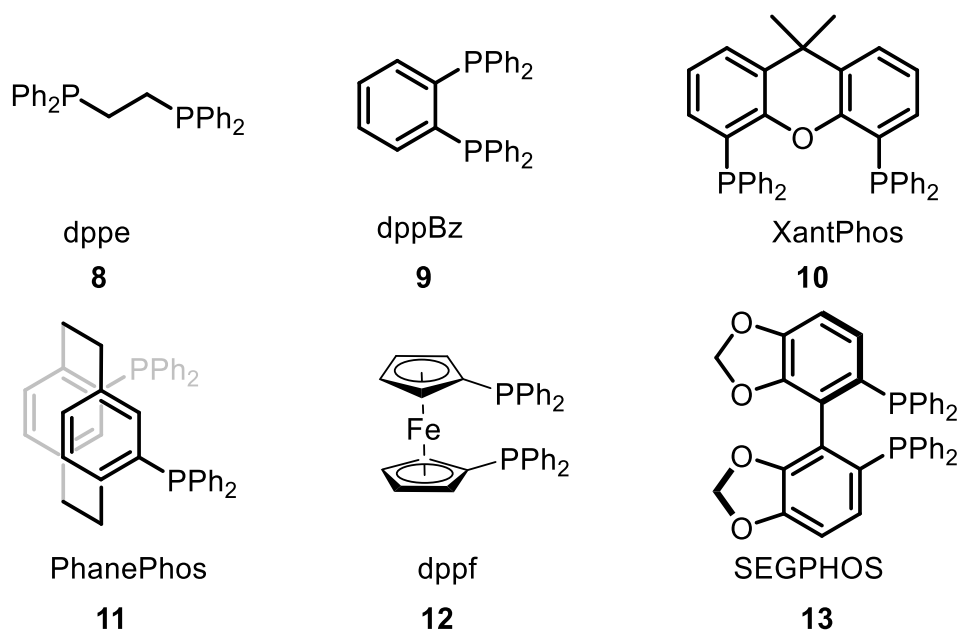
Figure 10. Examples of commonly used diphosphine ligands.

Diphosphine ligands are usually employed in ruthenium- and rhodium-catalysed asymmetric hydrogenation reactions.[35] These transformations are known as one of the most reliable and powerful methods of introducing chirality to the molecule, offering excellent control over absolute configuration of carbon atom adjacent to alcohol functionality.

The majority of chiral diphosphine ligands possesses C_2 symmetry and are either axially chiral (e.g. SEGPHOS)[36] or feature planar chirality (PhanePhos).[37] Over past decades, a library of tailored chiral diphosphines was synthetized to address the specific applications like imine reduction,[38] stereoselective hydroborylation,[39] oxidations [40] and many others.[41]

1.3.6 Electronic properties of phosphines

As it was already stated above depending on the substituents of phosphorus atom it is possible to tune the electronic properties of the phosphines. Until 1970s chemists were relying on a general rule of thumb, that σ-donating abilities of a phosphine ligand decreases when average electronegativity of substituents increases. In addition, π-accepting abilities of a ligand rise with the increase of electronegativity of substituents. In order to quantify these properties and categorize phosphines depending on their electronic specification, in 1970 Chadwick Tolman reported a parameter **v**.[42] Tolman electronic parameter (TEP) is determined by the measurement of CO infrared stretching frequency of the complexes, prepared from chosen ligand and tetracarbonylnickel(0). As a result, more electron-donating phosphines are corresponding to the lower CO stretching frequency. Stronger d_π–σ* interaction influences decreased C–O bond order and gives lower values of CO stretching frequency.

Figure 11. Tolman stereoelectronic map.

In 1977 Tolman plotted his electronic parameter against steric parameter θ in order to obtain Tolman stereoelectronic map (Figure 11). This chart is used up to date to identify and visualize both electron and steric abilities of new ligands.[43]

1.3.7 Electron-poor phosphine-type ligands

In parallel to many reactions in catalysis, which benefit from the application of phosphine ligands with electron-rich substituents placed on phosphorus atom (e.g. Buchwald-type ligands), there are few notable transformations in which electron-poor properties of the ligand are desired. For example, their introduction broaden the collection of tools used to control the mechanism of palladium catalyzed transformations. Most of them follow well-established elementary steps: oxidative addition- >transmetallation->reductive elimination. While a great number of ligands facilitating oxidative addition step were developed[44] designing ligands facilitating the rate of transmetallation and reductive elimination is challenging.

According to chemical logic introduction of electron-withdrawing substituents to the phosphine should affect the electronic properties of the ligand itself.

For example, in 1991 Krishnan and Farina investigated the role of ligand in Stille coupling reaction between iodobenzene (**14**) and tributyl vinyl tin (**15**) (Figure 12).[45]
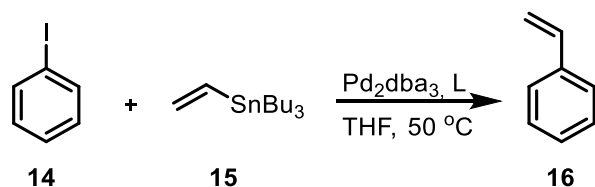
Entry	Used ligand	Yield of styrene [%]
1	PPh_3	15.2
2	$Ph_2PC_6F_5$	>95
3	$(2\text{-furyl})_3P$	>95
4	$MePPh_2$	< 2
5	$P(OPh)_3$	88

Figure 12. Investigation of ligand effect in Kosugi-Migita-Stille coupling.

The authors reported that using electron-poor ligands in this transformation leads to the increase of the yield of product **16**. They postulated that this phenomenon is probably attributed to the facilitated formation of a π-complex between stannane and palladium, by the use of electron-poor ligand , which is a rate-determining step. As shown in Figure 12, entries with fluorinated ($Ph_2PC_6F_5$) or oxygen-containing [$(2\text{-furyl})_3P$] phosphine as ancillary ligand yielded more of desired product in comparison with PPh_3.

Another application, where electron-poor ancillary ligands are beneficial, is catalysis using π-acids. The increase of π-accepting character of the ligand leads to the decrease of electron density on the metal which facilitates coordination to the metal center of substituents such as alkenes or alkynes. In comparison to classical ancillary ligands, electron-poor phosphines have proven their superiority in

transformations where the formation of π-complex between unsaturated substrate and transition metal is a rate determining step.[46]

In 2009 Gagné and co-workers showed an intermolecular reaction between electron-rich aromatic systems and allenes (Figure 13). Intermolecular hydroarylation using allenes is an attractive transformation giving access to highly functionalized unsaturated groups adjacent to aromatic system with excellent atom economy. However, one of the biggest challenges when using allenes in this type of transformation is control of the regioselectivity and expanding the scope of the reaction to non-heterocyclic electron-rich aromatic systems. In order to obtain the desired products, the group of Gagné applied electron-poor phosphites as electron-deficient ligands in this transformation, outperforming classical phosphines and expanding the scope of aromatic partner.[47]

12 examples
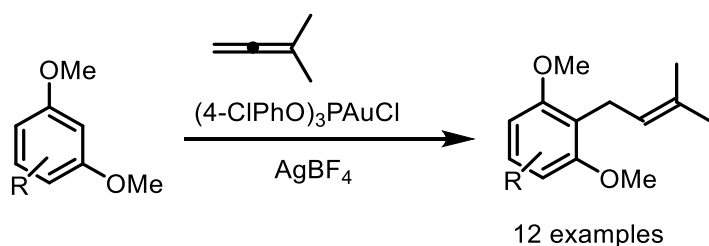
Figure 13. Hydroarylation reaction using gold phosphite complexes.

In 2010 Toste and co-workers reported a hydroazidation reaction of allenes (Figure 14). Investigation of reaction mechanism revealed that the pre-coordiation of allene to Au center is a rate-determining step. By changing the substitution pattern on the functionalized triphenylphosphine it was possible to increase the reaction rate up to 10 times by using *p*-CF$_3$-substituted ligand in comparison with electron-rich decorated phosphine.[48]
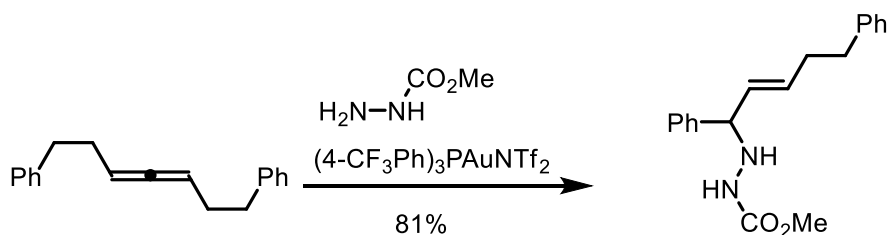
Figure 14. Intermolecular hydroazidation reaction.

Classical examples of electron-poor phosphorus-based ligands include polyhalogenated phosphines such as PCl_3, PF_3 or $P(CF_3)_3$ as well. It must be however noted that those molecules are not commonly used as ancillary ligands because of their tedious handling, explosive character and high toxicity.[49] These properties and shortcomings emphasize an immense need for new electron-poor ligands that would populate upper right fragment of Tolman's stereoelectronic map.

1.3.8 Classical ionic phosphine ligands

Although a vast majority of commonly used phosphine ligands are neutral species, there have been few precedential reports of introducing a charge to their structure.

One of the most quintessential examples of an ionic phosphine is tris(sodium-*m*-sulfonatophenyl)phosphane (**17**) commonly referred as NaTPPTS (Figure 15).[50] Since its introduction in 1984 it is used as a water-soluble alternative for classical phosphines. For instance, rhodium complexes of NaTPPTS are effective catalysts used for hydroformylation reaction in aqueous media.[51] This ligand was popularized and later successfully applied in industrial processes by Ruhrchemie company, because its use facilitate purification of desired organic product from transition metal contamination.[52]

In 1980s groups of Baird and Kinzel described synthesis and application of rhodium complexes of 2-(diphenylphosphino)ethyl]trimethylammonium hexafluorophosphate (**18**) (AMPHPHOS)[53] and its chelating analogue [(diphenylphosphino)methyl]-4-(diphenylphosphino)pyrrolidine tetrafluorobora-te (**19**) (DPPMDPPP) (Figure 15).[54] These monocationic ancillary ligands were successfully applied as constituents of rhodium catalysts used for hydrogenation and hydroformylation reactions in biphasic solvent system. Those ligands were historically first examples of cationic phosphines. Due to the presence of the aliphatic linker between the phosphine moiety and positively charged ammonium unit, it is considered that their electronic properties do not significantly differ from triphenylphosphine.
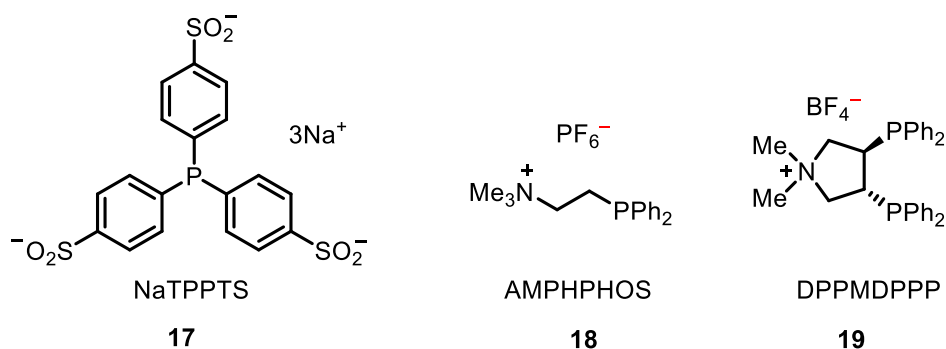
Figure 15. Classical phosphines ions.

1.4 α-Cationic phosphines

In the toolbox of readily available ligands, neutral and anionic species are predominant. Their expeditious development offer tailored-solutions to a variety of transition metal catalyzed reactions. Most of the accessible phosphines can be categorized as strong σ-donors and medium to weak π-acceptors.

At the same time the rapid increase of π-acid catalysis offered alternative approaches to synthesis of *inter alia* useful (hetero)aromatic motifs.[55] The catalytic performance of π-acids such as Au or Pt can be further tuned by the use of strong π-accepting ligands.[56,57] To this group belong rare examples of polyfluorinated phosphine ligands that possess required π-accepting properties. These ligands require tedious handling and are obtained in multi-step synthetic protocols.[58]

In order to address this scarcity and push the boundaries of extreme π-acid catalysts, α-cationic phosphines were developed, as positively charged, strong π-accepting ligands.

1.4.1 Definition and electronic properties

In the structure of the α-cationic phosphines, at least one of the substituents connected directly to phosphorus atom contains a cationic unit. This unit often corresponds to a heterocycle-derived cation; however, there are also other groups known in the literature.[59] Because of the direct connection to the phosphorus atom, σ-donating ability of these ligands is decreased. In addition, the energy of σ*(P–C)

orbital is lowered, leading to the raise of their π-accepting character. The combination of those two effects contracts the overall electron donation to the metal, making them perfect ligands for π-acid catalysis.

1.4.2 Imidazolium-derived phosphines

The first synthesis of a metal complex of α-cationic phosphine was described in 1995 by Komarov and coworkers (Figure 16).[60]
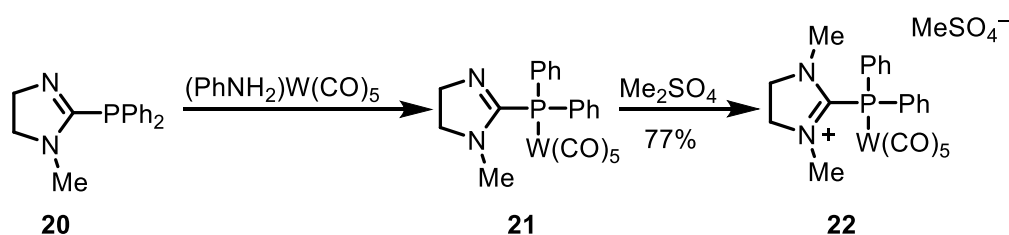
Figure 16. Synthesis of the tungsten complex 22 of imidazolium-derived phosphine.

They have demonstrated that using pentacarbonyl(aniline)tungsten in presence of neutral imidazole-derived phosphine **20** and subsequent methylation of one of the nitrogen atoms leads to the formation of a cationic complex **22**.

This work inspired Kuhn and coworkers, who showed in 1999, that the analogous free ligand **25** can be conveniently prepared from a free carbene and diarylchlorophosphine in one step (Figure 17).[61]
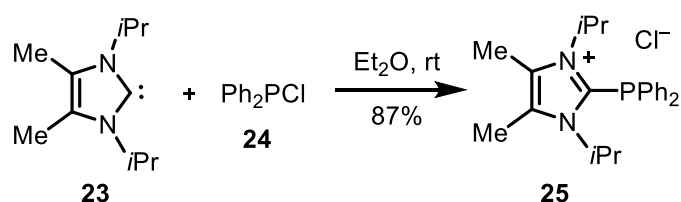
Figure 17. First synthesis of imidazolium-based cationic phosphine.

In 2007 the group of Andrieu reported an alternative route to the synthesis of imidazolium based phosphine.[62] They envisioned that the treatment of Ph_2PCl (**24**) by air stable imidazolium carboxylate zwitterion can result in formation of a cationic

phosphine. Their hypothesis was confirmed experimentally by synthesis of compound **27** (Figure 18) and others in 58–91% yield.
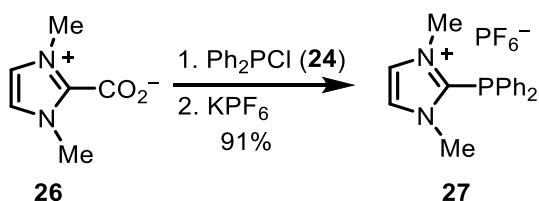
Figure 18. Synthesis of cationic phosphine using zwitterions.

1.4.3 Pyridinium-derived phosphines

Another examples of heterocycle-derived phosphine cations were developed in 2014 by Alcarazo and co-workers. In this new class of cationic phosphines ligands are based on pyridinium architecture.[63] It was hypothesized that by changing of the cationic moiety to pyridinium, a heterocyclic ion with low lying π^* orbital, more π-accepting character of the ligand would be obtained. In addition, similarly to Buchwald systems, pyridinium backbone is easier to modify, allowing introduction of additional substituents and, consequently, fine tuning of the ligand electronic properties.

In order to obtain desired molecules authors synthesized a series of 2-chloropyridinium salts **29** via a simple alkylation protocol. Afterwards, chloropyridinium ions were subjected to S_NAr reaction yielding final products **30** (Figure 19).
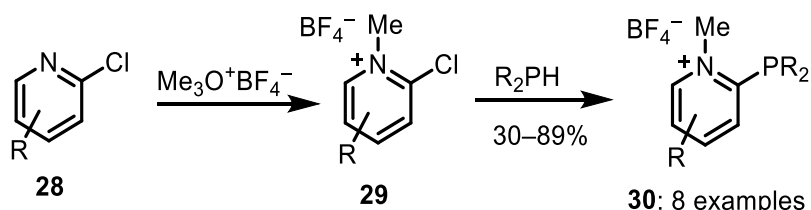
Figure 19, Synthesis of pyridinium-derived cationic phosphines.

In the same report Alcarazo and co-workers described coordination studies of new ligands to Au (I) and Pt(II) metals. In order to compare the reactivity of pyridinium-

derived cationic phosphines with classical electron-poor ancillary ligands authors performed a kinetic study of model hydroarylation reaction catalyzed by platinum complex (Figure 20).

As it can be observed on Figure 20, platinum (II) complexes with pyridinium phosphines as ancillary ligands have much higher kinetic coefficients than their neutral counterparts. Both of tested ligands reached full conversion of starting material **31** after just 5 minutes, whereas classical electron-poor ligands and platinum (IV) catalyst required much longer reaction times.
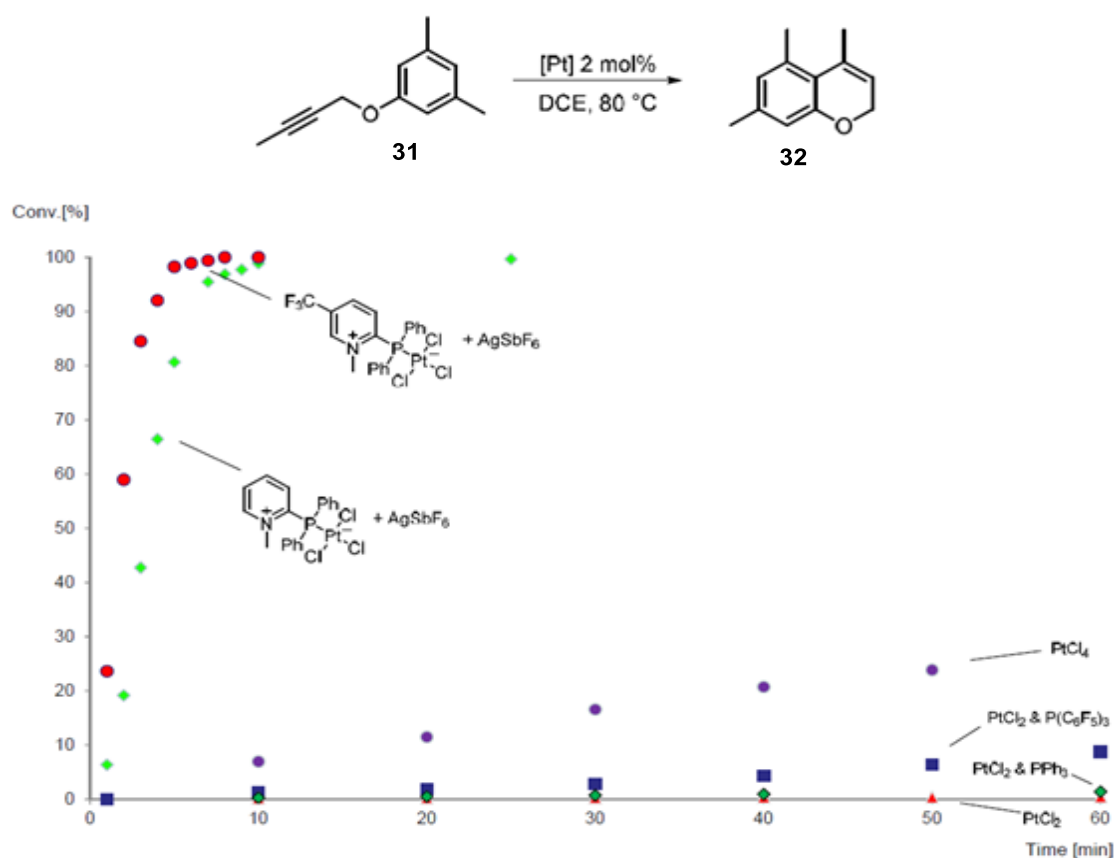
Figure 20. Comparative kinetic study of model hydroarylation.

1.4.4 Cyclopropenium-derived phosphines

In 2011 Alcarazo and co-workers demonstrated an unprecedented synthesis of cyclopropenium-derived cationic phosphine ligand – as the first example of non-heterocycle-derived α-cationic phosphine.[64] They discovered that treatment of chlorocyclopropenium salt **34** with secondary phosphines followed by anion exchange results in formation of the desired product **35** in good yield (Figure 21). The proposed synthetical method is complimentary to works of Kuhn[61] and Andrieu,[62] as it relies of a formal *Umpollung* of reagents.
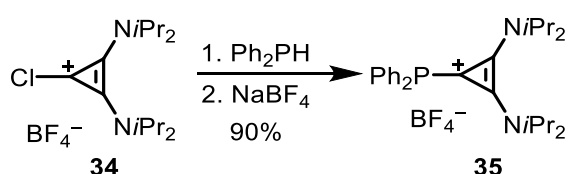
Figure 21. Synthesis of cyclopropenium-based cationic phosphine 35.

In the same report, the authors obtained gold(I) (**36**) and rhodium(I) (**37**) complexes of these ligands (Figure 22). The structures and connectivity of these complexes were confirmed by single crystal diffraction experiments.
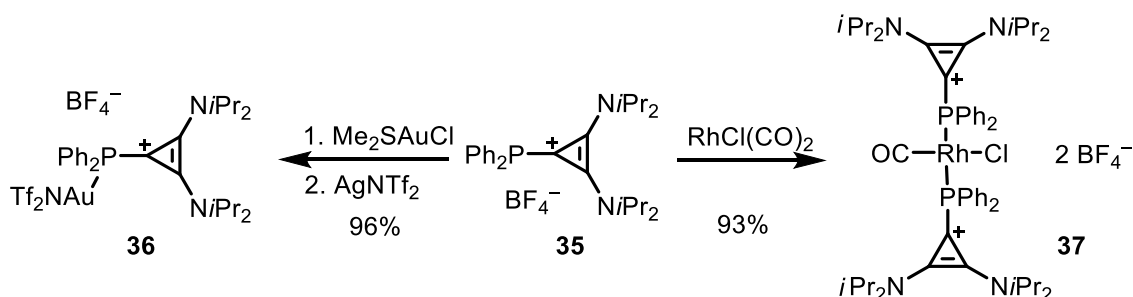
Figure 22. Synthesis of rhodium complexes of new cationic phosphines.

A model reaction – cyclization of allene **38** – was explored in order to confirm desired π-accepting properties of obtained complexes **36** and **37** (Figure 23). The product of this reaction depends on the nature of the ligands. If electron-poor, strongly π-accepting ligands are used, the intermediate **39** shows a strong carbocationic character; therefore, **pathway A** with 1,2-alkyl shift is promoted. In

the case of strong σ-donating and weak π-accepting ligands the nature of **39** is more of carbene-type. As result, **pathway B** and 1,2-hydride shift is observed.
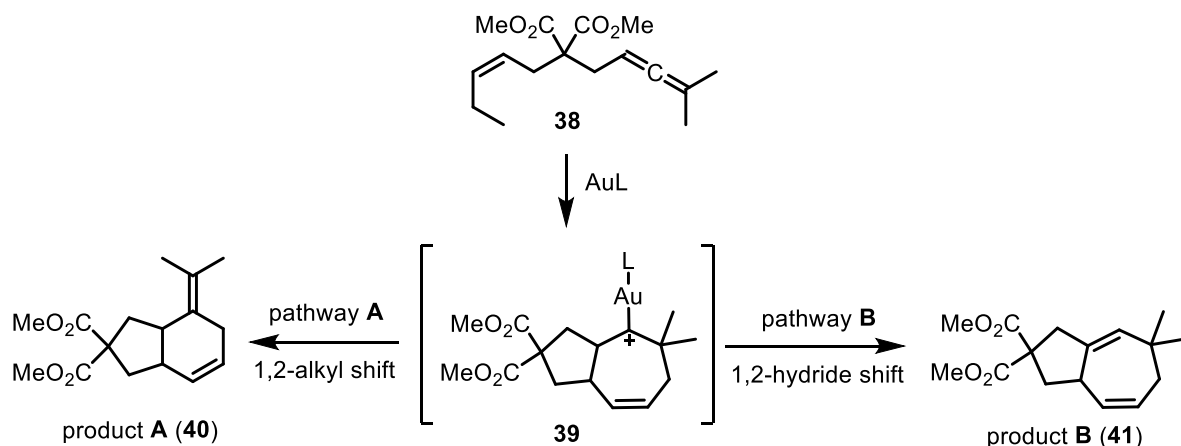
Figure 23. Model allene cyclization reaction.

Authors compared several commercially available ligands with the new cationic phosphine. The outcome of these studies is summarized below in the Table 1.

Table 1. Studies of reactivity using different ligands in allene cyclization.

Used ligand	Ratio 40/41	Yield [%]
PMe$_3$	55/45	84
PPh$_3$	75/25	75
P(OPh)$_3$	97/3	98
	87/13	92
	1/99	95

The reactivity studies have proven that **35** is indeed a strong π-accepting ligand, comparable to phosphite P(OPh)₃ and carbene. This study opened a new chapter in coordination chemistry of cationic phosphines.

1.4.5 Effect of cationic substituent on phosphines

It was demonstrated, that the introduction of cationic unit to the phosphine architecture significantly lowers both HOMOs and LUMOs, when referred to PPh₃ as neutral ligand (Figure 27). This effect can be quantified and calculated using DFT studies on B3LYP-D3/def2-TZVP level of theory.
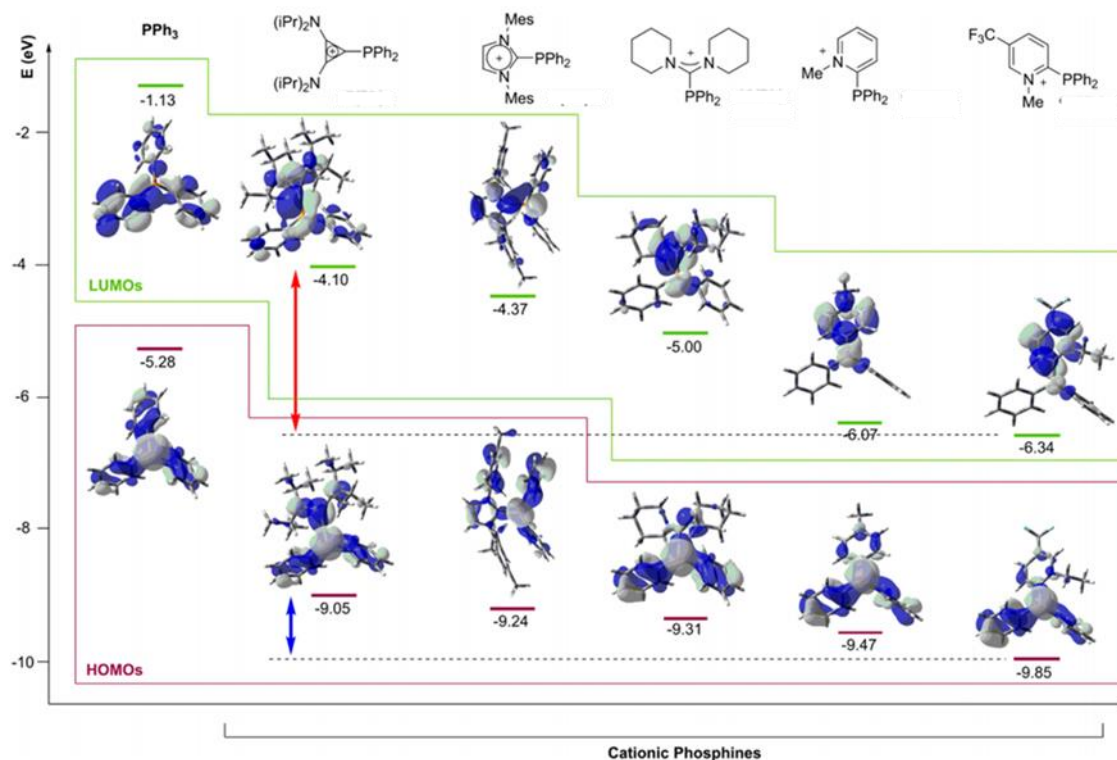
Figure 24. Energies of HOMO and LUMO in representative examples of cationic phosphines.[65]

Interestingly, lowering of HOMOs energy level is attributed to the introduction of a positive charge. Different substituents do not change this value in significant way. On the contrary, in LUMOs energy values depend significantly on the nature of

cationic moiety. This phenomenon enables a fine modification of HOMO-LUMO gap and further control over the reaction outcome.

1.4.6 Polycationic phosphines

In order to elaborate even more efficient approach to manage the electronic properties of cationic phosphines, in 2009 Andrieu and co-workers aimed the synthesis of the first dicationic phosphine (Figure 25). To achieve their goal, researchers used the mentioned above strategy condensing zwitterion **26** with chlorophosphine.[66]
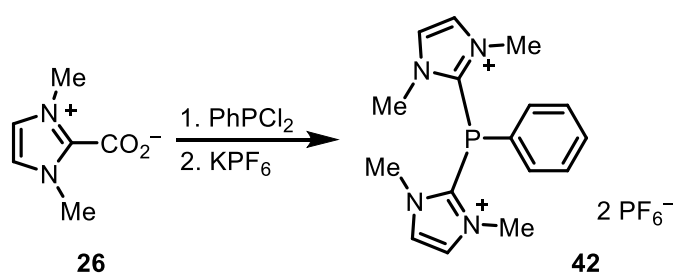
Figure 25. First synthesis of a dicationic phosphine.

The desired molecule **42** was obtained in low yield of 10%. This amount was sufficient to fully characterize the dicationic product, and prove its stability towards air and moisture. It was anticipated, that addition of second electron-withdrawing unit increases π-accepting properties of the ligand even further however no follow-up studies in this regard were presented due to difficult synthesis and tedious work-up protocol.

In 2013, the group of Alcarazo presented an elegant synthesis of dicationic cyclopropenium-derived phosphine **44** (Figure 26).[67] Authors envisioned the synthesis of this molecule based on a sequence of condensation reactions[64] however, after the first condensation the reaction was incomplete. To obtain **44**, uses of strong base and of an additional equivalent of electrophile were required.
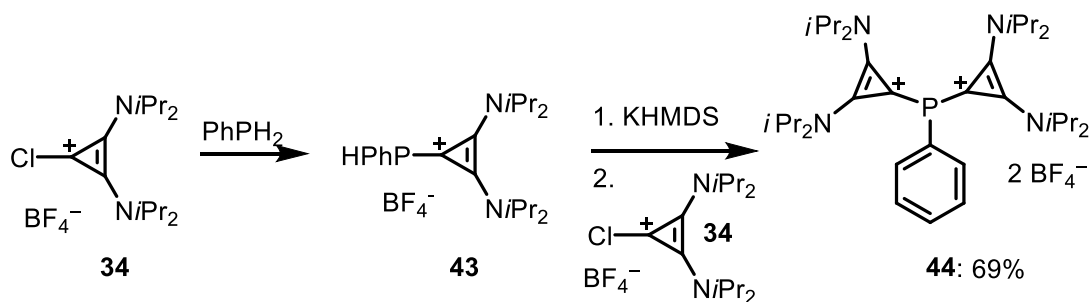
Figure 26. Synthesis of dicationic cyclopropenium-derived phosphine.

Phosphine **44** was successfully coordinated to gold (I) and platinum (II) centers. Unfortunately, all attempts to coordinate **44** to rhodium(I) or nickel(0) carbonyl precursors with a purpose to determine TEP were unsuccessful. On the other hand, this parameter was calculated using DFT methods and was estimated to be 2101 cm^{-1}.

The authors also investigated the catalytic activity of newly obtained ligand-based Au(I) complexes in a series of challenging hydroarylation reactions (Figure 27).
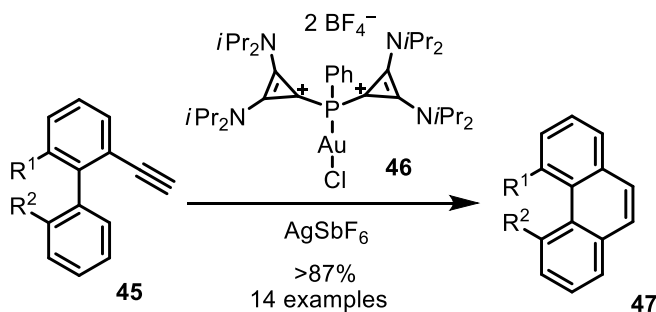
Figure 27. Model hydroarylation employed for the evaluation of catalytic activity of dicationic phosphine gold(I) complexes.

Dicationic phosphine-gold(I) complexes have proven to be very active in this transformation, giving access to a series of 1,9-disubstituted phenanthrenes **47** in excellent yields. In addition, authors presented a short synthesis of two natural products: *Ochrolide* and *Coeloginin* utilizing gold(I) dicationic phosphine complexes as catalysts for the hydroarylation reaction as a key step.

A new synthetic route, utilizing P(TMS)$_3$ allowed to obtain for the first time a tricationic phosphine ligand **48** (Figure 28).[68]
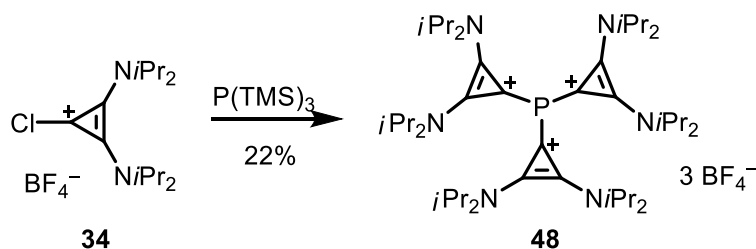
Figure 28. Synthesis of tricationic phosphine described by Alcarazo and coworkers.

Based on DFT studies, **48** was proven to be excellent π-acceptor and a very poor σ-donor. Furthermore, despite having three positive charges in its structure, **48** unexpectedly coordinate to platinum(II) metal center.

In 2015 Weigand and co-workers described a similar type of phosphines using silylimidazolium salts **49** and PCl$_3$ as starting materials (Figure 29).[69]
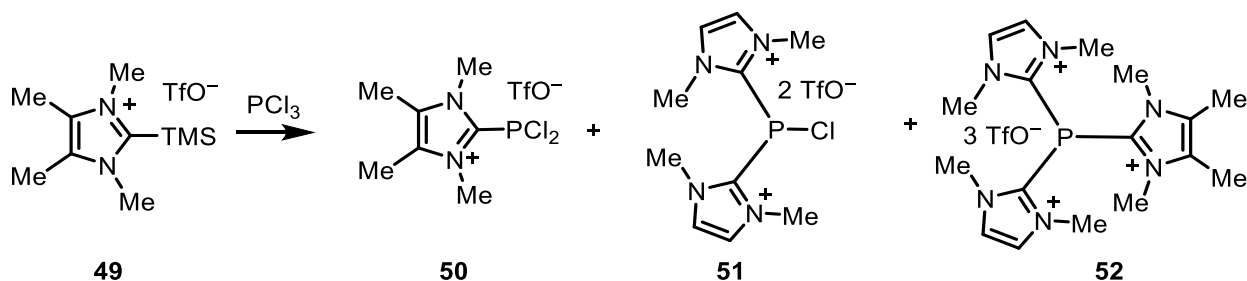
Figure 29. Synthesis of a tricationic phosphine by the group of Weigand.

Authors postulated that in solution, a tricationic phosphine (**52**) is involved in dynamic equilibrium with chloro- (**51**) and dichlorophosphines **50**. On the contrary to cyclopropenium derived tricationic system, this ligand was not able to coordinate either Au or Pt.

1.5 Use of bidentate phosphines as ancillary ligands for rhodium and iridium – selected examples

In 2013 group of van Leeuwen envisioned, synthetized and evaluated the catalytic properties of a new class of electron poor phosphines based on N-pyrrolyl moiety. The authors chose a model hydroformylation reaction in order to test their hypothesis that strong π-acceptor ligands show higher activity in this transformation then classical phenyl substituted phosphines. Noteworthy, in addition to higher activity N-pyrrolyl substituted systems proved to be more selective than Phenyl (Figure 30)[70].
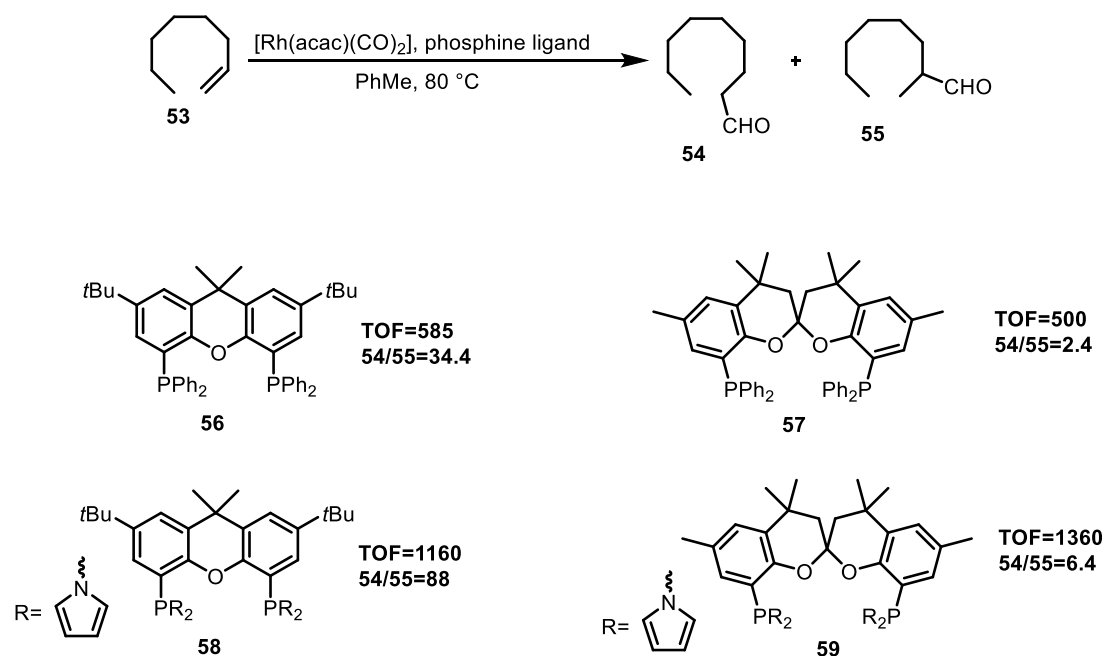
Figure 30. Use of pyrrolyl substituted phosphines in hydroformylation of n-octene.

In addition to reactivity studies, authors performed HPNMR and HPIR studies showing that pyrrolyl substituted ligands favour formation of bisequatorial rhodium complexes under reaction conditions.

In 2012 group of Kwong described a stereoselective hydroalkynylation of norbornadienes catalyzed by chiral iridium complexes. Authors performed a detailed screening of different chiral diphosphines that were successfully applied as ancillary ligands for this transformation (Figure 31).[71]
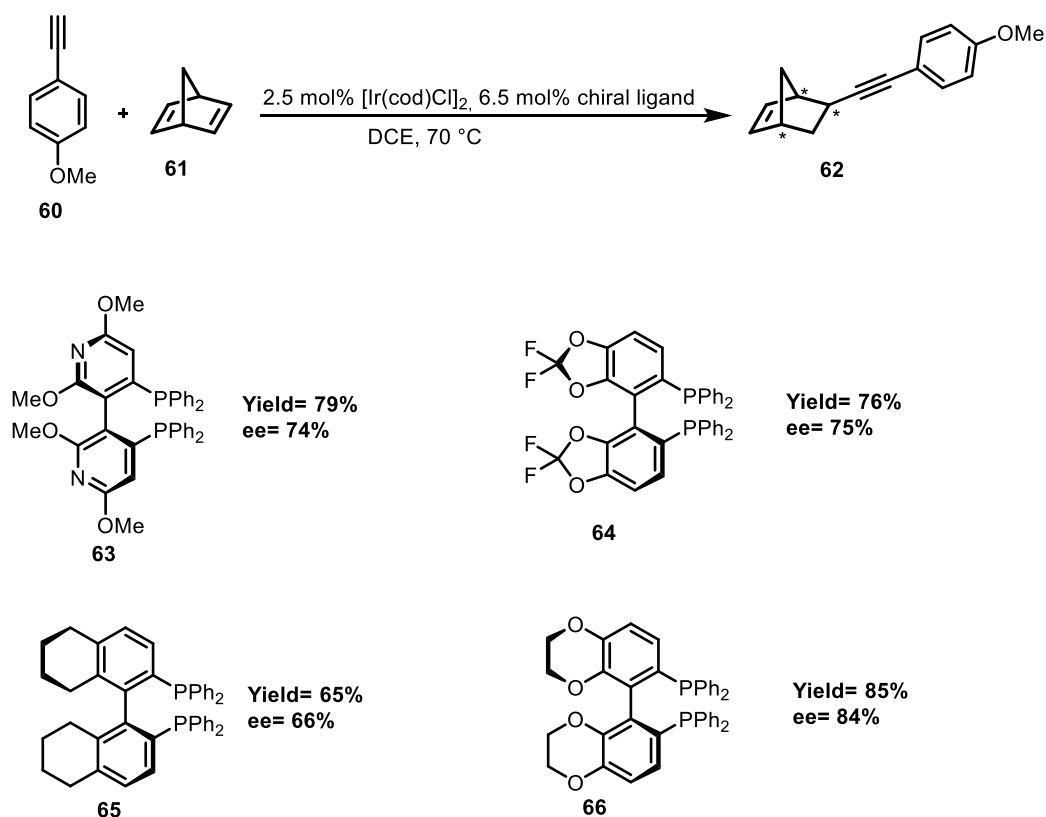
Figure 31. Use of chiral bidentate phosphines in iridium catalyzed hydroalkynylation of norbornadiene

The results obtained using electron rich BINAP type ligands versus electron poor 65 ligands led to the drop of reaction yield and enantioselectivity. The highest yield and stereochemical outcome however were obtained using bulky SYNPHOS ligand 66 showing that steric parameter plays more significant role in this transformation than the electronic properties of ancillary ligand.

1.6 1,3-Conjugated dienes

The term 1,3-conjugated dienes refers to derivatives of 1,3-butadiene. This molecule has four electrons in the π-system, placed on the two bonding orbitals: without and with one node (Figure 32).[72]
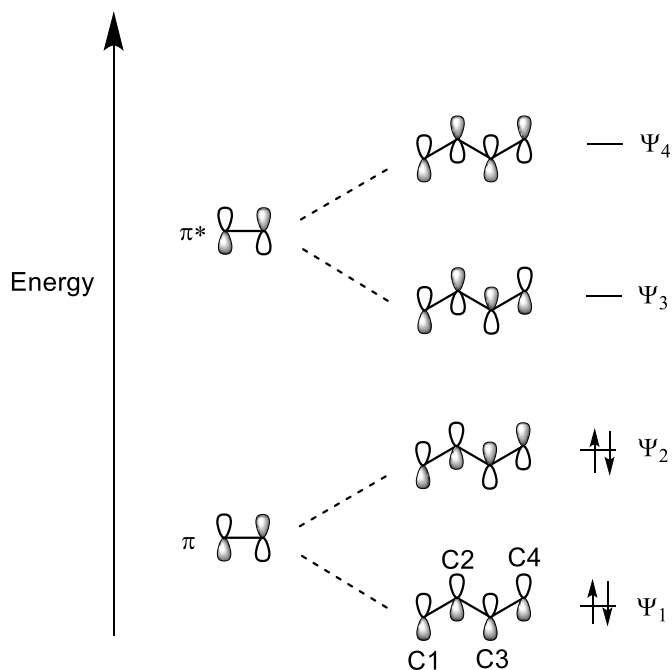
Figure 32. Electron distribution in 1,3-butadiene.

In the orbital with lowest energy ψ_1, all electrons are delocalized equally over four carbon atoms. In ψ_2 the bonding between atoms C1 and C2 and C3 and C4 and an antibonding interaction between C2 and C3 can be distinguished. Consequently, 1,3-dienes have a resonance structure of 1,4 dipole. A single bond between carbons in butadiene has a preference for planarity and is shorter (1.45 Å) than usual C–C single bond (1.54 Å). This results in two possible conformers – s-*cis* and s-*trans*, when referring to the position of both double bonds around a single bond in 1,3 conjugated dienes (Figure 33). The rotation barrier between them is determined to be about 2.3 kcal/mol.
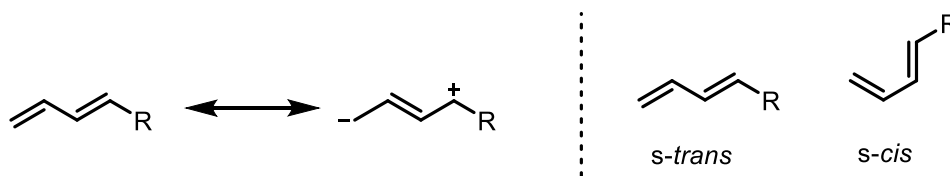
Figure 33. Resonance structure and conformers of 1,3-dienes.

Because of this unique electronic structure conjugated 1,3-dienes have been used as substrates in a variety of organic transformations.[73]

1.6.1 Electrophilic additions

Due to the unique structure of butadiene, its HOMO possesses higher energy than the HOMO of ethylene. Consequently, 1,3-conjugated dienes are more reactive towards electrophiles than simple alkenes. Depending on the reaction conditions, they can react with an electrophile via either 1,2- or 1,4-addition reaction mechanism. Transformations, which proceed under kinetic control (performed at lower temperatures) are giving 1,2-product, whereas at higher temperatures, more stable intermediate – allylic carbocation – is formed, and 1,4-addition product prevails (Figure 34).[74]
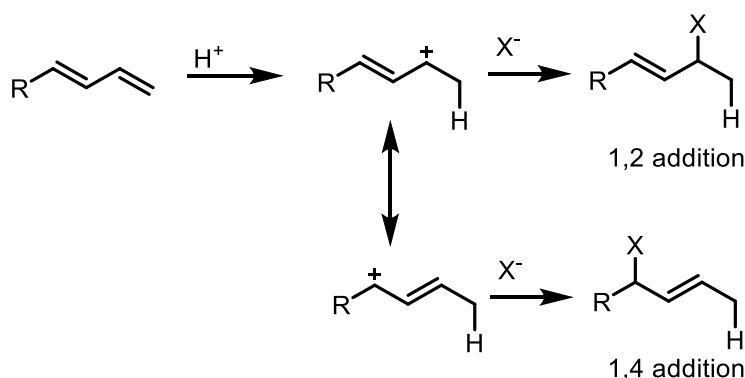
Figure 34. Mechanism of electrophilic 1,2- and 1,4-addition to butadienes.

1.6.2 Cycloaddition reactions

1,3-Dienes react with dienophiles in [4+2] Diels-Alder cycloaddition reaction (Figure 35). This reactivity involves 4π electrons of diene and 2π electrons of dienophile. In order for the reaction to proceed, the difference of energy between

HOMO of diene and LUMO of dienophile have to be small enough for the molecular orbitals to overlap and form two new σ-bonds that possess lower energy than the π-bonds of both reactants.[75]
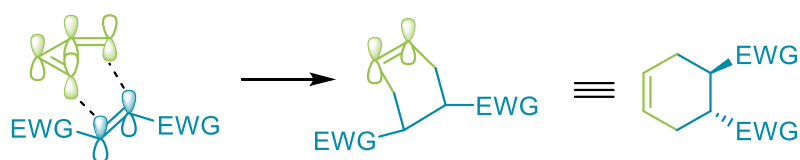
Figure 35. Mechanism of 4+2 cycloaddition reaction.[72]

Diels-Alder reaction is one of the most powerful methods of C–C bond formation.[76] For its discovery Otto Diels and Kurt Adler were awarded Nobel Prize in Chemistry in 1950.

1.6.3 Metal-catalyzed hydrofunctionalization reactions

Over the past decades rapid development of metal catalyzed hydro-functionalization reactions of carbon-carbon multiple bonds enabled access to a variety of different structural motifs. This type of reactions offers excellent atom economy, and is often tolerating various functional groups. A great majority of reports in this field utilizes simple alkenes, alkynes or allenes as substrates leaving the conjugated dienes, an alluring alternative towards functionalized unsaturated carbon chains.[77] One of the main challenges in the field of functionaliztion of 1,3-conjugated dienes is the regioselectivity of this transformation, tackled so far only in few reports.

In 2008 group of Hiyama reported an entry towards nickel-catalyzed functionalization of 1,3-dienes with fluoroarenes (Figure 36).[78]
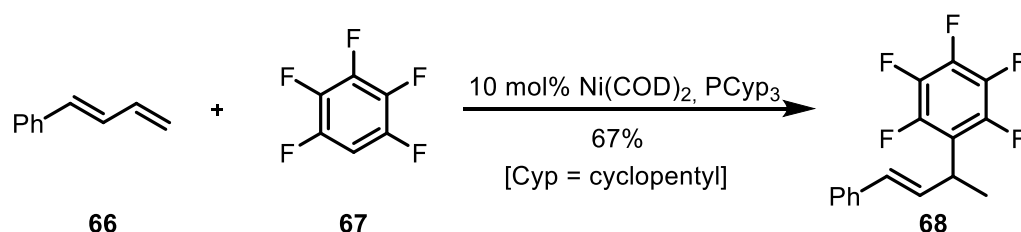
Figure 36. Nickel-catalyzed hydroarylation of phenylbutadiene 53.

Authors postulated that this reaction proceeds via C–H activation of fluoroarene and migratory insertion of Ni(II) species in C–C multiple bond. In this example the use of a bulky and electron-rich phosphine stabilizes Ni(II) intermediate and governs the regioselectivity.

In 2006 group of He explored gold-catalyzed hydroamination of 3-methyl-1,3-pentadiene (**69**) (Figure 37). Authors reported that applied Ph₃PAuOTf is an effective π-acid catalyst for this transformation.
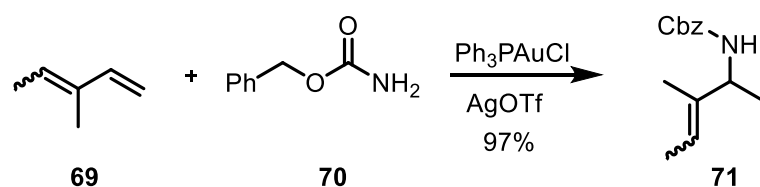
Figure 37. Gold (I)-catalysed hydroamination of 1,3-dienes.

In 2014 Meek and co-workers reported synthesis and coordination chemistry of a new chelating carbodicarbene (CDC) ligand. They have successfully applied rhodium complex of CDC (**72**) in hydroamination reaction of 1,3-dienes.[79] In the following report, the same group utilized **72** in hydroarylative transformation of 1,3-dienes using electron-rich heterocycles as nucleophiles (Figure 38).[80]
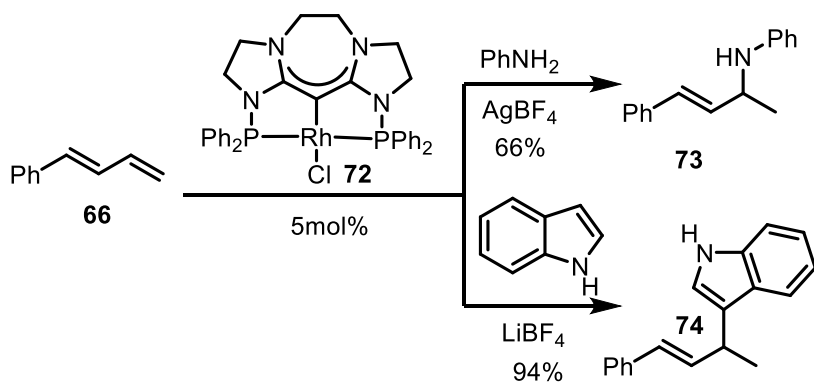
Figure 38. Hydroamination and hydroarylation of indoles using rhodium CDC complexes.

Group of Meek proved that rhodium-CDC complexes were efficient and regioselective catalysts for this transformation. Despite high yields of over 70% and good regioselectivities, one of the main limitations of these reactions was their limited substrate scope and necessity to use external inorganic salt.

2 CHELATING DICATIONIC PHOSPHINES – SYNTHESIS AND STRUCTURE

2.1 Synthesis

One of the uttermost shortcomings of the highly π-accepting cationic phosphine ligands such as di- and tricationic phosphines is their low ability to coordinate transition metals because of charge repulsion. In fact, up to date, only Au (I), Pt (II) and Rh (I) complexes were described in the literature.[66,68,81] In addition, electron-poor phosphines have been successfully applied as ancillary ligands in a variety of rhodium complexes used for catalysis.[82]

In order to address this inherent limitation and expand the coordination chemistry of polycationic phosphines we conceptualized the new, tailored ligand, in which the dicationic phosphine moiety is tethered to the strong σ-donating unit such as diphenylphosphine (-PPh$_2$). We envisioned that this coordination anchor, as well the use of the rigid linker will be able to bring the polycationic phosphine to the proximity of the coordination sphere of a metal, which in turn will prompt the coordination of the cationic group (Figure 39).
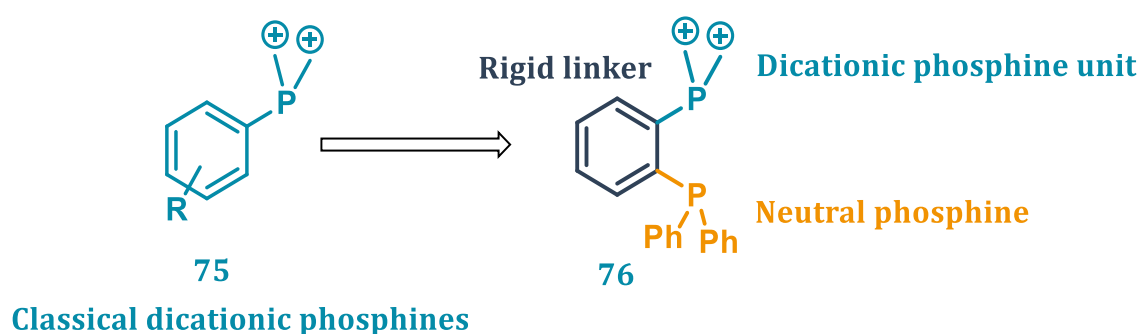
Figure 39. Rational design of the chelating dicationic phosphine.

Using retrosynthetical analysis, we have concluded that our synthetic goal can be achieved in a three step reaction sequence using either nucleophilic or electrophilic P-atom synthons (Figure 40).
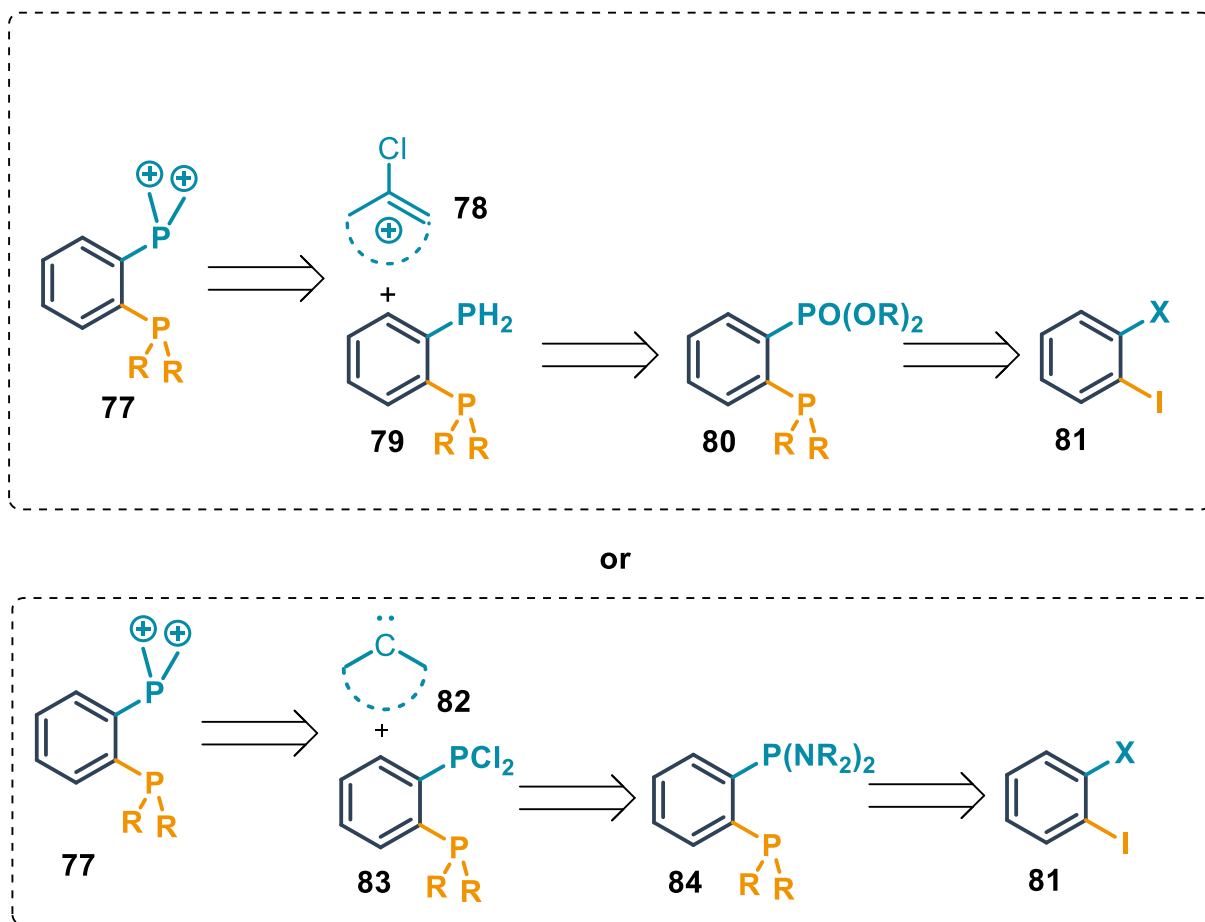
Figure 40. Retrosynthetical analysis of the dicationic chelating phosphine.

The first strategy, based on previously described approach by Alcarazo and co-workers, involves the incorporation of tertiary phosphine and phosphate moieties to the backbone via metalation followed by quenching with an electrophile. Subsequent reduction to the primary phosphine and condensation with an electrophilic agent is expected to deliver the final product.

The second approach involves formation of phosphodiamidate followed by acidolysis to give the corresponding phosphine dichloride. After condensation with carbene, this species would yield the desired molecule.

Despite the requirement of using and handling highly reactive and sensitive primary phosphine, we decided to apply the first strategy, since it looked more straightforward and logical to be carried out on the laboratory scale.

Monophosphine **86** was prepared with a high yield via modified procedure of C–P bond formation by Pd-catalyzed cross-coupling reaction of **85**.[83] Subsequent metalation with *t*BuLi and quenching with diethylchlorophosphate yielded **87**, which was later reduced using LiAlH$_4$ furnishing the diphosphine **88** in 52% overall yield.
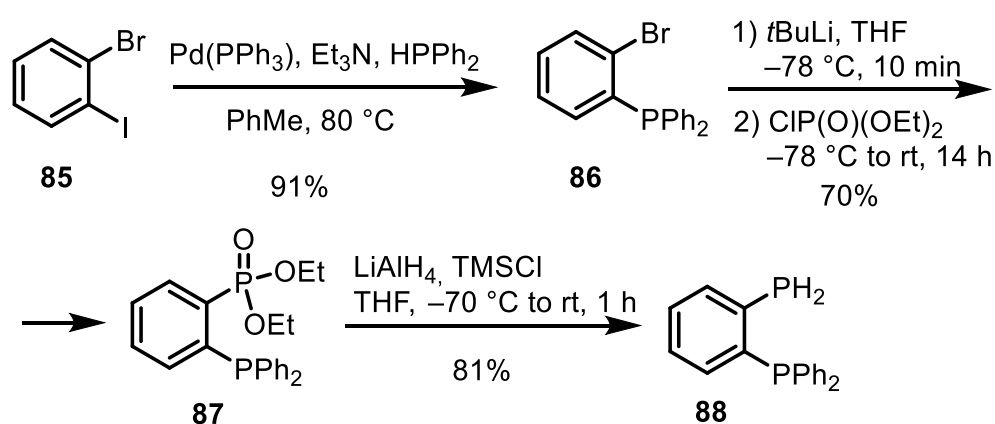
Figure 41. Synthesis of the synthon 88.

With the synthon **88** in hand, we continued with the final synthetic steps towards the target ligands. We envisioned that primary phosphine is a strong nucleophile readily reacting with different C-electrophiles giving access to different families of dicationic ligands.

2.1.1 Bisimidazolinium chelating phosphines

First we aimed the synthesis of bisimidazolinium chelating phosphines. We envisioned to prepare the required reagent **91** bearing the imidazolium unit from a commercially available 1,3-dimethyl-2-imidazolidinone (**89**). The desired chlorodihydroimidazolinium salt (**91**) was obtained by the treatment of **89** with oxalyl chloride and subsequent counterion exchange in the Vilsmeier-type intermediate **90** (Figure 42).
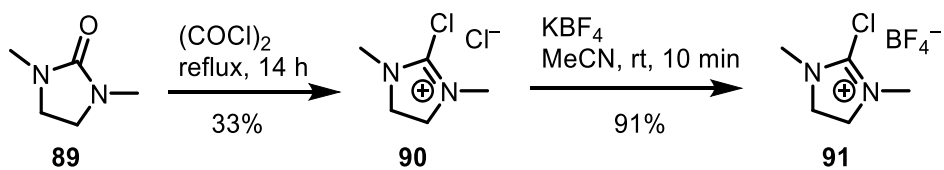
Figure 42 Synthesis of the Vilsmeier-type intermediates.

Afterwards, treatment of diphosphine **88** with **91** in the presence of NEt$_3$ followed by anion exchange afforded expected dicationic structure **92** (Figure 43).[I]
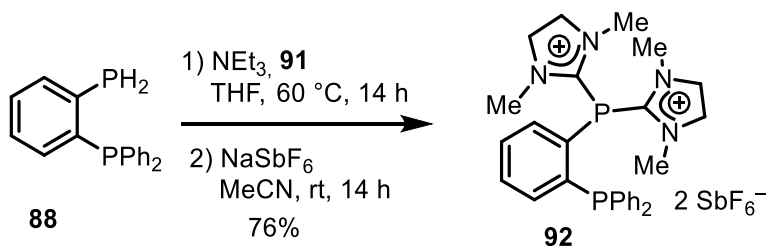
Figure 43 Synthesis of imidazolium-derived dicationic phosphine

The ^{31}P NMR spectrum of **92** consists of two doublet of doublet signals (121 MHz, acetonitrile-d$_3$) δ:- -11.3 and -46.8 ppm and shows the coupling between neutral and cationic phosphorus atoms

The structure and connectivity of **92** were confirmed by monocrystal diffraction measurement (Figure 44). Interestingly, the distance between both phosphorus atoms in the solid state is 3.094 Å and it is smaller than in its neutral analogue 1,2-bis(diphenylphosphino)benzene (3.165 Å).[84] This difference might be the consequence of an attraction between both phosphorus centers in the obtained chelating phosphine, which is not present in the neutral equivalent.

[I] Compound **92** was obtained, characterized and crystallized by Dr. Lianghu Gu.

Figure 44. Single crystal structure of 92, thermal ellipsoids at 50% probability; hydrogen atoms, solvent molecules and hexafluoroantimonate counterions have been omitted for clarity.

Obtained compound shows remarkable stability in the presence of moisture and air, showing no oxidation after 1 week in solution. This is remarkable for phosphine ligands.

2.1.2 Bispyridinium chelating phosphines

In order to modify the architecture and to obtain a small library of chelating dicationic ligands, we decided to introduce alkylpyridinium moiety into their structure. We have anticipated that, in fact, it could be possible to obtain both *orto-* and *para*-alkylpyridinium regioisomers by simple nucleophilic aromatic substitution with **88** in *orto-* or *para*-substituted halopyridinium salts. The corresponding salts **94** and **96** were prepared using alkylation of commercially available starting materials **93** and **95** with either Meerwein salt or ethyl triflate, respectively.
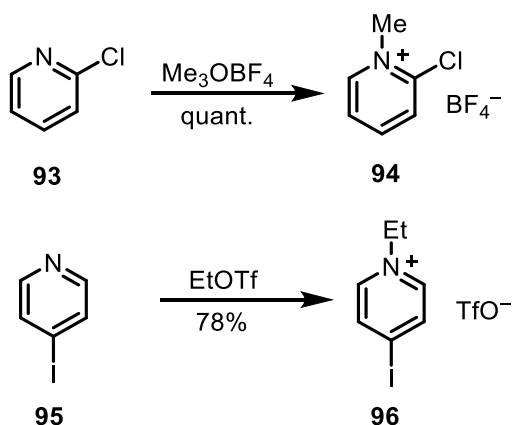
Figure 45. Synthesis of halopyridinium salts.

With the above mentioned salts **94** and **96** in hand, we have performed condensation reactions with **88** in the presence of NEt₃ (Figure 46).
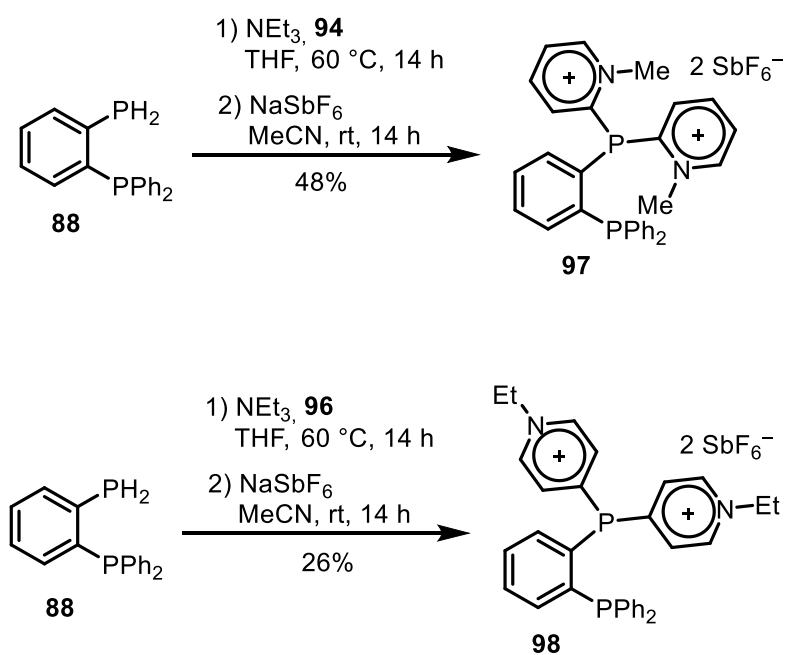
Figure 46. Synthesis of chelating dicationic pyridinium phosphines.

Similarly to **92**, the ³¹P NMR spectrum of **97** consists of two doublets of doublet signals: (162 MHz, CD₃CN) δ = -12.45, -23.85. (. Interestingly, in the case of **98** the chemical shift of both phosphorus atoms is so small, that strong 'roof' effect in AB

system is observed: (162 MHz, acetonitrile-d$_3$) δ = -10.87 (d, J = 152.1 Hz), -12.19 (d, J = 153.5 Hz) (Figure 47).
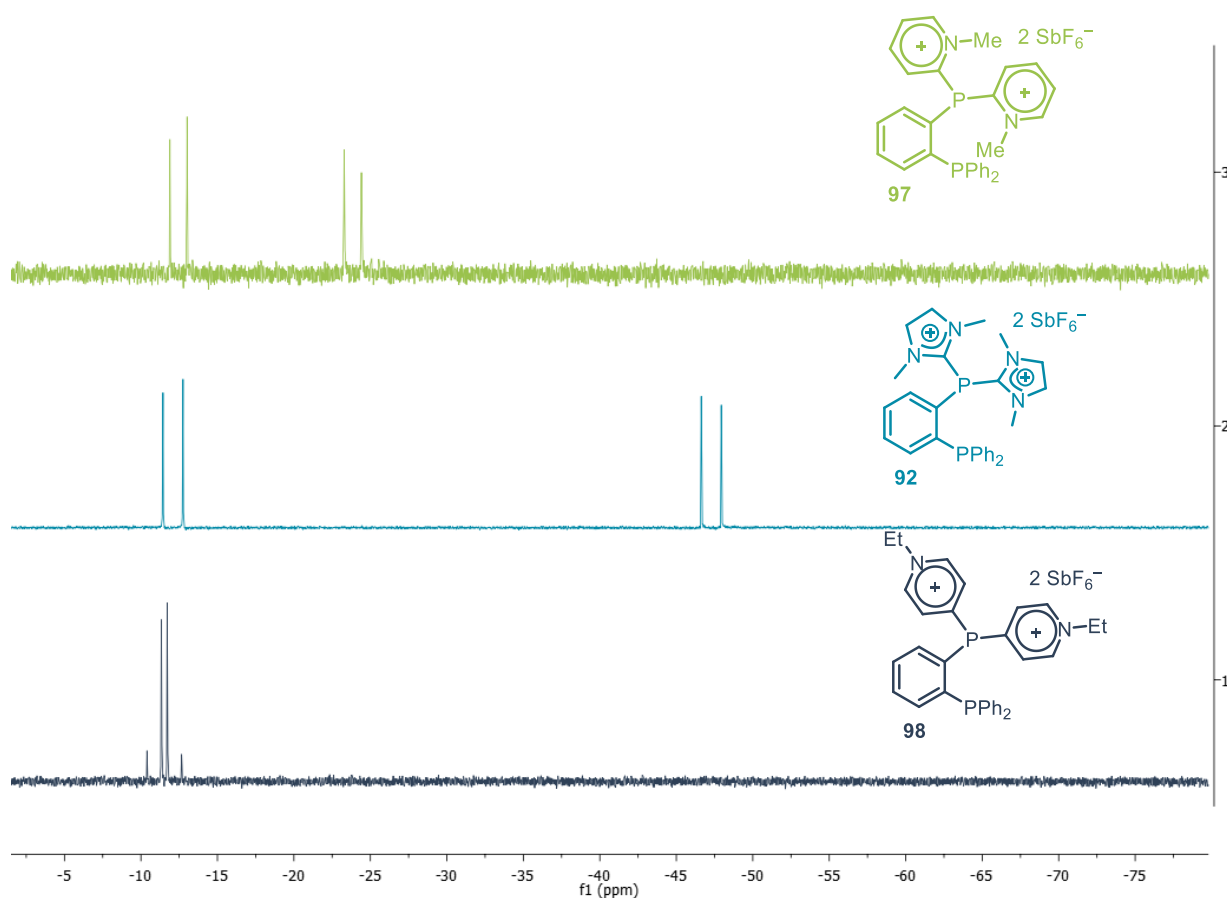
Figure 47. Comparison of 31P NMR spectra of the obtained ligands.

These compounds proved to be moisture and air sensitive, showing considerable amount of hydrolysis product after one hour in solution.

Suitable for X-ray diffraction analysis monocrystals of both pyridinium-derived phosphine ligands **97** and **98** were obtained by slow evaporation of acetonitrile from their saturated solutions.

In both obtained compounds C–P and C–C bonds lengths are within the usual range. In case of **97** (Figure 48) the distance between P1 and P2 (3.140 Å) is longer than in **92** (3.094 Å), but it is still slightly shorter than the bonds lengths observed in bis(diphenylphosphino)benzene (3.165 Å).
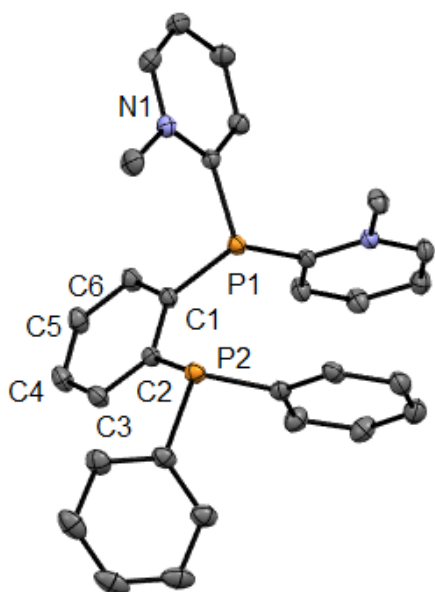
Figure 48. Monocrystal structure of 97, thermal ellipsoids at 50% probability; hydrogen atoms, solvent molecules and hexafluoroantimonate anions have been omitted for clarity.

In case of **98** (Figure 49) the distance between P1 and P2 is slightly shorter (3,091Å) than compared to **92**, which might indicate the strongest dative interaction between both phosphorus atoms in the whole series of ligands.

Figure 49. Single crystal structure of 98, thermal ellipsoids at 50% probability; hydrogen atoms, solvent molecules and hexafluoroantimonate anions have been omitted for clarity.

2.2 Synthesis of the chelating dicationic phosphine with paracyclophane backbone

In order to develop a chiral version of the obtained ligands we decided to modify the structure by changing its backbone. Specifically, we decided to use a [2.2]paracyclophane structure. Incorporation of this moiety might offer an access to a new type of chiral dicationic ligands similar to PhanePhos **11**.[39]

Similarly to the synthesis of ligands with the benzene ring embedded in their core, we started the synthetic chain towards chiral ligands from dibromoderivative of cyclophane **99** (Figure 50). Initial monolithiation of **99** followed by the addition of diphenylchlorophosphine gave monosubstituted product **100** in 67% yield. The second lithiation and quenching with diethylchlorophosphate yielded **101** in 44% yield. Reduction of the latter with LiAlH₄ smoothly furnished the primary phosphine derivative **102**, which was condensed with Vilsmeier-type salt **91** to deliver the target compound **103** after counterion exchange with NaSbF₆.
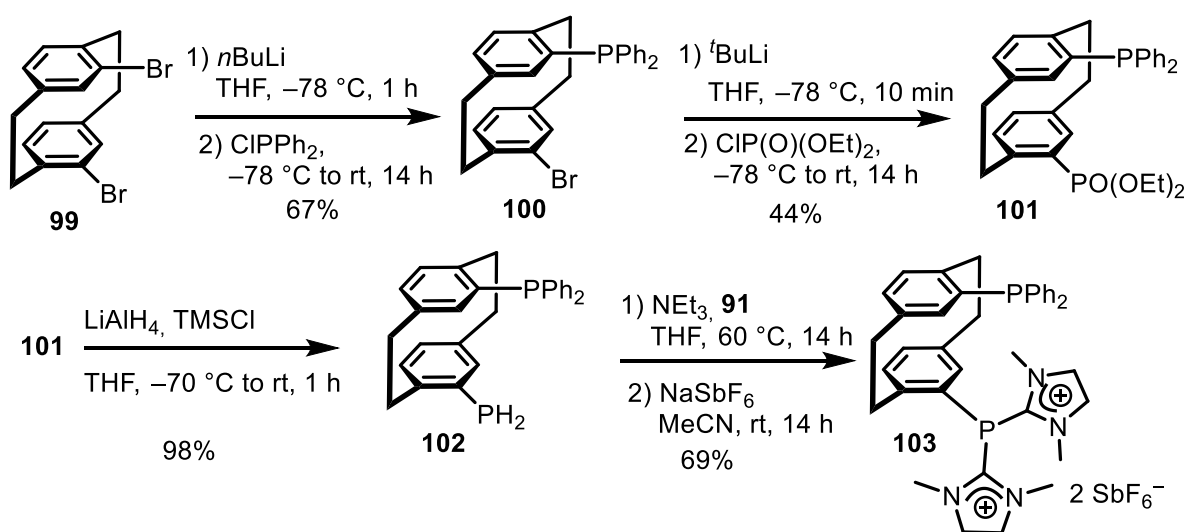
Figure 50. Synthesis of cyclophane-derived dicationic phosphine.

Interestingly, ^{31}P NMR spectrum of **103** consists of two singlets observed at δ = -0.33and -41.73 ppm. The chemical shifts of both phosphorus atoms are very similar to ones observed for **92**, indicating similar electronic properties of both molecules.

Suitable for crystal diffraction analysis single crystals of partially oxidized **103** were obtained by slow evaporation of the solvent form its saturated acetonitrile solution. Their analysis confirmed the connectivity and the structure (Figure 51).
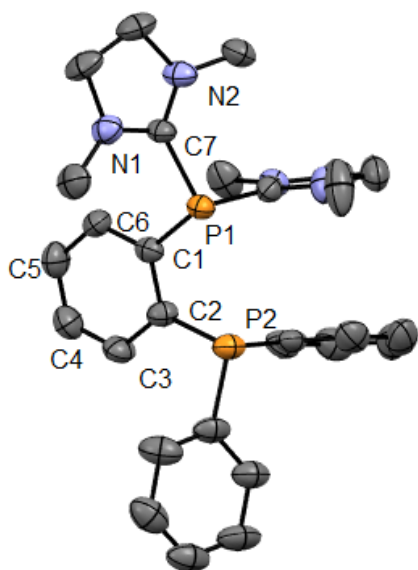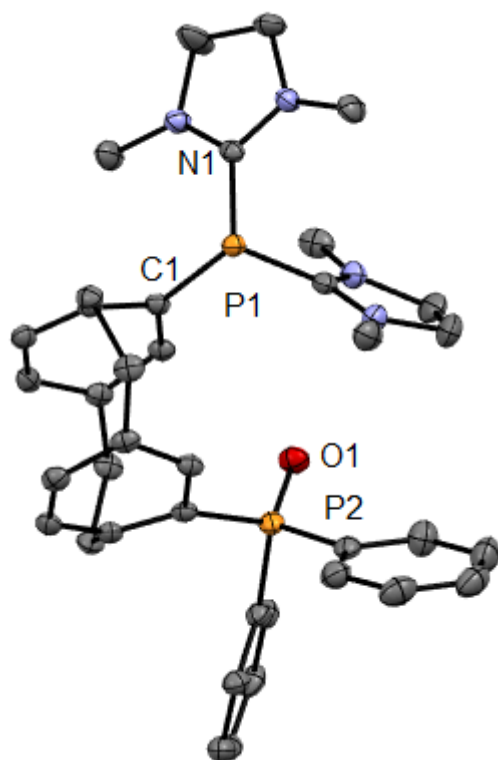

Figure 51. Single crystal structure of [O]-103, thermal ellipsoids at 50% probability; hydrogen atoms, solvent molecules and hexafluoroantimonate anions have been omitted for clarity.

Compound **103** turned out to be extremely sensitive to air atmosphere, oxidizing in minutes after exposition to air.

2.3 Attempts of synthesis of the chelating dicationic phosphine with ferrocene backbone

Another type of backbone structure, which we intended to build into the dicationic ligand's core, was ferrocene. This aromatic moiety offers possibility of selective functionalization as well as a variety of follow up reactions leading to highly

functionalized motifs. Motivated by the versatility and easy access to this platform, as well as potential preparation of future chiral versions, we targeted the synthesis of dicationic dppf analogue.

We started our synthesis sequence with 1,1'-dibromoferrocene. Similarly to previously discussed preparations, we have introduced both phosphine and a phosphate moieties in two sequential lithiation-electrophilic substitution reactions. Afterwards the phosphate was smoothly reduced using previously described protocol and primary phosphine (**107**) was isolated with excellent yield. Surprisingly, after multiple attempts of condensation with **91** in presence of base the only isolated compound containing phosphorus was **108** – the product of dehydrogenative P–P cyclotetramerization (Figure 52).
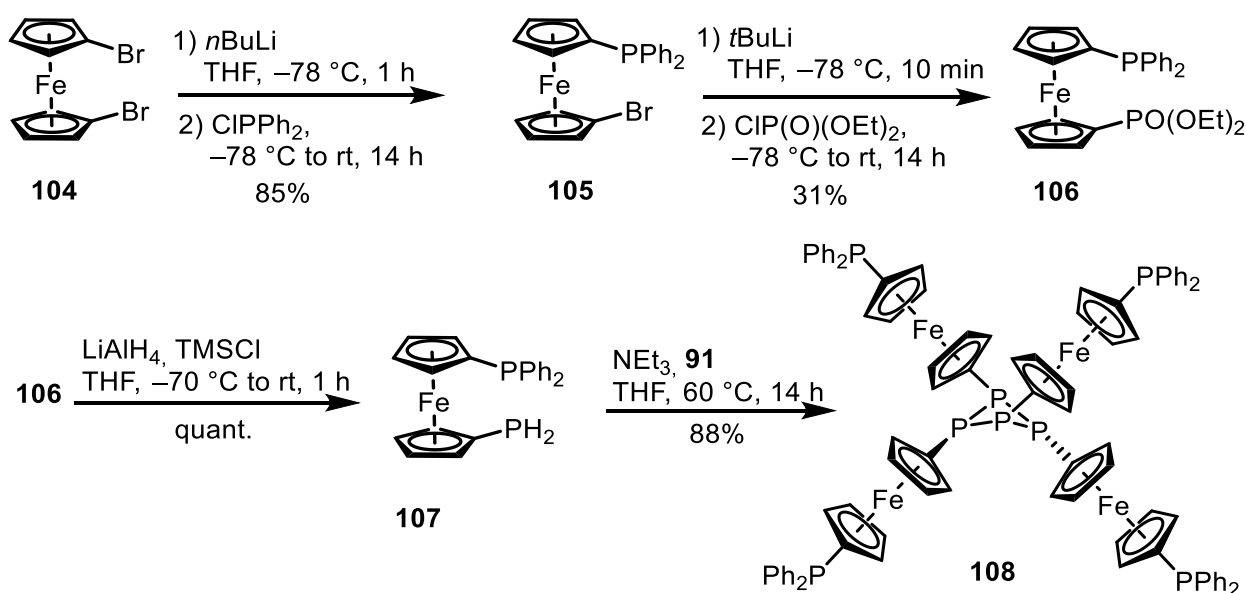
Figure 52. Attempted synthesis of ferrocene-based ligand.

The structure of **108** could be confirmed by single crystal analysis, ultimately proving the number of ferrocene units in the structure and its connectivity (Figure 53).
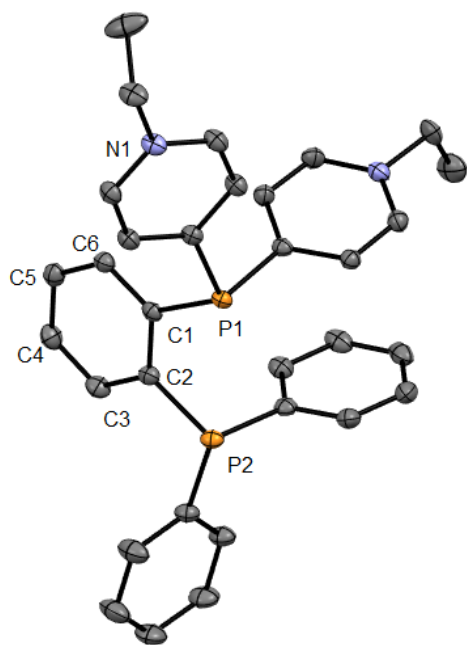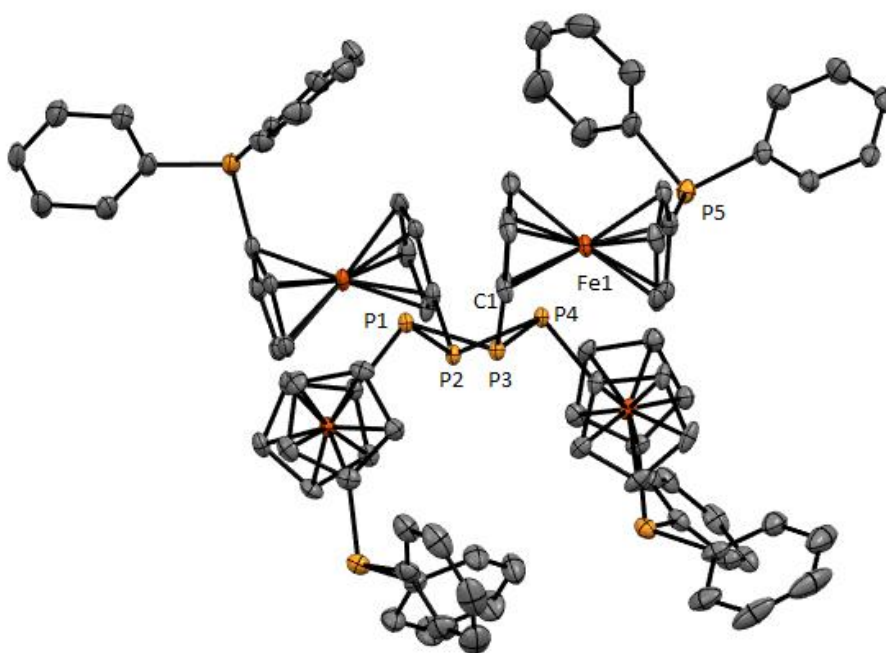
Figure 53. Single crystal structure of 108, thermal ellipsoids at 50% probability; hydrogen atoms, solvent molecules have been omitted for clarity.

Interestingly, **108** is the only oligomer of $(Ph_2PFcP)_x$ isolated from the reaction mixture; therefore, the reaction shows remarkable selectivity for the formation of that tetrameric species. To the best of our knowledge, this is the first and only example of non-metal mediated dehydrogenative P–P coupling.

The ^{31}P NMR spectrum of **108** shows to singlet signals at (162 MHz, CD$_3$CN) δ = -17.39 and -71.53 ppm. This might indicate no P–P dative interaction between the phosphorus atoms forming the ring and the tertiary phosphine.

The above described observations allow proposing the following plausible mechanism for the formation of **108** (Figure 54). The first step involves condensation of **107** with Vilsmeier-type reagent **91** followed by nucleophilic attack on the activated phosphorus center by another molecule of primary phosphine. This mechanism is supported by the isolation of protonated carbene **110** from the reaction mixture.

We are currently investigating the detailed mechanism, general aspect of this reaction and possibility of using it as a ligand in coordination chemistry of transition metals.
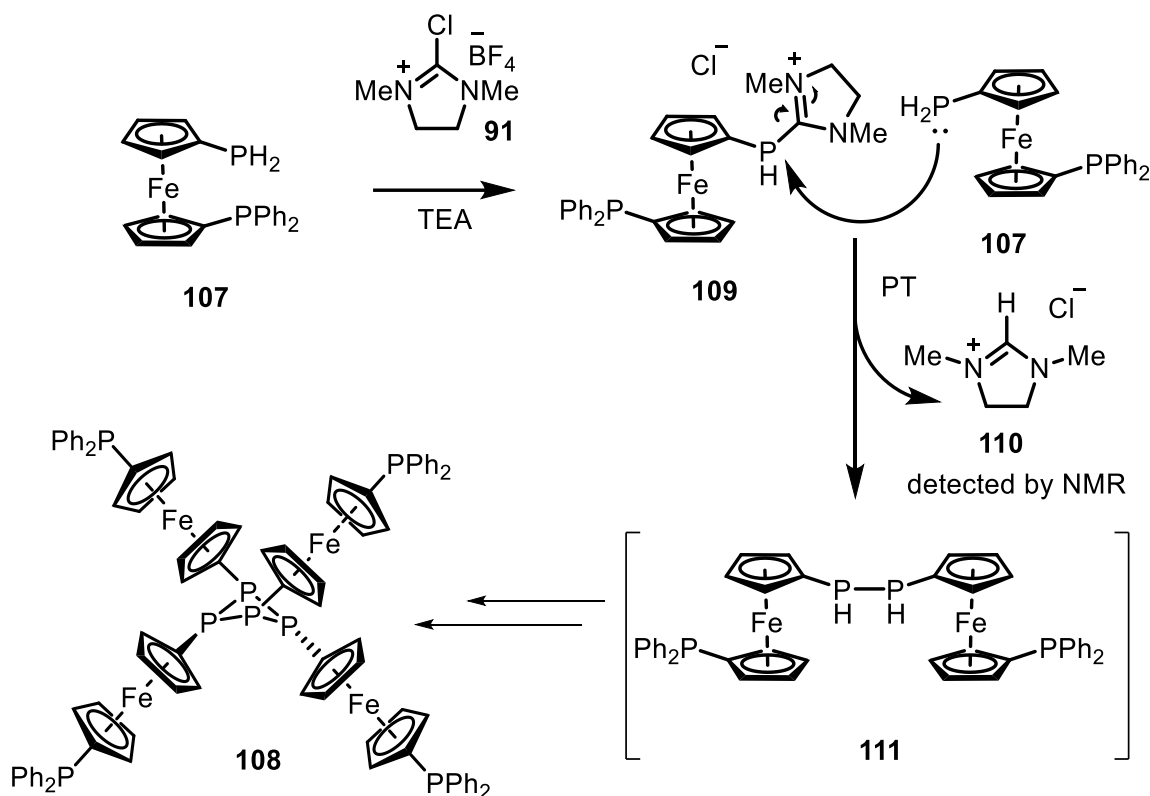
Figure 54. Proposed mechanism for the formation of 108.

2.4 Evaluation of electronic properties of obtained ligands

In order to determine the electronic properties of newly obtained ligands we decided to compare CO stretching frequency in transition metal complexes derived from metal carbonyls. As all our attempts to obtain nickel and rhodium carbonyl derivatives were unsuccessful, we decided to use $Mo(CO)_6$ as a metal precursor. Representative dicationic phosphine molybdenum complexes (**112** and **113**) were obtained in acceptable yields (Figure 55). Additionally dppb and polyfluorinated phosphine complexes were synthetized for comparison.
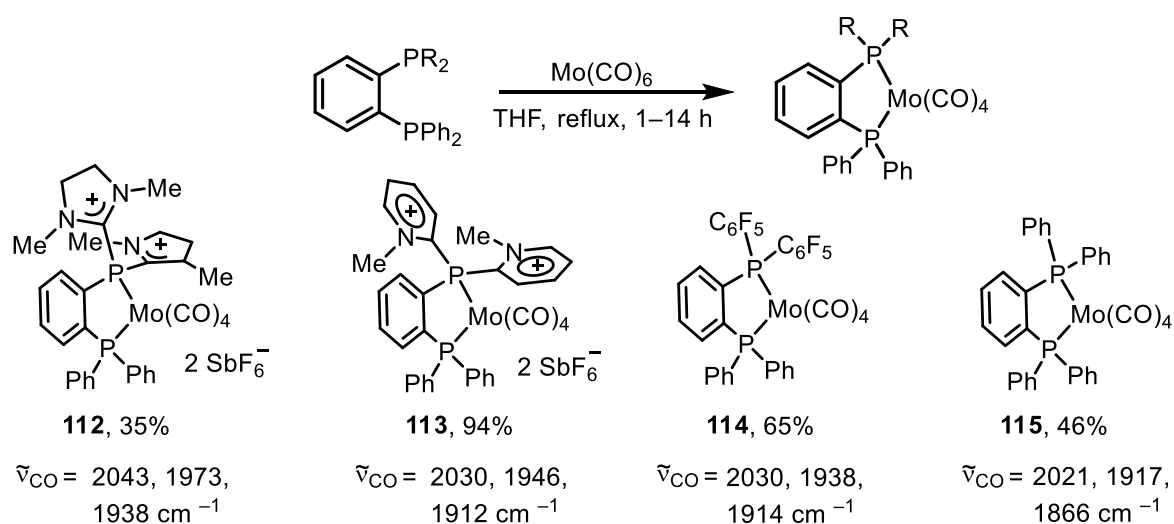
Figure 55. Synthesis of Mo complexes and their CO stretching frequency in IR spectroscopy.

The evaluation of the measured $\tilde{\nu}_{CO}$ values revealed that both dihydroimidazolium- and pyridinium-derived phosphines have stronger π-accepting properties than bis(diphenylphosphino)benzene (dppb). Moreover, **92** appeared to be the strongest π-acceptor from the whole series, whereas electronic properties of **97** are similar to those of polyfluorinated analogue.

Structure and connectivity of **112** and **113** were determined by single crystal diffraction (Figure56).[§§]
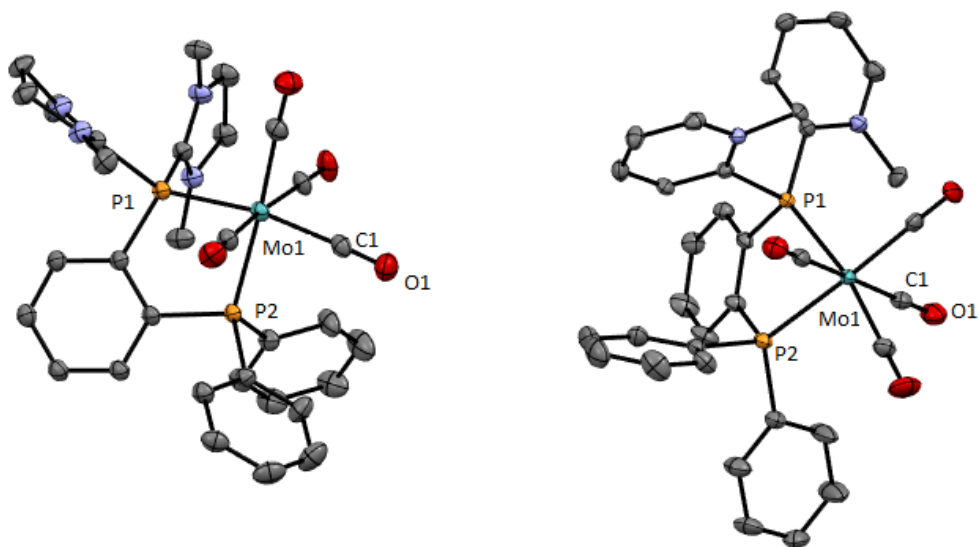
Figure 56. Molecular structure of 112 and 113 in the crystal. Thermal ellipsoids at 50% probability; hydrogen atoms and solvent molecules have been omitted for clarity.

§§Synthesis and evaluation of electronic properties of **112**, **114** and **115** were performed by Dr. Lianghu Gu.

In addition we performed cyclic voltammetry studies (Table 2). Ligands **92** and **97** show oxidation peaks at 1.05 V and 1.22 V, respectively. These voltage values are assigned to the oxidation of neutral phosphine moieties (like e.g. PPh_2), which are significantly higher values than the one of DPPB (0.69 V). The reduction potentials of –1.53 V and –1.24 V are attributed to the chemical reduction of the dication not present in DPPB.

Table 2. Results of cyclic voltammetry measurement of 92 and 97 and their comparison with data for model phosphine.

Entry[II]	Ligand	E^{OX}	E^{RED}
1	DPPB	0.69 V	-
2[I§]	92[III]	1.05 V	–1.53 V
3	97	1.22 V	–1.24 V

[II] Oxidation/reduction peaks potential reported in V and calibrated versus $Cp^*_2Fe/Cp^*_2Fe^+$, Bu_4NPF_6 (0.1 M) in CH_2Cl_2.

[III] CV of 92 was measured by Dr. Lianghu Gu.

3 Coordination of Chelating Dicationic Phosphines to Transition Metals

As it was stated in the beginning of the previous chapter, transition metal complexes of dicationic phosphines, coordinated to other metal centers than Au (I) and Pt (II) were not described in literature. With the ligands **92**, **97**, **98** and **103** in hands we decided to explore this unknown territory.

3.1.1 Coordination to Rhodium

We have started our investigations by an attempt to form a metal complex of **92** and rhodium using [Rh(cod)Cl]₂.
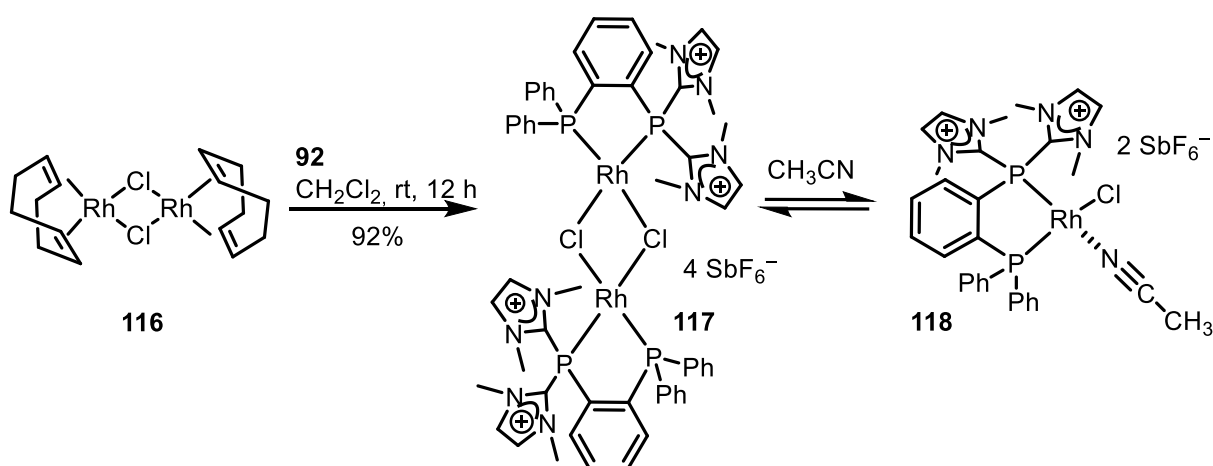
Figure 57. Synthesis of the rhodium complex of 92.

After stirring the ligand **92** for 1 hour in CH₂Cl₂ at room temperature in the presence of metal precursor we isolated and characterized the expected product of the displacement of olefins with the dicationic diphosphine ligands – the dimeric tetractionic system **117** (Figure 57).

The obtained complex was analyzed above all by ³¹P NMR measurement in acetonitrile. This study to our surprise revealed that in acetonitrile the dimeric form

is engaged in the dynamic equilibrium with the solvent molecule giving monomeric species **118**. This dication with coordinated acetonitrile moiety gave rise to two sets of signals observed at δ = 74.08 – 70.58 (m) and at 34.66 – 23.04 (m) ppm.

Single crystals of both compounds were obtained by slow evaporation of the saturated solutions in DCM and their X-Ray analysis confirmed the structures and connectivities (Figure 58 and Figure 59).[IV]

Figure 58. Molecular structure of 117 in the crystal. Thermal ellipsoids at 50% probability; hydrogen atoms, hexafluoroantimonate counterions and solvent molecules have been omitted for clarity.

[IV] Compounds **117** and **118** were crystalized by Dr. Lianghu Gu.

Figure 59. Molecular structure of 118 in the crystal. Thermal ellipsoids at 50% probability; hydrogen atoms, hexafluoroantimonate counterions and solvent molecules have been omitted for clarity.

As it can be seen from the solid state structure of both **117** and **118**, the P1–Rh1 bond length is slightly shorter (2.135 Å) than P2–Rh1 (2.195 Å) which might indicate stronger interactions between the atoms and significant π-backdonation in the case of cationic phosphine in comparison to the neutral. All the other values of the bonds lengths are in the usual range

Similarly to **92**, **97** reacts with [Rh(cod)Cl]₂ forming dinuclear teatracationic complex **119**. The NMR study, performed in the same manner as for **117**, showed that 2-pyrydinium analogue in the acetonitrile solution is in the equilibrium with mononuclear complex **120** (Figure 60).
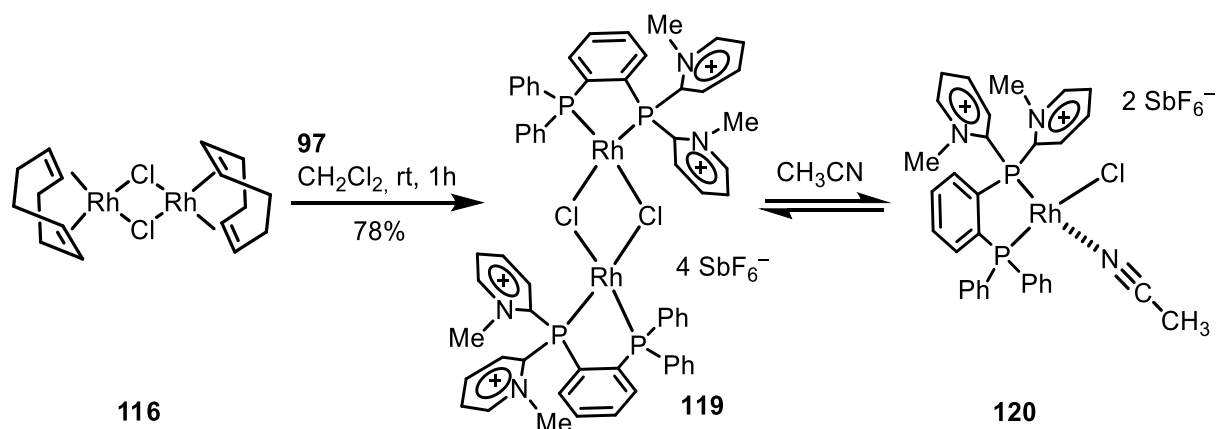
Figure 60. Synthesis of rhodium complexes coordinated by pyridinum phosphine ligands.

In ^{31}P NMR spectrum of **119** and **120** in equilibrium we could observe two sets of signals at 69.56 and 61.25 ppm, which interestingly are more similar in comparison with the ones observed for the mixture of **117** and **118**.
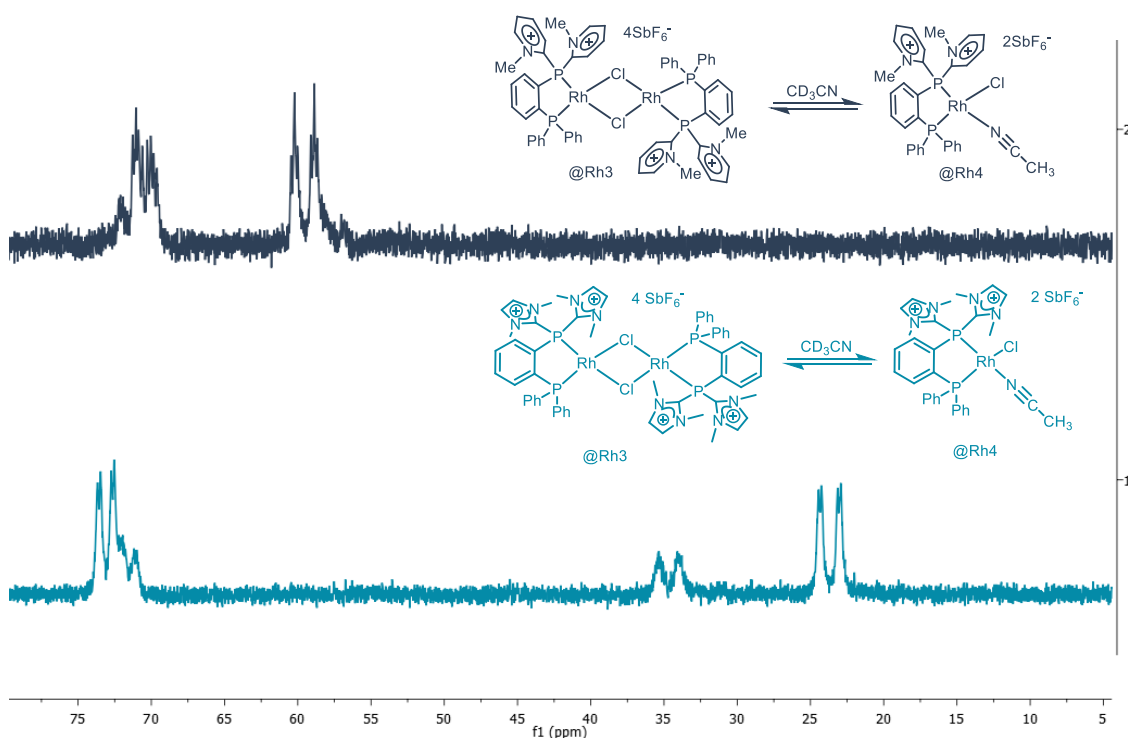
Figure 61. Comparison of 31P NMR spectra of 119/120 (top) and 117/118 (bottom) mixtures.

3.1.2 Coordination to Iridium

The next transition metal which we were interested in coordinating our ligands to was iridium. After stirring **92** with [Ir(cod)Cl]₂ (**121**) we isolated well defined species **122**. Careful analysis of ^{1}H NMR spectrum indicated that the desired tetracationic complex analogues to Rh was not formed. Instead, the 2D NMR spectra analysis allowed us to assign the signals to the unexpected structure of iridium complex **122**, as presented in Figure 62. Apparently, the coordination of the electron-poor phosphine to the iridium atom facilitated the C–H activation reaction in a methyl group from one of the imidazolium moieties.
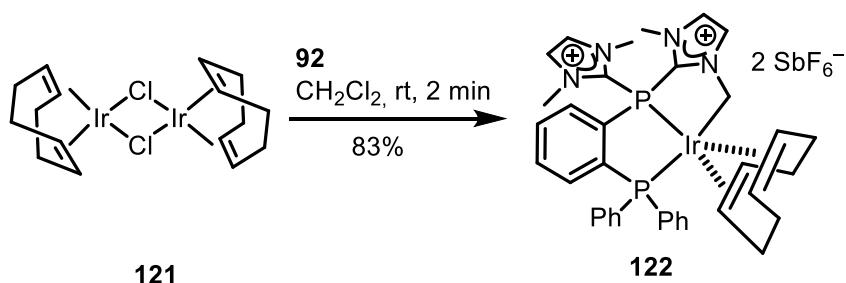
Figure 62. Synthesis of 122.

The structure of **122** was confirmed by single crystal diffraction (Figure 63).
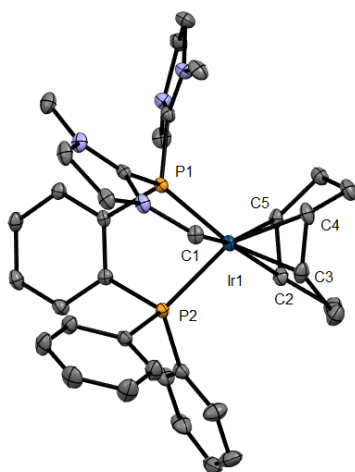
Figure 63. Molecular structure of 122 in the crystal. Thermal ellipsoids at 50% probability; hydrogen atoms, hexafluoroantimonate counterions and solvent molecules have been omitted for clarity.

Similarly to mononuclear Rh complex, in **122** P1–Ir1 bond is shorter (2.22 Å) than P2–Ir1 bond(2.33 Å). Another interesting bond to be mentioned is C1–Ir1 which length is 2.10 Å. That value is much shorter than in most Ir–C^{sp3} complexes.

We have anticipated that by using appropriate metal precursor without chelating olefin in its structure, we might be able to obtain desired iridium complexes by replacing the alkene ligand and avoiding C–H activation event in the dicationic ligand.

We have tested our hypothesis by synthetizing [Ir(coe)$_2$Cl]$_2$ (**123**) and using it as a starting material in complex formation. We chose coe because of its weaker coordination to metal center then those of cod. Much to our delight we could obtain analogous to Rh tetracationic binuclear system **124** by applying this approach (Figure 64).
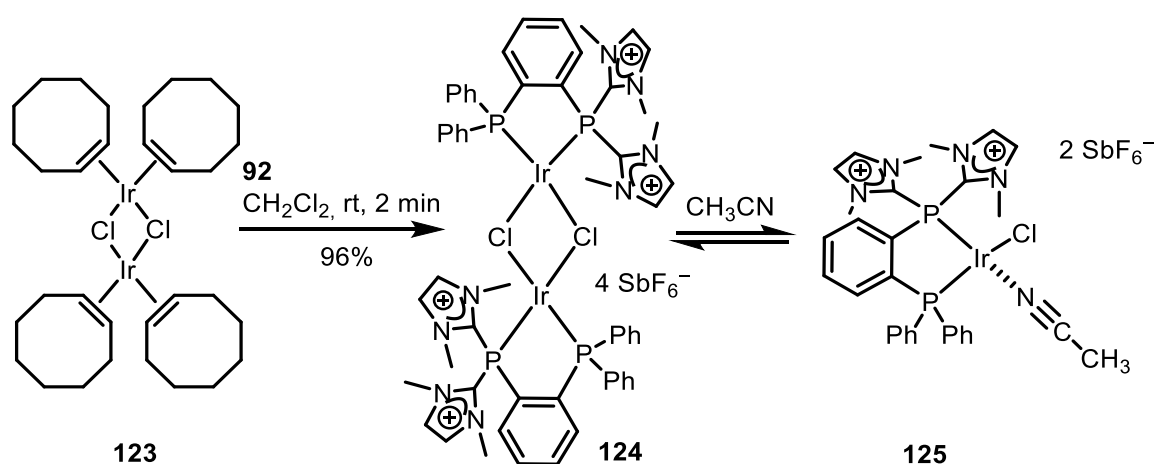
Figure 64. Synthesis of dinuclear complex 124.

The structure of **124** was unambiguously confirmed by NMR measurement in acetonitrile. Akin to **117**, **124** is involved in equilibrium between dinuclear tetracation and mononuclear dicationic species **125**.

Structure and connectivity of **124** and **125** were confirmed by single crystal diffraction (Figure 65 and Figure 66). The monocrystals suitable for X-Ray analysis were obtained from slow evaporation of DCM-Et$_2$O solution.
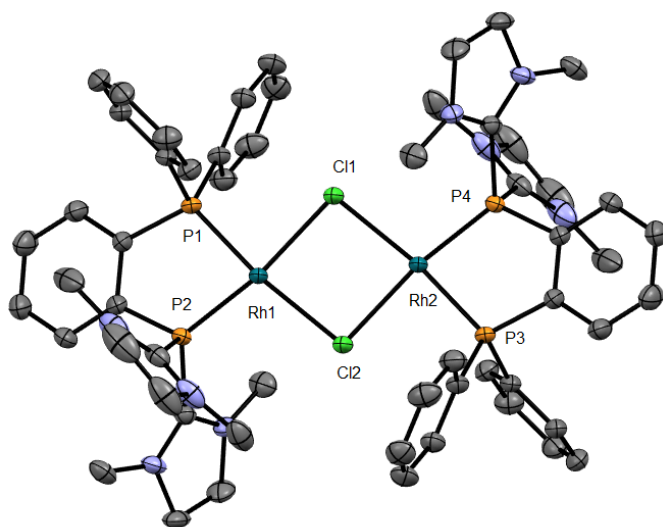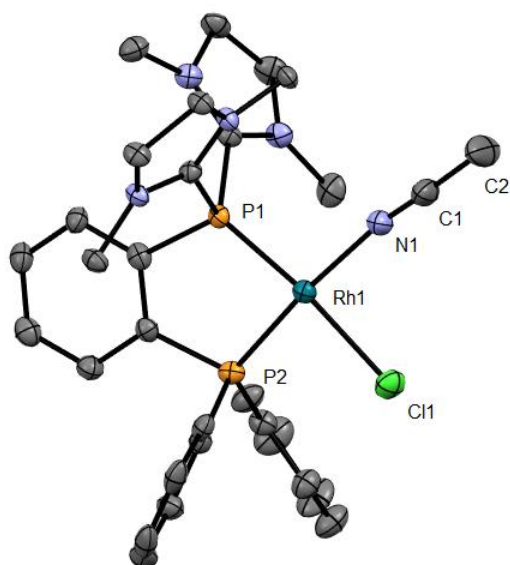
Figure 65. Molecular structure of 124 in the crystal. Thermal ellipsoids at 50% probability; hydrogen atoms, hexafluoroantimonate counterions and solvent molecules have been omitted for clarity.
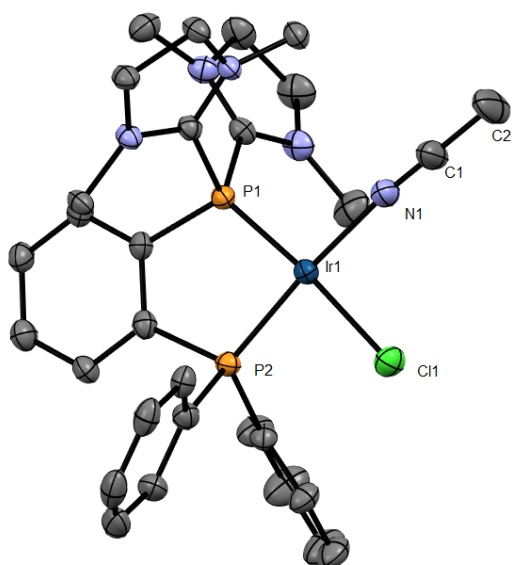
Figure 66. Molecular structure of 125 in the crystal. Thermal ellipsoids at 50% probability; hydrogen atoms, hexafluoroantimonate counterions and solvent molecules have been omitted for clarity.

Analogously to the whole family of Rh and Ir complexes, the bond length between P(cationic)–Ir atoms in **125** are shorter (2.14 Å) than in case of P(neutral)–Ir (2.21

Å). For **124** this difference in bond lengths is less significant than in corresponding rhodium complex and the C–H activated complex **122**.

Careful analysis of the ^{31}P NMR spectrum of the mixture of **124** and **125** revealed two discreet sets of signals confirming the dynamic equilibrium between both forms, as measured in acetonitrile. The signals are much sharper than the ones observed for Rh complexes (*cf.* Figure 61), which we propose is connected to the much slower rate of the equilibrium.
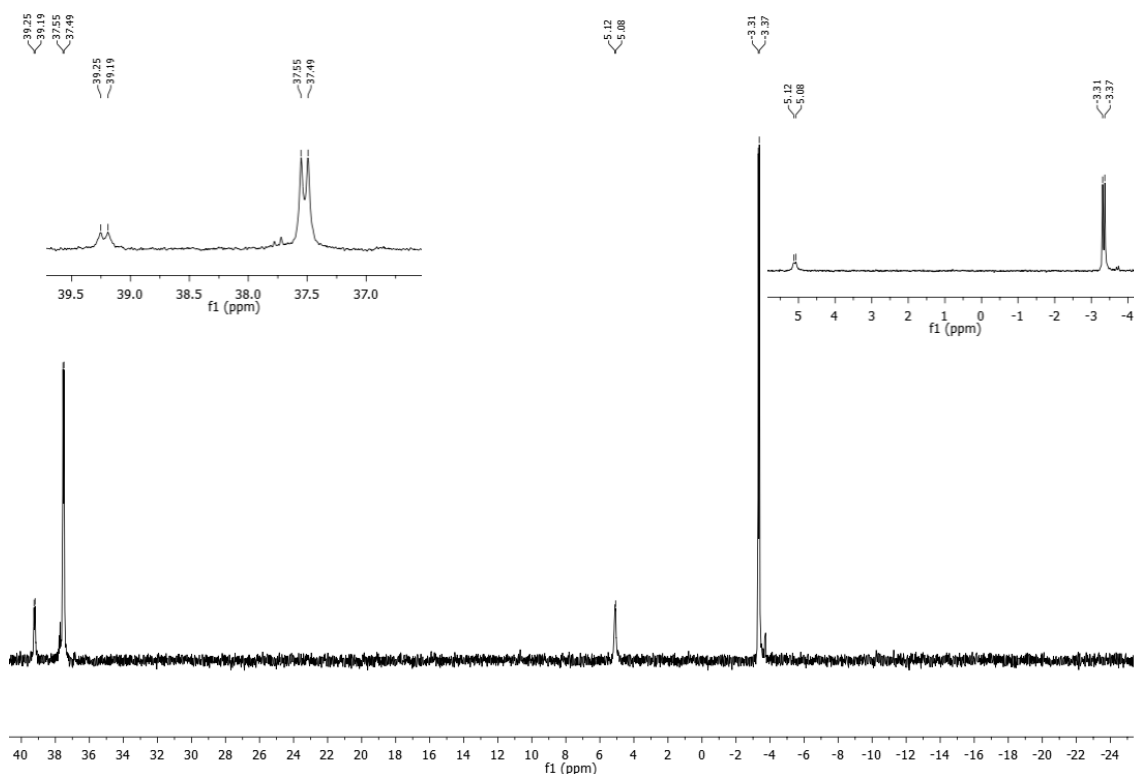
Figure 67. ^{31}P NMR spectrum of 124 and 125 in the mixture.

Encouraged by previous successful results, we tried to synthesize the Ir complexes with ligand **97**. Unfortunately, despite multiple attempts we could not obtain desired products.

We envisioned that coordination of *p*-cyclophane-derived ligand **103** to rhodium and iridium could be achieved using the same conditions as described above. Our investigations was started by performing a reaction of **103** with [Rh(cod)Cl]$_2$ (**116**). After stirring for 2 min at ambient temperature, a well-defined product **126** was isolated in 77% yield (Figure 68). A ^{31}P NMR spectrum of the new complex contained two signals at 50.92 and –43.68 ppm (Figure 69). This indicated that only neutral phosphine moiety is coordinated to the metal center, whereas the dicationic part of the ligand was not active.
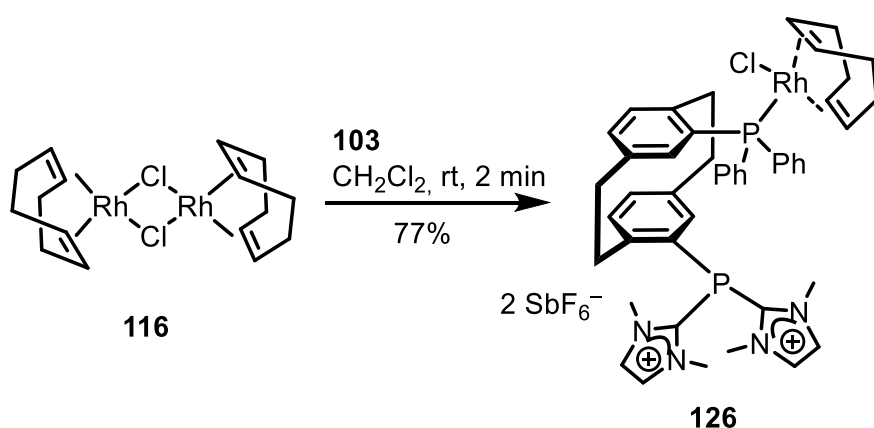
Figure 68. Synthesis of the rhodium complex of 103.
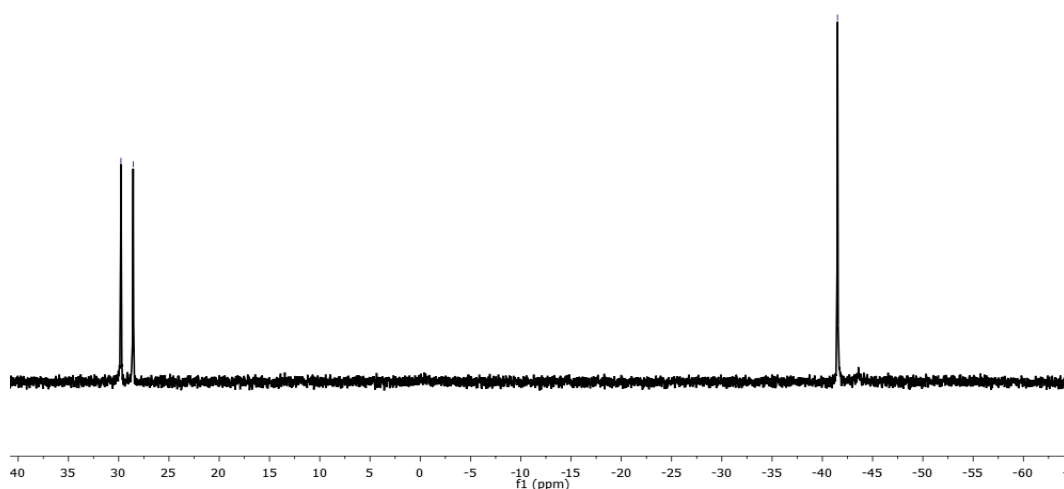
Figure 69. ^{31}P NMR spectrum of the rhodium complex of 103.

Despite several attempts to use different rhodium precursors such as [Rh(coe)$_2$Cl]$_2$ and [RhCO$_2$Cl]$_2$, we could never obtain a complex with two phosphine units coordinated to a metal center.

Nevertheless, we continued our studies in exploration of coordination chemistry of **103** with the aim of coordinating it to iridium. Keeping in mind our previous successful attempts with different ligands, we used [Ir(cod)Cl]$_2$ as a metal precursor for this experiment. After 1 h of stirring it in CH$_2$Cl$_2$ in the presence of **103**, we could isolate quantitatively a coordination product (Figure 70). Similarly to the case described above, after analysis of ^{31}P NMR spectrum, we identified new product as a complex **127** of only neutral phosphine (Figure 71).
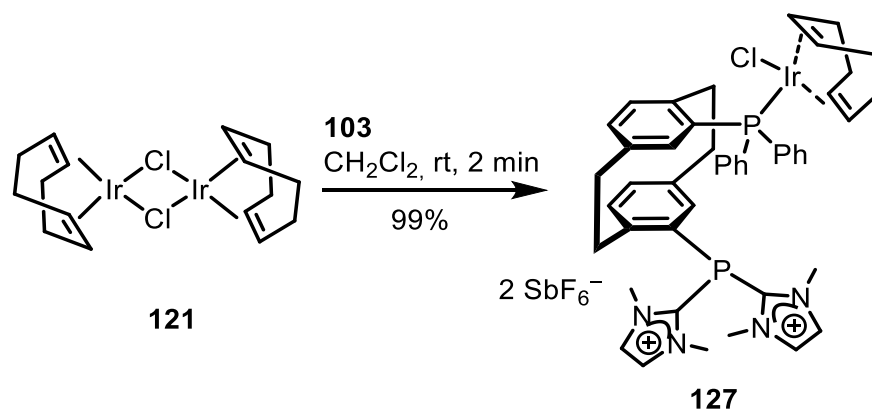
Figure 70. Synthesis of iridium complex of 103.
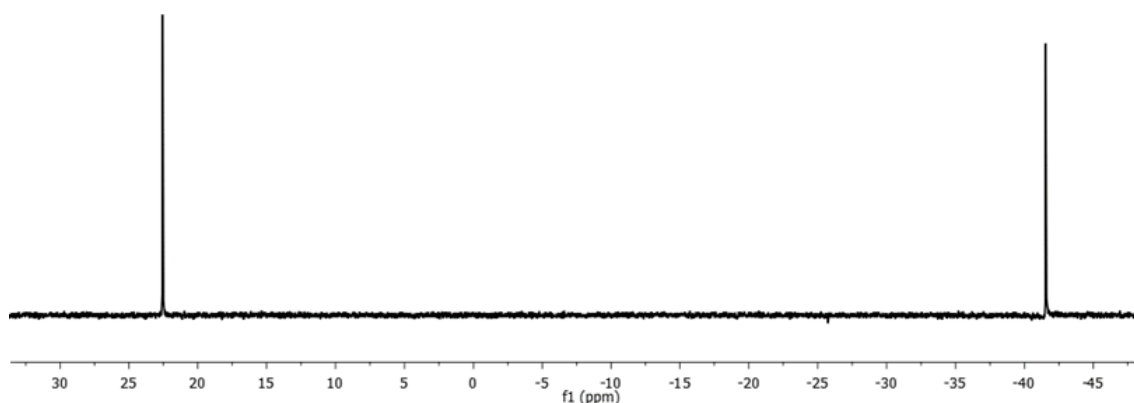
Figure 71. ^{31}P NMR spectrum of the iridium complex of 103.

Structure of **127** was confirmed by single crystal diffraction, as depicted in Figure 72. The monocrystals appropriate for diffraction measurements were obtained from slow evaporation of saturated acetonitrile solution.
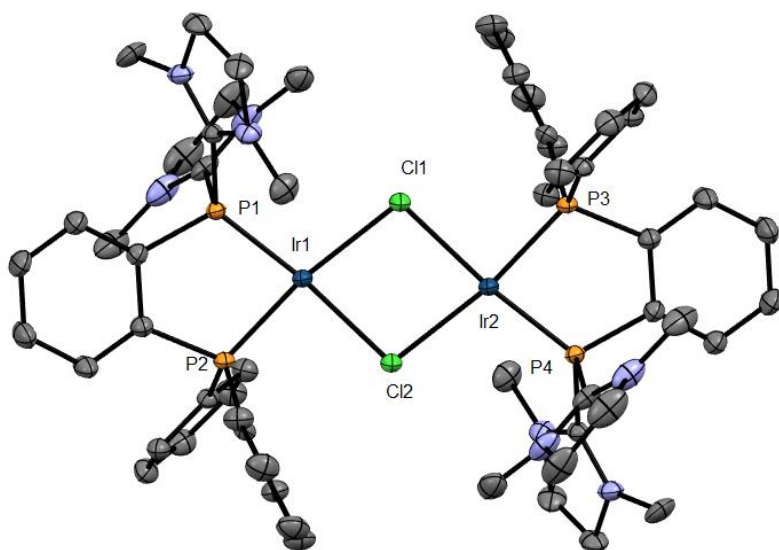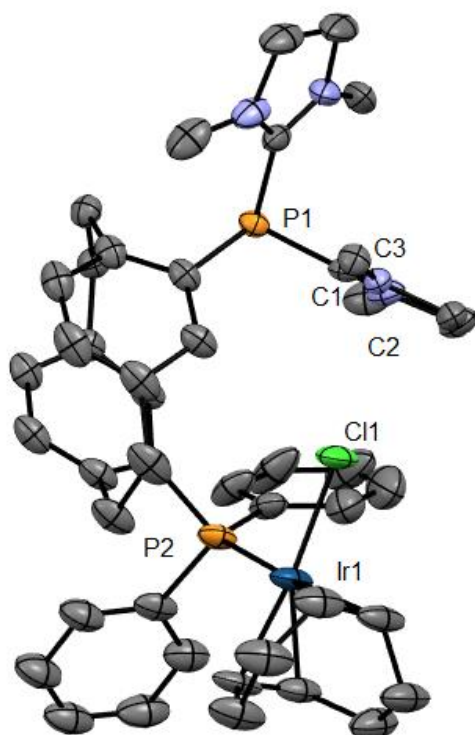

Figure 72. Molecular structure of 127 in the crystal. Thermal ellipsoids at 50% probability; hydrogen atoms, hexafluoroantimonate counterions and solvent molecules have been omitted for clarity.

Interestingly, in the solid structure of Ir complex the distance between P1 and P2 is 5.80 Å, which is much longer than in case of free ligands (5.04 Å). This phenomena might be attributed to the strong Coulomb repulsion between metal center and dicationic phosphine unit, which disfavors the coordination between them.

Despite our attempts of using different Ir precursor, like [Ir(coe)₂Cl]₂ we did not obtain a product of coordination of dicationic phosphine to the metal center. The possible reason for this is an enhanced distance between neutral and dicationic phosphine moieties: 3.094 Å for **92** and **97** and of 3.140 Å for **98**.

4 HYDROARYLATION OF DIENES

The development of new catalytic reactions characterized by high atom economy is of an objective in chemical synthesis.[85–87] One of the important challenges in such transformations is regioselective formation of C–C bonds using inactivated aryl systems. Encouraging example in this field is a remarkably atom economical process of catalytic hydroarylation of 1,3-dienes. In this reaction electron-rich (hetero)arene is added selectively across one of the carbon-carbon double bonds. This results in the formation of a highly functionalized aromatic system, in which the second C=C bond stays intact and can be transformed later in different reaction. Examples of such transformation, catalyzed by transition metal complexes, features generally low turnover number of catalysts together with inferior functional group tolerance, which significantly limits it applicability.[88]

Due to the above mentioned reasons, hydroarylation of 1,3-dienes attracted our interest as a model transformation to test the catalytic performance of the previously described Rh and Ir complexes (Figure 73). We rationalized the fact that the strong π-accepting properties of complexes such as **119** or **124**, might lead to increased catalytic performance and expansion of this methodology.

Figure 73. General scheme of 1,3-diene hydroarylation reaction.

To begin with, we performed the screening for the best conditions for this transformation using 1-phenyl-1,3-butadiene (**66**) and indole as starting materials. We decided to use [RhCl(CO)$_2$]$_2$ as the metal precursor without olefinic ligand, that might inhibit the reactivity of our system towards desired diene.
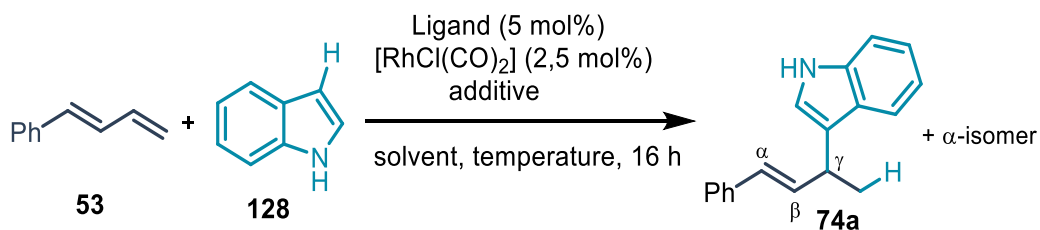
Figure 74. Model transformation used for the optimization of reaction conditions.

Table 3. Optimization of the conditions of model hydroarylation reaction.

Entry	Ligand	Solvent	Temp.	Additive	GC Conversion
1	92	DCM	25°C	-	<5%
2	92	DCE	40°C	-	12%
3	92	DCE	70°C	-	28%
4	92	DCE	100°C	-	<5%
5	92	DCE	70°C	CH_3CN (5 mol%)	<5%
6	92	DCE	70°C	$KB(C_6F_5)_4$ (5 mol%)	48%
7	92	DCE	70°C	$KB(C_6F_5)_4$ (10 mol%)	91%
8	92	THF	70°C	$KB(C_6F_5)_4$ (10 mol%)	<5%
9	92	$PhCH_3$	70°C	$KB(C_6F_5)_4$ (10 mol%)	25%
10	92	$PhCF_3$	70°C	$KB(C_6F_5)_4$ (10 mol%)	62%
11	92	CH_3CN	70°C	$KB(C_6F_5)_4$ (10 mol%)	<5%
12	92	Acetone	70°C	$KB(C_6F_5)_4$ (10 mol%)	11%
13	97	DCE	70°C	$KB(C_6F_5)_4$ (10 mol%)	72%

14	98	DCE	70°C	KB(C$_6$F$_5$)$_4$ (10 mol%)	33%
15	dppb	DCE	70°C	KB(C$_6$F$_5$)$_4$ (10 mol%)	8%
16	-	DCE	70°C	KB(C$_6$F$_5$)$_4$ (10 mol%)	8%

We quickly realized that the model transformation is leading to the desired product in 70°C in DCE. In order to address the issue of low solubility of dicationic phosphine in the solvent of choice we decided to add KB(C$_6$F$_5$)$_4$ as an anion-exchanging agent, that led to much higher conversions of the starting material. Strong coordinating solvents such as CH$_3$CN or acetone inhibited the reaction. From the whole library of ligands synthetized in this project, **92** was giving highest conversions of starting material in our hands. It is worth noting that other dicationic chelating phosphines were also leading to the formation of desired product. This observation indicates that the studied reaction requires the use of electron-poor ligand.

After establishing the proper reaction conditions we investigated its scope and limitations. Selected electron-rich aromatic systems and representative 1,3-butadiene derivatives were subjected to the reaction (Figure 75).
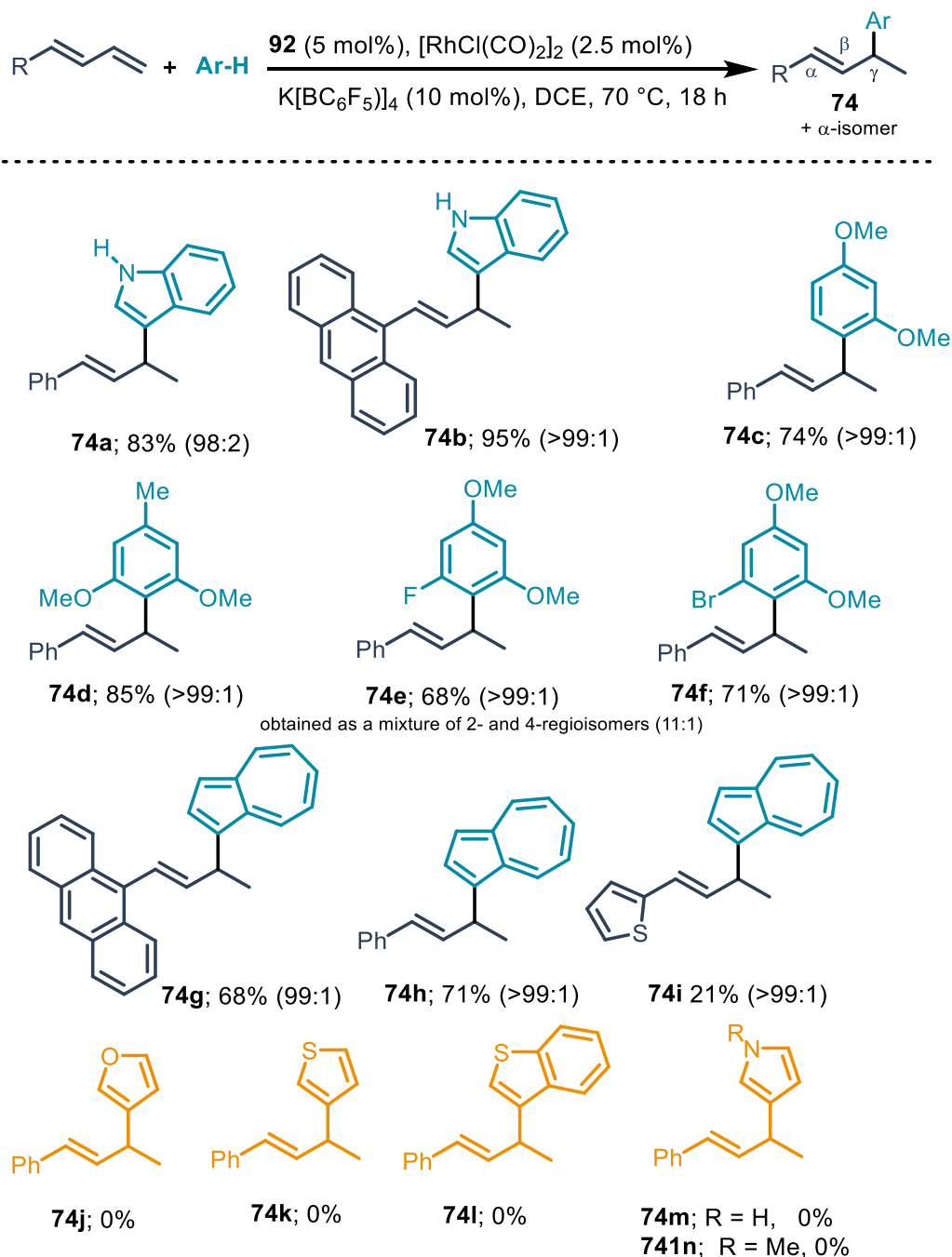
Figure 75. Scope and limitations of the hydroarylation reaction.

We also proved that the reaction proceeds smoothly using indole derivatives and dienes with (poly)aromatic system affording **74a** and **74b**. Encouraged by this results we performed the reaction with electron-rich aromatic system, such as dimethyl resorcinol. Much to our delight we observed the formation of desired product **74c** in good yields. We continued to evaluate the reactivity of our system

with different dimethylresorcinol derviatives. Again, the reaction turned out to tolerate various substitution patterns on the nucleophile, successfully furnishing **74d–f**. To our delight we isolated azulene derivative **74h** in excellent yield, extending this methodology to nucleophiles without any heteroatoms. The reaction could be performed with other 1,3-butadiene derviatives such as 9-anthranyl or 2-tiophenyl as well, although in the last case the yield of **74i** was significantly lower. Structure and connectivity of the product **74g** was confirmed by crystallization and single crystal diffraction (Figure 76). Unfortunately, using different electron-rich heterocycles as nucleophiles such as benzofurane and tiophene showed the limitation of the scope reaction[v].
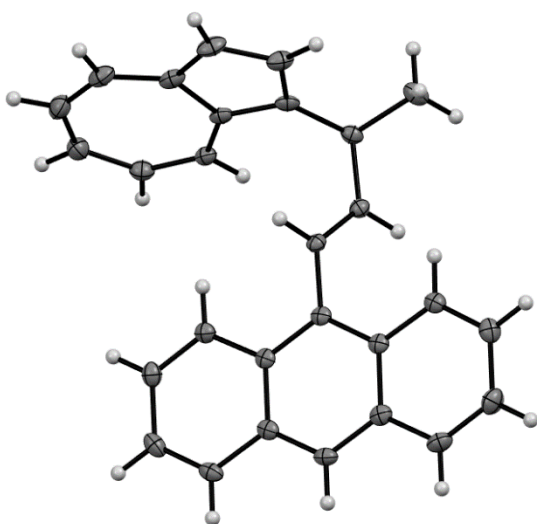
Figure 76. Molecular structure of 74g in the crystal. Thermal ellipsoids at 50% probability.

---

[v] Synthesis of compounds 74a and 74c was performed together with Dr Lianghu Gu

According to the postulated mechanism (Figure 77), the reaction starts with coordination of the diene **66** to the Rh(I) complex (**A**) to form η^2 (**B**) or η^4 (**B'**) complex. Afterwards a nucleophilic attack with indole (**128**) takes place to form an intermediate (**C**), which after subsequent rotation over C–C bond undergoes hydrogen transfer to the Rh metal center. At this stage Rh(III) complex (**E**) forms, which easily undergoes reductive elimination because of the properties of the ligand to deliver the product and forms back the catalytically active species (**A**).
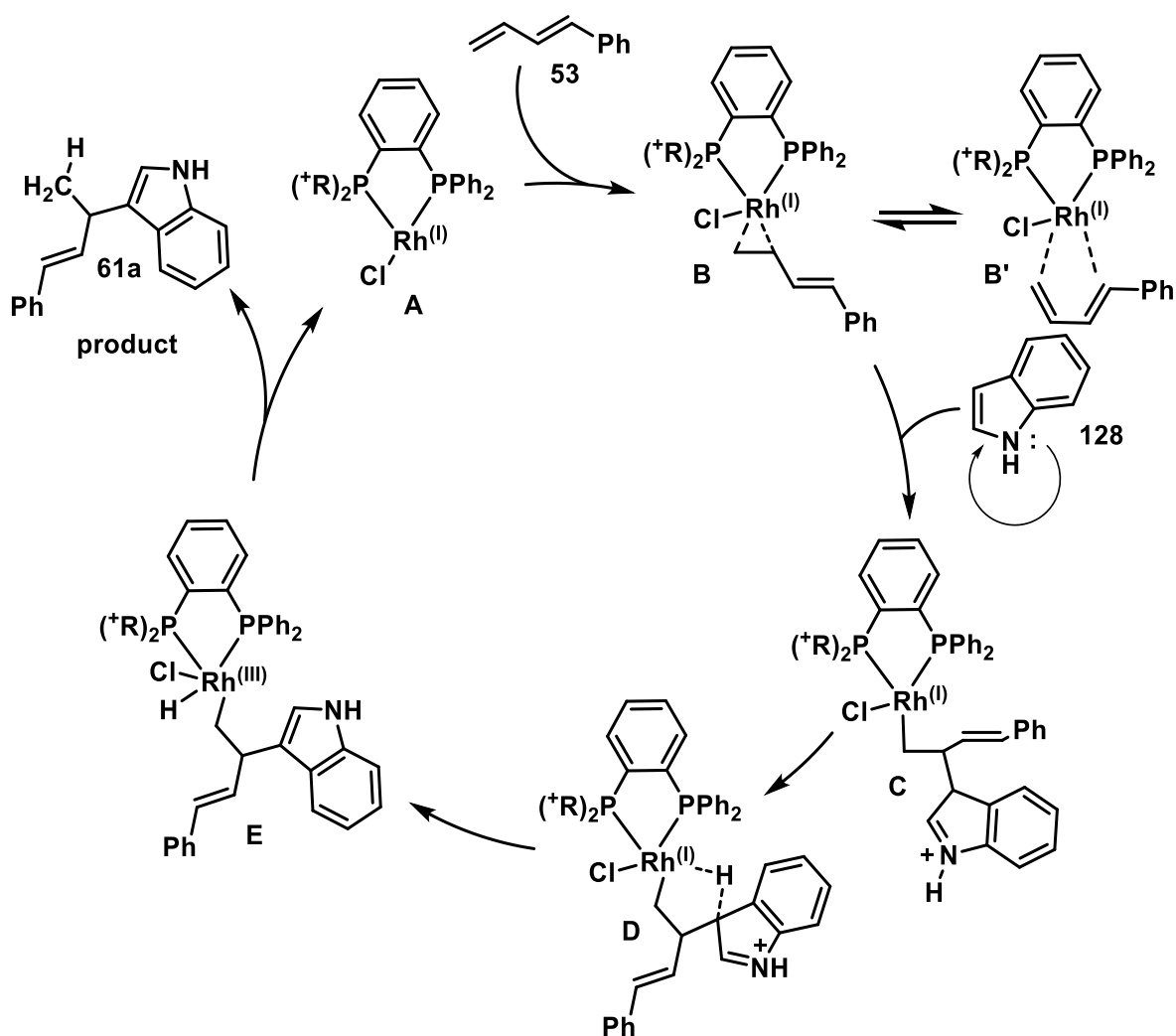
Figure 77. Postulated mechanism of diene hydroarylation catalyzed by rhodium complex.

Proposed mechanism as well as theoretical mechanism involving hypothetical monocationic analogue of **92** was studied in details using density functional theory by the group of Prof. Walther Thiel (Figure 78).
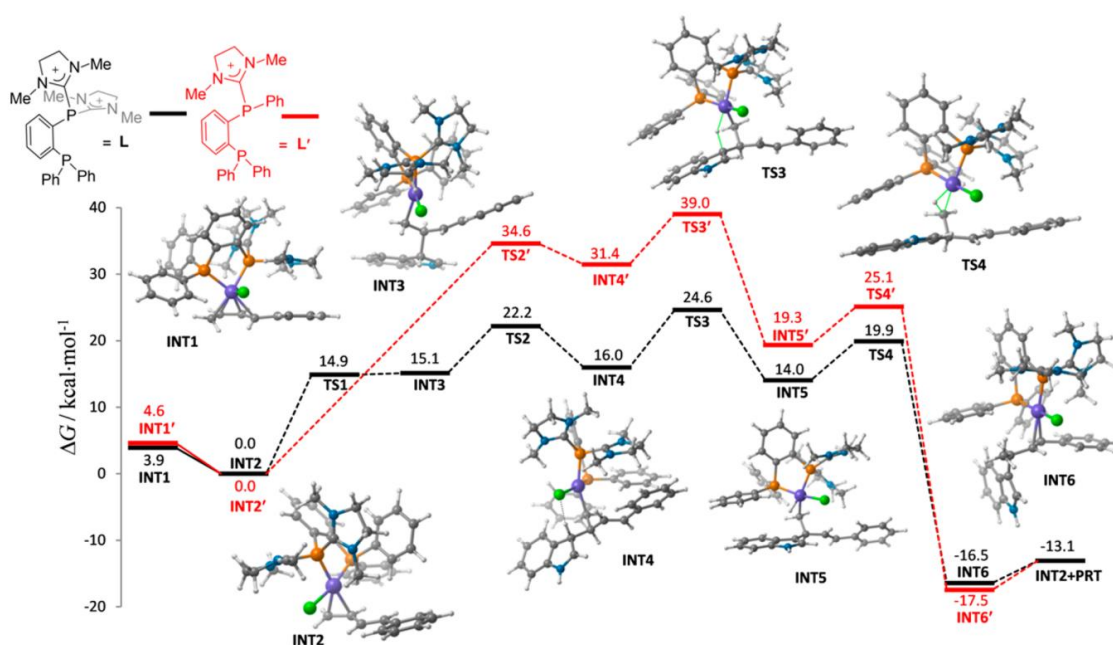
Figure 78. Gibbs free energy profile of the model hydroarylation reaction at the BP86-D3(CPCMDCE)/def2-TZVP//BP86-D3/def2-SVP level of DFT.

The Gibbs free energies calculated for the intermediate as well as transition states shows that the free energy of activation of B or B' complexes by indole molecule is 14,9 kcal/mol. According to the above depicted calculation results, proton transfer reaction and formation of Rh(III) center are states with the highest energy value in the whole catalytic cycle.

In addition to the calculations performed for the investigated reaction, the theoretical study of the analogous transformation, but with the use of a monocationic ligand (depicted in red in Figure 78) was performed. The results clearly show that the hypothetical monocationic ligand requires significantly higher energy barrier, justifying the use of dicationic phosphine for this reaction.

Finally we performed a series of kinetic experiments using 3-[H]- and 3-[D]-labeled indoles **128**, respectively, to determine kinetic isotope effect (Figure 79). We

analyzed the conversion of these starting materials over a period of 60 to 300 minutes with an interval of 1 hour, applying calibrated GC method to determine the conversion.
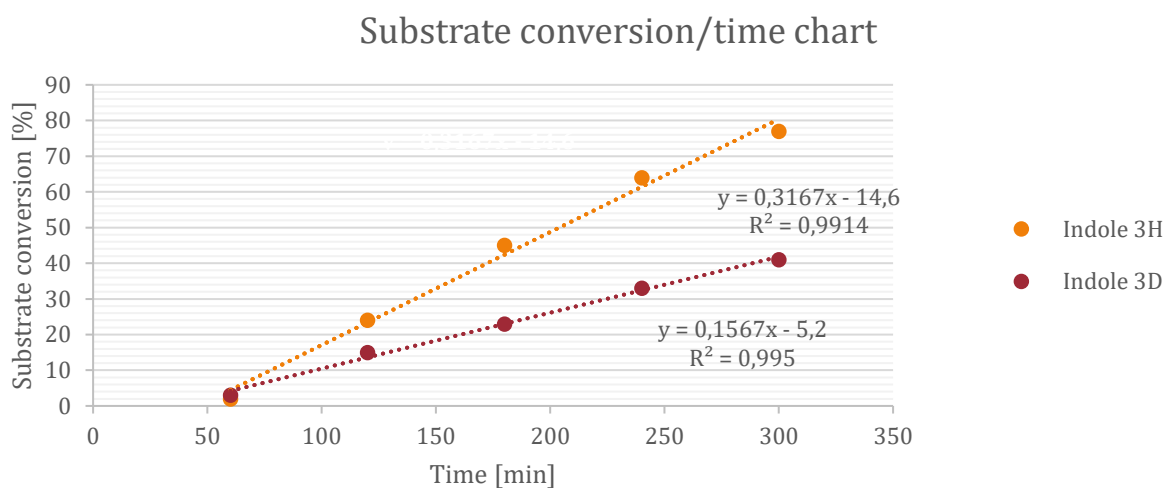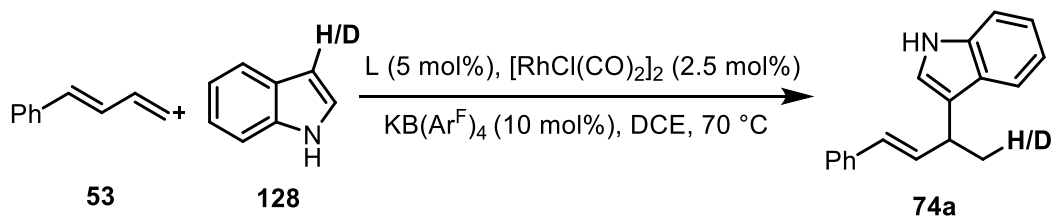
Figure 79. KIE studies.

The kinetic isotope effect was calculated to be 2.02, thus additionally proving proposed mechanism and nonlinear transfer of the proton to rhodium center.

5 POLYCYCLIC NONAROMATIC HYDROCARBONS

Since the first synthesis in 1941 by Vladimir Prelog, adamantane (131, Figure 80) became one of most important examples of well-defined cyclic aliphatic hydrocarbons.[89] Its highly symmetric structure, high crystallinity and applications in chemical synthesis have fascinated chemists for over a century.[90] In 1957 Paul von Ragué Schleyer proposed an elegant two step protocol for the synthesis of this molecule, giving access to multi-gram scale and making it commercially available (Figure 80).[91]
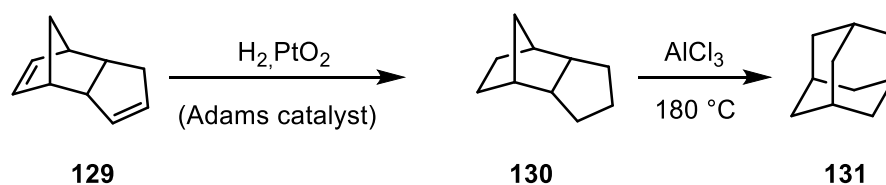
Figure 80. Schleyer's synthesis of adamantane.

This precedential report inspired other research groups to investigate this class of compounds, known as *cage hydrocarbons*, in order to develop new synthetic routes, check their reactivity and discover their functionalization methods.[92–94] Their study expanded cage hydrocarbons family by e.g. isogarudane (**132**), cubane, prismane, diamantane or dodecahedrane (Figure 81).

Isogarudane Williams 1961	Cubane Cole 1964	Prismane Katz 1973
132	**133**	**134**

Diamantane von Schleyer 1965	Dodecahedrane Paquette 1982	Octahedrane de Meijere 1993
135	**136**	**137**
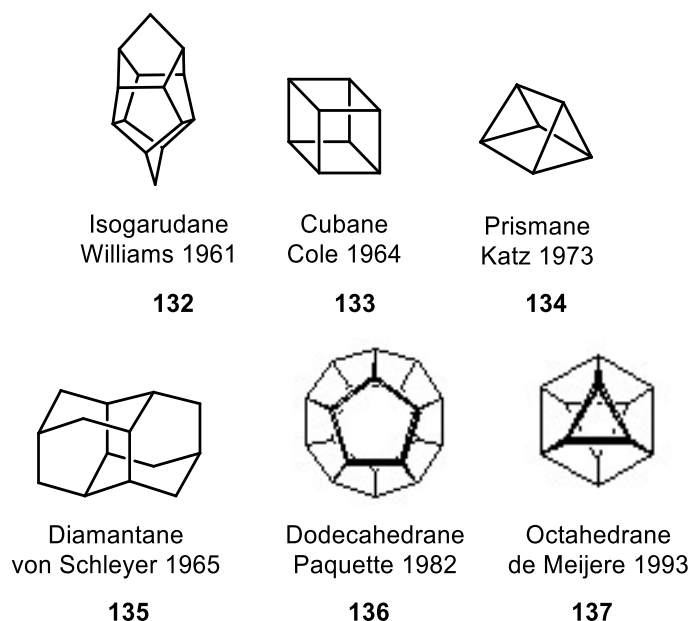
Figure 81. Selected examples of cage hydrocarbons.

Cage hydrocarbons are challenging targets for modern synthetic organic chemistry and in addition possess potential applications in pharmaceutical industry, as high energy fuels and functional materials.[95] These factors inspired chemists to synthetize cubane (**133**),[96] prismane (**134**),[97] diamantane (**135**),[98] dodecahedrane (**136**)[99] and octahedrane (**137**)[100] proving their existence and properties.

5.1.1 Dimerization of norbornadiene

One of the most fascinating classes of polycyclic nonaromatic hydrocarbons are dimers of norbornadiene **61**.

In 1961 Williams and co-workers investigated reactions of diene **61** with metal carbonyls.[101] Authors described treatment of norbornadiene with iron pentacarbonyl, diiron nonacarbonyl, triiron dodecacarbonyl or dicobalt octacarbonyl. In all the cases similar reaction mixture was obtained. Besides several liquid products, Williams and co-workers isolated a highly symmetric norbornadiene dimer with melting point at 164°C in yield of 4%. Nuclear magnetic resonance spectra of this compound consisted of only two signals in ratio 3:1.

Authors suggested two possible structures for this dimer: garudane (**139**) or heptacyclo-[6.6.0.0^{2,6}.0^{3,13}.0^{4,11}.0^{5,9}.0^{10,14}]tetradecane (isogarudane **132**, Figure 81).
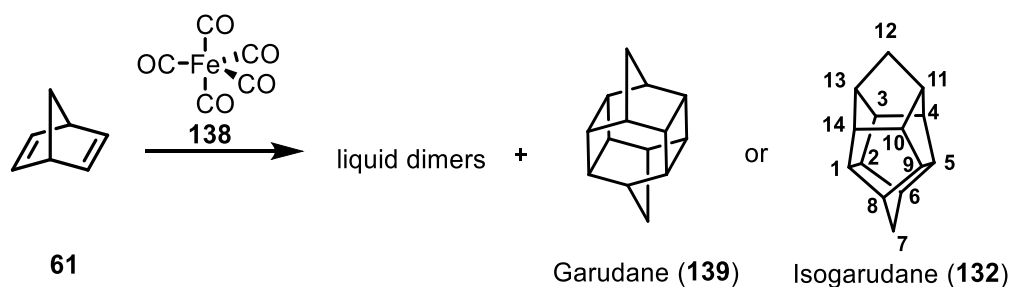
Figure 82. Possible structures of highly symmetric norbornadiene dimer as proposed by Williams.

The exact connectivity and structure of this compound remained unknown until 1972, when Katz et al. proved that it corresponds to isogarudane (**132**). Garudane (**139**) was synthetized fifteen years later in a multiple step sequence.[102] As of 2019, garudane was never obtained via direct dimerization of norbornadiene.

In 1966 Fosselius and coworkers investigated dimerization of norbornadiene with binuclear carbonyl catalyst: $Zn[Co(CO)_4]_2$. Authors found that these type of bimetallic complexes are promoting formation of a new norbornadiene dimer – Binor-S (**140**) (Figure 83).[103]
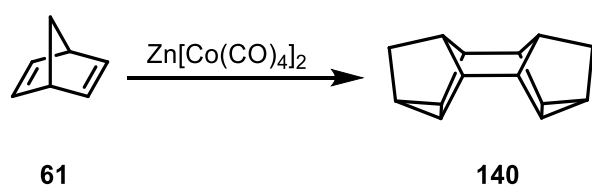
Figure 83. Synthesis of Binor-S.

The empirical formula of Binor-S corresponds to the data of elemental analysis, and its structure was proven unequivocally using NMR and mass spectroscopy. It was envisioned that coordination of two norbornadiene molecules by cobalt atoms of the catalyst brings them into proximity and allows reaction to occur with excellent regioselectivity. Binor S (**140**) is one of the most industrially significant dimers of

norbornadiene, as it is commonly used as a starting material for the synthesis of diamantane.[104]
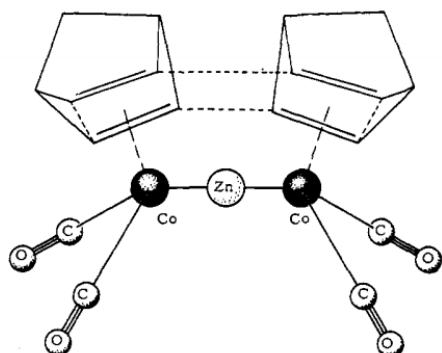
Figure 84. Proposed structure of cobalt-complexed norbornadiene intermediate.[103]

In 1972 group of Katz investigated rhodium-catalyzed dimerization of norbornadiene (**61**).[105] They have reported that after refluxing norbornadiene for 5 days in the presence of Wilkinson's catalyst, a complex mixture of dimers and trimers was obtained (Figure 85).
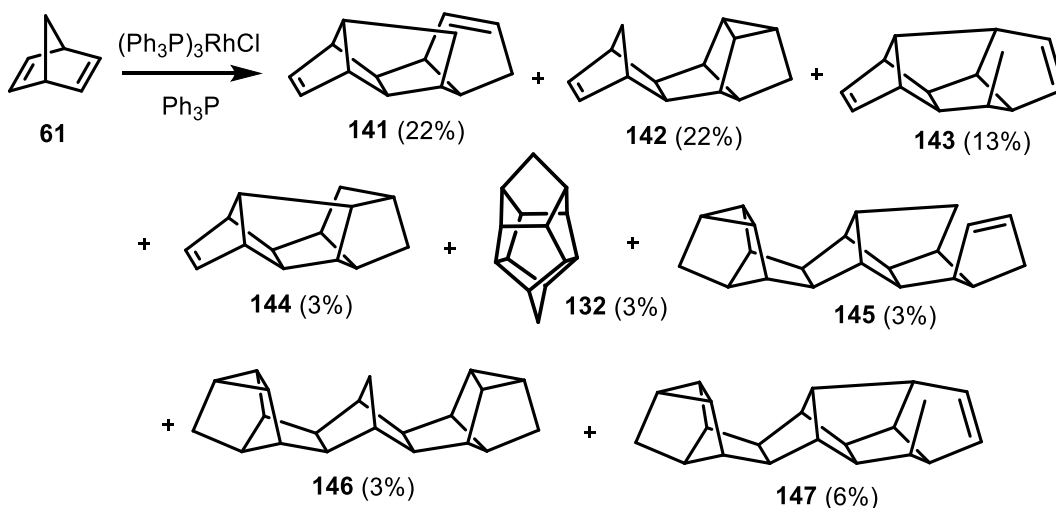
Figure 85. Mixture of norbornadiene dimers and trimers obtained by Katz.

Katz et al. analyzed and characterized each of these products. They reported plausible mechanistic explanation for their formation and investigated

hydrogenation of unsaturated dimers. Although all of the molecules have been characterized, the authors did not describe selective synthesis of the single dimer.

In 1987 group of Chow reported selective dimerization of norbornadiene to isogarudane (**132**) using $Mo(CO)_6$ catalyst (Figure 86).[106]
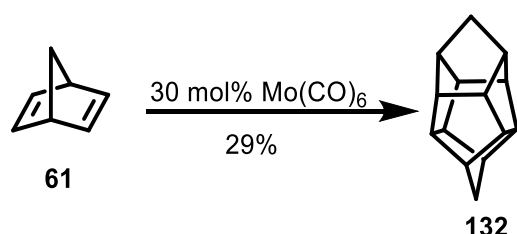
Figure 86. Synthesis of isogarudane (132) promoted by molybdenum carbonyl.

The Authors suggested that the reaction proceeds via organometallic intermediate, where two norbornadienes molecules are coordinated to one molybdenum center at D_{2D} symmetry in respect to each other. Chow and co-workers isolated and characterized these molybdenum intermediates. Despite its high selectivity, major drawbacks of this method are high toxicity of metal complex and relatively low yield of the product.

In 2016 Dong and co-workers published a synthetic protocol towards the derivatives of isogarudane **150** using ruthenium catalyst (Figure 87).[107]
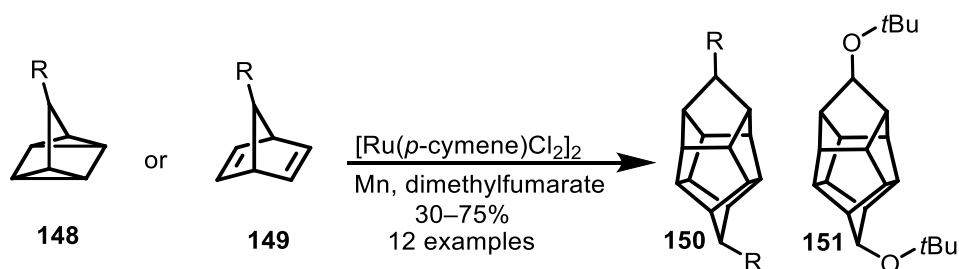
Figure 87. Synthesis of functionalized isogarudanes using ruthenium catalyst.

The authors reported a practical method yielding desired products in moderate to good yields with good selectivity. Group of Dong investigated post-synthetic

modifications of bis(*tert*-buthoxyl) derivative of garudane **151** in the same report giving access to natural motifs functionalized by cyclic hydrocarbon moieties.

Despite the numerous reports discussed above, a catalytic synthesis of polycyclic hydrocarbons is challenging up to date. The mechanism of these transformations is often not completely understood, and the number of examples of the use of different carbon-based backbones in highly functionalized molecules is very limited.[108–110]

6 Catalytic dimerization of norbornadiene derivatives

6.1.1 Serendipitous discovery of norbornadiene dimerization

Encouraged by the high reactivity of rhodium complexes with dicationic chelating phosphines as ancillary ligand in conjugated diene hydroarylation reaction, we envisioned that cyclic non-conjugated dienes, such as norbornadiene (**61**), might be adequate substrates to further expansion of this methodology.[111] Surprisingly, after reacting one equivalent of norbornadiene with one equivalent of indole (**128**) under standard reaction conditions, instead of expected hydroarylation product we isolated a dimer of norbornadiene (Figure 88) among other products.

L (5 mol%), [RhCl(CO)$_2$]$_2$ (2.5 mol%)

KB(C$_6$F$_5$)$_4$ (10 mol%), DCE, 70 °C

no hydroarylation product, norbornadiene dimer isolated

61 **128**
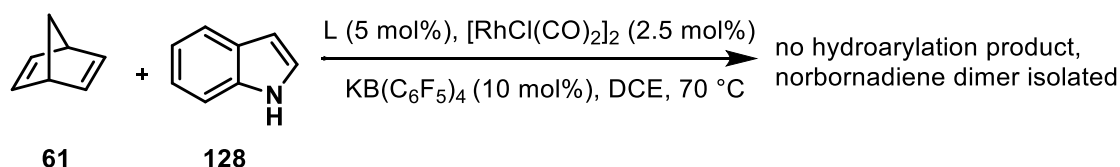
Figure 88. An attempt towards hydroarylation of norbornadiene.

The empirical formula and mass of obtained dimer were confirmed by GC-MS and HR-MS measurements. In ^{1}H NMR spectrum of isolated dimer only 2 singlets at 2.39 and 1.76 ppm can be observed (Figure 89). The 3:1 intensity ratio between these signals corresponds to 12 and 4 equivalent protons, respectively, according to the empirical formula of norbornadiene dimer C$_{14}$H$_{16}$. This conclusion indicates a high symmetry of obtained compound. In ^{13}C NMR spectrum only 3 signals at 53.2, 51.0 and 42.7 ppm are observed (Figure 90). In the Attached Proton Test (APT) ^{13}C NMR spectrum of this compound, two signals appear as positive and one as negative (Figure 91). Based on this experiment, it is possible to conclude that there are two groups of chemically equal tertiary carbon atoms and one group of equal secondary carbon atoms. After comparison of obtained spectral data with the reported ones,[106,107] we assigned the structure of obtained product to isogarudane (**132**).
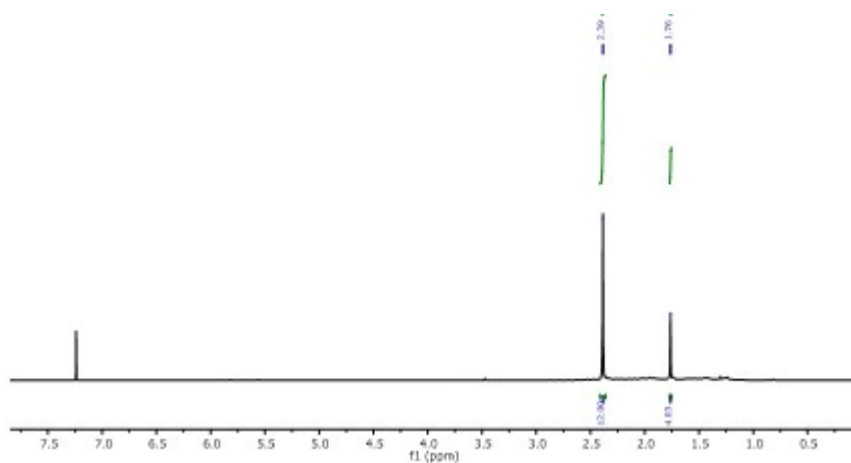
Figure 89. ^{1}H NMR (500 MHz, 25 °C, CDCl$_3$) spectrum of norbornadiene dimer.
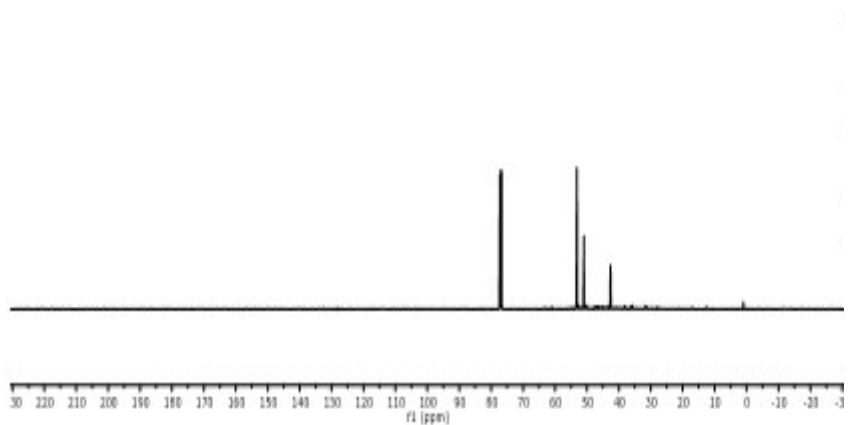
Figure 90. ^{13}C NMR (125 MHz, 25 °C, CDCl$_3$) of norbornadiene dimer.
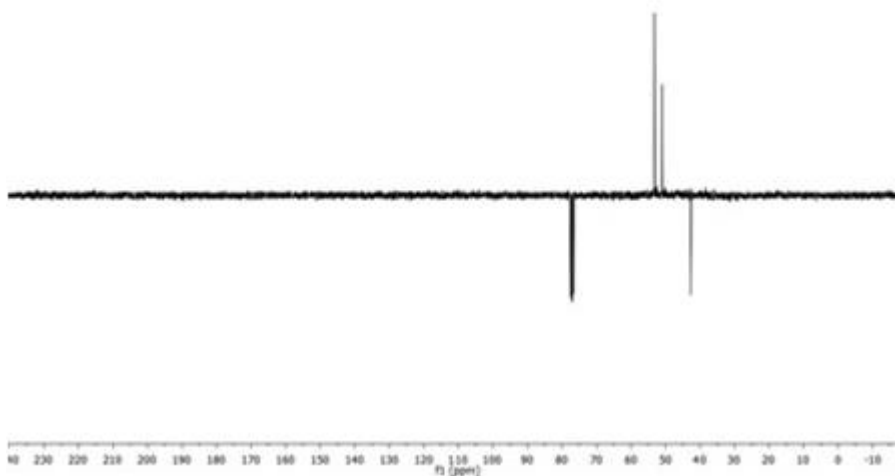
Figure 91. APT ¹³C NMR 125 MHz, 25 ˚C, CDCl₃) spectrum of norbornadiene dimer.

Additionally the structure of obtained compound **132** was proven by single crystal diffraction (Figure 92; *cf.*[107]).
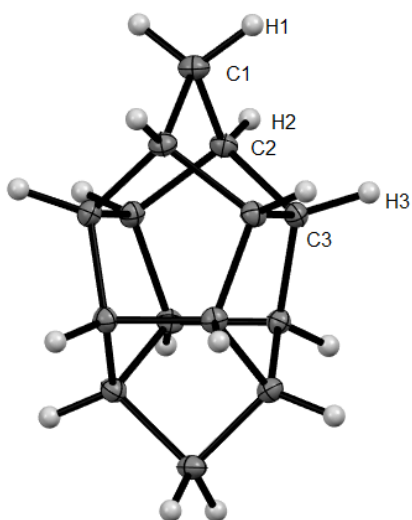
Figure 92. Molecular structure of norbornadiene dimer in the crystal; thermal ellipsoids at 50% probability.

All the C–C bond distances lie within the range of typical carbon–carbon single bond length (1.53–1.57 Å). Obtained molecule is composed of five-membered rings

arranged in D_{2D} symmetry and characterized with remarkable chemical stability with melting point of 158 °C.

6.1.2 Optimization of the dimerization conditions

Encouraged by these preliminary results we screened different reaction conditions to find optimized protocol for synthesis of this compound **132** and possibly of its derivatives (Figure 93). After initial experiments summarized in Table 4 we limited the use of metal precursor to 1,5-cyclooctadienerhodium(I) chloride dimer and the use of solvent to 1,2-dichloroethane (entry 1).
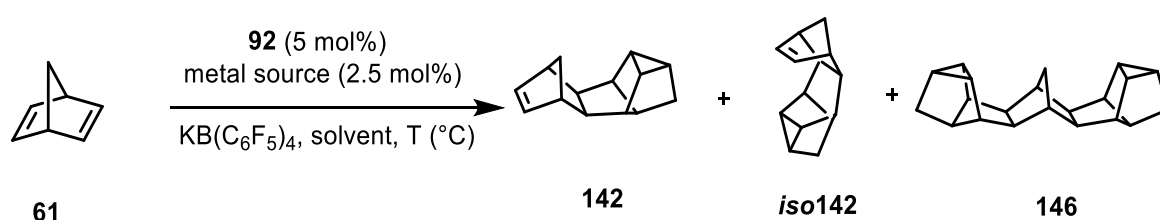
Figure 93. Investigations towards optimized conditions of norbornadiene dimerization.

Table 4. Optimization of the conditions of dimerization reaction.

Entry	Metal source	Solvent	GC Conversion of **61**
1	[Rh(cod)Cl]₂	DCE	58%
2	[Rh(coe)₂Cl]₂	DCE	55%
3	[Rh(CO)₂Cl]₂	DCE	52%
4	[Rh(cod)Cl]₂	EtOAc	<10%
5	[Rh(cod)Cl]₂	THF	<10%
6	[Rh(cod)Cl]₂	PhCH₃	31%
7	[Rh(cod)Cl]₂	PhCF₃	Complex mixture

8	[Rh(cod)Cl]$_2$	CH$_3$CN	<5%
9	[Rh(cod)Cl]$_2$	Acetone	<5%
10	[Rh(cod)Cl]$_2$	THF	<5%

Depending on the reaction conditions, the mixture of dimers containing either **142**, **iso142** or **146** as the main product proportions was formed. (Figure 93).

Results of our further efforts towards searching the better dimerization conditions and employing ligands **92**, **97** and **98** are presented in Table 5.[VI]
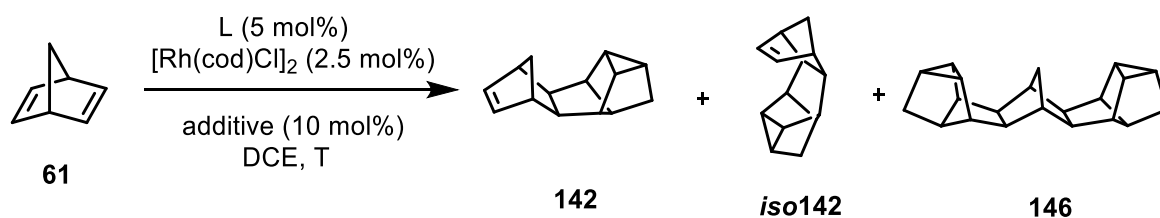
Figure 94. Further investigations towards optimized conditions of norbornadiene dimerization.

[VI] Optization of the reaction conditions and analysis of the ratio between the products was performed in cooperation with Dr. Xavier Marset

Table 5. Further optimization of dimerization conditions.

Entry	Ligand (mol%)	Additive (mol%)	Solvent (M)	T (°C)	142	*i*142	146
1	**92** (2)	KB(C₆F₅)₄ (4)	DCE (0.30)	70	8	48	33
2	**92** (2)	NaB(C₆F₅)₄ (4)	DCE (0.30)	90	7	53	30
3	**92** (2)	KB(C₆F₅)₄ (4)	DCE (0.30)	90	4	42	51
4	**92** (2)	NaB(C₆F₅)₄ (4)	DCE (0.50)	90	9	79	12
5	**92** (2)	KB(C₆F₅)₄ (4)	DCE (0.30)	90	4	82	11
6	**92** (2)	NaB(C₆F₅)₄ (4)	DCE (0.30)	90	8	76	15
7	**92**(2)	KB(C₆F₅)₄ (4)	DCE (0.05)	90	10	89	-
8	**97** (2)	KB(C₆F₅)₄ (4)	DCE (0.05)	90	10	20	-
9	**98** (2)	KB(C₆F₅)₄ (4)	DCE (0.05)	90	<5	20	-
10	**92**(2)	KB(C₆F₅)₄ (4)	CH₃CN (0.05)	90	-	<5	-

Interestingly we realized that after analyzing the reaction mixture by NMR we did not see formation of desired product. We hypothesized that **132** is formed by

isomerization of **142** and **iso142** catalyzed by acid. We performed additional experiments, where isolated **142** was treated with different proton sources.[VII]

Table 6. Optimization of proton catalyzed isomerisation of norbornadiene derivatives
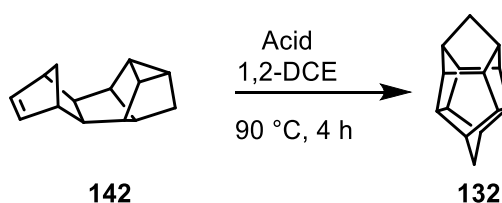
Entry	Acid (mol%)	Concentration (M)	Yield (%)
1	F_3CSO_3H (1 mol%)	0.2	34
2	$HBF_4 \cdot Et_2O$ (3 mol%)	0.04	33
3	HCl (5 mol%)	0.04	1
4	$BF_3 \cdot Et_2O$ (3 mol%)	0.04	62
5	$BF_3 \cdot Et_2O$ (5 mol%)	0.04	25
6	$HSbF_6$ (3 mol%)	0.04	10
7	*p*-Toluenesulfonic acid (3 mol%)	0.04	0
8	$[H(OEt_2)_2][B(C_6F_5)_4]$ (1 mol%)	0.04	67

[VII] Optimization of the acid catalyzed isomerization of norbornadiene dimers was performed by Dr. Xavier Marset

To our delight we could isolate the desired product with moderate yield. We suspected that the formation of **132** in our preliminary experiments (Figure 88) was probably due to the contamination of perfluorophenylborate salt with free acid. Structure and connectivity of **142** and **146** were confirmed by ^{1}H and ^{13}C NMR spectra. The latter are identical to the previously published data.[86] In addition, **146** could be crystalized from dichloromethane/methanol mixture giving monocrystals suitable for single diffraction experiments (Figure 95).
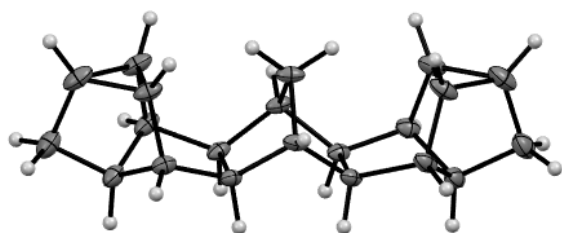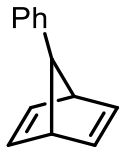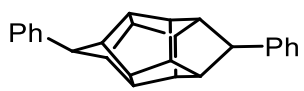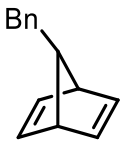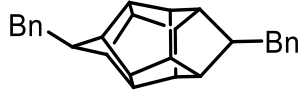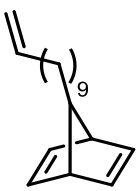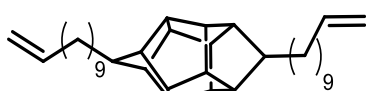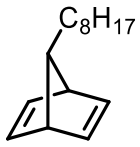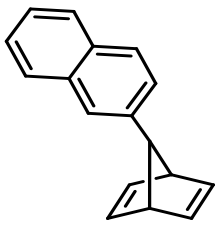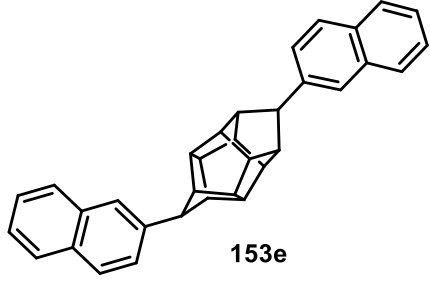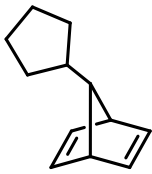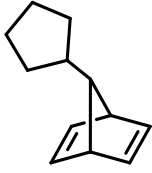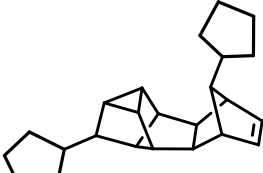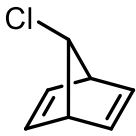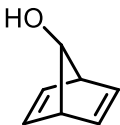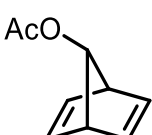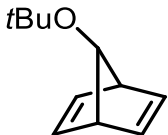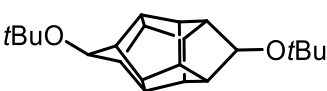
Figure 95. Single crystal structure of norbornadiene trimer 79; thermal ellipsoids at 50% probability.

After finding optimized conditions (Table 5, entry 7), we explored the scope and limitations of the described methodology. We applied the standard reaction conditions to series of 7-substituted norbornadienes **152** in order to achieve new derivatives of isogarudane **153** (Table 7).

Table 7. Scope and limitations of norbornadiene derivatives dimerization.
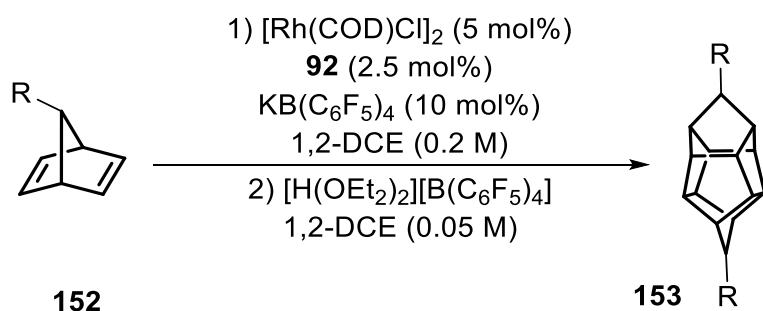
Entry	Substrate	Product	Isolated yield [%]	Comment
1	**152a** (Ph substituted norbornadiene)	**153a** (Ph substituted product)	57	Obtained as a 7:3 mixture with the second isomer
2	**152b** (Bn substituted norbornadiene)	**153b** (Bn substituted product)	64	-
3	**152c** (alkenyl substituted norbornadiene)	**153c** (alkenyl substituted product)	59	-
4*	**152d** (C$_8$H$_{17}$ substituted norbornadiene)	**153d** (C$_8$H$_{17}$ substituted product)	71	-
5	**152e** (naphthyl substituted norbornadiene)	**153e** (naphthyl substituted product)	42	Obtained as a 5:1 mixture with the second isomer

6	152f	-	-	Complex mixture under standard conditions
7	152f	155	93	Using 10 mol% of KB[3,5-(CF$_3$)$_2$C$_6$H$_3$]$_4$ as an additive
8	152g	-	-	Complex mixture
9	152h	-	-	Complex mixture
10	152i	-	-	Complex mixture
11	152j	153j	46	-

We proved that hydrocarbon-substituted norbornadienes **152** yield desired cage products **153** in moderate to good yields. If the aliphatic substituent is present (entries 3 and 4), isogarudane derivative **153** is the sole reaction product. In the

case of aromatic derivatives, a formation of the second, minor isomers are observed (entries 1 and 5). Because of difficult work up procedures it is impossible to isolate the minor isomer quantitatively and completely characterize it. When using bulky cyclopentyl derivative (entry 6)[VIII] we obtained a complex and inseparable mixture of products. Surprisingly, employing different counterion source led selectively to an *endo* dimer **155** of the starting material (entry 7).

In contrast to the recently reported Ru/Mn-catalyzed dimerizations of norbornenes,[107] heteroatom-functionalized derivatives of norbornadiene did not yield the desired products under applied reaction conditions with exception of bulky 7-*tert*-butoxy norbornadiene **153j** (entry 11). All the obtained compounds are characterized with exceptional thermal stability and high degree of crystallinity. We managed to crystalize and perform the single crystal diffraction experiments of reaction products from entries 1, 7 and 11, ultimately proving their structure and connectivity (Figure 96). All atom distances are within the typical ranges of C–C and C–O bond lengths.
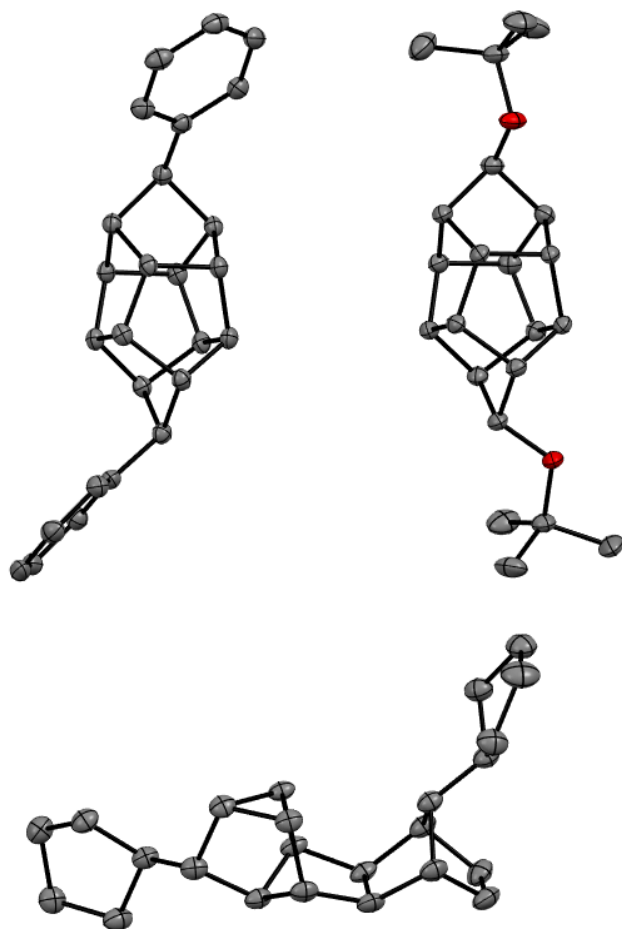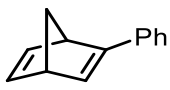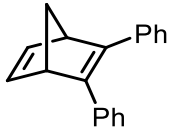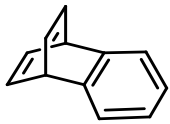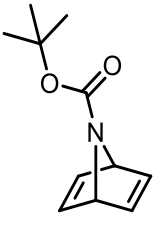
Figure 96. Molecular structures of 153a, 153j and 155in the crystals. Thermal ellipsoids at 50% probability; hydrogen atoms and disorder of tert-butyl substituent have been omitted for clarity.

In order to test compatibility of our catalytic system with different starting materials we envisioned a series of experiments where we use a variety of olefins as starting materials for dimerization (Table 8).

Table 8. Investigation of dimerization reaction of different bicyclic dienes.

Entry	Substrate	Product	Isolated Yield [%]	Comment

1	**156**	-	-	Quantitative re-isolation of starting material
2	**157**	-	-	Quantitative re-isolation of starting material
3	**158**	-	-	Complex reaction mixture, traces of dimer in GC-MS
4	**159**	-	-	Quantitative re-isolation of starting material
5	**160**	-	-	Complex reaction mixture, decomposing upon exposing to air, moisture, light and at room temperature
6	**161**	Unidentified dimer	33	Dimeric product isolated after column chromatography; mass confirmed by HRMS measurement; decomposing upon exposure to air

After testing a variety of different starting materials we concluded that reaction conditions do not tolerate the substitution in positions 1 and 2 in norbornadiene (entries 1 and 2). In the case of benzobarrelene (**159**, entry 4) we re-isolated the

starting materiala, whereas dihydrobarrelene (**158**, entry 3) was yielding traces of dimer, isolation of which from the reaction mixture appeared to be impossible. 7-Oxanorbornadiene (**160**, entry 5) caused rapid decomposing of the metal catalyst. In the case of *N-tert*-butoxycarbonyl 7-azanorbornadiene (**161**, entry 6) we managed to isolate with a yield of 33% the dimerization product. Unfortunately, due to its low stability we could not elucidate the structure of the dimeric product during the time of doctoral program.

6.1.3 Proposed mechanism of rhodium-catalysed norbornadiene dimerization

In order to explain the formation of different products under applied reaction conditions we propose the following mechanism consisting of two cycles.

In catalytic cycle rhodium diphosphine dimeric complex **A** is coordinated by one molecule of norbornadiene forming η^4 complex **B**. In the case of ligand **92** formation of this intermediate **B** = **162** was confirmed by its isolation followed by crystallization from the reaction mixture. Single crystals suitable for an X-ray diffraction experiment were obtained and analyzed (Figure 97).
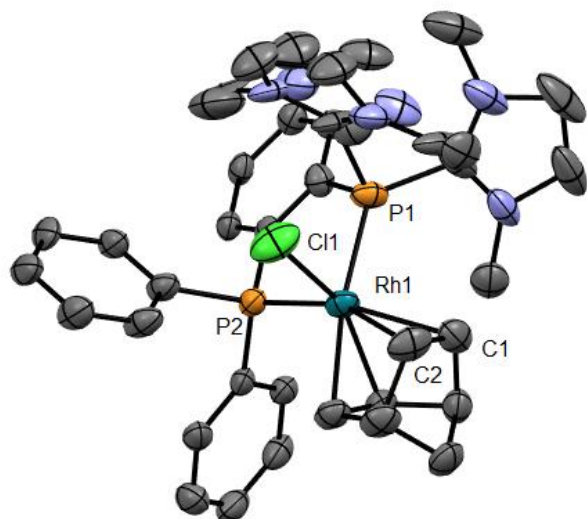
Figure 97. Molecular structure of the η4 norbornadiene-rhodium diphosphine complex 162 in the crystal. Thermal ellipsoids at 50% probability; hexafluoroantimonate counterions and solvent molecules have been omitted for clarity.

Afterwards a 2+2+2 Homo Diels-Alder reaction occurs. Depending on the reaction conditions, preferentially either *endo*-complex (**C**, see Figure 98) or *exo*-complex is formed. This elementary step governs the outcome of the reaction – formation of **132** or *iso***132**.
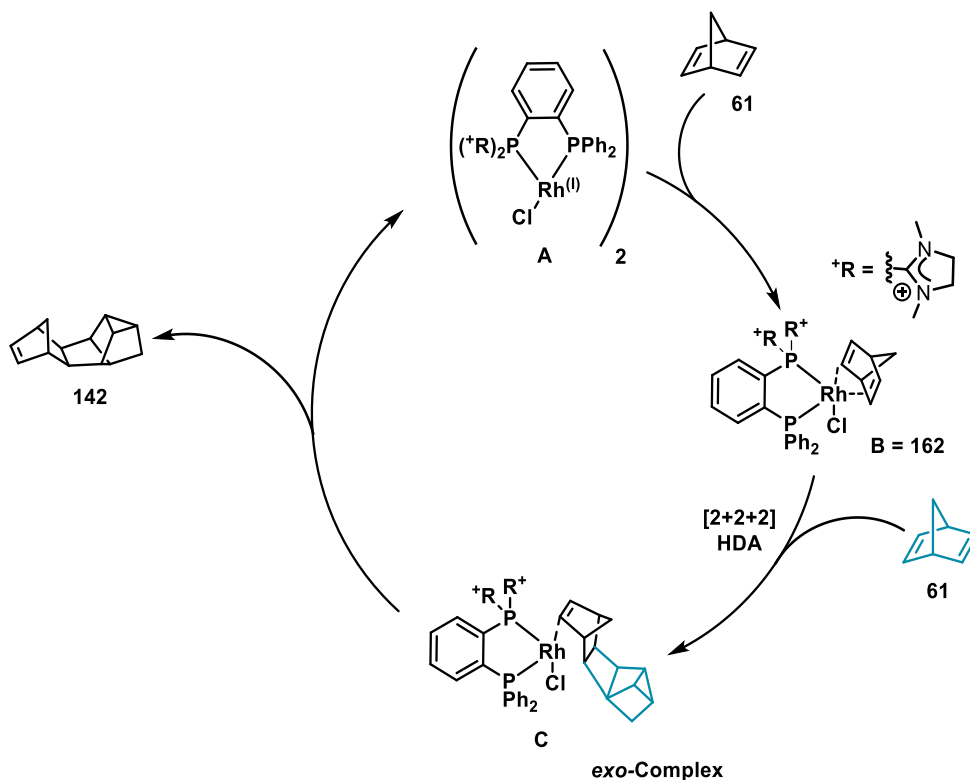
Figure 98. Postulated mechanism of rhodium-catalyzed dimerization of norbornadiene leading to the formation of isogarudane 132.

In the next step one decoordination of the olefin from Rhodium complex occurs, a dimer of norbornadiene is released and Rhodium catalyst is regenerated.

In the second step of the synthetic sequence leading to **132** we postulate the proton catalyzed rearrangement of **142** and **iso142** to desired product. This is in line with the previous findings of Katz and coworkers.
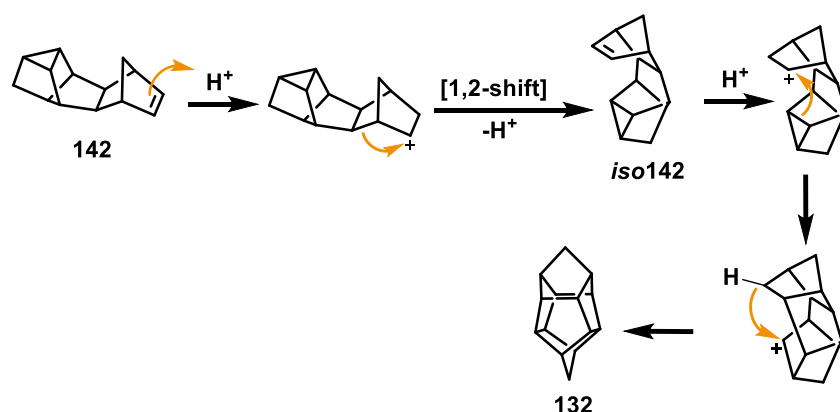
Figure 99. Postulated mechanism proton catalyzed rearrangement of 142 to isogarudane.

In order to confirm our mechanistic hypothesis we tested if the isolated η^4 norbornadiene rhodium diphosphine complex **162** can catalyse the dimerization.

We prepared **162** via treatment of rhodium precursor [Rh(cod)Cl]$_2$ with excess (10 equivalents) of norbornadiene (**61**) in the presence of the diphosphine ligand **92**. Complex **162** was obtained in acceptable yield, and its structure and connectivity was confirmed using ^{1}H, ^{13}C and ^{31}P NMR spectroscopy as well as X-ray crystal structure analysis (Figure 97).
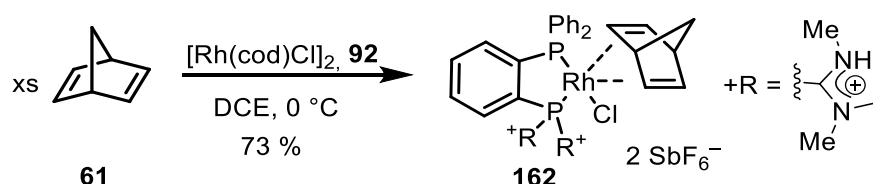
Figure 100. Preparation of η4 norbornadiene-rhodium diphosphine complex 162.

Employing our standard reaction conditions (Table 5, entry 7) in the presence of the synthetized complex **162** and norbornadiene followed by addition of the acid resulted in formation of the expected product **132**.

Additional theoretical investigation[IX] using density functional theory (at the PBE0-D3BJ(PCM)/def2-TZVPP//TPSS-D3BJ/def2-SVP level of theory) aimed to confirm our postulated mechanism and explain why dppbz, which is a neutral analogue of **92** does not favor formation of norbornadiene dimers. Indeed, the calculated mechanism (Figure 101) begins with an addition of external norbornadiene to the norbornadiene-Rhodium complex **162.** Energy barrier of this elementary step was calculated to be 16.1 kcal/mol for *endo* complex and 13.8 for an *exo* complex. Afterwards an oxidative cyclization event occurs, still favoring *exo* pathway. The energy profile calculations reveled this elementary step to be rate determining.

The second carbon-carbon bond is formed via carbometallation. Finally, reductive elimination occurs in a final step releasing the polycyclic carbon system and regenerating the Rhodium catalyst.

[IX] Performed by Prof. Dr. Lawrence M. Wolf from University of Massachusetts
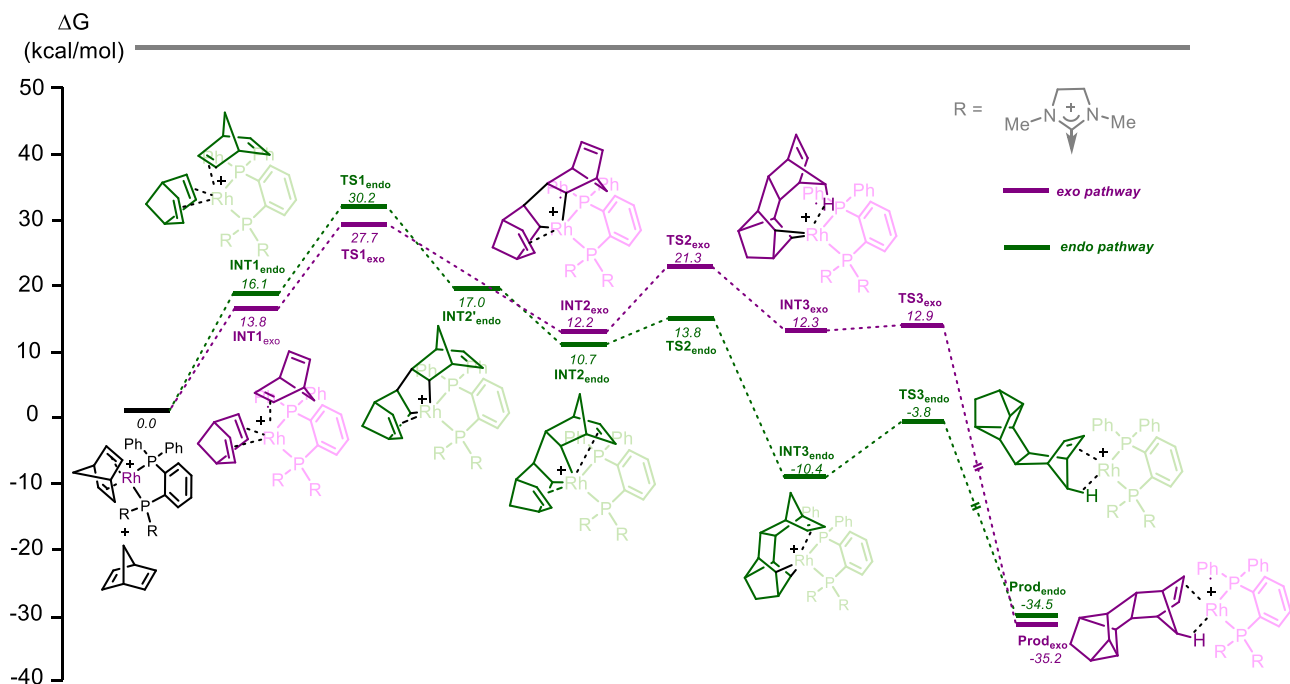
Figure 101. Gibbs free energy profile of the dimerization reaction.

We postulate that the use of electron poor bidentate phosphines is crucial, since monodentate phosphines involves bicoordination of two norbornadienes to metal center. A notable example of such reactivity is Rhodium catalyzed formation of binor S. In addition classical electron rich bidentate phosphines enable coordination of only 1 norbornadiene unit and thus inhibit further reactivity.[112]

6.1.4 Functionalization of norbornadiene dimers

After proving the scope and limitations of our catalytic system we were intrigued to figure out whether, we could introduce any functional groups to isogarudane skeleton via post-synthetic modification. This would provide a synthetic approach to 1-fuinctionalized isogarudanes, whereas dimerization of norbornadienes affords usually the 7,12-disubstituted ones. Because of its notorious chemical stability isogarudane (**132**) is one of the underrepresented motifs in the chemistry of polycyclic aliphatic hydrocarbons. Hydrocarbons are known to be demanding substrates in terms of selectively functionalizing C–H bonds. In fact, only several methods of introducing C–O, C–N or C–X functionalities are known up to date, and most of them are exclusively applied to adamantane derivatives.[113]

We started our investigations with the attempt of introducing a halogen atom into isogarudane structure by simple bromination reaction using molecular bromine. Unfortunately we did not observe any conversion of starting material using classical electrophilic or radical bromination protocols (Figure 102 and Table 9).
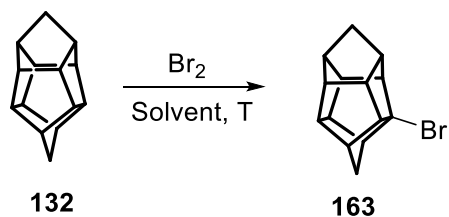
Figure 102. Bromination of isogarudane 132.

Table 9. Initial screening of isogarudane bromination.

Entry	Solvent	T	Result	Comment
1	CHCl$_3$	rt	No conversion	Reaction in the dark
2	CHCl$_3$	rt	No conversion	Reaction in the presence of sunlight
3	CHCl$_3$	rt	No conversion	Reaction with blue LED light
4	CHCl$_3$	reflux	No conversion	-
5	neat	rt	No conversion	-
6	neat	reflux	No conversion	-

After unsuccessful initial attempts we decided to follow the protocol developed by Schreiner group utilizing Phase Transfer Catalytic (PTC) conditions (Figure 103 and Table 10).[114]
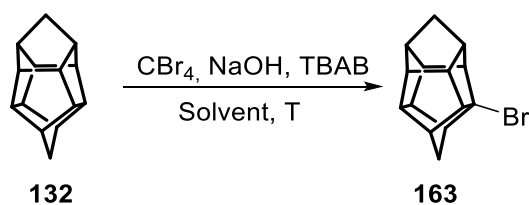
Figure 103. Bromination of isogarudane 132 under PTC conditions.

Table 10. Screening of bromination conditions under PTC.

Entry	Solvent	T	Result	Comment
1	DCM	rt	5% **163**, 95% 132	Literature conditions
2	DCM	rt	6% **163**, 94% 132	Double excess of CBr$_4$
3	DCM	reflux	60% **163**, 40% **132**	-
4	DCE	reflux	45% **163**	-
5	DCM	60 °C	78% **163**,* 22% **132**	Reaction in the pressure vial

*Isolated in 59% yield after column chromatography.

After intensive screening we were very happy to notice, that the brominated isogarudane **163** was prepared in moderate yield utilizing modified literature protocol.

This bromoisogarudane **163** was used as a starting material to ensure further functionalizations and to obtain three different derivatives **164**, **165** and **166** in 99%, 99% and 85% yield, respectively (Figure 104).
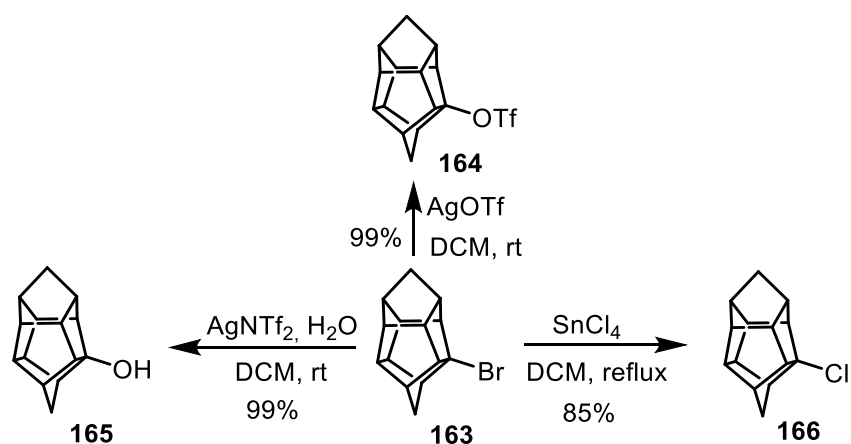
Figure 104. Further functionalization of bromoisogarudane 163.

In addition to the functionalization of isogarudane skeleton, we were interested if it is possible to modify the second dimer **142**, obtained as the minor product of dimerization reaction.

We envisioned, that using an active olefin metathesis catalyst,[115] as well as excess of styrene (**16**) as the cross metathesis partner and the solvent, should result in desymmetrization of **142**. We were pleased to observe that cross metathesis product **167** was obtained in high yield, as inseparable mixture of *E* and *Z* isomers (Figure 105).
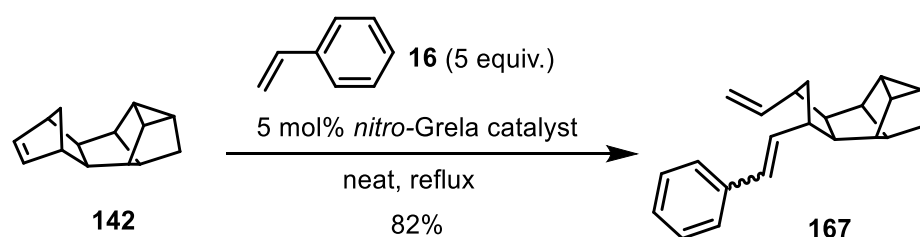
Figure 105. Desymmetrization of 142 using olefin metathesis reaction.

As the transformation of a double bond into a single one would reduce the molecular complexity of **167**, we subjected obtained stereoisomeric mixture of **167** to hydrogenation reaction under 1 atm of hydrogen pressure and in the presence of

Pd/C catalyst. After 24 h, we quantitatively isolated reduction product **168** (Figure 106). It is worth noting, that the straightforward reaction sequence dimerization-metathesis-reduction delivered a hydrocarbon of complex structure which, to the best of our knowledge, would require multistep protocol using classical synthetic methods.
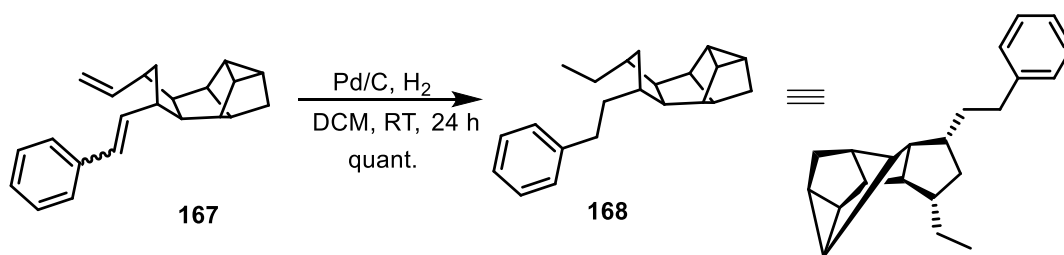
Figure 106. Hydrogenation of cross metathesis product 167.

7 SUMMARY

In summary we designed and synthetized three new dicationic phosphine ligands with phenyl backbone and different substitution pattern on the cationic moiety. We obtained a paracyclophane derived dicationic ligand and we attempted a synthesis of ferrocene decorated ligand leading to formation of unexpected dehydrogenative P-P coupling product. All of the new ligands were characterized using spectroscopic methods and X-ray diffraction. We evaluated the electronic properties of the newly obtained species by comparison of CO stretching frequency of molybdenum carbonyl complexes and using cyclic voltammetry.

With the ligands in hand we obtained a family of new rhodium and iridium complexes. In case of ligands with phenyl backbone we observed coordination of both phosphines to the metal, whereas paracyclophane decorated ligands coordinated rhodium and iridium with only neutral phosphine. While analyzing NMR spectra of rhodium and iridium complexes with **92**, **97** and **98** we observed a dynamic equilibrium between tetracationic dimeric complexes and dicationic monomeric species. Structure of all of the complexes was confirmed using spectroscopic methods and most of them were crystalized and their connectivity was analyzed using X-ray diffraction.

We successfully used the obtained rhodium complexes as effective catalysts for hydroarylation of butadiene derivatives with strong nucleophiles. Our system proved to be outperforming electron poor neutral ligands and enabled us to obtain a family of indole, dimethyl resorcinol and azulene substituted olefins. The mechanism of this transformation was studied using KIE experiments and DFT calculations proving a need for using dicationic ligands in this transformation.

We discovered a serendipitous reactivity between rhodium complexes and norbornadiene. We conceptualized that homodimerization of norbornadiene under reaction conditions proceeds via [2+2+2] homo Diels-Alder mechanism catalyzed by electron deficient rhodium complexes. A new family of 7-substituted

heptacyclotetradecanes was obtained using a simple protocol employing dimerization reaction and subsequent acid catalyzed rearrangement. We successfully performed post synthetic modification of obtained isogarudane. The mechanism of the dimerization was studied using computational methods, again proving necessity of using dicationic complexes as efficient catalysts.
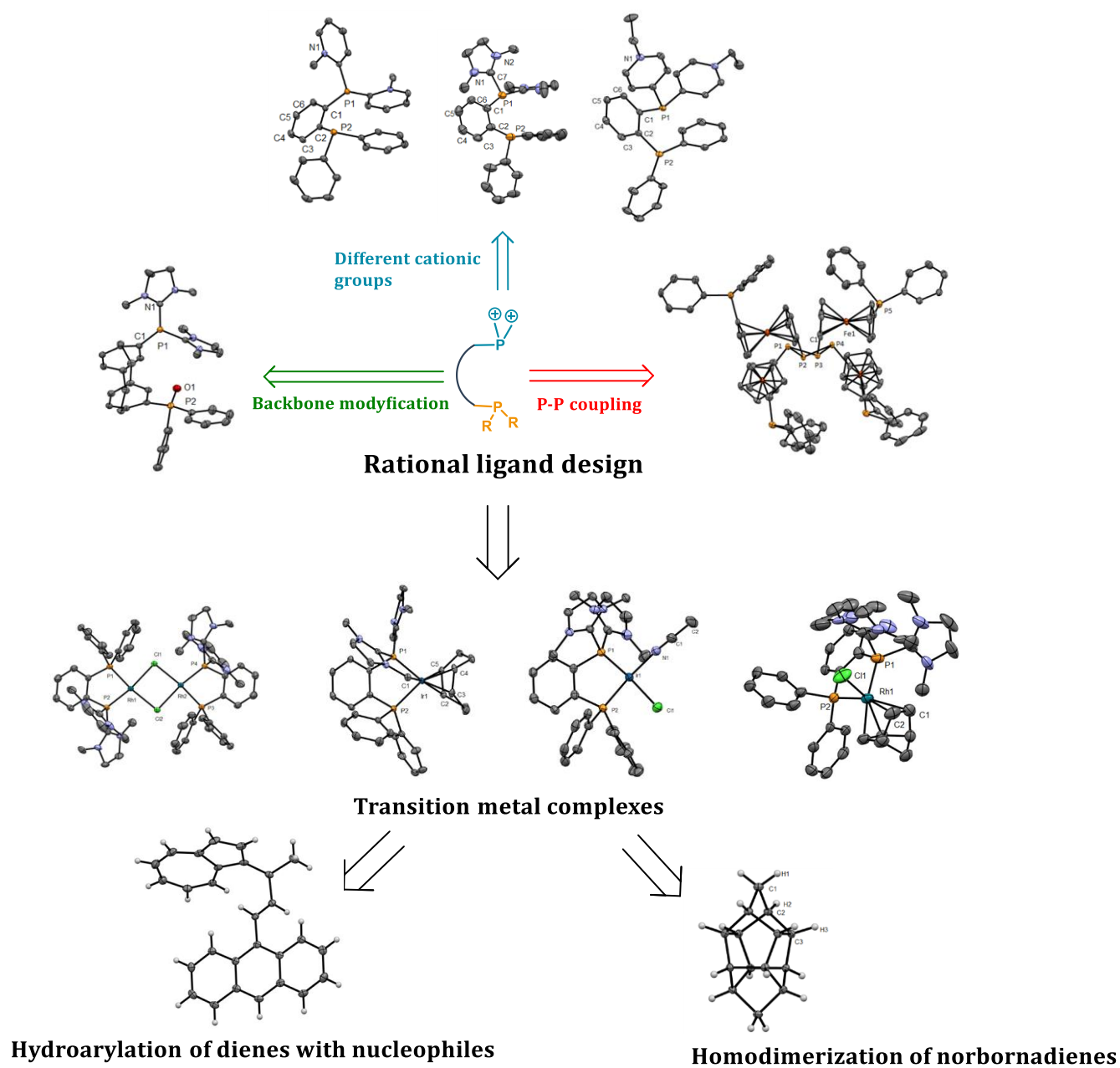

Figure 107. Graphical summary of experimental studies performed during Doctoral Thesis.

8 Experimental part

8.1.1 General remarks

All commercially available solvents were used as received, unless stated otherwise. Anhydrous solvents (THF, Et$_2$O, MeCN, DCM, DCE) were obtained using Solvent Purification System MBraun (SPS), stored over 4 Å molecular sieves and degassed before use. Unless otherwise stated, all reactions were carried out in flame-dried glassware under nitrogen, using Schlenk or glovebox techniques. Infrared (IR) measurement were performed on: Nicolet FT-7199 and FT/IR-4100 (Jasco) instruments, wavenumbers in cm^{-1}. Mass determination (HR-MS) was performed on Finnigan MAT 8200 (70 eV), Finnigan MAT 95 or Finnigan LCQ instruments; high resolution mass (HR-MS) determinations were performed on Bruker APEX III FT-MS (7 T magnet) or APEX IV 7T FTICR instruments. Nuclear magnetic resonance (NMR): Spectra were recorded on a Bruker AV600, AV500, AV400, DPX300, Varian Mercury 300 or Varian Inova 500 spectrometers, as stated for each case; ^{1}H and ^{13}C chemical shifts (δ) are given in ppm relative to TMS, using the solvent signals as references and converting the chemical shifts to the TMS scale. ^{31}P chemical shifts (δ) are given in ppm relative to H$_3$PO$_4$ respectively (external standard). Coupling constants (J) are given in Hz. Deuterated solvents (CDCl$_3$, CD$_3$CN) were stored in Schlenk flasks over molecular sieves (4 Å for CDCl$_3$ or 3 Å for CD$_3$CN). Chromatographic separations: type of the used column as well as specific conditions are stated for each compound. Reactions were controlled by thin-layer chromatography (TLC) analysis, performed using polygram SILG/UV254 from Macherey Nagel, and visualized by UV irradiation (λ = 254 nm, 366 nm). All commercially available compounds (Acros, ABCR, Alfa Aesar, Sigma-Aldrich, TCI, J and K Scientific) were used as received, unless stated otherwise. 4 Å and 3 Å molecular sieves were activated by heating under high vacuum at 200 °C for 3 days.

8.1.2 Experimental procedures and characterizations

(2-Bromophenyl)diphenylphosphane (**86**):
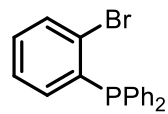
Distilled and dried NEt$_3$ (12.0 g, 16.5 mL, 118.4 mmol, 1.10 equiv.), diphenylphosphine (20.0 g, 107.4 mmol, 1.00 equiv.) and tetrakis(triphenylphosphine)palladium (1.0 g, 865 µmol, 0.8 mol%) were added to the solution of 1-bromo-2-iodobenzene (**85**) (31.56 g, 111.6 mmol, 1.04 equiv.) in dry PhMe (250 mL). The reaction mixture was stirred at 80 °C for 14 h and, after cooling down to RT, the organic phase was extracted with H$_2$O (3 × 100 mL) and the aqueous phase with DCM (3 × 100 mL). The organic phase was dried over Na$_2$SO$_4$ and concentrated under vacuum to give a yellow solid residue. The latter was dissolved in a small amount of DCM and, after adding EtOH, a precipitate was formed. After filtration and drying, the product was isolated as a yellow solid (33.4 g, 98.0 mmol, 91%), ^{1}H NMR (300 MHz, CDCl$_3$): 7.62 – 7.44 (m, 1H), 7.44 - 7.26 (m, 10H), 7.24 - 7.16 (m, 2H), 6.79 – 6.72 (m, 1H) ppm. ^{31}P{^{1}H } NMR (121 MHz, CDCl$_3$): -5.11 ppm. ^{1}H and ^{31}P NMR spectra matched the characterization in the literature.

Diethyl [2-(Diphenylphospheneyl)phenyl]phosphonate (**87**):
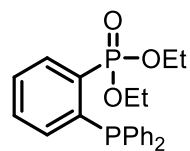
tBuLi (2.5 M in hexane, 27 mL, 67.5 mmol, 1.12 equiv.) was slowly added to a solution of **86** (20.6 g, 60.4 mmol, 1.00 equiv.) in THF (500 mL) at −78 °C. After stirring for 10 min at this temperature, diethyl chlorophosphate (12.54 g, 10.5 mL, 72.7 mmol, 1.2 equiv.) was added at −78 °C and the mixture was stirred for 14 h. After removal of the cooling bath, the reaction mixture was stirred for another 30 min at RT. The reaction was quenched through addition of saturated aqueous NH$_4$Cl-solution (150 mL). The aqueous phase was extracted with Et$_2$O (3 × 200 mL). The combined extracts were dried over Na$_2$SO$_4$, the solvent was removed under reduced pressure and, after purification by column chromatography (EtOAc/Hex 1:1), the pure product (16.78 g, 42.1 mmol, 70%) was isolated as a colorless oil. ^{1}H NMR (300 MHz, CDCl$_3$): 8.18 – 8.10 (m, 1H), 7.48 – 7.39 (m, 2H), 7.37 – 7.27 (m, 6H), 7.25 – 7.18 (m, 4H), 7.18 – 7.11 (m, 1H), 4.17 – 4.02 (m, 2H), 4.00 – 3.86 (m, 2H), 1.13 (t, $^3J_{H-H}$ = 7.0 Hz, 6H) ppm. ^{31}P{^{1}H } NMR (121 MHz,

CDCl$_3$): δ= 18.07, -9.03 ppm. ^{1}H and ^{31}P NMR spectra matched the characterization in the literature.

Diphenyl(2-phosphaneylphenyl)phosphane (**88**):
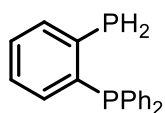
Trimethylchlorosilane (14.71 g, 17.0 mL, 135.4 mmol, 3.22 equiv.) was slowly added to a suspension of LiAlH$_4$ (5.8 g, 152.8 mmol, 3.63 equiv.) in THF (150 mL) *via* syringe at −70 °C. The reaction mixture was stirred for 10 min, warmed to RT and stirred for 1 h. Subsequently **87** (16.78 g, 42.1 mmol, 1.00 equiv.) in THF (150 mL) was slowly transferred into the reaction mixture and stirred for 18 h. The reaction was carefully quenched at 0 °C with H$_2$O (120 mL) and NaOH (1 M, 120 mL). The aqueous layer was extracted with Et$_2$O (150 mL, 3 × 80 mL). The organic phase was concentrated *in vacuo* to yield the product **88** as a white solid (10.0 g, 34 mmol, 81%), ^{1}H NMR (300 MHz, CDCl$_3$): 7.61 – 7.54 (m, 1H), 7.40 – 7.26 (m, 10H), 7.25 – 7.17 (m, 1H), 6.93–6.87 (m, 1H), 3.97 (dd, $^1J_{P-H}$ = 205.8, J_{H-H} = 11.9 Hz, 2H) ppm. ^{31}P{^{1}H } NMR (121 MHz, CDCl$_3$): -11.3 (d, $^3J_{P-P}$ = 98.0 Hz), -125.0 (d,$^3J_{P-P}$ = 98.0 Hz) ppm. ^{1}H and ^{31}P NMR spectra matched the characterization in the literature.

2-Chloro-1,3-dimethyl-4,5-dihydro-1*H*-imidazol-3-ium chloride (**90**):
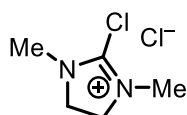
Oxalyl chloride (28,12 g, 19.0 mL, 221.5 mmol, 1.2 equiv.) was added to a solution of 1,3-dimethyl-2-imidazolidinone (**89**) (21.0 g, 20.0 mL, 184.0 mmol, 1.0 equiv.) in THF (80 mL). The reaction mixture was stirred under reflux for 14 h. After cooling down to rt, the precipitate was filtered off and washed with portions of Et$_2$O until the filtrate became a colorless solid. After drying, 10.24 g (60.6 mmol, 33%) of **90** was obtained. ^{1}H NMR (300 MHz, CD$_3$CN): 3.95 (s, 4H), 3.13 (s, 6H) ppm. ^{1}H NMR spectrum matched the characterization in the literature.
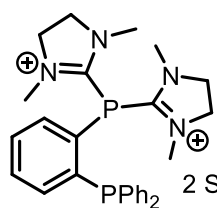
2-Chloro-1,3-dimethyl-4,5-dihydro-1*H*-imidazol-3-ium Tetrafluoroborate (**91**):
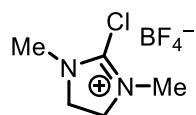
2-Chloro-1,3-dimethylimidazolium chloride **90** (10.24 g, 60.6 mmol, 1.0 equiv.) in MeCN (100 mL) was treated with KBF$_4$ (7.63 g, 60.6 mmol, 1.0 equiv.). The precipitate was filtered off, dissolved in a small amount of MeCN and recrystallized from Et$_2$O to afford a white solid (12.15 g, 55.1 mmol, 91%), ^{1}H NMR (300 MHz, CD$_3$CN): δ= 3.92 (s, 4H), 3.12 (s, 6H) ppm.^{1}H NMR spectrum matched the characterization in the literature.

2,2'-{[2-(diphenylphosphaneyl)phenyl]phosphanediyl}bis(1,3-dimethyl-4,5-dihydro-1*H*-imidazol-3-ium) Bis(hexafluoroantimonate) (**92**):

2-Chloro-1,3-dimethyl-4,5-dihydro-1*H*-imidazol-3-ium Tetrafluoroborate **91** (7.49 g, 34.0 mmol, 2.0 equiv.) and NEt$_3$ (3.63 g, 5.0 mL, 35.9 mmol, 2.11 equiv.) were added to the solution of **88** (5.0 g, 17.0 mmol, 1.00 equiv.) in THF (150 mL), and reaction mixture was stirred at 60°C for 14 h. The resulting yellowish precipitate was filtered off and washed with CHCl$_3$. After removing the solvents *in vacuo*, the solid residue was dissolved in MeCN (50 mL) and treated with NaSbF$_6$ (9.67 g, 37.4 mmol, 2.20 equiv.). The reaction mixture was stirred overnight at RT, the precipitate was filtered off and washed with DCM. After removal of the solvents *in vacuo*, the product was dried to afford **92** as a white solid (12.44 g, 12.93 mmol, 76%), ^{1}H NMR (300 MHz, CD$_3$CN): δ= 7.78 – 7.66 (m, 4H), 7.53 – 7.45 (m, 6H), 7.36 – 7.27 (m, 4H), 3.82 (s, 8H), 2.97 (s, 12H) ppm. ^{31}P{^{1}H } NMR (121 MHz, CD$_3$CN): δ= -11.3 (d, $^3J_{\text{P-P}}$ = 212.8 Hz), -46.8 (d, $^3J_{\text{P-P}}$ = 212.8 Hz) ppm. HRMS calcd. for C$_{28}$H$_{34}$N$_4$SbF$_6$P$_2$$^+$ [M – SbF$_6$]$^+$: 723.11956; found: 723.11904; IR (neat, cm^{-1}) $\tilde{v}$: 422, 456, 518, 653, 699, 745, 767, 934, 998, 1090, 1107, 1300, 1335, 1412, 1434, 1445, 1521, 1576, 3103.

2,2'-{[2-(Diphenylphosphaneyl)phenyl]phosphanediyl}bis(1-methylpyridin-1-ium) Bis(hexafluoroantimonate) (**97**):
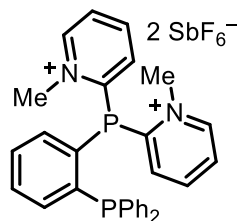
2-Chloro-*N*-methylpyridinium tetrafluoroborate (**94**, 7.32 g, 34.0 mmol, 2.0 equiv.) and NEt₃ (3.63 g, 5.0 mL, 35.9 mmol, 2.11 equiv.) (5 mL, 35.9 mmol, 2.10 equiv.) were added to a solution of **88** (5.0 g, 17.0 mmol, 1.00 equiv.) in THF (150 mL) and stirred at 60 °C for14 h. The resulting yellow precipitate was filtered and washed with CHCl₃. After removing the solvent *in vacuo*, the solid was dissolved in MeCN (50 mL) and treated with NaSbF₆ (9.67 g, 37.4 mmol, 2.20 equiv.). The reaction mixture was stirred over night at rt. The precipitate was filtered and washed with DCM. After removal of solvent *in vacuo*, the product was dried to afford a white crystalline solid (7.71 g, 8.1 mmol, 48%).
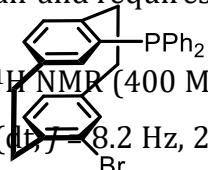
¹H NMR (300 MHz, CD₃CN) δ= 8.94 – 8.79 (m, 2H), 8.27 (td, *J* = 8.0, 1.5 Hz, 2H), 8.04 (ddd, *J* = 7.8, 6.0, 1.6 Hz, 2H), 7.71 (td, *J* = 7.6, 1.3 Hz, 1H), 7.57 (d, *J* = 7.5 Hz, 1H), 7.45 (dd, *J* = 8.0, 1.5 Hz, 2H), 7.41 – 7.27 (m, 6H), 7.28 – 7.10 (m, 4H), 7.12 (dt, *J* = 8.7, 4.4 Hz, 1H), 4.30 (d, *J* = 2.2 Hz, 6H) ppm. ³¹P NMR (162 MHz, CD₃CN) δ = -12.45 (d, *J* = 181.9 Hz), -23.85 (d, *J* = 182.4 Hz) ppm. ¹³C NMR (75 MHz, CDCl₃) δ =145.0, 140.7, 136.5, 134.9, 134.7, 130.2, 89.6, 54.3, 21.8, 20.5. HRMS calcd. for C₃₀H₂₈F₆N₂P₂Sb⁺ [M – SbF₆]⁺ 713.0665; *found* 713.0669. IR (neat, cm⁻¹) ṽ: 457, 541, 609, 692, 1063, 1118, 1286, 1386, 1437, 1634, 3360.

4,4'-((2-(λ¹-phosphaneyl)phenyl)phosphanediyl)bis(1-ethylpyridin-1-ium) Bis-(hexafluoroantimonate) (**98**):
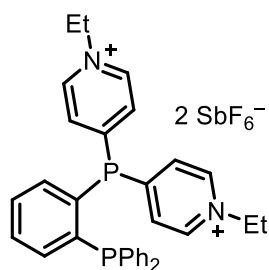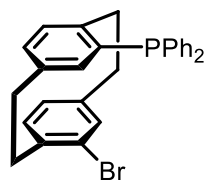
4-Iodo-*N*-methylpyridinium trifluoromethanesulfonate (**96**, 13.0 g, 34.0 mmol, 2 equiv.) and NEt₃ (3.63 g, 5.0 mL, 35.9 mmol, 2.10 equiv.) were added to a solution of **88** (5.0 g, 17.0 mmol, 1.00 equiv.) in THF (150 mL), and reaction mixture was stirred at 60 °C for 14 h. The resulting yellow precipitate was

filtered and washed with CH_2Cl_2 and $CHCl_3$. After removing the solvent *in vacuo*, the solid was dissolved in MeCN (50 mL) and treated with $NaSbF_6$ (9.67 g, 37.4 mmol, 2.20 equiv.). The reaction mixture was stirred over night at rt. The precipitate was filtered and washed with DCM. After removal of solvent *in vacuo*, the product was dried to afford a yellow solid (4.3 g, 4.40 mmol, 26%). The compound is unstable on air and requires storage under inert conditions.

^{1}H NMR (400 MHz, CD_3CN) δ= 8.61 (d, J = 6.2 Hz, 4H), 7.73 (d, J = 5.1 Hz, 4H), 7.53 (d, J = 8.2 Hz, 2H), 7.42 – 7.14 (m, 12H) , 4.56 (q, J = 7.3 Hz, 4H), 1.58 (t, J = 7.3 Hz, 6H) ppm. ^{31}P NMR (162 MHz, CD_3CN) δ = -10.87 (d, J = 152.1 Hz), -12.19 (d, J = 152.5 Hz) ppm. ^{13}C NMR (75 MHz, CD_3CN) δ =164.1, 140.6, 136.6, 136.1, 130.2, 129.6, 125.4, 120.7, 21.6, 11.4. HRMS calcd. for $C_{32}H_{32}F_6N_2P_2Sb^+$ [M – SbF_6]$^+$ 741.0978; *found* 741.0986. IR (neat, cm^{-1}) $\tilde{v}$: 472, 544, 611, 685, 1112, 1289, 1388, 1636, 3357.

4-Bromo-12-diphenylphosphino-*p*-cyclophane (**100**):

*n*BuLi (2.5 M in hexane, 4 mL, 10 mmol) was slowly added to a solution of 4,12-dibromo-*p*-cyclophane (**99**, 3.66 g, 10.0 mmol, 1.00 equiv.; kindly provided by Dr. Sergei I. Kozhushkov and Marvin Blaue) in THF (100 mL) at –78 °C and stirred for 1 h. Subsequently, chlorodiphenylphosphine (11.0 mmol, 2.43 g) was added at –78 °C, and the reaction mixture was stirred for additional 14 h at this temperature and then, after removal of the cooling bath, for another 30 min at RT. The reaction was quenched through addition of saturated aqueous NH_4Cl solution (50 mL). The aqueous phase was extracted with Et_2O (3 × 200 mL) and dried over Na_2SO_4. The solvent was removed under low pressure and after purification by column chromatography (EtOAc/Hex 1:5) the pure product **100** (3.16 g, 6.7 mmol, 67%) was isolated as a colorless solid.

^{1}H NMR (300 MHz, $CDCl_3$) δ = 7.54 (ddt, J = 9.5, 5.7, 2.1 Hz, 2H), 7.45 – 7.15 (m, 8H), 6.69 – 6.43 (m, 4H), 6.35 (dd, J = 8.1, 1.8 Hz, 2H), 3.52 – 3.24 (m, 3H), 3.20 – 2.63 (m, 5H) ppm. ^{31}P NMR (121 MHz, $CDCl_3$) δ = -1.60 ppm. This compound was not fully characterized due to time limitations during the doctoral programme.

Diethyl (12-Diphenylphosphino-*p*-cyclophan-4-yl)phosphonate (**101**):
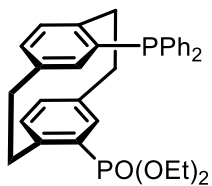
*t*BuLi (2.5 M in hexane, 2 mL, 5 mmol) was slowly added to a solution of **100** (2.36 g, 5.0 mmol, 1.00 equiv.) in THF (50 mL) at −78 °C and stirred for 1 h. Subsequently, diethyl chlorophosphate (949 mg, 795 μL, 5.5 mmol, 1.1 equiv.) was added at −78 °C, and the reaction mixture was stirred for additional 14 h at this temperature and then, after removal of the cooling bath, for another 30 min at RT. The reaction was quenched through addition of saturated aqueous NH_4Cl solution (25 mL). The aqueous phase was extracted with Et_2O (3 × 100 mL) and dried over Na_2SO_4. The solvent was removed under low pressure and after purification through column chromatography (EtOAc/Hex 1:1) the pure product **101** (1.17 g, 2.21 mmol, 44%) was isolated as a white waxy solid.

^{1}H NMR (300 MHz, CDCl$_3$) δ= 7.81 (dt, *J* = 15.7, 1.5 Hz, 1H), 7.55 (dq, *J* = 8.5, 3.0, Hz, 2H), 7.40 – 7.18 (m, 8H), 6.76 – 6.51 (m, 4H), 6.10 (dd, *J* = 8.4, 1.8 Hz, 1H), 4.14 (dp, *J* = 9.9, 6.9 Hz, 1H), 4.02 – 3.77 (m, 3H), 3.57 (ddd, *J* = 12.7, 9.9, 7.2 Hz, 2H), 3.36 (dd, *J* = 13.6, 9.8 Hz, 1H), 3.16 (dd, *J* = 13.1, 10.2 Hz, 1H), 3.06 – 2.85 (m, 3H), 2.75 (dddd, *J* = 13.0, 9.9, 7.2, 2.2 Hz, 1H), 1.17 (dt, *J* = 10.9, 7.1 Hz, 6H) ppm. ^{31}P NMR (121 MHz, CDCl$_3$) δ = 18.27, -0.85 ppm. This compound was not fully characterized due to time limitations during the doctoral programme.

Diphenyl[4^3-phosphaneyl-1,4(1,4)-dibenzenacyclohexaphane-1^2-yl]phosphane   or (12-Diphenylphosphino-*p*-cyclophan-4-yl)phosphane (**102**):
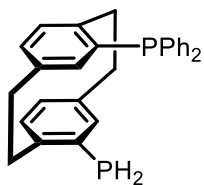
Trimethylchlorosilane (329 mg, 380 μL, 3.0 mmol) was slowly added to a suspension of $LiAlH_4$ (142.6 mg, 3.8 mmol) in THF (15 mL) *via* syringe at −70 °C. The reaction mixture was stirred for 10 min, then warmed to RT and stirred for 1 h. Subsequently **101** (544 mg, 1.0 mmol, 1.00 equiv.) in THF (10 mL) was slowly cannulated into the reaction mixture and stirred for 18 h. The reaction was carefully quenched at 0 °C with H_2O (5 mL) and NaOH (1 M, 5 mL). The aqueous layer was extracted with Et_2O (15 mL, 3

× 10 mL). The organic phase was concentrated *in vacuo* to yiled the product **102** (431 mg, 0.98 mmol, 98%) as a white solid, .

^{1}H NMR (300 MHz, CDCl$_3$) δ = 7.63 (ddt, *J* = 8.0, 5.6, 1.8 Hz, 2H), 7.47 – 7.37 (m, 2H), 7.33 (d, *J* = 8.6 Hz, 1H), 7.19 – 7.06 (m, 4H), 7.03 – 6.93 (m, 3H), 6.43 (dt, *J* = 7.9, 1.6 Hz, 1H), 6.37 – 6.21 (m, 5H), 3.97 – 3.74 (m, 1H), 3.62 – 3.09 (m, 4H), 2.88 – 2.42 (m, 5H), ppm. ^{31}P NMR (121 MHz, C CDCl$_3$) δ = -2.28, -129.16 ppm. This compound was not fully characterized due to time limitations during the doctoral programme.

2,2'-[(4^3-(Diphenylphosphaneyl)-1,4(1,4)-dibenzenacyclohexaphane-1^2-yl)phos-phanediyl]bis(1,3-dimethyl-4,5-dihydro-1H-imidazol-3-ium)   Bis-(hexafluoroanti-monate) (**103**):
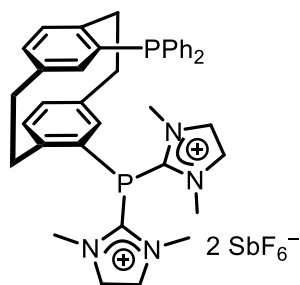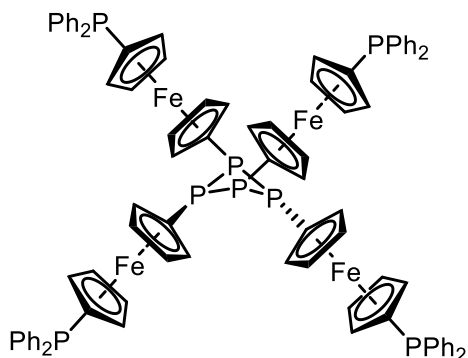

2-Chloro-1,3-dimethyl-4,5-dihydro-1*H*-imidazol-3-ium Tetrafluoroborate (**91**, 440 mg, 2.0 mmol, 2 equiv.) and NEt$_3$ (223 mg, 307 μL, 2.2 mmol, 2.10 equiv.) were added to the solution of **102** (431 mg, 1.0 mmol, 1.00 equiv.) in THF (5 mL), and reaction mixture was stirred at 60°C for 14 h. The resulting white precipitate was filtered and washed with THF. After removing the solvent *in vacuo*, the solid residue was dissolved in CH$_3$CN (2 mL) and treated with NaSbF$_6$ (569 mg, 2.2 mmol, 2.20 equiv.). The reaction mixture was stirred overnight at RT. The precipitate was filtered and washed with CH$_2$Cl$_2$. After removal of solvent *in vacuo*, the product was dried to afford **103** as a white solid (752 mg, 0.69 mmol, 69%), .

^{1}H NMR (300 MHz, CD$_3$CN) δ = 7.75 (s, 1H), 7.31 (q, *J* = 36.4, 31.7 Hz, 6H), 7.01 – 6.48 (m, 2H), 6.13 (d, *J* = 11.8 Hz, 1H), 4.20 (s, 2H), 3.80 (d, *J* = 30.4 Hz, 6H), 3.30 – 2.45 (m, 20H), 1.86 (s, 4H), 1.20 (tt, *J* = 7.9, 4.4 Hz, 8H) ppm. ^{31}P NMR (121 MHz, CD$_3$CN) δ = -0.33, -41.73 ppm. This compound was not fully characterized due to time limitations during the doctoral programme.

Tetrakis(1'-diphenylphosphinoferrocen-1-yl)-1λ^2,2λ^2,3λ^2,4λ^2-tetraphosphetane (**108**):


1-(Diphenylphosphino)-1'-phosphino-ferrocene (**107**, 910 mg, 2.26 mmol; prepared as indicated above in Figure 60 using the literature procedure[96]) and 2-Chloro-1,3-dimethyl-4,5-dihydro-1*H*-imidazol-3-ium Tetrafluoroborate (**91**, 1.0 g, 4.53 mmol, 2 equiv.) were added to flame-dried schlenk flask under nitrogen atmosphere. Anhydrous THF (20 mL) was added followed by dropwise addition of freshly distilled NEt$_3$ (454 mg, 625 µL, 4.50 mmol). The reaction mixture was stirred at 60 °C for 14 h. Then all volatiles were removed *in vacuo*, the remaining solid was re-dissolved in ethyl acetate and filtered over a pad of silica gel. Column chromatography (EtOAc/Hex 1:9) afforded the product **108** (796 mg, 88%) as a brick red solid. Crystals suitable for X-ray analysis were obtained by slow evaporation of the DCM solution.

^{1}H NMR (400 MHz, CD$_2$Cl$_2$) δ = 7.42 – 7.17 (m, 40H), 4.38 (t, *J* = 1.8 Hz, 8H), 4.31 (t, *J* = 1.8 Hz, 8H), 4.27 (t, *J* = 1.8 Hz, 8Hz), 4.10 (q, *J* = 1.9 Hz, 8H) ppm. ^{31}P NMR (162 MHz, CD$_2$Cl$_2$) δ = -17.39, -71.53 ppm. ^{31}P NMR (162 MHz, CD$_2$Cl$_2$) δ = -17.39, -71.53. ^{13}C NMR (101 MHz, CD$_2$Cl$_2$) δ = 139.1, 139.0, 133.5, 133.3, 128.5, 128.2, 128.1, 77.1, 76.9, 75.5, 73.4, 71.6 ppm. HRMS calcd. for C$_{88}$H$_{72}$Fe$_4$P$_4$ [M]$^+$ 1600.0933; *found* 1600.0938. IR (neat, cm^{-1}) $\tilde{v}$: 417, 693, 738, 818, 1025, 1216, 1346, 1540, 1738.

2,2'-{[2-(Diphenylphosphaneyl)phenyl]phosphanediyl}bis(1-methylpyridin-1-ium)/Tetracarbonylmolybdenum Complex Bis(hexafluoroantimonate) (**113**):
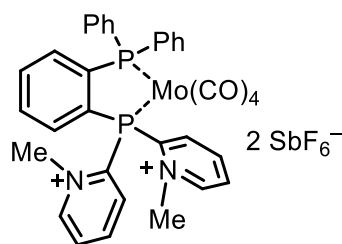
Mo(CO)$_6$ (26.4 mg, 100.0 μmol, 1.2 equiv.) and **97** (78.9 mg, 83.3 μmol, 1.0 equiv.) were suspended in dry THF (2 mL) and stirred for 1 hour at reflux. After the filtration over a Schott filter, the product **113** (90.4 mg, 78 μmol, 94%) was obtained as a white solid, .

^{1}H NMR (400 MHz, CD$_3$CN) δ = 8.89 (s, 1H), 8.57 (t, J = 8.0 Hz, 1H), 8.27 (t, J = 7.0 Hz, 1H), 8.17 – 7.96 (m, 2H), 7.94 – 7.82 (m, 3H), 7.77 (tdd, J = 6.8, 3.3, 2.0 Hz, 1H), 7.60 – 7.24 (m, 7H), 7.09 (t, J = 6.9 Hz, 1H), 4.40 (d, J = 83.5 Hz, 6H) ppm. ^{31}P NMR (75 MHz, CD$_3$CN) δ = 32.05 (d, J = 87.3 Hz), 14.45 (d, J = 87.3 Hz) ppm. ^{13}C NMR (282 MHz, CD$_3$CN) δ = 215.1, 213.4, 208.7, 206.1, 152.2, 151.3, 146.5, 146.4, 143.0, 136.8, 136.4, 135.6, 135.4, 135.3, 133.9, 132.4, 132.3, 131.8, 131.6, 130.9, 130.8, 130.7, 129.8, 129.1, 50.0, 48.6 ppm. HRMS calcd. for C$_{33}$H$_{28}$F$_6$MoN$_2$O$_3$P$_2$Sb$^+$ [M – CO –SbF$_6$]$^+$ 894.9566; *found* 894.9572. IR (neat, cm^{-1}) $\tilde{v}$: 517, 565, 654, 764, 863, 1026, 1094, 1157, 1435, 1479, 1603, 1911, 2031.

Dirhodium Complex **117**:
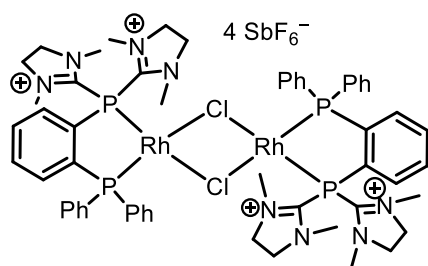
[RhCl(COD)]$_2$ (**116**, 5.0 mg, 10 μmol, 0.75 equiv. [Rh]) and **92** (24.7 mg, 25.7 μmol) were dissolved in CH$_2$Cl$_2$ (2 mL) and stirred at rt overnight. After removal of the solvent in vacuo, the solid thus obtained was washed with pentane affording the desired product **117** as an orange solid (26.3 mg, 11.9 μmol, 92%). Orange crystals of **117** suitable for X-ray crystallography were directly obtained by cooling CH$_3$CN/CH$_2$Cl$_2$/Et$_2$O solutions of the title compound. ^{1}H and ^{31}P NMR spectra of solutions of **117** in CD$_3$Cl showed two species, with **117** being the major component. ^{1}H NMR (400 MHz, CD$_3$CN): δ = 8.05 – 7.45 (m, 14H), 3.99 (s, 8H), 3.21 (s, 12H) ppm. ^{31}P NMR (162 MHz, CD$_3$CN): δ = 74.08 – 70.58 (m), 34.66 (d, J = 217.7 Hz), 23.04 (d, J = 38.1 Hz) ppm. ^{13}C NMR (101 MHz, CD$_3$CN): δ = 155.88, 135.07, 134.92, 134.71,

134.01, 133.94, 133.53, 133.38, 131.57, 130.88, 128.73, 52.41, 50.59, 47.05, 36.82, 34.05, 33.85, 22.05, 13.33, 8.26 ppm. HRMS calcd. for $C_{28}H_{34}ClF_6N_4P_2RhSb^+$ [M/2 – SbF$_6$]$^+$ 860.9939; *found* 863.0102.

Dirhodium Complex **119**:
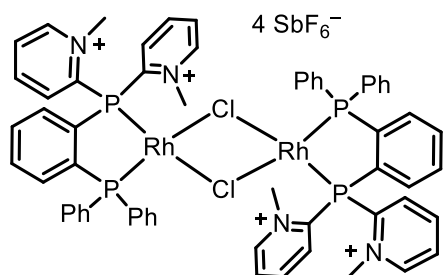
[RhCODCl]$_2$ (**116**, 49.3 mg, 100.0 μmol, 2.88 equiv. [Rh]) and **97** (66.0 mg, 69.4 μmol, 1.0 equiv.) have been dissolved in DCM (2 mL) and stirred for 1 h at RT. The resulting red precipitate was washed with dry Et$_2$O. After the filtration, the product **119** was obtained as a red solid (59.0 mg, 27.1 μmol, 78%).

^{1}H NMR (400 MHz, CD$_3$CN) δ = 8.94 (d, J = 45.8 Hz, 2H), 8.53 (d, J = 8.4 Hz, 1H), 8.29 (s, 1H), 7.89 (d, J = 54.4 Hz, 6H), 7.65 (d, J = 40.4 Hz, 2H), 7.57 – 7.34 (m, 7H), 7.47 – 7.15 (m, 4H), 6.80 (s, 1H), 5.03 – 4.54 (m, 6H) ppm. ^{31}P NMR (162 MHz, CD$_3$CN) δ = 69.56 (dd, J = 149.6, 42.9 Hz), 61.25 (d, J = 193.5 Hz) ppm. ^{13}C NMR (101 MHz, CD$_3$CN) δ = 152.2, 151.3, 146.6, 146.4, 136.6, 136.4, 135.6, 135.5, 135.3, 133.9, 132.5, 132.4, 131.8, 131.7, 131.0, 130.9, 130.7, 129.8, 129.1, 50.1, 48.6 ppm. HRMS calcd. for $C_{30}H_{28}ClF_6N_2P_2SbRh^+$ ([M/2 – SbF$_6$]$^+$) 850.9408; *found* 850.9416. IR (neat, cm^{-1}) $\tilde{v}$: 497, 564, 617, 692, 752, 930, 1034, 1215, 1410, 1536, 1580, 2118, 2296, 2970.

Iridium complex **122**:
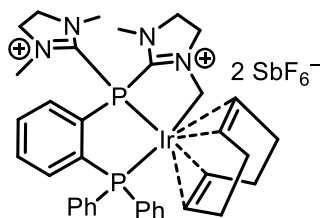
[IrcodCl]$_2$ (**121**, 66.3 mg, 98.7 μmol, 2.38 equiv [Ir]) and **92** (80.0 mg, 83.2 μmol, 1.0 equiv.) were dissolved in DCM (2 mL) and stirred for 2 minutes at rt. After the filtration over a Schott filter, the product **122** was obtained as a red solid (87.0 mg, 69,2 μmol, 83%). ^{1}H NMR (400 MHz, CD$_3$CN): 8.36 – 8.28 (m, 1H), 7.98 – 9.92 (m, 1H), 7.90 – 7.83 (m, 1H), 7.82 – 7.76 (m, 1H), 7.70 –

7.62 (m, 2H), 7.59 – 7.52 (m, 3H), 7.42 – 7.36 (m, 3H), 7.16 – 7.08 (m, 1H), 4.36 – 3.95 (m, 6H), 3.65 (s, 2 H), 3.49 – 3.16 (m, 12H), 2.89 – 2.76 (m, J = 12.3 Hz, 1H), 2.76 – 2.71 (m, 3H), 2.61 – 2.47 (m, 1H), 2.33 – 2.23 (m, 1H), 1.83 – 1.69 (m, 2H) ppm. ^{13}C NMR (101 MHz, CD$_3$CN): δ = 139.0, 138.9, 135.0, 134.9, 134.2, 134.1, 132.1, 132.0, 131.60, 131.6, 131.0, 131.0, 129.9, 129.9, 129.8, 129.8, 60.3, 54.0, 54.0, 50.4, 50.3, 40.1, 40.0, 39.6, 37.3, 37.3, 35.9, 29.7 ppm. ^{31}P{^{1}H } NMR (162 MHz, CD$_3$CN): δ = 32.0 (d, $^3J_{P-P}$ = 87.2 Hz), 14.5 (d, $^3J_{P-P}$ = 87.2 Hz) ppm. HRMS calculated m/z for C$_{28}$H$_{33}$IrN$_4$P$_2^+$ [M – cod – 2 SbF$_6$]$^+$: 340.0899; $found$ 340.0890. IR (neat, cm^{-1}) $\tilde{v}$: 528, 655, 767, 925, 1026, 1293, 1517.

Iridium complex **124**:
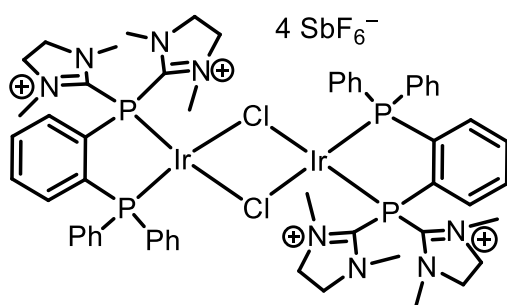
[Ir(coe)$_2$Cl]$_2$ (**123**, 86.4 mg, 96.4 μmol, 2.32 equiv. [Ir]) and **92** (80 mg, 83.2 μmol, 1.0 equiv.) were dissolved in DCM (2 mL) and stirred for two minutes at RT. The product was obtained as a red solid (95.0 mg, 40.0 μmol, 96%). After the dimer was dissolved in a mixture of CH$_2$Cl$_2$ and CH$_3$CN and crystallized from Et$_2$O, its structure was verified through X-ray diffraction measurements. ^{1}H NMR (400 MHz, CD$_3$CN): 8.05 – 7.94 (m, 1H), 7.93 – 7.85 (m, 1H), 7.82 – 7.67 (m, 6H), 7.59 – 7.44 (m, 6H), 3.94 (s, 8H), 3.18 (s, 12H) ppm. ^{31}P{^{1}H} NMR (162 MHz, CD$_3$CN): 39.2 (d, $^3J_{P-P}$ = 9.3 Hz), 37.2 (d, $^3J_{P-P}$ = 9.5 Hz), 5.1 (d, $^3J_{P-P}$ = 9.3 Hz), -3.3 (d, $^3J_{P-P}$ = 9.5 Hz) ppm

Rhodium complex **126**:
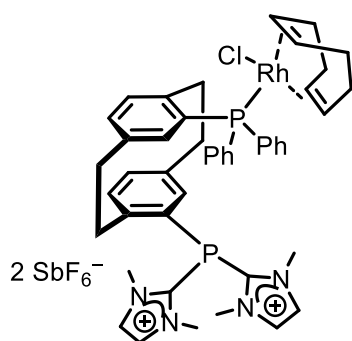
[Rh(cod)Cl]₂ (**116**, 49.3 mg, 100.0 μmol, 2.36 equiv. [Rh]) and **103** (92.3 mg, 84.7 μmol, 1.0 equiv.) were dissolved in DCE (2 mL) and stirred for 2 minutes at rt. After the filtration over a Schott filter and washing with diethyl ether (1 mL), the product **126** was obtained as an orange solid (87.7 mg, 65.6 μmol, 77%), .

^{1}H NMR (400 MHz, CD₃CN) δ = 8.20 (s, 2H), 7.79 – 7.51 (m, 5H), 7.39 – 6.87 (m, 8H), 6.67 (d, J = 9.5 Hz, 3H), 5.96 – 5.57 (m, 2H), 5.47 (s, 3H), 4.34 – 3.65 (m, 13H), 3.57 – 2.20 (m, 28H), 2.17 – 1.78 (m, 11H), 1.49 – 1.16 (m, 2H), 0.91 (t, J = 6.8 Hz, 1H) ppm. ^{31}P NMR (162 MHz, CD₃CN) δ = 29.62 (d, J = 147.8 Hz), -41.28.

Iridium complex **127**:
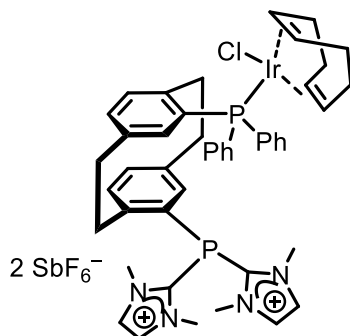
[Ir(cod)Cl]₂ (67.1 mg, 100.0 μmol, 2.36 equiv. [Ir]) and **103** (92.3 mg, 84.7 μmol, 1.0 equiv.) were dissolved in DCE (2 mL) and stirred for 2 minutes at rt. After the filtration over a Schott filter and washing with Et₂O (1 mL), the product **127** was obtained as an orange solid (118.4 mg, 81 μmol, 99%). ^{1}H NMR (400 MHz, CD₃CN) δ = 7.57 (ddd, J = 8.3, 7.4, 1.6 Hz, 2H), 7.52 – 7.44 (m, 2H), 7.42 – 7.30 (m, 6H), 7.23 (d, J = 11.4 Hz, 1H), 7.06 – 6.93 (m, 2H), 6.81 (dd, J = 7.8, 1.9 Hz, 1H), 6.71 (dd, J = 7.8, 4.7 Hz, 1H), 6.25 (dt, J = 10.8, 1.7 Hz, 1H), 4.30 (s, 4H), 4.06 – 3.80 (m, 6H), 3.73 – 3.63 (m, 1H), 3.58 (dd, J = 14.3, 9.6 Hz, 1H), 3.36 – 2.90 (m, 15H), 2.84 – 2.57 (m, 9H) ppm. ^{31}P NMR (162 MHz, CD₃CN) δ = -0.45, -43.07 ppm.

Compounds **74a** to **74i** were obtained using the following general procedure 1 (GP1):

Diphosphine ligand **92** (9.6 mg, 10 μmol), [RhCl(CO)$_2$]$_2$ (1.94 mg, 5 μmol) and KB(C$_6$F$_5$)$_4$ (14.4 mg, 20 μmol) were weighted on air in the 4-mL flame-dried microwave vial equipped with magnetic stirring bar. The vial was transferred to the nitrogen-flushed glovebox, and DCE (1 mL) was added in one portion. The brick red solution thus obtained was stirred for 15 minutes at room temperature inside the glovebox. After this, respective phenylbutadiene derivative (200 μmol) and the nucleophile (220 μmol) were added in one portion. The microwave vial was tightly sealed inside the glovebox and transferred to the preheated (70 °C) oil bath on the heating plate outside the glovebox. The reaction mixture was stirred at this temperature for 18 h. After cooling down to the room temperature, the reaction mixture was transferred to a round-bottom flask, and 300 mg of silica gel was added in one portion. Solvent was removed *in vacuo*, the pre-absorbed mixture was transferred to the chromatography column and purified by column chromatography (SiO$_2$, EtOAc/pentane/cyclohexane gradient) affording the desired hydroarylation product **74**.

(*E*)-3-(4-Phenylbut-3-en-2-yl)-1*H*-indole (**74a**):
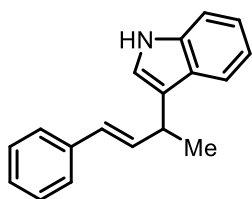
Colorless oil (41.0 mg, 165.7 μmol, 83%). ^{1}H NMR (400 MHz, CDCl$_3$): δ = 7.95 (br, 1H), 7.69 (dd, *J* = 7.9 Hz, *J* = 0.6 Hz, 1H), 7.40 – 7.35 (m, 3H), 7.31 – 7.27 (m, 2H), 7.23 – 7.17 (m, 2H), 7.10 (ddd, *J* = 7.9 Hz, *J* = 7.8 Hz, *J* = 0.6 Hz, 1H), 7.03 (dd, *J* = 2.3 Hz, *J* = 0.6 Hz, 1H), 6.51 – 6.48 (m, 2H), 3.95 (p, *J* = 6.8 Hz, 1H), 1.58 (d, *J* = 7.0 Hz, 3H) ppm. ^{13}C NMR (100 MHz, CDCl$_3$): δ = 137.9, 136.7, 135.6, 128.6, 128.3, 127.0, 126.9, 126.3, 122.1, 120.6, 120.5, 119.8, 119.4, 111.2, 34.4, 20.8 ppm. HRMS *calcd.* for C$_{18}$H$_{18}$N$^+$ [M + H]$^+$: 248.14338; *found* 248.14337. IR (neat, cm^{-1}) $\tilde{v}$: 424, 497, 581, 693, 742, 765, 807, 928, 966, 1009, 1095, 1221, 1244, 1337, 1417, 1455, 1492, 1598, 1618, 2869, 2927, 2963, 3024, 3055, 3417.

(*E*)-3-[4-(Anthracen-9-yl)but-3-en-2-yl]-1*H*-indole (74b):
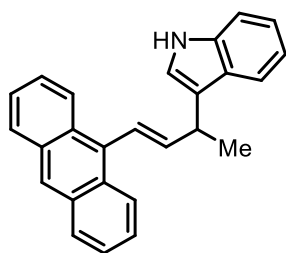
Pale yellow solid (66.0 mg, 190 μmol, 95%). ^{1}H NMR (400 MHz, C$_6$D$_6$) δ = 8.44 – 8.40 (m, 2H), 8.15 (s, 1H), 7.93 – 7.89 (m, 1H), 7.83 – 7.80 (m, 2H), 7.29 – 7.24 (m, 6H), 7.11 – 7.08 (m, 2H), 6.62 (s, 1H), 6.53 (d, *J* = 2.4 Hz, 1H), 6.21 (dd, *J* = 16.1, 7.0 Hz, 1H), 4.05 – 3.99 (m, 1H), 1.58 (d, *J* = 7.0 Hz, 3H) ppm.

^{13}C NMR (100 MHz, C$_6$D$_6$) δ = 143.97, 132.06, 130.30, 128.89, 126.67, 126.36, 125.34, 125.23, 124.46, 122.30, 120.43, 120.10, 119.60, 111.49 ppm. HRMS *calcd.* for C$_{26}$H$_{21}$N$^+$: 347.1674; *found* 347.1667. IR (neat, cm^{-1}) $\tilde{v}$: 668, 737, 1012, 1338, 1351, 1417, 1456, 1488, 1621, 1654, 1670, 1683, 1698, 2341, 2360, 2869, 2926, 2964, 3049, 3421, 3627, 3733.

(*E*)-2,4-Dimethoxy-1-(4-phenylbut-3-en-2-yl)benzene (74c):
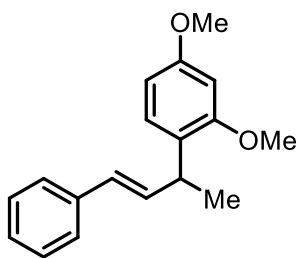
Colorless oil (37.8 mg, 140.9 μmol, 70% yield). ^{1}H NMR (400 MHz, CDCl$_3$,): δ = 7.37 – 7.34 (m, 2H), 7.30 – 7.27 (m, 2H), 7.20 – 7.15 (m, 1H), 7.10 (d, *J* = 8.2 Hz, 1H), 6.47 – 6.40 (m, 4H), 4.00 – 3.97 (m, 1H), 3.83 (s, 3H), 3.80 (s, 3H), 1.39 (d, *J* = 7.0 Hz, 3H) ppm. ^{13}C NMR (100 MHz, CDCl$_3$,): δ = 159.3, 157.9, 138.1, 135.4, 128.6, 128.1, 128.0, 126.9, 126.7, 126.2, 104.3, 98.9, 55.6, 55.5, 34.8, 20.3 ppm. HRMS *calcd.* for C$_{18}$H$_{21}$O$_2^+$ [M + H]$^+$: 269.153610 ; *found* 269.135605. IR (neat, cm^{-1}) $\tilde{v}$: 495, 634, 692, 737, 798, 909, 966, 1034, 1117, 1156, 1179, 1206, 1259, 1290, 1417, 1453, 1503, 1586, 1610, 2835, 2928, 2959, 3024.

(*E*)-1,3-Dimethoxy-5-methyl-2-(4-phenylbut-3-en-2-yl)benzene (74d):
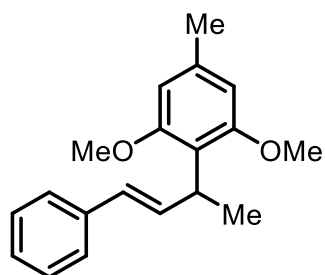
Colorless oil (48.0 mg, 170.0 μmol, 85%). ^{1}H NMR (400 MHz, CDCl$_3$) δ = 7.38 – 7.33 (m, 3H), 7.31 – 7.24 (m, 4H), 7.23 – 7.13 (m, 1H), 6.71 (dd, *J* = 15.9, 7.4 Hz, 1H), 4.29 (td, *J* = 7.2, 1.3 Hz, 1H), 3.83 (s, 6H), 2.35 (s, 3H), 1.45 (d, *J* = 7.1 Hz, 3H) ppm. ^{13}C NMR (101 MHz, CDCl$_3$) δ = 158.0, 138.4,

137.1, 135.5, 128.2, 127.5, 126.3, 126.0, 119.0, 105.5, 55.8, 32.7, 21.8, 19.2 ppm. HRMS *calcd.* for $C_{19}H_{23}O_2^+$ [M + H]$^+$: 283.1693; *found* 283.1693. IR (neat, cm^{-1}) $\tilde{v}$: 669, 801, 882, 943, 963, 1008, 1027, 1167, 1253, 1453, 2341, 2360, 2872, 2927, 2966, 3024.

(*E*)-1-fluoro-3,5-dimethoxy-2-(4-phenylbut-3-en-2-yl)benzene (**74e'**) and (*E*)-5-Fluoro-1,3-dimethoxy-2-(4-phenylbut-3-en-2-yl)benzene (**74e''**):
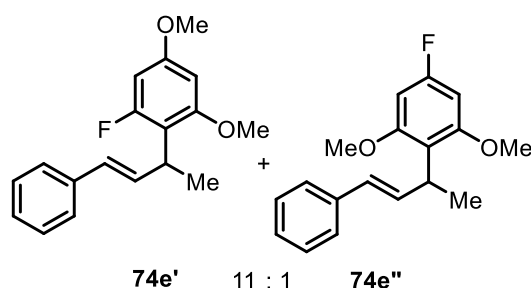

Colorless oil (39.0 mg, 136.2 μmol, 68%). ^{1}H NMR (400 MHz, CDCl$_3$) δ = 7.35 – 7.30 (m, 2H), 7.28 – 7.21 (m, 3H), 7.18 – 7.11 (m, 1H), 6.54 (ddd, *J* = 15.9, 7.3, 2.1 Hz, 1H), 6.36 (d, *J* = 15.9 Hz, 1H), 6.27 – 6.18 (m, 2H), 4.13 – 4.04 (m, 1H), 3.82 (s, 1H), 3.80 (s, 2H), 3.75 (s, 3H), 1.46 – 1.37 (m, 3H) ppm. ^{19}F NMR (282 MHz, CDCl$_3$) δ = -100.01 ppm. ^{13}C NMR (101 MHz, C$_6$D$_6$) δ = 163.6, 161.2, 159.7, 159.6, 158.9, 158.7, 156.7, 138.0, 138.0, 134.1, 134.0, 133.9, 128.8, 128.3, 126.7, 126.2, 95.2, 95.2, 93.5, 93.2, 55.1, 54.9, 54.6, 32.7, 19.6, 19.6 ppm. HRMS *calcd.* for $C_{18}H_{19}FO_2^+$ [M]$^+$: 286.1369; *found* 286.1372. IR (neat, cm^{-1}) $\tilde{v}$: 745, 803, 820, 964, 1017, 1053, 1198, 1213, 1422, 1438, 1454, 1493, 1584, 1620, 2360, 2934, 2961.

(*E*)-9-[3-(Azulen-1-yl)but-1-en-1-yl]anthracene (**74g**):
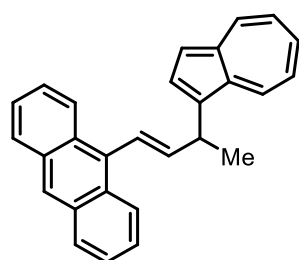
Blue solid (48.8 mg, 136.1 μmol, 68%). ^{1}H NMR (400 MHz, C$_6$D$_6$) δ = 8.31 (ddd, *J* = 7.7, 3.9, 1.9 Hz, 3H), 8.10 (s, 1H), 7.96 (d, *J* = 9.3 Hz, 1H), 7.88 (d, *J* = 3.9 Hz, 1H), 7.79 – 7.75 (m, 2H), 7.31 (d, *J* = 4.0 Hz, 1H), 7.24 – 7.17 (m, 5H), 6.96 (dt, *J* = 16.2, 1.2 Hz, 1H), 6.84 (t, *J* = 9.8 Hz, 1H), 6.72 (t, *J* = 9.6 Hz, 1H), 6.18 (dd, *J* = 16.1, 6.6 Hz, 1H), 4.34 – 4.25 (m, 1H), 1.59 (d, *J* = 7.0 Hz, 3H) ppm. ^{13}C NMR (100 MHz, C$_6$D$_6$) δ = 144.2, 137.0, 136.5, 135.2, 133.2, 131.7, 129.9, 128.5, 126.2, 126.0, 125.0, 124.9, 123.8, 122.1, 121.3, 117.4, 35.7, 21.7 ppm. HRMS *calcd.* for $C_{28}H_{22}^+$ [M]$^+$: 358.1722; *found* 358.1716. IR (neat, cm^{-1}) $\tilde{v}$: 543, 720, 773, 784, 800, 845, 887, 973, 1015, 1046, 1260, 1394, 1448, 1575, 2360, 2851, 2922.

(*E*)-1-(4-Phenylbut-3-en-2-yl)azulene (**74h**):
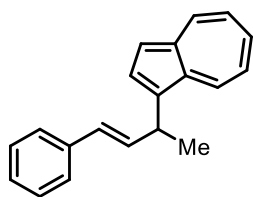
Blue solid (36.5 mg, 141.3 μmol, 71%). ^{1}H NMR (400 MHz, C$_6$D$_6$) δ = 8.37 (d, *J* = 9.7 Hz, 1H), 8.27 (dd, *J* = 9.4, 1.0 Hz, 1H), 7.87 (d, *J* = 3.9 Hz, 1H), 7.58 – 7.49 (m, 1H), 7.38 – 7.29 (m, 3H), 7.26-7.24 (m, 2H), 7.19 – 7.04 (m, 3H), 6.51 (dd, *J* = 15.9, 6.4 Hz, 1H), 6.39 (dd, *J* = 15.8, 1.2 Hz, 1H), 4.38 – 4.25 (m, 1H), 1.63 (d, *J* = 7.0 Hz, 3H) ppm. ^{13}C NMR (101 MHz, CDCl$_3$) δ = 140.8, 137.7, 137.4, 136.6, 135.9, 135.1, 134.9, 133.7, 133.3, 128.4, 127.85, 126.8, 126.1, 122.3, 121.6, 116.9, 35.0, 21.8 ppm. HRMS *calcd.* for C$_{20}$H$_{18}$$^+$ [M]$^+$: 258.1409; *found* 258.1411. IR (neat, cm^{-1}) $\tilde{v}$: 529, 577, 671, 712, 771, 846, 870, 893, 943, 961, 1015, 1028, 1198, 1296, 1370, 1392, 1412, 1430, 1447, 1493, 1533, 1574, 2925, 2959, 3021.

(*E*)-2-[3-(azulen-1-yl)but-1-en-1-yl]thiophene (**74i**):

Blue solid (11.1 mg, 42.0 μmol, 21% yield). ^{1}H NMR (400 MHz, C$_6$D$_6$) δ = 8.35 (d, *J* = 9.8 Hz, 1H), 8.31 – 8.23 (m, 1H), 7.86 (d, *J* = 3.9 Hz, 1H), 7.55 (td, *J* = 9.8, 1.1 Hz, 1H), 7.37 (d, *J* = 3.9 Hz, 1H), 7.14 – 7.03 (m, 3H), 6.92 – 6.86 (m, 1H), 6.83 (dd, *J* = 3.6, 1.2 Hz, 1H), 6.51 – 6.43 (m, 1H), 6.41 – 6.32 (m, 1H), 4.30 (p, *J* = 6.8 Hz, 1H), 1.61 (d, *J* = 7.1 Hz, 3H) ppm. ^{13}C NMR (101 MHz, CDCl$_3$) δ = 143.0, 140.8, 137.4, 136.6, 135.9, 135.2, 134.9, 133.3, 133.2, 127.1, 124.5, 123.2, 122.3, 121.7, 121.3, 116.9, 34.8, 21.7 ppm. HRMS *calcd.* for C$_{18}$H$_{16}$S [M]$^+$: 264.0973; *found* 264.0975. IR (neat, cm^{-1}) $\tilde{v}$: 559, 669, 579, 898, 1053, 1205, 1259, 1394, 1475, 1558, 1652, 2360, 2966, 3674, 37

Compounds **153a**–**153j** were obtained using the general procedure 2 (GP2):

General procedure for the synthesis of norbornadiene dimers (GP2)[X]:

Diphosphine ligand **92** (24 mg, 0.025 mmol), [Rh(COD)$_2$Cl]2 (6.3 mg, 0.0125 mmol) and KB(C$_6$F$_5$)$_4$ (36 mg, 0.050 mmol) were weighted on air to a 10 mL flame-dried Schlenk flask equipped with magnetic stirring bar. The Schlenk flask was evacuated and filled with nitrogen (x3) and 1,2-DCE (2.5 mL) was added in one portion. The brick red solution thus obtained was stirred for 15 minutes at room temperature. After that time, 0.500 mmol of the desired norbornadiene derivative was added in one portion. The reaction flask was transferred to a preheated (90 ˚C) oil bath. The reaction mixture was stirred for 18 h. After cooling down to the room temperature, the reaction mixture was added dropwise over a solution of [H(OEt$_2$)$_2$][B(C$_6$F5)$_4$] (25 mg, 0.030 mmol) in 10 mL of DCE at rt under nitrogen atmosphere. The corresponding mixture was stirred at rt 4 h and transferred to a roundbottom flask with 500 mg of silica gel. The solvent was removed in vacuo and the resulting solid was transferred to a chromatography column. The reaction mixture purified by column chromatography (SiO2, pentane/cyclohexane gradient) to give the desired dimerization product.

Heptacyclo-[6.6.0.0^{2,6}.0^{3,13}.0^{4,11}.0^{5,9}.0^{10,14}]tetradecane (**132**):

Colorless solid (38 mg, 206.2 μmol, 82%). R_f = 0.75 (cyclohexane), ^{1}H NMR (400 MHz, CDCl$_3$) δ = 2.39 (s, 12H), 1.76 (s, 4H) ppm. ^{13}C NMR (100 MHz, CDCl$_3$) δ = 53.2, 51.0, 42.7 ppm. HRMS calcd. for C$_{14}$H$_{16}$$^+$ [M]$^+$: 182.1252; *found* 182.1254. The obtained data are in agreement with the previously reported characterization.[86]
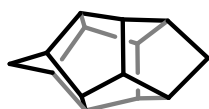
7,12-Diphenylheptacyclo-[6.6.0.0^{2,6}.0^{3,13}.0^{4,11}.0^{5,9}.0^{10,14}]tetradecane (**153a**):

[X] General Procedure 2 was optimized in cooperation with Dr. Xavier Marset
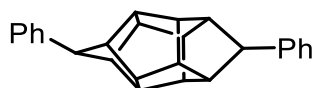
Colourless solid (48 mg, 57% yield) Rf = 0.65 (cyclohexane), ^{1}H NMR (400 MHz, CD$_2$Cl$_2$) δ 7.29 – 7.05 (m, 10H), 3.62 (s, 2H), 2.84 (d, J = 9.3 Hz, 4H), 2.68 (s, 4H), 2.51 (s, 4H). ^{13}C NMR (100 MHz, CDCl$_3$) δ = 142.9, 128.1, 127.7, 125.5, 59.8, 55.2, 54.0, 53.1, 52.7, 51.3, 50.9. HRMS calcd. for C26H24 (M+) 336.1878 found 336.1884. IR (neat, cm-1) $\tilde{v}$ = 456, 504, 617, 278, 1027, 1260, 1338, 1494, 2949, 3020. The analytical data correspond to the previously reported ones.[88]

7,12-Dibenzylheptacyclo-[6.6.0.0^{2,6}.0^{3,13}.0^{4,11}.0^{5,9}.0^{10,14}]tetradecane (**153b**):
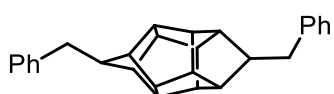
Colorless solid (58 mg, 64% yield) Rf = 0.65 (cyclohexane). ^{1}H NMR (400 MHz, CDCl$_3$) δ = 7.32-7.15(m, 10 H), 2.81 – 2.75 (m, 2H), 2.73 – 2.67 (m, 2H), 2.65-2.60 (m, 4H), 2.56 – 2.44 (m, 4H), 2.41 – 2.32 (m, 4H), 2.26-2.21 (m, 2H).^{13}C NMR (100 MHz, CDCl$_3$) δ = 142.8, 128.8, 128.3, 125.6, 58.7, 54.6, 53.5, 52.9, 52.7, 51.0, 50.8, 37.5. HRMS calcd. for C28H28 (M+) 364.2191 found 364.2188. IR (neat, cm-1) $\tilde{v}$ = 418, 517, 616, 681, 795, 913, 1276, 1351, 1540, 1998, 2157, 2920. The obtained data is in agreement with the previously reported characterization. The analytical data correspond to the previously reported ones.[88]

7,12-Di-*n*-undec-1-ene-11-ylheptacyclo-[6.6.0.0^{2,6}.0^{3,13}.0^{4,11}.0^{5,9}.0^{10,14}]tetradecane (**153c**):
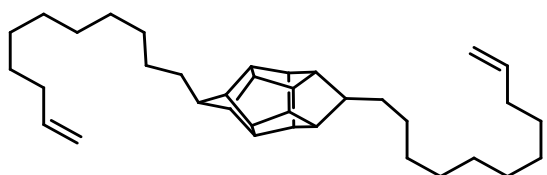
Colorless oil (72 mg, 147.3 μmol, 59%). R_f = 0.80 (cyclohexane), ^{1}H NMR (400 MHz, CDCl$_3$) ^{1}H NMR (400 MHz, CDCl$_3$) δ = 5.80 (ddt, J = 17.0, 10.2, 6.7 Hz, 2H), 5.09 – 4.77 (m, 4H), 2.60 – 2.29 (m, 6H), 2.30 – 2.11 (m, 4H), 2.09 – 1.96 (m, 4H), 1.42 – 1.13 (m, 36H) ppm. ^{13}C NMR (101 MHz, CDCl$_3$) δ = 139.3, 114.1, 56.8, 54.6, 53.5, 52.7, 52.6, 50.8, 50.6, 45.4, 33.8, 30.6, 30.0, 29.7, 29.6, 29.5, 29.2, 29.2, 29.0, 29.0, 25.4 ppm. HRMS calcd. for C$_{36}$H$_{56}$$^+$ [M]$^+$: 488.4382; *found* 488.4386 IR (neat, cm^{-1}) $\tilde{v}$: 549, 627, 715, 907, 989, 1216, 1365, 1466, 1640, 1783, 3075, 3445

7,12-Di-*n*-octylheptacyclo-[6.6.0.0^{2,6}.0^{3,13}.0^{4,11}.0^{5,9}.0^{10,14}]tetradecane (**153d**):
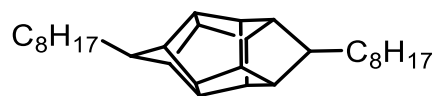
C$_8$H$_{17}$——[structure]——C$_8$H$_{17}$ Colorless solid (73 mg, 178.6 µmol, 71%), (Lit.:[88] 43–45 °C). R_f = 0.85 (cyclohexane), ^{1}H NMR (400 MHz, CDCl$_3$) δ = 2.53 (p, J = 4.8 Hz, 4H), 2.47 – 2.35 (m, 4H), 2.31 – 2.26 (m, 2H), 2.22 (q, J = 4.6, 3.7 Hz, 4H), 1.39 – 1.19 (m, 28H), 0.94 – 0.86 (t, 6H) ppm. ^{13}C NMR (101 MHz, CDCl$_3$) δ = 56.8, 54.6, 53.5, 52.7, 52.6, 50.8, 50.6, 32.0, 30.6, 30.0, 29.7, 29.4, 29.1, 22.7, 14.1 ppm. HRMS calcd. for C$_{30}$H$_{48}^+$ [M]$^+$: 408.3756; *found* 408.3758. IR (neat, cm^{-1}) $\tilde{v}$: 428, 790, 1466, 2852, 2877, 2922, 2957. The analytical data correspond to the previously reported ones.[88]

7,12-Bis(naphthalen-2-yl)heptacyclo[6.6.0.0^{2,6}.0^{3,13}.0^{4,11}.0^{5,9}.0^{10,14}]tetradecane (**153e**):
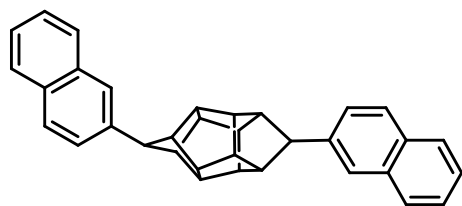
Colorless solid (46 mg, 105.4 µmol, 42%), (Lit.:[88] 203–205 °C). R_f = 0.55 (cyclohexane), ^{1}H NMR (400 MHz, CDCl$_3$) δ = 7.87 – 7.61 (m, 8H), 7.52 – 7.31 (m, 6H), 3.77 (s, 2H), 2.95 (d, J = 23.7 Hz, 4H), 2.75 (s, 4H), 2.59 (d, J = 11.9 Hz, 4H) ppm. ^{13}C NMR (100 MHz, CDCl$_3$) δ = 140.3, 133.5, 131.8, 127.6, 127.5, 127.3, 126.9, 125.7, 125.3, 125.0, 59.9, 55.0, 54.0, 53.1, 52.6, 51.2, 50.8 ppm. HRMS calcd. for C$_{34}$H$_{28}^+$ [M]$^+$: 436.2191; *found* 436.2190. IR (neat, cm^{-1}) $\tilde{v}$: 472, 517, 621, 795, 900, 961, 1081, 1216, 1364, 1456, 1634, 2357, 2476, 3014. The analytical data correspond to the previously reported ones.[88]

7,12-Di-*tert*-butoxyheptacyclo[6.6.0.0^{2,6}.0^{3,13}.0^{4,11}.0^{5,9}.0^{10,14}]tetradecane (**153j**):
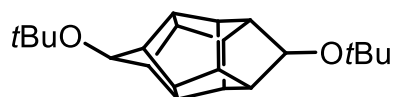
*t*BuO——[structure]——O*t*Bu Colorless solid (38 mg, 115.7 µmol, 46%), (Lit.:[87a] 123–125 °C). R_f = 0.55 (cyclohexane), ^{1}H NMR (400 MHz, CDCl$_3$) δ = 4.29 (s, 2H), 3.51 (br, s, 2H), 2.77 (s, 4H), 2.35 (s, 7H), 1.20 (s, 18H) ppm. ^{13}C NMR (100 MHz, CDCl$_3$) δ = 86.0, 72.7, 55.7, 53.2, 51.8, 51.3, 48.9, 48.3, 28.6 ppm. HRMS calcd. for C$_{22}$H$_{33}$O$_2^+$ [M + H]$^+$: 329.2475; *found* 329.2487. IR (neat, cm^{-1}) $\tilde{v}$:619, 668, 759, 971, 1035, 1362, 1455, 1506. The analytical data correspond to the previously reported ones.[87a,88]

7,12-Diaza-7,12-di(*tert*-butoxycarbonyl)heptacyclo-[6.6.0.0^{2,6}.0^{3,13}.0^{4,11}.0^{5,9}.0^{10,14}]-tetradecane (**154**)

exo,endo-Hexacyclo[9.2.1.0^{2,10}.0^{3,8}.0^{4,6}.0^{5,9}]tetradec-12-ene (**142**):
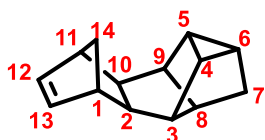
Colorless oil (8 mg, 43.4 µmol, 17%). R_f = 0.81 (cyclohexane), ^{1}H NMR (400 MHz, CDCl$_3$) δ = 6.18 (t, *J* = 1.8 Hz, 2H), 2.65 – 2.55 (m, 2H), 2.47 (d, *J* = 8.8 Hz, 1H), 2.02 – 1.92 (m, 1H), 1.94 – 1.80 (m, 4H), 1.40 – 1.23 (m, 3H), 1.19 (dt, *J* = 8.7, 1.4 Hz, 1H), 0.81 (dd, *J* = 4.8, 1.0 Hz, 2H) ppm. This spectrum corresponds to the previously reported one.[86a] ^{13}C NMR (126 MHz, CDCl$_3$) δ = 140.4, 47.5, 46.1, 45.1, 42.6, 42.5, 28.7, 18.7, 12.8 ppm. This spectrum is identical to the previously reported one.[86c] HRMS calcd. for C$_{14}$H$_{16}^+$ [M]$^+$ 182.1252; *found* 182.1250. IR (neat, cm^{-1}) $\tilde{v}$: 581, 648, 712, 943, 1004, 1251, 1616, 2753.

endo,exo,endo-Decacyclo[9.9.1.0^{2,10}.0^{3,8}.0^{4,6}.0^{5,9}.0^{12,20}.0^{13,19}.0^{14,16}.0^{15,19}]heneicosane (**146**):
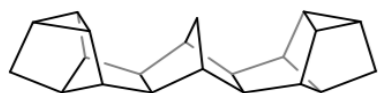
Colorless solid (24 mg, 86.8 µmol, 52%), (Lit.:[86a] 176–178 °C). R_f = 0.72 (cyclohexane), ^{1}H NMR (400 MHz, CDCl$_3$) δ = 2.14 (s, 4H), 1.99 – 1.91 (m, 4H), 1.75 (dt, *J* = 1.5, 0.8 Hz, 2H), 1.69 (t, *J* = 2.3 Hz, 4H), 1.32 – 1.21 (m, 6H), 0.83 (dq, *J* = 4.8, 1.0 Hz, 4H) ppm. ^{13}C NMR (100 MHz, CDCl$_3$) δ = 50.8, 47.0, 44.5, 39.1, 29.1, 27.7, 17.7, 12.9 ppm. This spectrum is identical to the previously reported one.[86c] HRMS calcd. for C$_{21}$H$_{24}^+$ [M]$^+$ 276.1878; *found* 276.1885. IR (neat, cm^{-1}) $\tilde{v}$:798, 803, 816, 833.

7,14-Di(cyclopentyl)-*exo,endo*-hexacyclo[9.2.1.0^{2,10}.0^{3,8}.0^{4,6}.0^{5,9}]tetradec-12-ene (**154***):
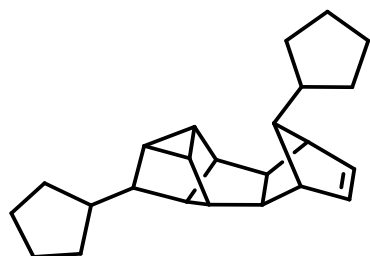
Colorless solid (74 mg, 92% yield), . R_f = 0.75 (cyclohexane), ^{1}H NMR (400 MHz, CDCl$_3$) δ = 6.03 (s, 2H), 2.96 (d, J = 9.6 Hz, 1H), 2.52 (d, J = 11.2 Hz, 2H), 2.20 – 2.07 (m, 1H), 2.01 – 1.42 (m, 20H), 1.41 – 1.00 (m, 8H), 0.90 (t, J = 4.4 Hz, 2H) ppm. ^{13}C NMR (101 MHz, CDCl$_3$) δ = 136.7, 136.7, 58.1, 51.3, 47.5, 46.4, 46.3, 46.1, 45.9, 45.9, 42.1, 41.1, 37.6, 32.6, 32.2, 31.5, 25.5, 25.3, 25.3, 24.1, 15.0, 13.7 ppm. HRMS calcd. for C$_{24}$H$_{32}$ [M]$^+$ 320.2504; *found* 320.2499. IR (neat, cm^{-1}) $\tilde{v}$: 547, 726, 1287, 1640, 2911.

Rhodium complex **162**:
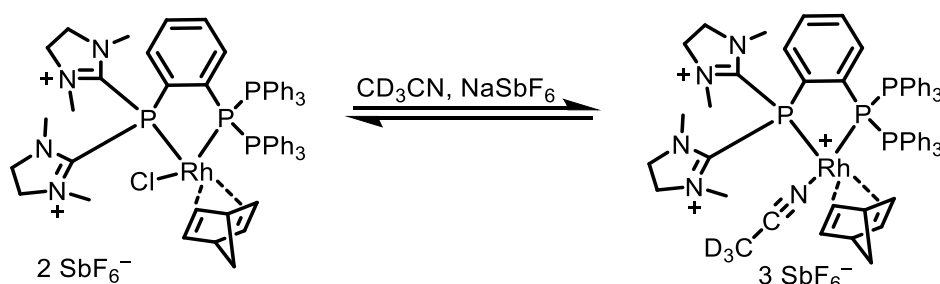
A flame-dried Schlenk flask was charged with [Rh(cod)Cl]$_2$ (49.3 mg, 100 μmol) and diphosphine ligand **92** ((192 mg, 200 μmol))under argon atmosphere. Anhydrous DCE (1 mL) was added, the reaction mixture was stirred for 30 minutes at room temperature and then cooled to 0 ℃. Freshly distilled norbornadiene (**61**, 1.81 g, 2.0 mL, 19.7 mmol) was added in one portion. The reaction mixture was stirred for 4 h maintaining the temperature below 0 ℃. Addition of anhydrous pentane (5 mL) to the Schlenk flask furnished yellow precipitate. The latter was filtered under argon atmosphere and washed with dry pentane (3 × 10 mL) followed by dry diethyl ether (3 × 5 mL). Clean product **162** was obtained as a yellow solid senstivie to moisture,

yield 73%. Redissolving the solid in dry acetonitrile and layering the solution with diethyl ether afforded yellow crystals suitable for X-ray crystal structure analysis.

Yellow solid (178 mg, 73.0 μmol 73%). ^{1}H NMR (400 MHz, CD$_3$CN) δ = 7.84 (t, J = 46.5 Hz, 8H), 7.64 – 7.22 (m, 6H), 3.96 (s, 8H), 3.88 (s, 1H), 3.55 (q, J = 1.9 Hz, 2H), 3.16 (s, 12H) ppm. ^{31}P NMR (162 MHz, CD$_3$CN) δ = 73.03 (d, J = 154.2 Hz), 23.73 (d, J = 224.3 Hz) ppm. ^{13}C NMR (101 MHz, CD$_3$CN) δ = 143.2, 134.9, 134.7, 133.9, 128.8, 74.9, 52.4, 50.1, 36.9 ppm.

(2S,3R,3aS,3bR,4S,6R,6aS,7R,7aR,8S)-4-Ethyl-6-phenethyldecahydro-1H-2,3,7-(epimethanetriyl)cyclopenta[a]pentalene (**167**):
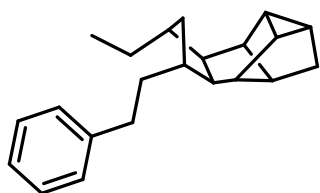
A flame-dried 4-mL microwave vial was charged with ruthenium benzylidene *nitro*-Grela catalyst* (6,7 mg, 10 μmol, 10 mol%). The vial was transferred into the nitrogen flushed glovebox. A mixture of norbornadiene dimer **142** (18,4 mg, 100 μmol) and freshly distilled styrene (52.0 mg, 57.2 μL, 499 μmol, 5 equiv.) was added in one portion. The microwave vial was tightly sealed and transferred to the preheated (100 °C) oil bath on the heating plate outside the glovebox. After 18 h stirring at this temperature, the reaction mixture was cooled down to the room temperature and filtered through a silica pad washing with pentane. After removal of all volatiles, dichloromethane (5 mL) was added, the solution of crude diene **167** was transferred to a Schlenk flask equipped with a magnetic stirring bar and 10 mg of 10% Pd/C (1 mg Pd, 10 μmol, 10 mol%) were added. After replacing glass stopper with septum and purging the system with hydrogen, the reaction mixture was stirred at room temperature for 24 h. Then all the volatiles were removed *in vacuo* and the residue was purified using column chromatography affording hydrocarbon **168**.

Colorless oil (23.6 mg, 80.6 μmol, 81%). R_f = 0.9 (pentane), ^{1}H NMR (400 MHz, CDCl$_3$) δ = 7.31 – 7.13 (m, 5H), 2.63 (qdd, J = 13.8, 9.2, 6.8 Hz, 2H), 2.27 – 2.01 (m, 3H), 2.01

– 1.82 (m, 4H), 1.81 – 1.69 (m, 1H), 1.49 (t, J = 1.4 Hz, 2H), 1.44 – 1.20 (m, 2H), 1.14 – 0.80 (m, 7H) ppm ^{13}C NMR (101 MHz, CDCl$_3$) δ = 143.2, 128.3, 128.2, 125.5, 53.8, 53.5, 47.2, 46.2, 46.2, 45.3, 43.9, 41.7, 38.1, 35.2, 31.6, 28.8, 13.9, 13.3, 12.0, 11.9 ppm. HRMS calcd. for $C_{22}H_{28}^+$ [M]$^+$: 292.2191; *found* 292.2197. IR (neat, cm^{-1}) $\tilde{v}$: 683, 915, 1543, 2166.

*(1,3-Dimesitylimidazolidin-2-ylidene)dichloro(2-isopropoxy-5-nitrobenzylidene)ruthenium(II)

1-Bromoheptacyclo-[6.6.0.0^{2,6}.0^{3,13}.0^{4,11}.0^{5,9}.0^{10,14}]tetradecane (**163**):
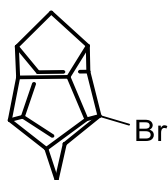
A 4-mL microwave vial equipped with a magnetic stirring bar was charged with norbornadiene dimer **132** (300 mg, 1.63 mmol), CBr$_4$ (640 mg, 1.93 mmol), benzyltriethylammonium chloride (26 mg. 114 µmol,), 50% aq. NaOH (0.6 mL) and dichloromethane (0.6 mL). The vial was tightly sealed, and the reaction mixture was stirred at 70 °C for 18 h. After this the reaction mixture was cooled down to room temperature and subsequentially transferred to separation funnel. 10mL of distilled water were added and the mixture was extracted with dichloromethane (3 × 25mL). Combined organic fractions were dried over anhydrous Na$_2$SO$_4$. After filtration and removal of all the volatiles *in vacuo* the mixture was filtered on a pad of silica (pentane) and purified using column chromatography (hexane). Bromide **163** was obtained as a pale solid.

Pale solid. Rf = 0.50 (pentane), ^1H NMR (300 MHz, CDCl$_3$) δ = 2.87 (ap t, J = 5.5 Hz, 1H), 2.85 – 2.70 (m, 3H), 2.56 – 2.38 (m, 7H), 2.25 – 2.14 (m, 1H), 1.88 – 1.77 (m, 3H). ^{13}C NMR (101 MHz, CDCl$_3$) δ = 79.2, 66.7, 63.0, 59.9, 53.4, 53.3, 52.1, 52.0, 51.6, 51.5, 51.5, 49.1, 42.3, 41.2. HRMS calcd. for C14H15Br (M+) 262.0357 found 262.0361. IR (neat, cm-1) $\tilde{v}$ = 628, 699, 770, 891, 1196, 1399, 2871.

Heptacyclo-[6.6.0.0^{2,6}.0^{3,13}.0^{4,11}.0^{5,9}.0^{10,14}]tetradecyl Trifluoromethanesulfonate (**164**):

163 (262 mg, 1.0 mmol) was weighed into a flame dried Schlenk tube equipped with magnetic stirring bar. 0.1 mL of dry CH_2Cl_2 was added in one portion and 514 mg (2 mmol) of AgOTf was added. The reaction mixture was sealed and stirred overnight in room temperature. After that time all the volatiles were removed in vacuo and the cure product was extracted with pentane.
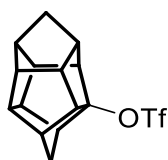
Pale solid (330 mg, 950 µmol, 99%). R_f = 0.45 (pentane), ^{1}H NMR (300 MHz, C_6D_6) δ = 2.97 – 2.86 (m, 2H), 2.73 – 2.63 (m, 1H), 2.57 (t, J = 5.9 Hz, 1H), 2.31 – 2.00 (m, 7H), 1.96 – 1.86 (m, 1H), 1.57 – 1.43 (m, 3H) ppm. ^{19}F NMR (282 MHz, C_6D_6) δ = -76.81 ppm. ^{13}C NMR (101 MHz, C_6D_6) δ = 55.0, 53.8, 53.5, 53.1, 52.8, 51.7, 51.5, 51.2, 50.8, 50.6, 49.4, 49.2, 48.9, 42.1, 40.4 ppm. HRMS calcd. for $C_{15}H_{15}F_3O_3S^+$ [M][+]: 332.0694; *found* 332.0691 IR (neat, cm[-1]) $\tilde{\nu}$: 628, 699, 770, 891, 1141, 1195, 1398, 2871, 2953.

1-Hydroxyheptacyclo-[6.6.0.0^{2,6}.0^{3,13}.0^{4,11}.0^{5,9}.0^{10,14}]tetradecane (**165**):

163 (262 mg, 1.0 mmol) was weighed into a flame dried Schlenk tube equipped with magnetic stirring bar. 0.1 mL of dry CH_2Cl_2 was added in one portion and 776 mg (2 mmol) of AgNTf$_2$ was added. The reaction mixture was sealed and stirred overnight in room temperature. After that time all the volatiles were removed in vacuo and the cure product was extracted with pentane.
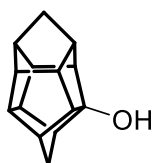
Pale solid (198 mg, 0.99 µmol, 99%), . R_f = 0.5 (pentane), ^{1}H NMR (400 MHz, C_6D_6) δ = 2.70 – 2.63 (m, 1H), 2.49 – 2.37 (m, 2H), 2.36-2.25 (m, 6H), 2.22 (dd, J = 4.7, 2.0 Hz, 1H), 2.14 (t, J = 5.4 Hz, 1H), 2.08 – 2.01 (m, 1H), 1.81 – 1.60 (m, 3H) ppm. ^{13}C NMR (101 MHz, C_6D_6) δ = 98.1, 63.4, 58.0, 55.2, 53.5, 52.9, 52.0, 51.7, 51.0, 50.5, 49.6, 48.9, 42.7, 40.8 ppm. HRMS calcd. for $C_{14}H_{17}O^+$ [M - H][+]: 201.1274; *found* 200.1203. IR (neat, cm[-1]) $\tilde{\nu}$: 594, 708, 795, 849, 1046, 1235, 1454, 1659, 2927, 3212.

1-Chloroheptacyclo-[6.6.0.0^{2,6}.0^{3,13}.0^{4,11}.0^{5,9}.0^{10,14}]tetradecane (**166**):

163 (262 mg, 1.0 mmol) was weighed into a flame dried Schlenk tube equipped with magnetic stirring bar. 0.1 mL of dry DCM was added in one portion and 1040 mg (10 mmol) of $SnCl_4$ was added. The reaction mixture was sealed and stirred overnight in reflux. After that time the reaction was cooled down to room temperature, all the volatiles were removed in vacuo and the cure product was extracted with pentane.
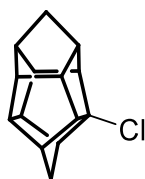
Pale solid (185 mg, 0.85 μmol, 85%). R_f = 0.55 (pentane), ^{1}H NMR (300 MHz, $CDCl_3$) δ = 2.81 (s, 1H), 2.72 – 2.35 (m, 10H), 2.19 (dd, J = 10.8, 1.5 Hz, 1H), 1.91 – 1.73 (m, 3H) ppm. ^{13}C NMR (101 MHz, $CDCl_3$) δ = 65.8, 61.5, 58.5, 53.2, 53.1, 51.9, 51.6, 51.4, 51.3, 50.7, 49.0, 42.3, 41.0. HRMS calcd. for $C_{14}H_{15}Cl^+$ [M]$^+$ 218.0862; *found* 218.0869. IR (neat, cm^{-1}) $\tilde{v}$: 628, 698, 772, 891, 1179, 1385, 2860.

8.1.3 NMR Spectra

Compound **86** ^{1}H NMR (300 MHz, CDCl$_3$):

Br

PPh$_2$

1.44
10.14
1.84
1.01

11.0 10.5 10.0 9.5 9.0 8.5 8.0 7.5 7.0 6.5 6.0 5.5 5.0 4.5 4.0 3.5 3.0 2.5 2.0 1.5 1.0 0.5 0.0 -0.5 -1
f1 (ppm)
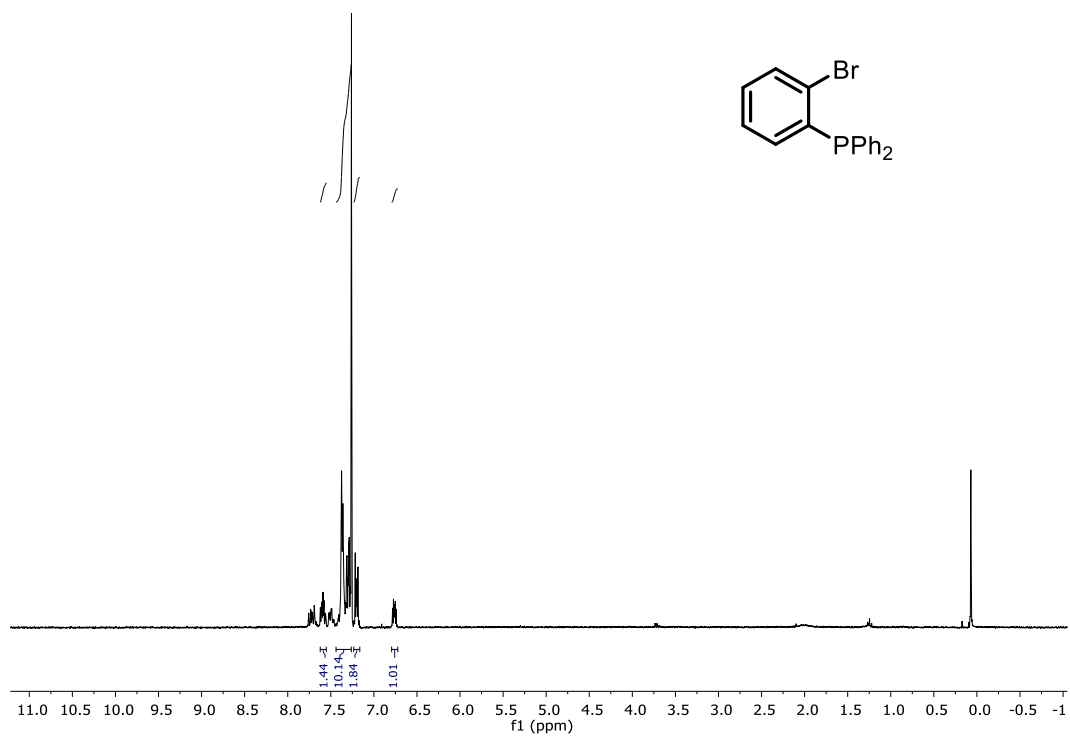
Compound **86** ^{31}P{^{1}H} NMR (121 MHz, CDCl$_3$):

Br

PPh$_2$

160 140 120 100 80 60 40 20 0 -20 -40 -60 -80 -100 -120
f1 (ppm)

Compound **87** ¹H NMR (300 MHz, CDCl₃):
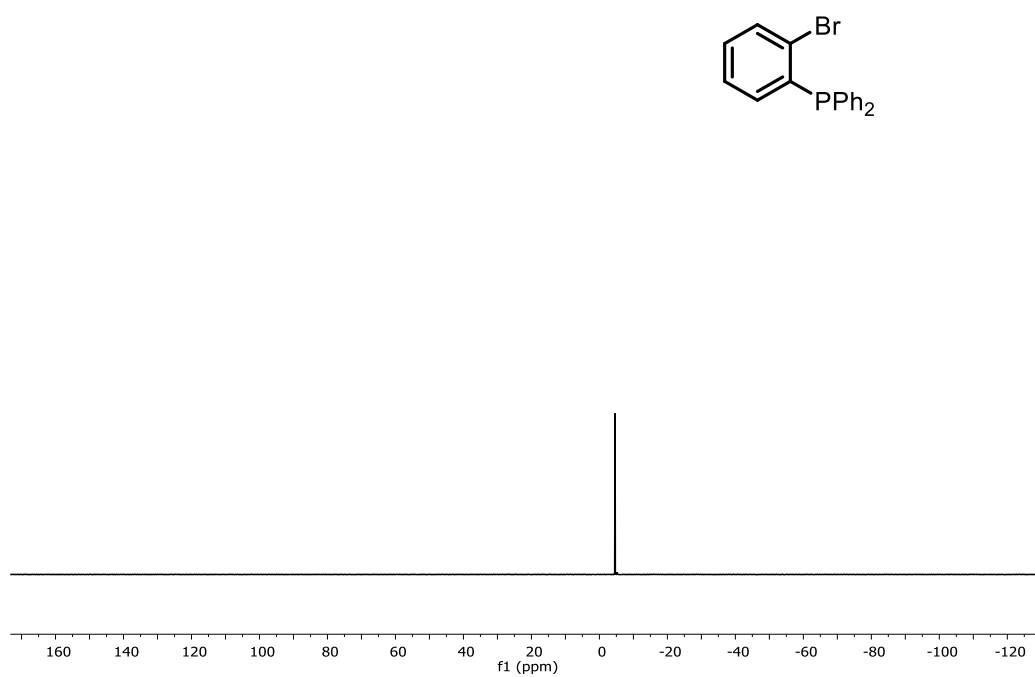
Compound **87** ¹H NMR (300 MHz, CDCl₃):
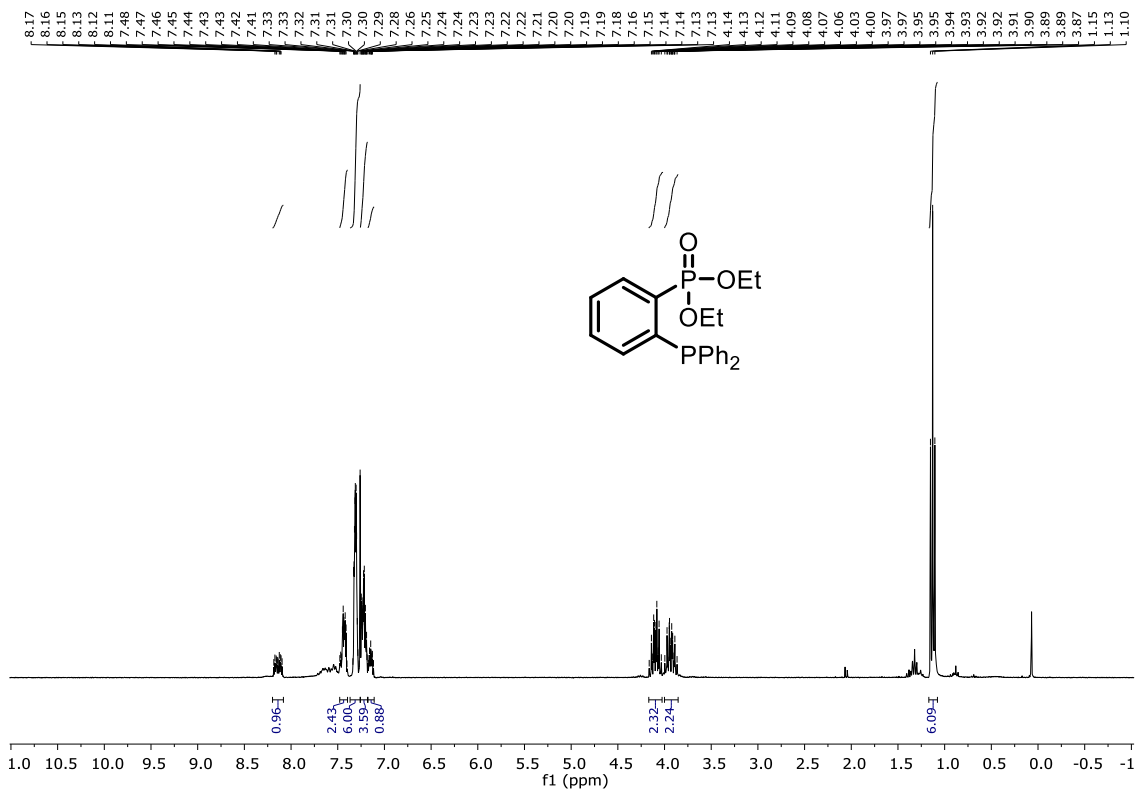
Compound **87** ³¹P{¹H } NMR (121 MHz, CDCl₃):
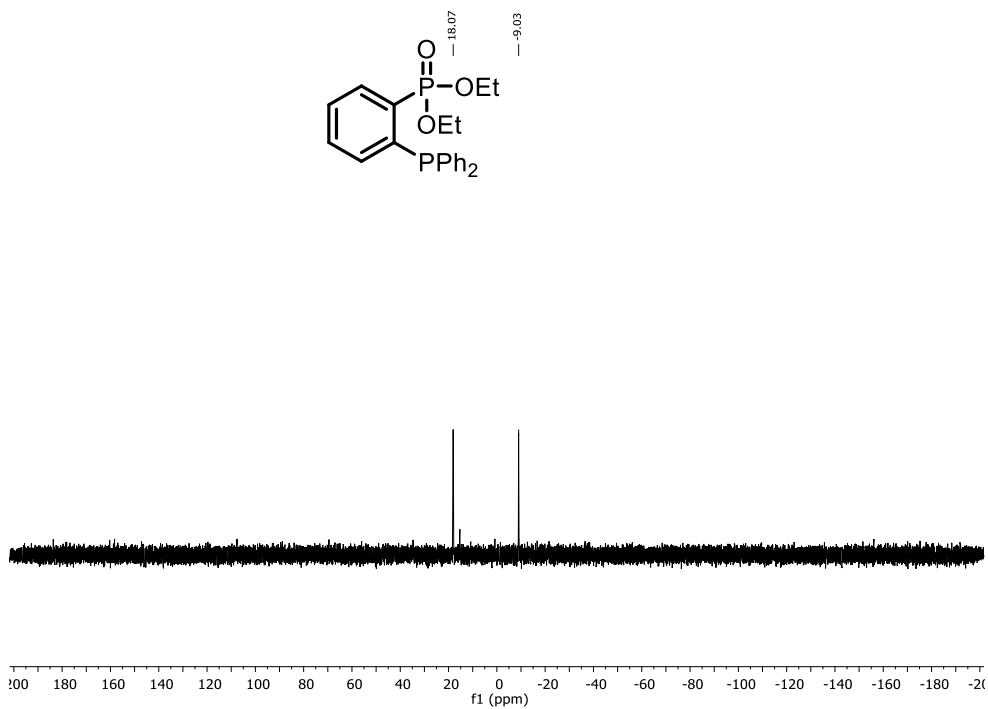
Compound **88** ^{1}H NMR (300 MHz, CDCl$_3$):
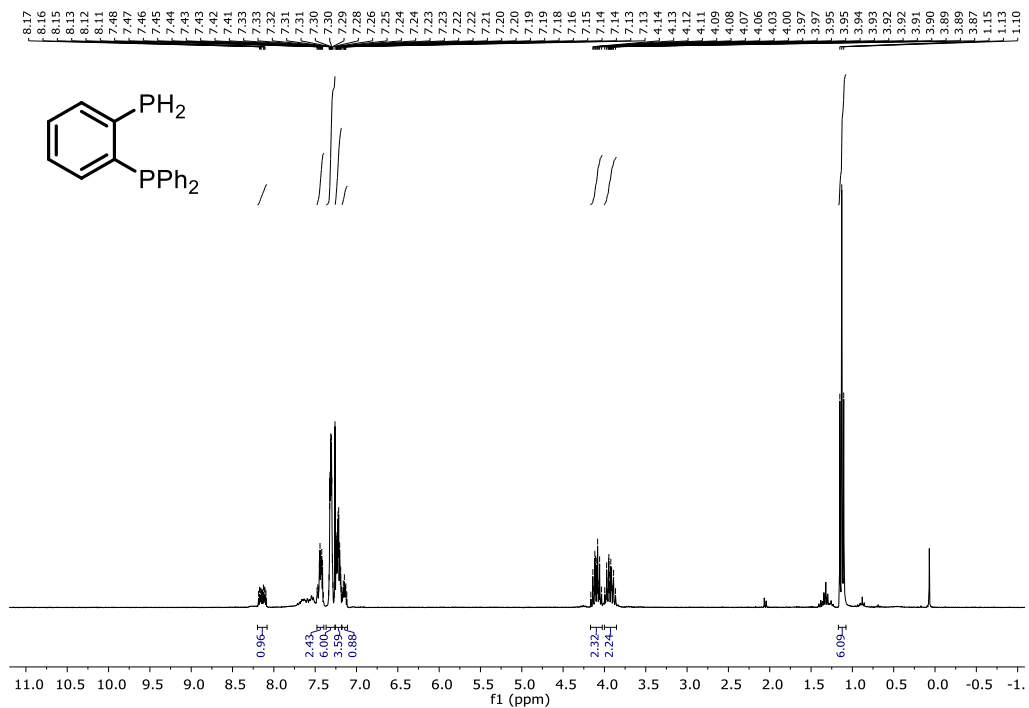
Compound **88** ^{31}P{^{1}H } NMR (121 MHz, CDCl$_3$):
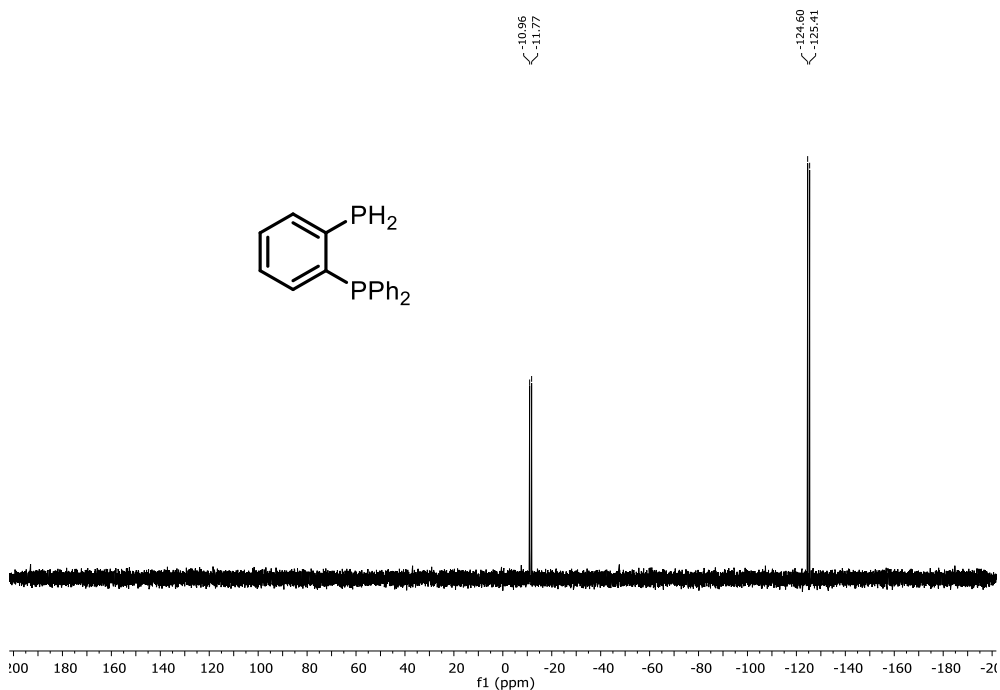
Compound **91** ^{1}H NMR (300 MHz, CDCl$_3$):
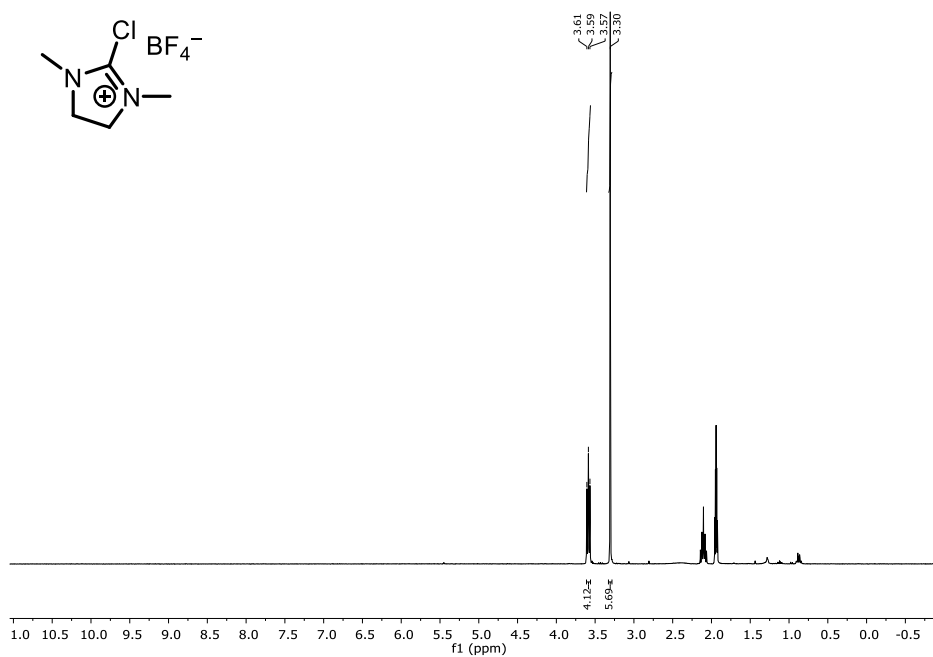
Compound **92** ^{1}H NMR (300 MHz, CDCl$_3$):
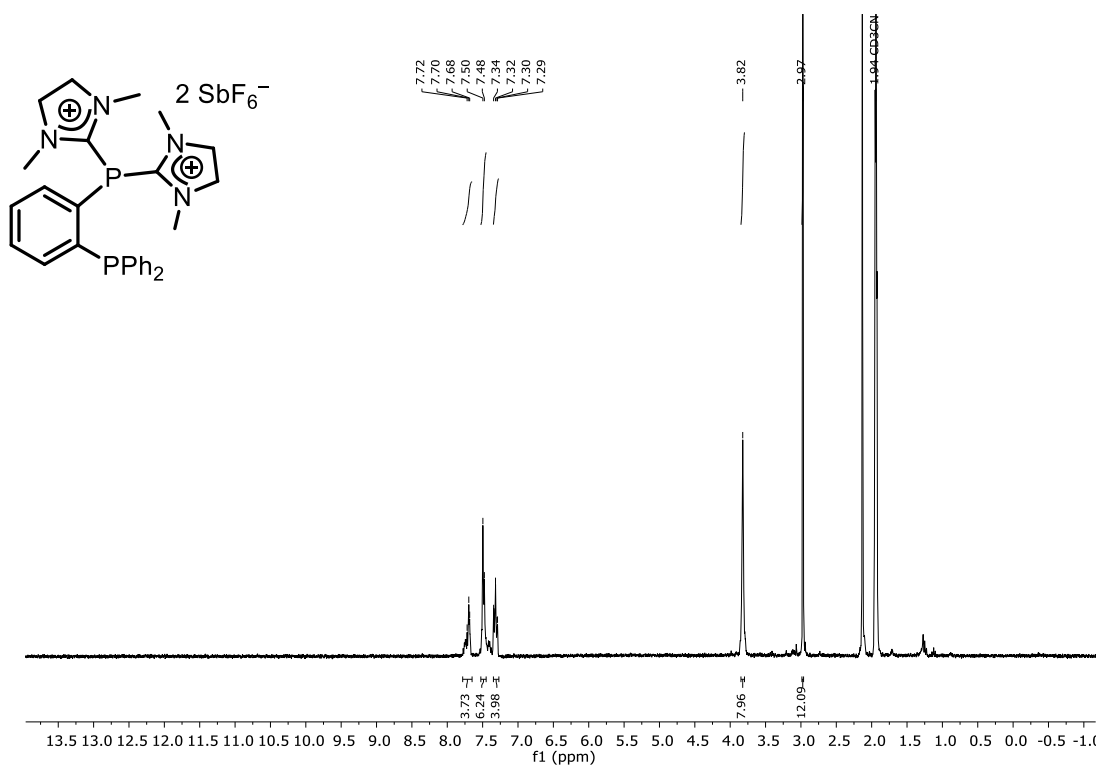
Compound **92** ^{31}P{^{1}H } NMR (121 MHz, CDCl$_3$):
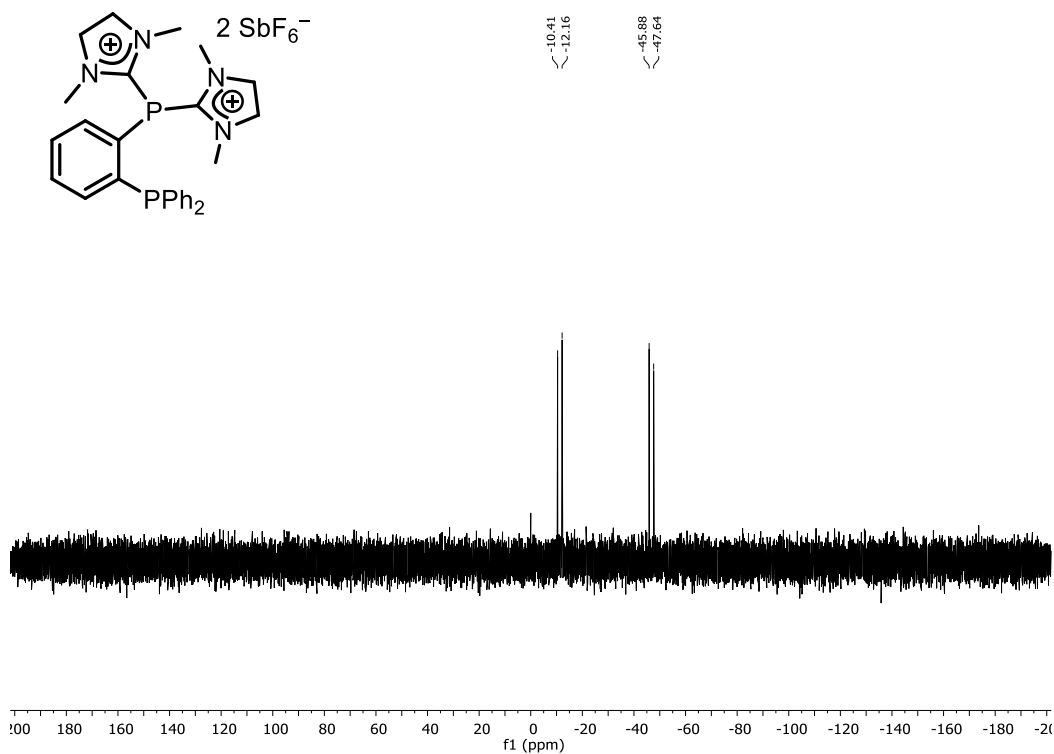
Compound **97** ^{1}H NMR (300 MHz, CD$_3$CN)
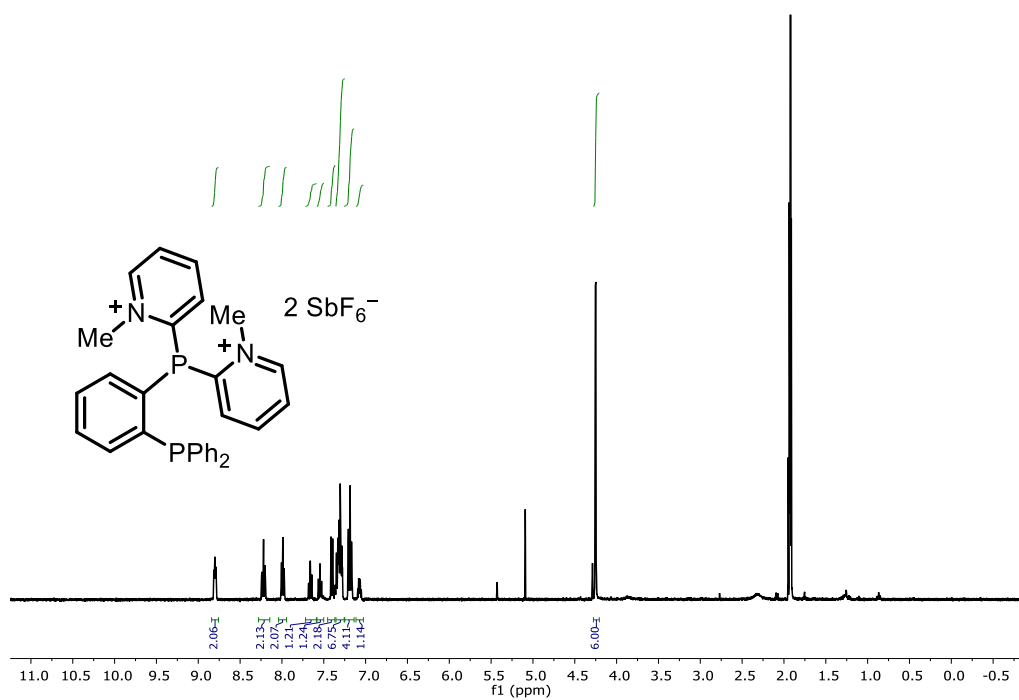
Compound **97** ^{31}P NMR (75 MHz, CD$_3$CN)
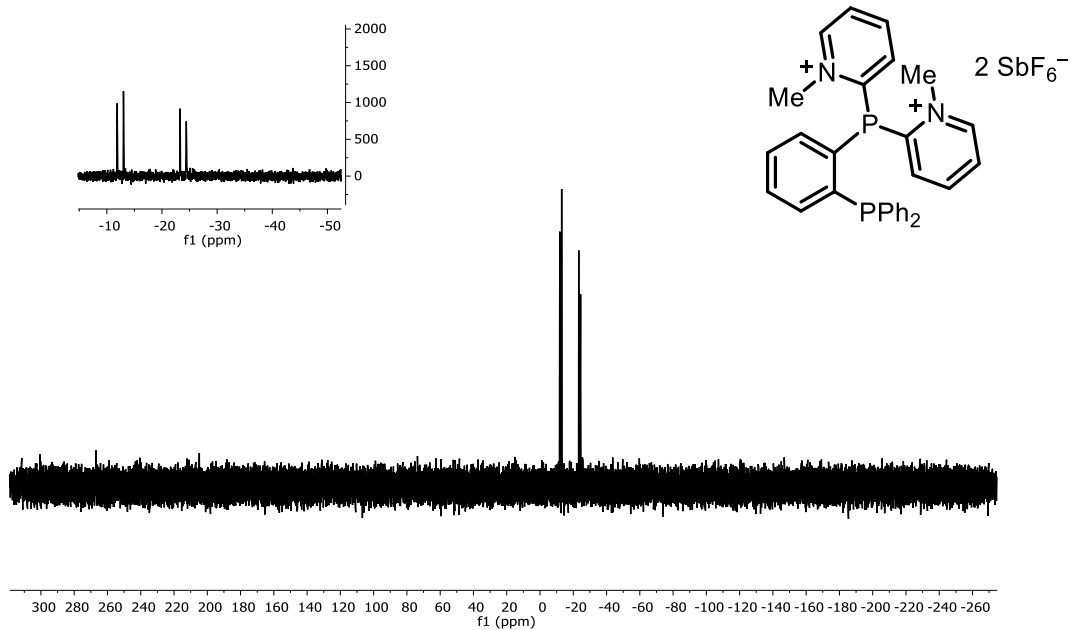
Compound **97** ^{13}C NMR (75 MHz, CD$_3$Cl)
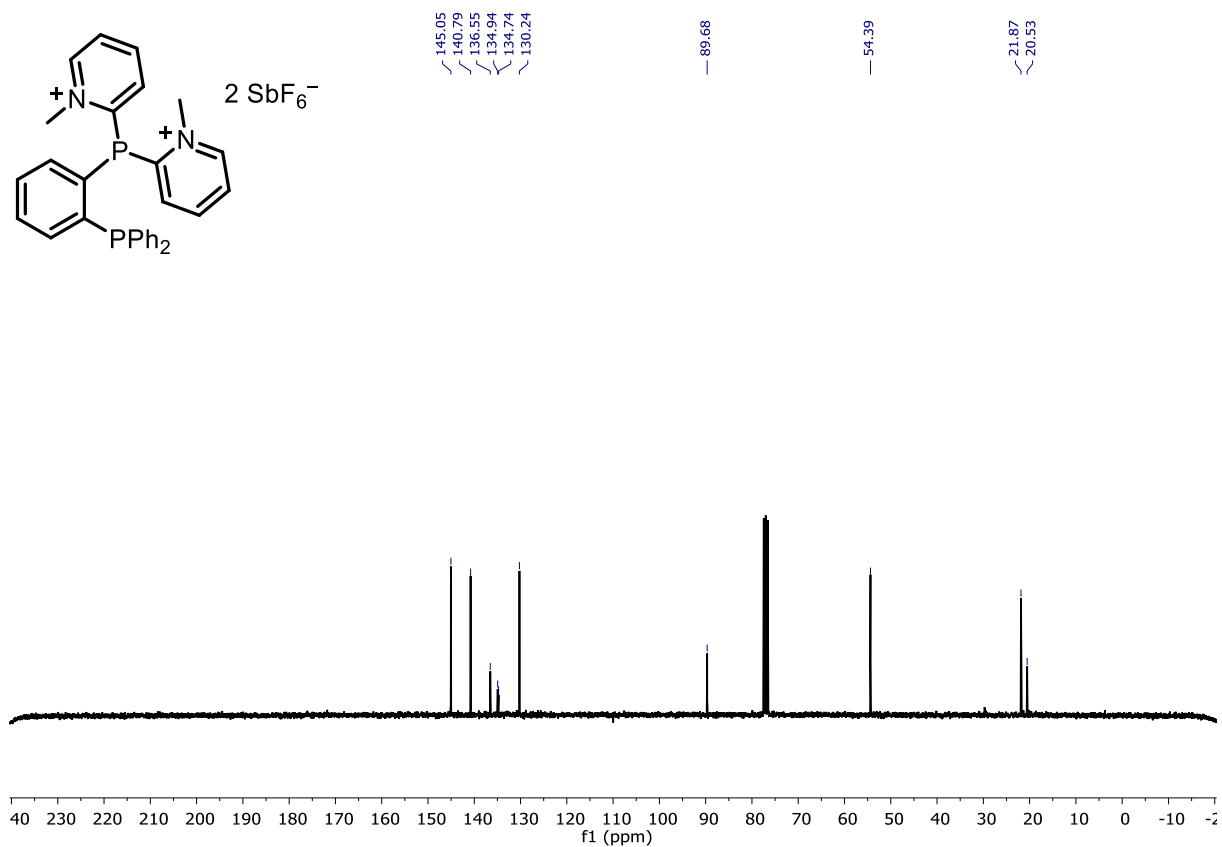
Compound **98** ¹H NMR (400 MHz, CD₃CN
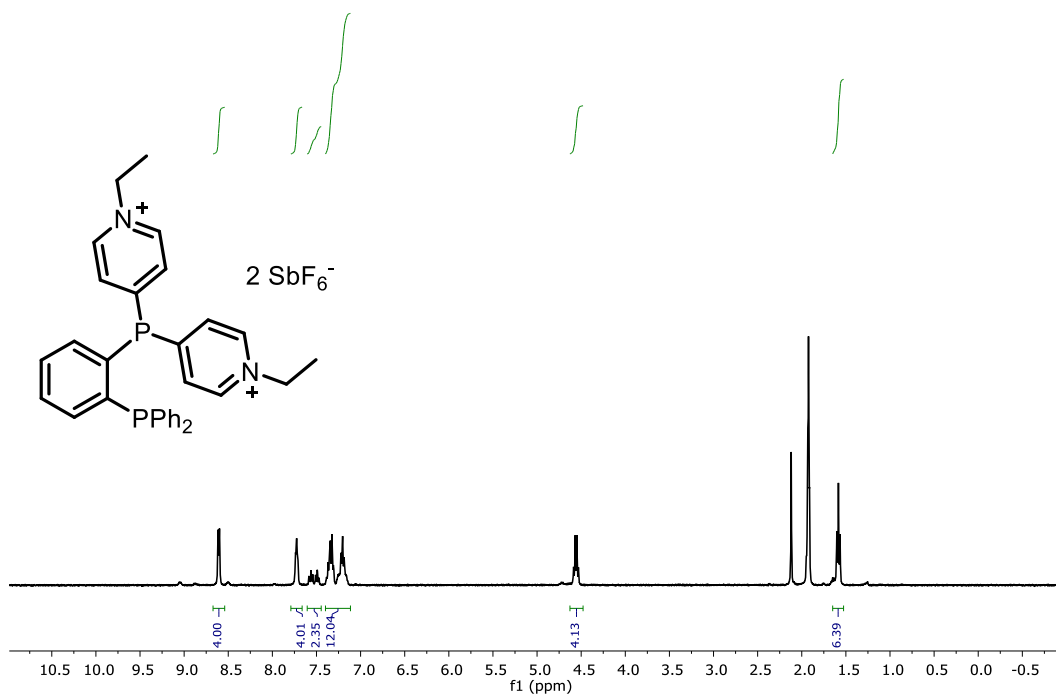
Compound **98** ³¹P NMR (162 MHz, CD₃CN)
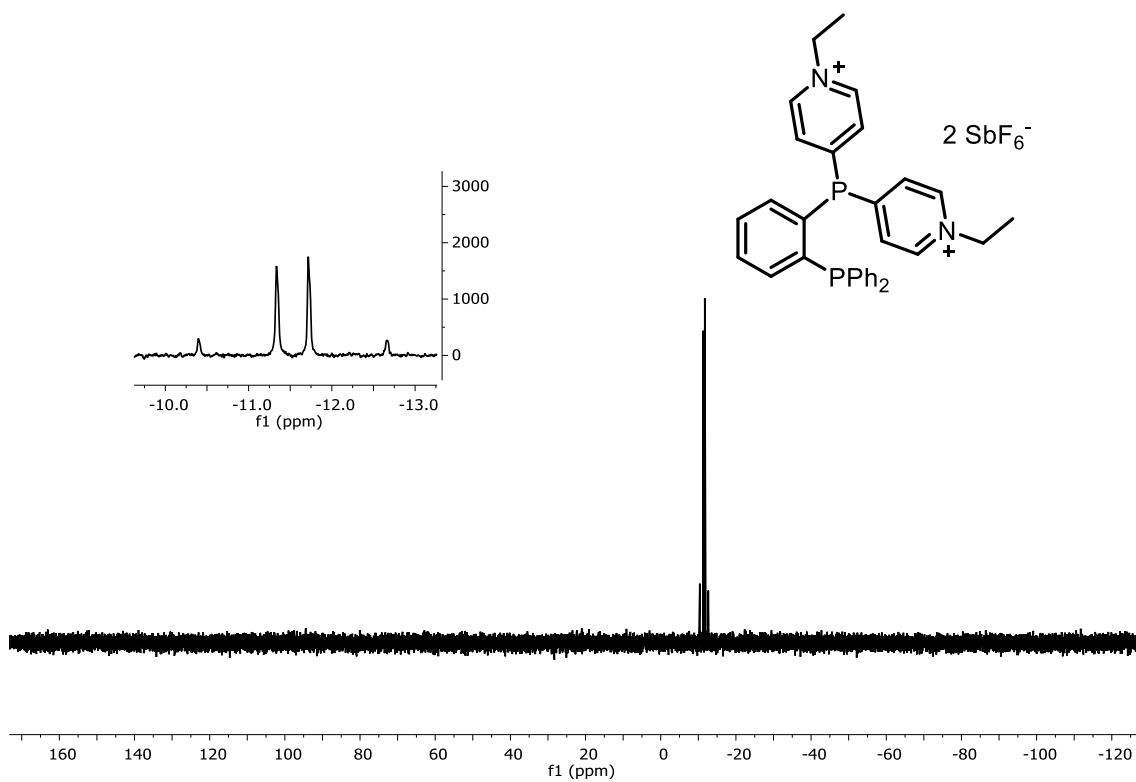
Compound **98** ^{13}C NMR (101 MHz, CD$_2$Cl$_2$)
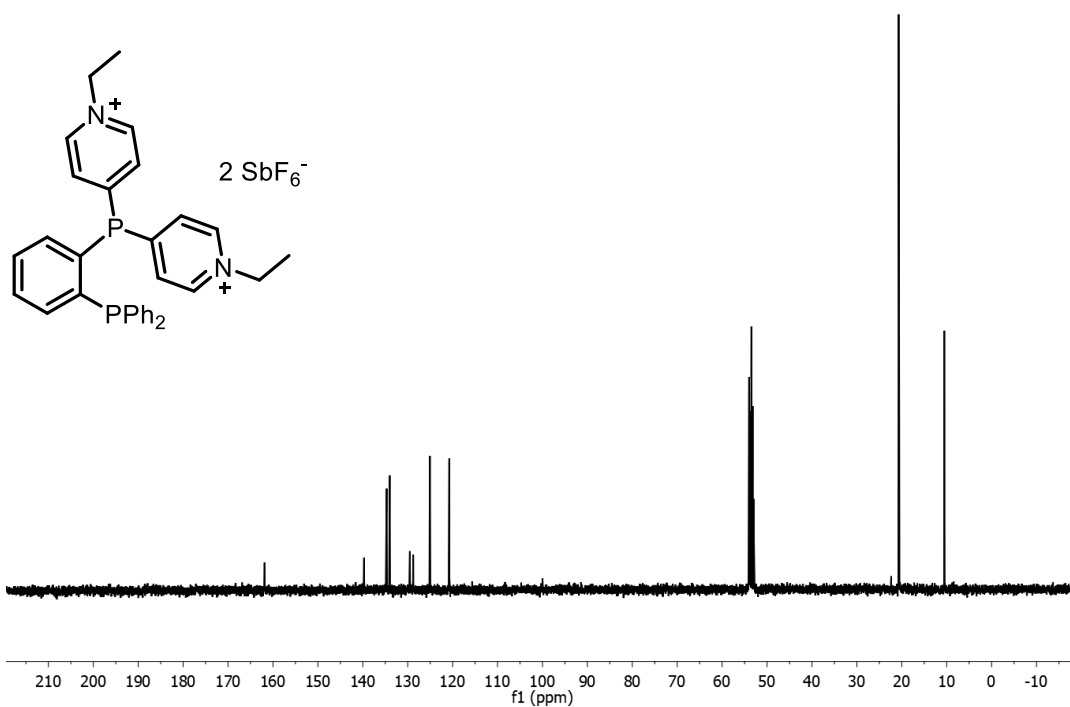
Compound **100** ^{1}H NMR (300 MHz, CDCl$_3$)
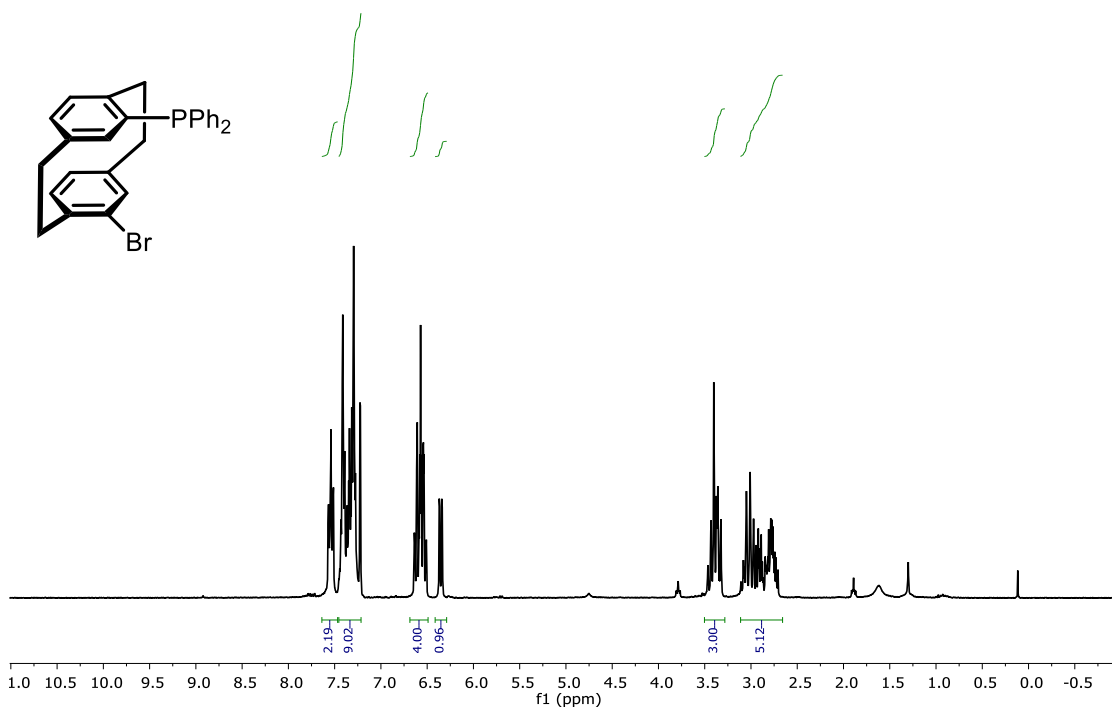
Compound **100** ^{31}P NMR (121 MHz, CDCl$_3$)
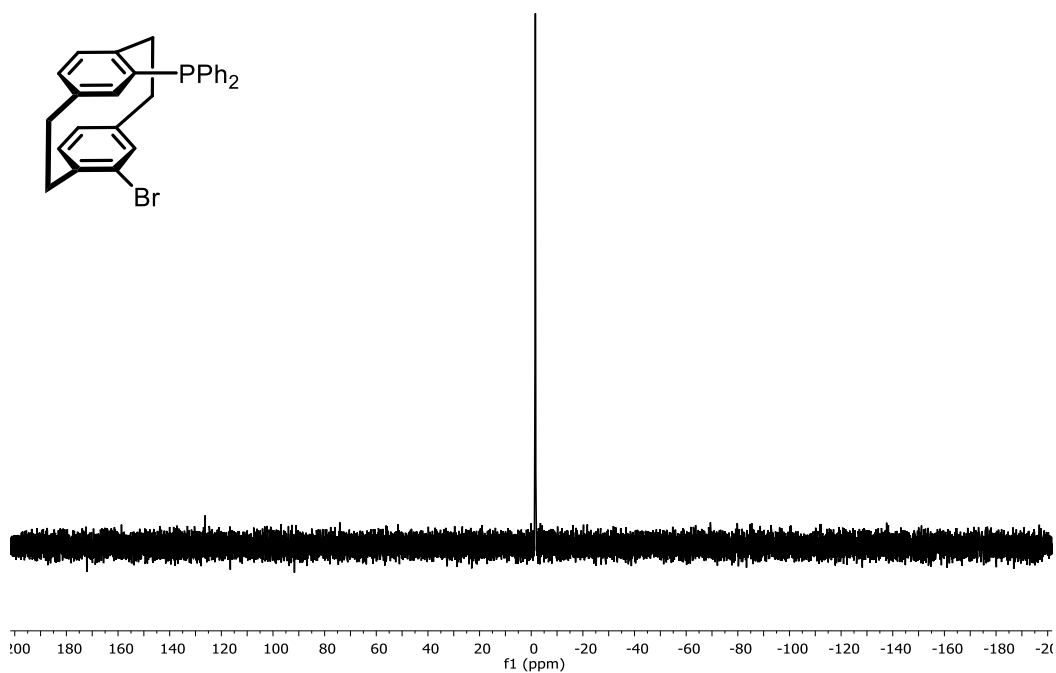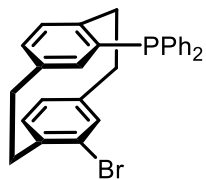
Compound **101** ^{1}H NMR (300 MHz, CDCl$_3$)
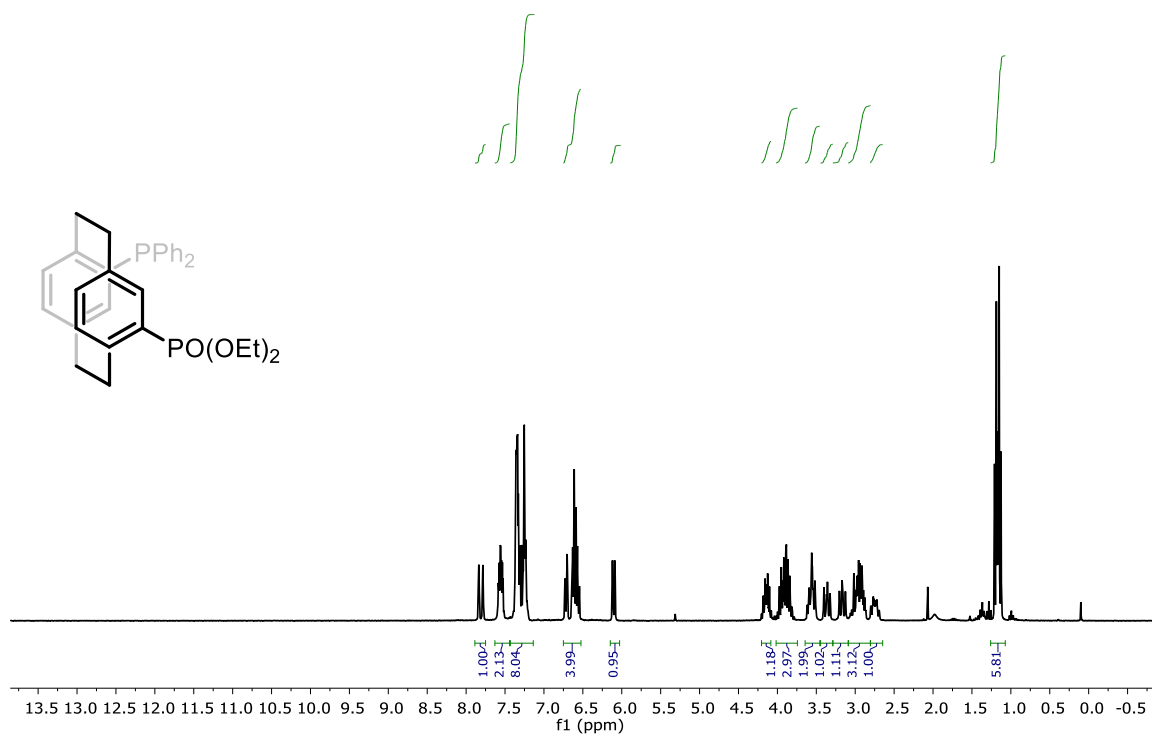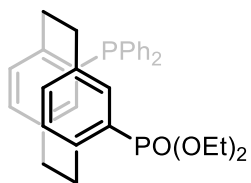
Compound **101** ^{31}P NMR (121 MHz, CDCl$_3$)
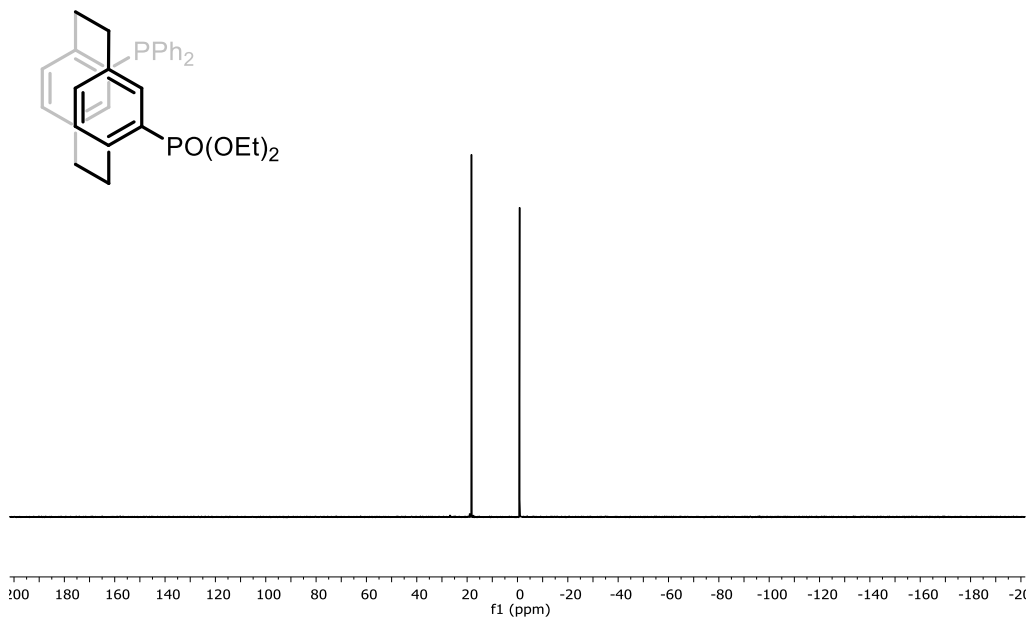
Compound **102** ^{1}H NMR (300 MHz, CDCl$_3$)
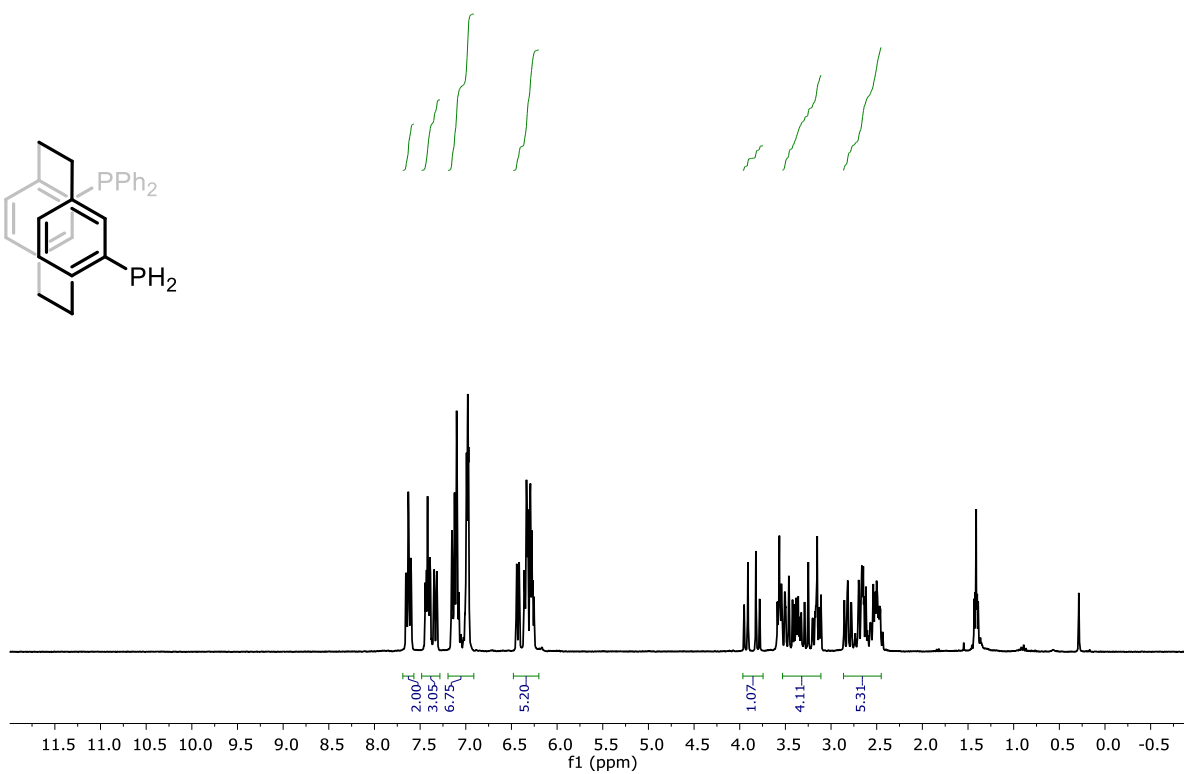
Compound **102** ³¹P NMR (121 MHz, CDCl₃)
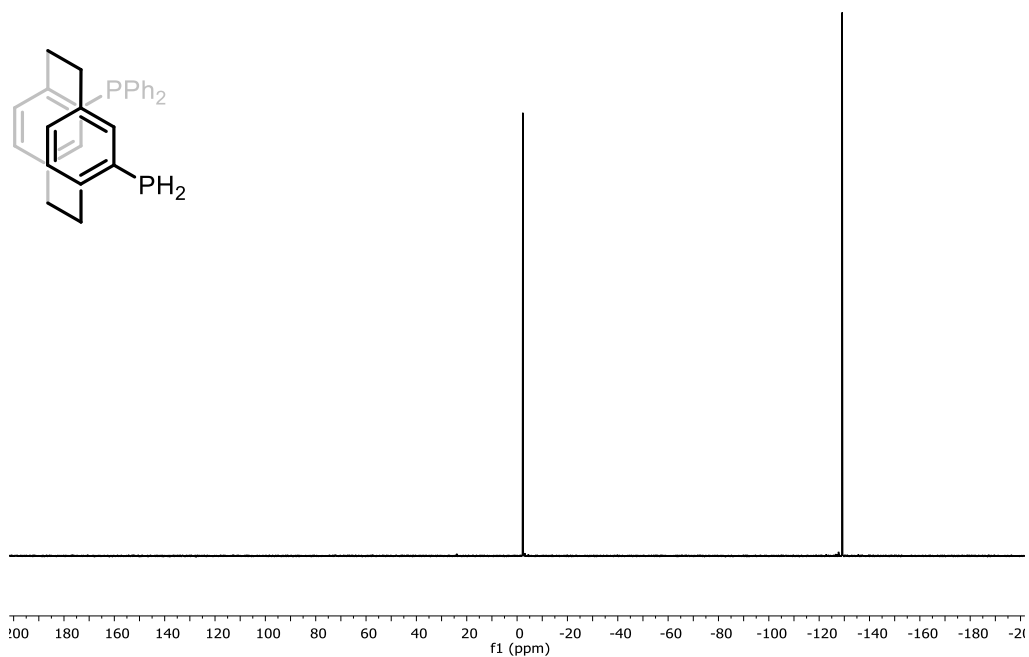
Compound **103** ¹H NMR (300 MHz, CD₃CN)
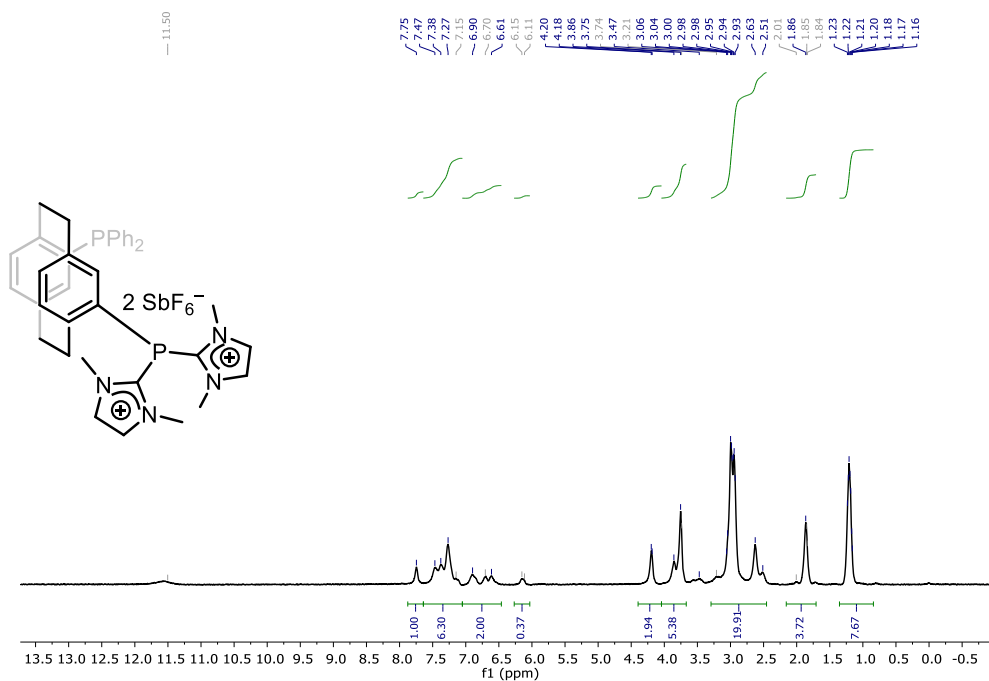
Compound **103** ^{31}P NMR (121 MHz, CD$_3$CN)
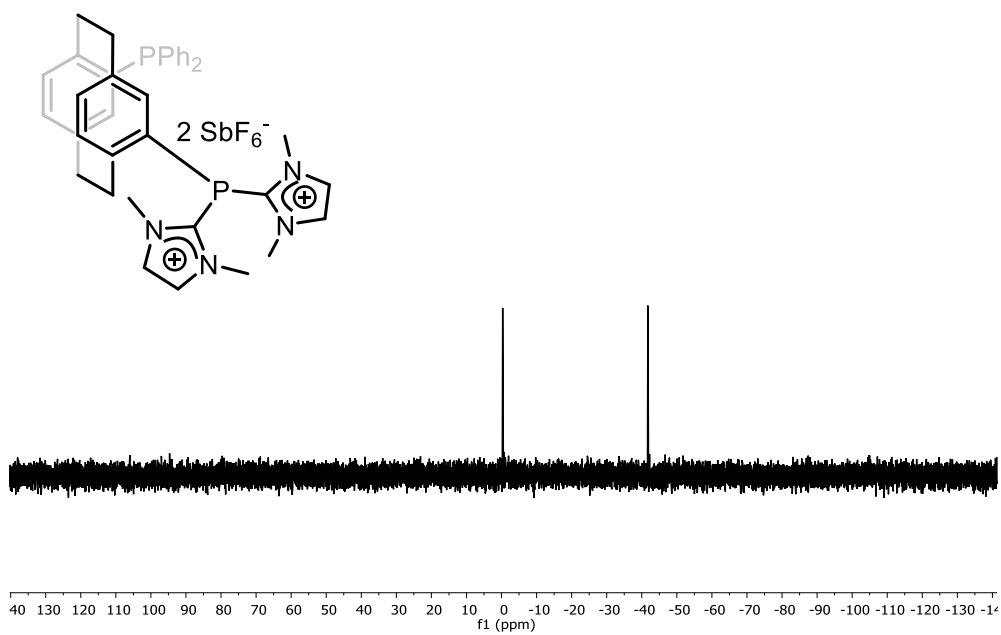
Compound **108** ¹H NMR (400 MHz, CD₂Cl₂)
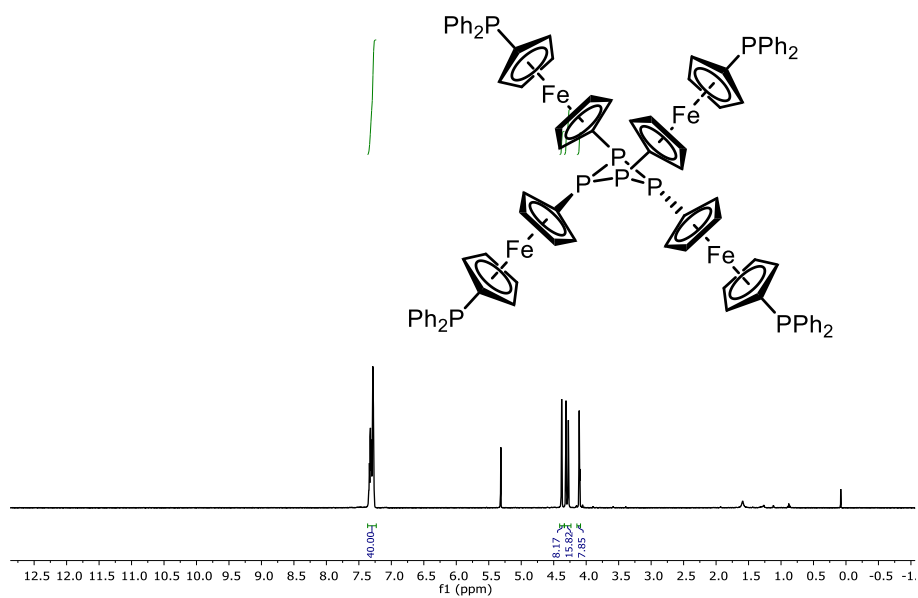
Compound **108** ³¹P NMR (162 MHz, CD₂Cl₂)
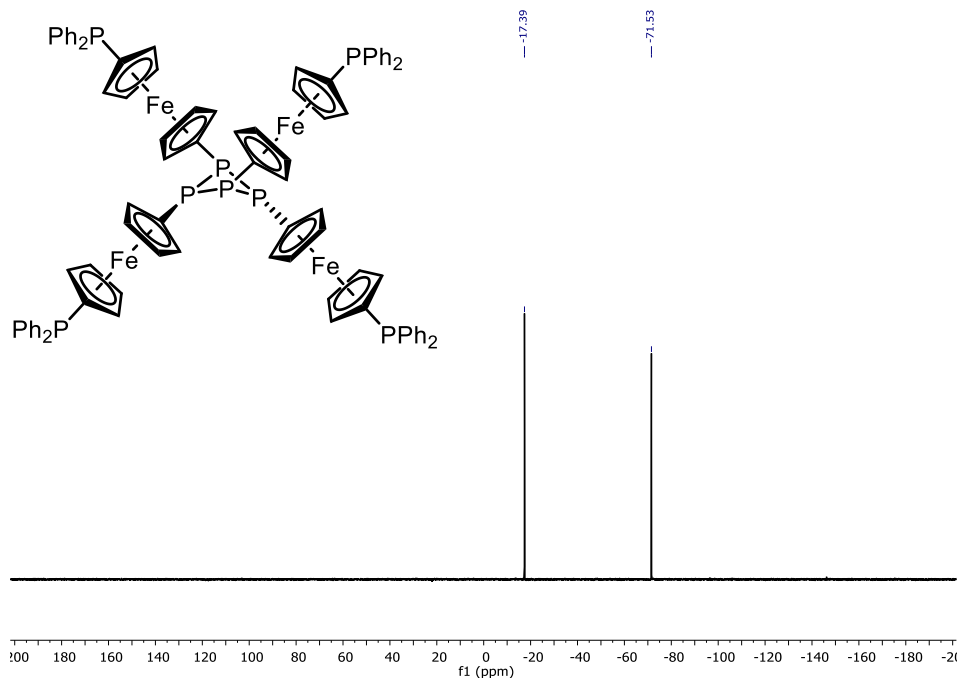
Compound **108** ^{13}C NMR (101 MHz, CD$_2$Cl$_2$)
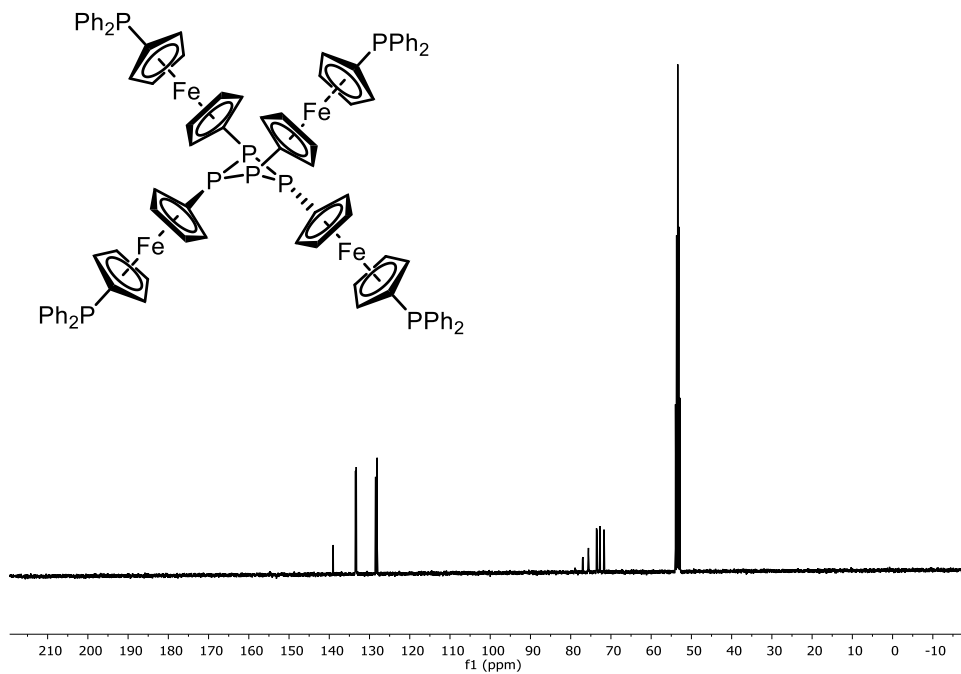
Compound **113** ^{1}H NMR (400 MHz, CD$_3$CN)
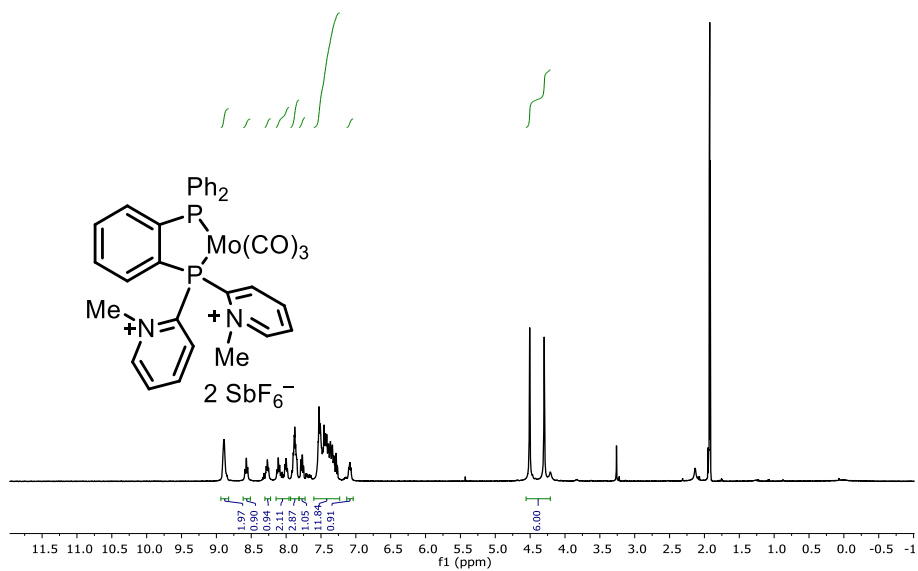
Compound **113** ^{31}P NMR (75 MHz, CD$_3$CN)
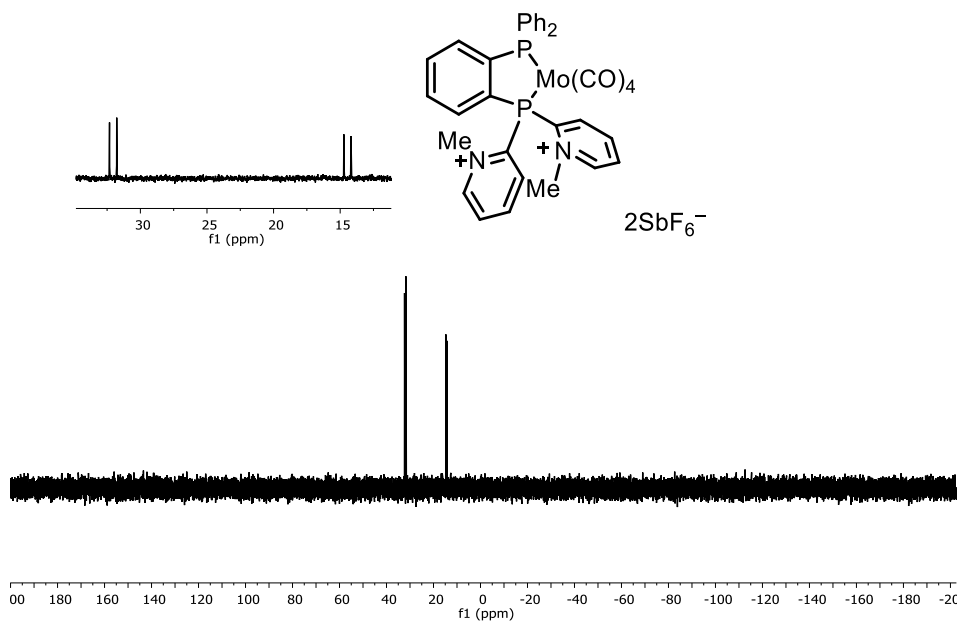
Compound **113** ^{13}C NMR (282 MHz, CD$_3$CN)
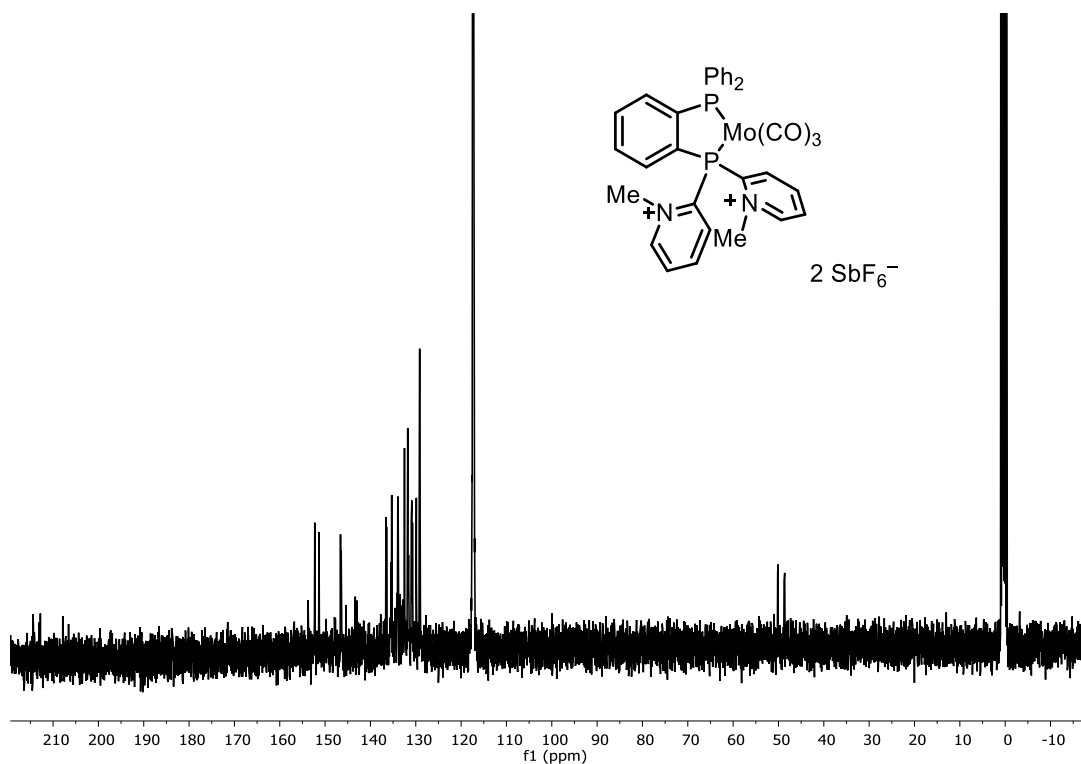
Compound **113** IR (neat)
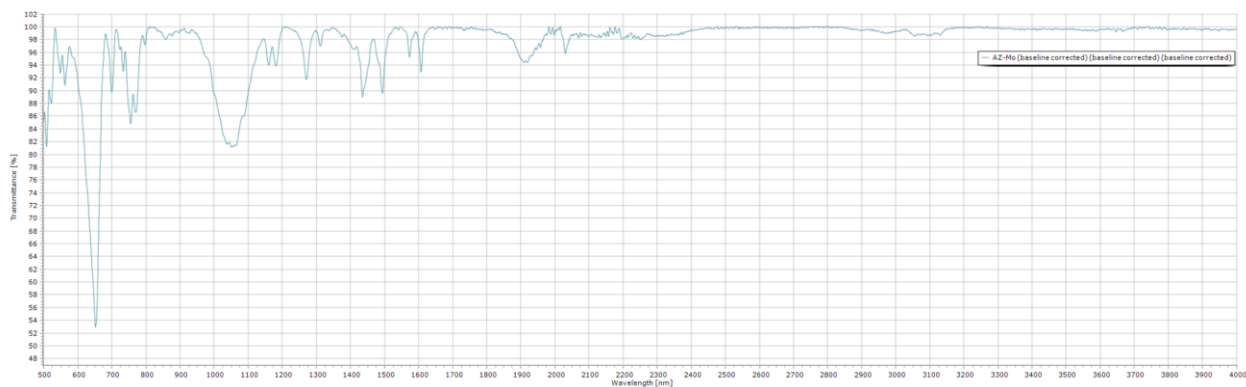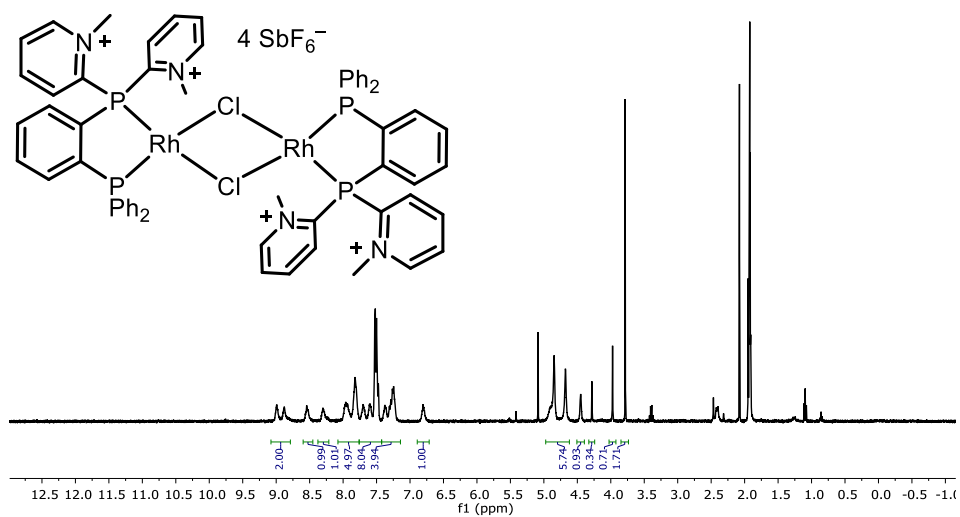

Compound **117** ^{1}H NMR (400 MHz, CD$_3$CN)
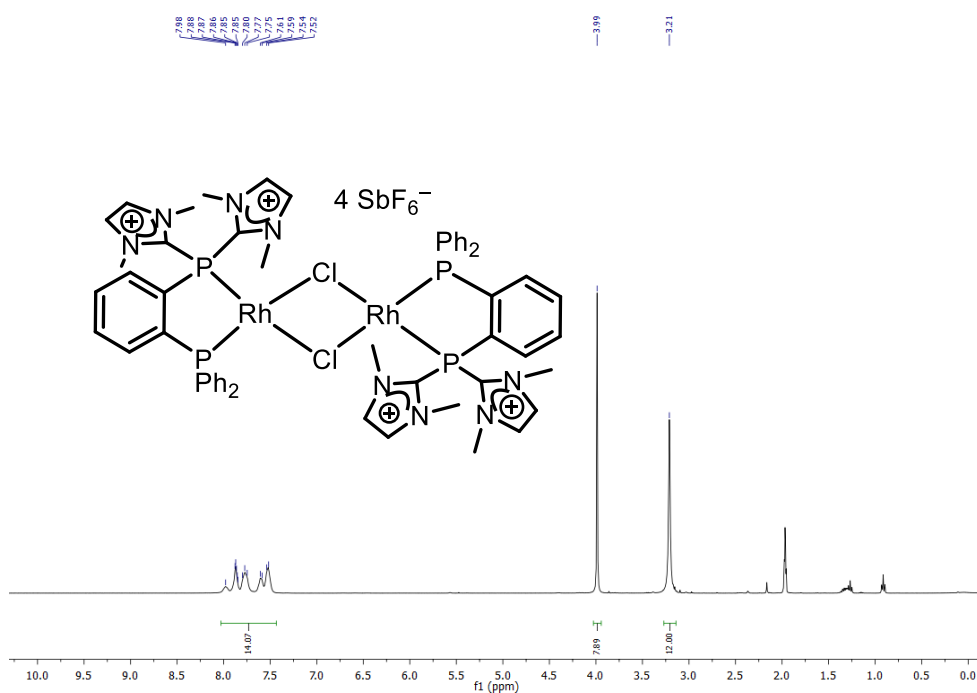
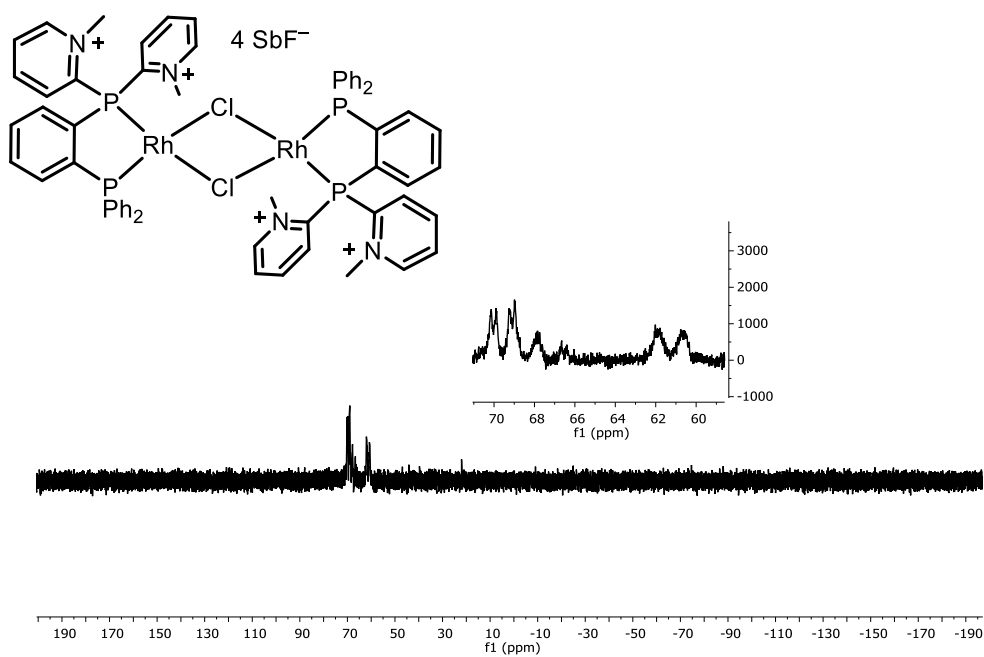Compound **117** ^{31}P NMR (162 MHz, CD$_3$CN)
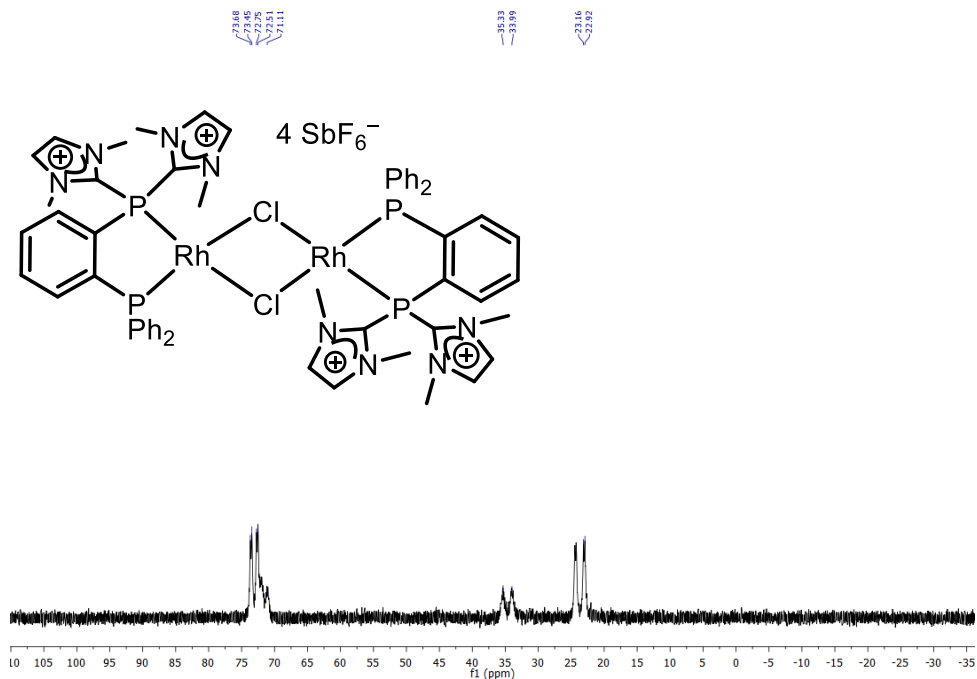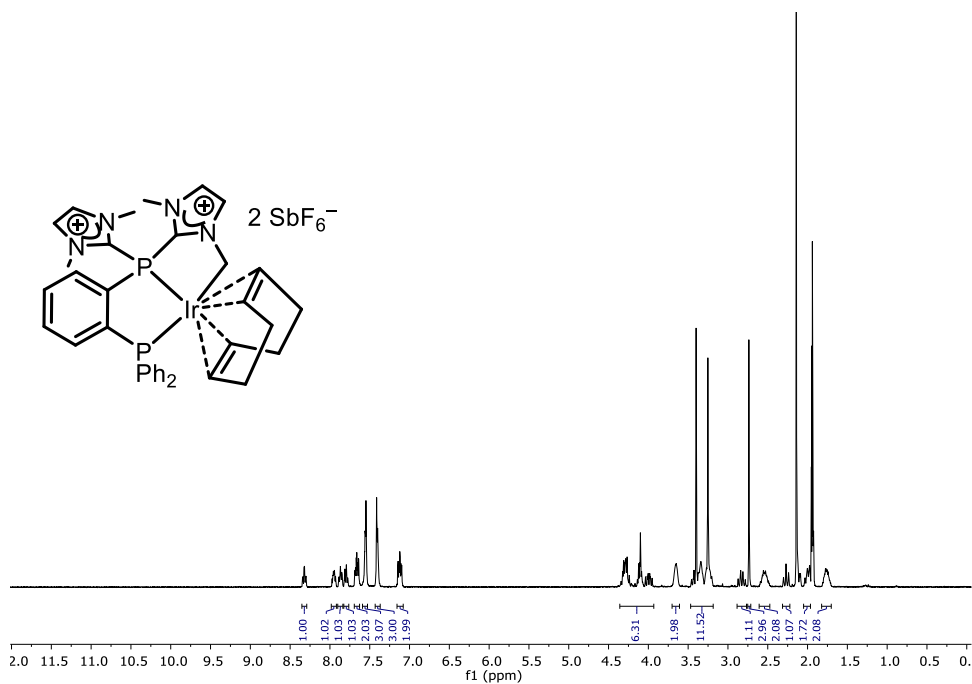

Compound **117** ^{13}C NMR (101 MHz, CD$_3$CN)
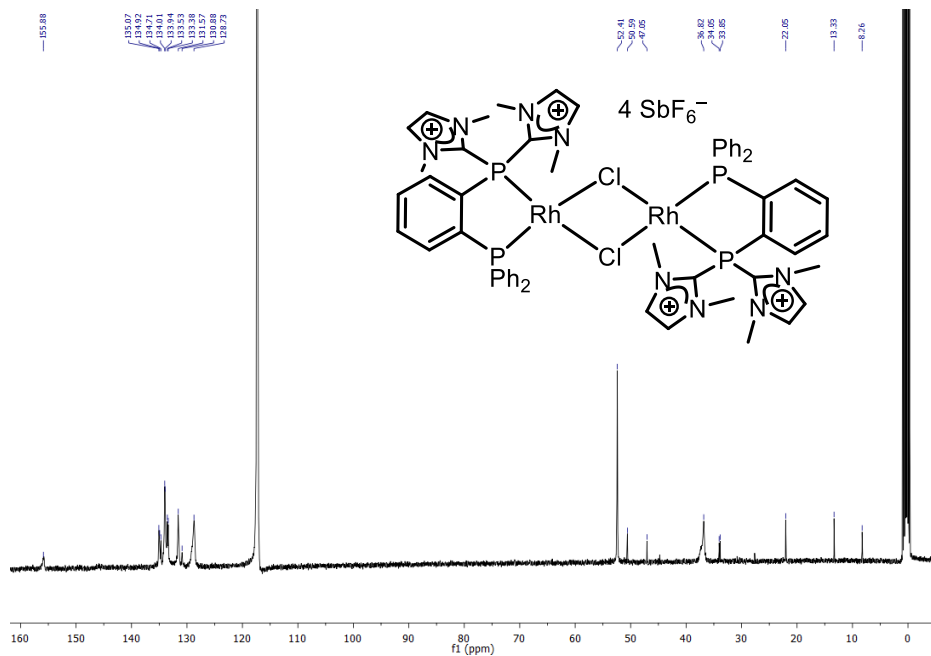
Compound **119** ^{1}H NMR (400 MHz, CD₃CN)
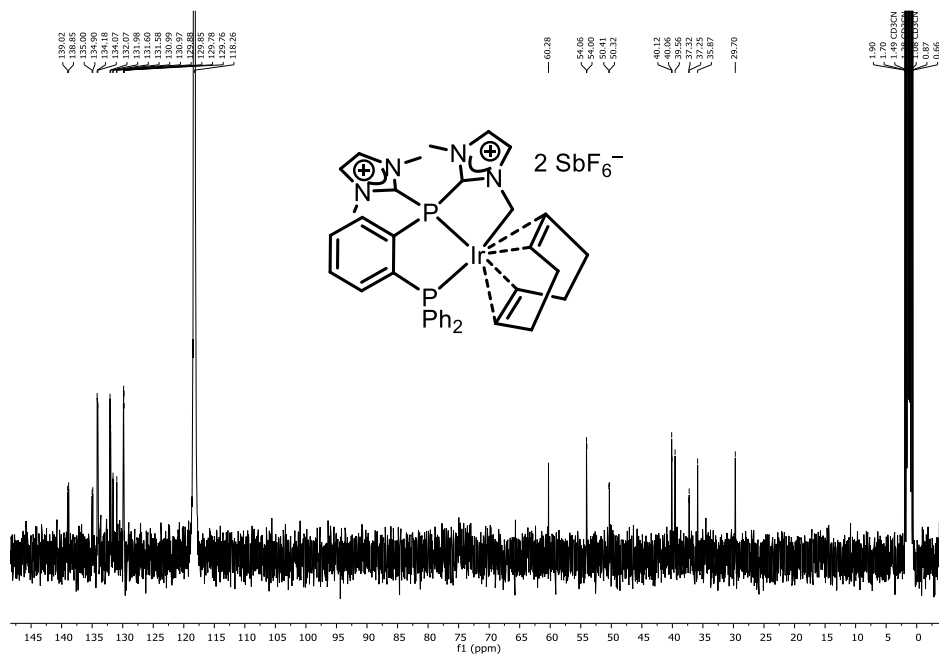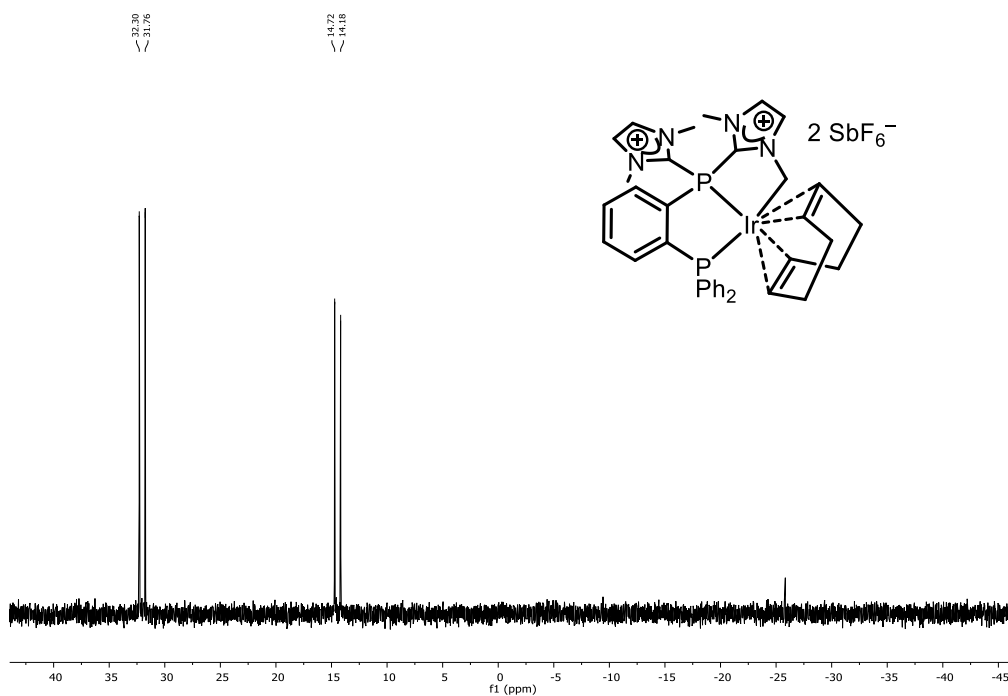

Compound **119** ^{31}P NMR (162 MHz, CD₃CN)

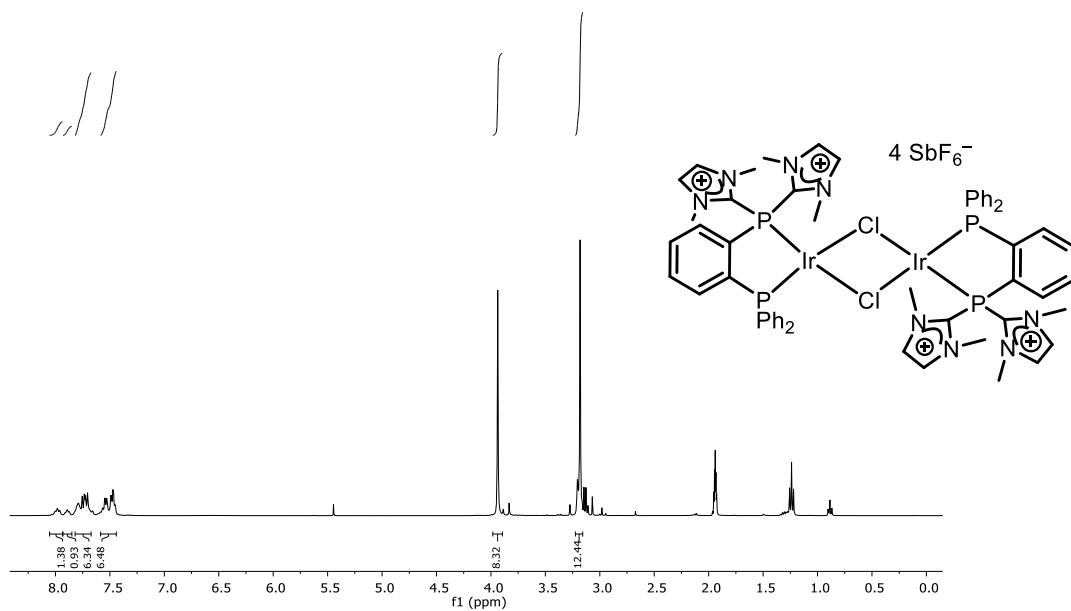Compound **122** ¹H NMR (400 MHz, CD₃CN)

Compound **122** ¹³C NMR (101 MHz, CD₃CN)

Compound **122** ^{31}P NMR (162 MHz, CD$_3$CN)

Compound **124** ^{1}H NMR (400 MHz, CD$_3$CN)

Compound **124** ^{31}P NMR (162 MHz, CD$_3$CN)

Compound **124** ^{13}C NMR (282 MHz, CD₃CN)

64

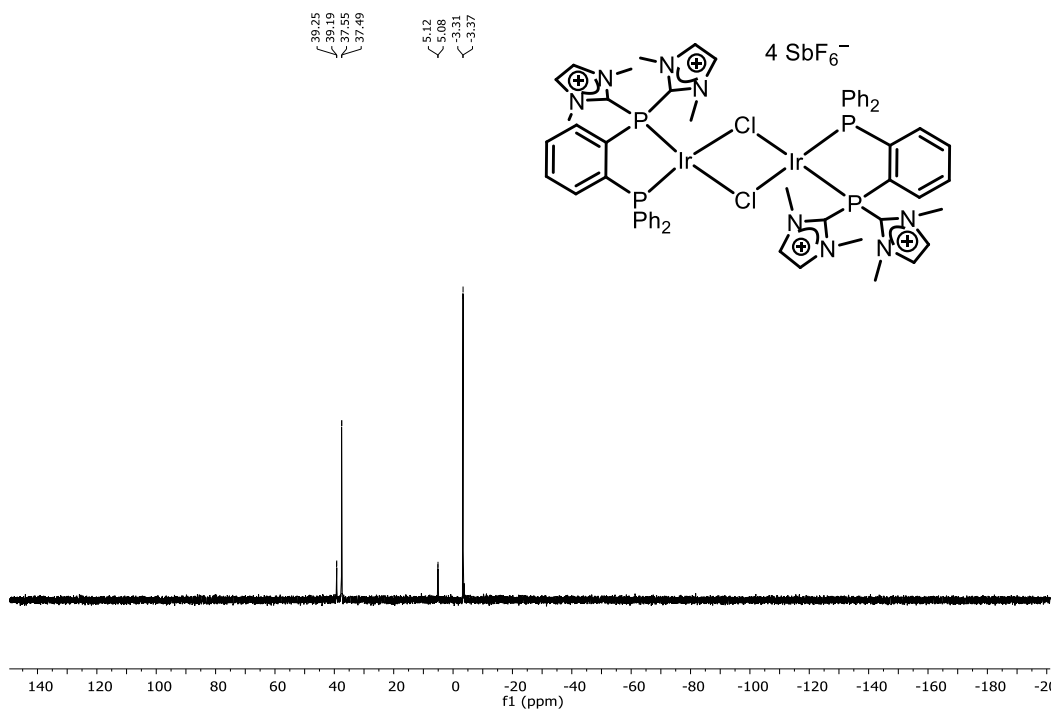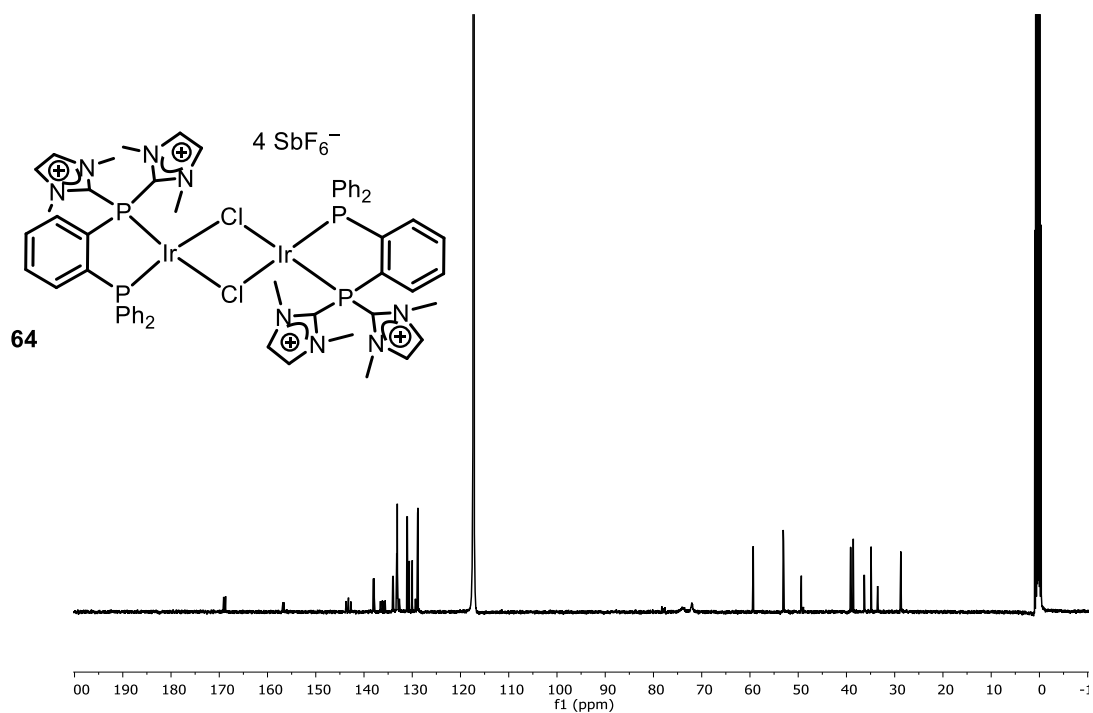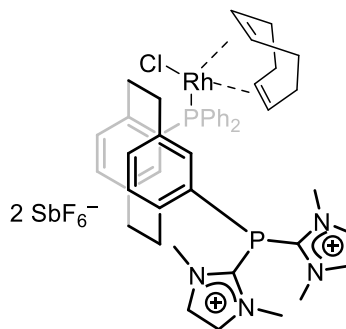Compound **126** ^{1}H NMR (400 MHz, CD$_3$CN)
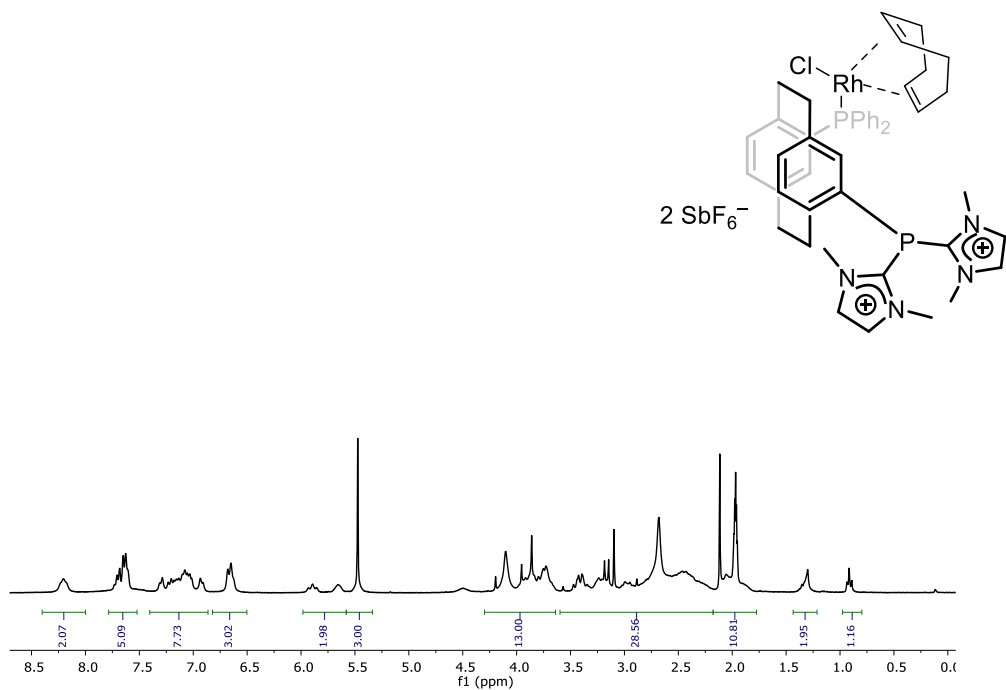
Compound **126** ^{31}P NMR (162 MHz, CD$_3$CN)
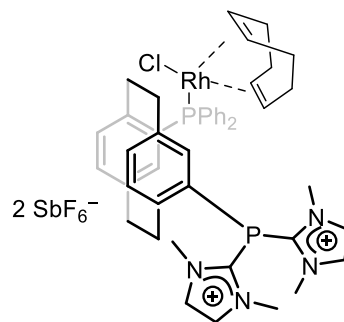
Compound **127** ¹H NMR (400 MHz, CD₃CN)

Compound **127** ³¹P NMR (162 MHz, CD₃CN)
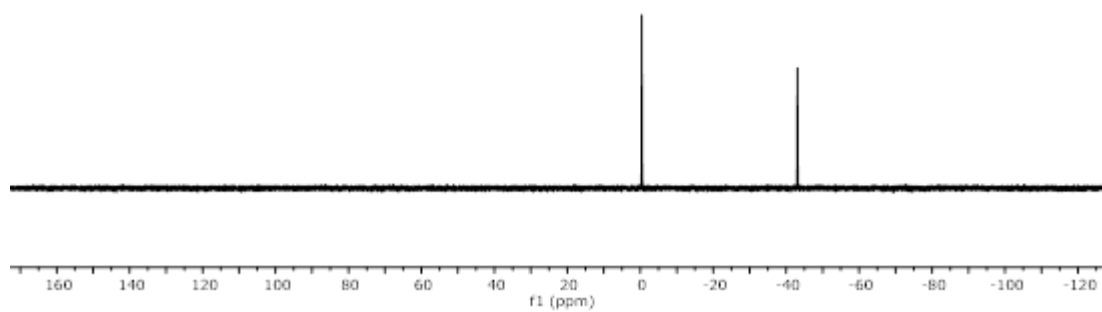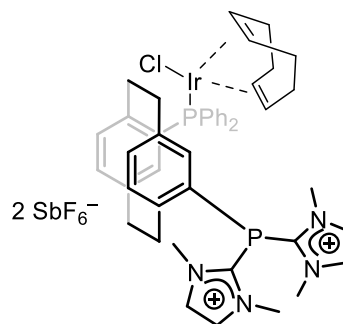
Compound **74a** ^{1}H NMR (400 MHz, CDCl$_3$)
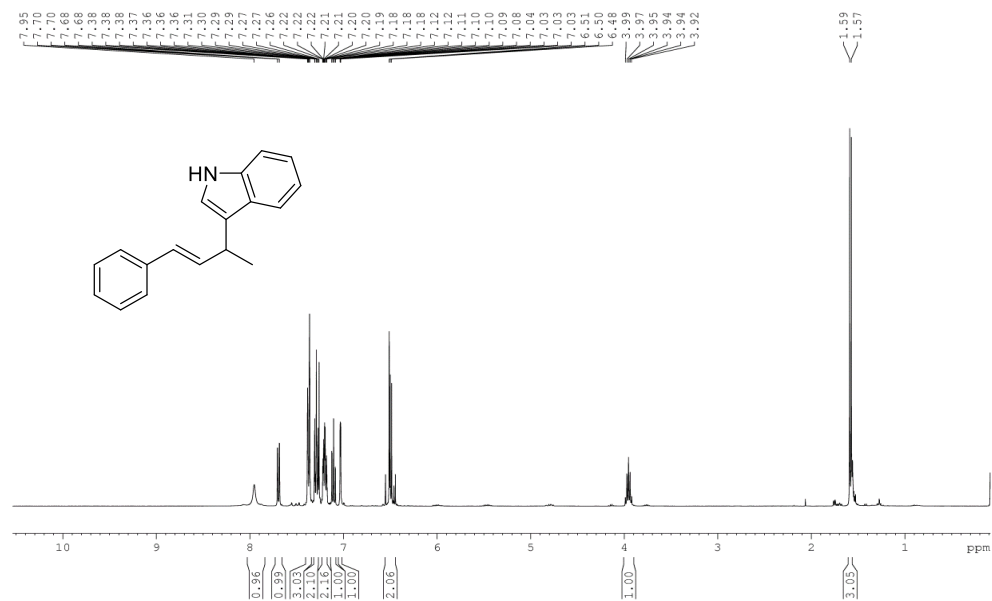
Compound **74a** ^{13}C NMR (100 MHz, CDCl$_3$)
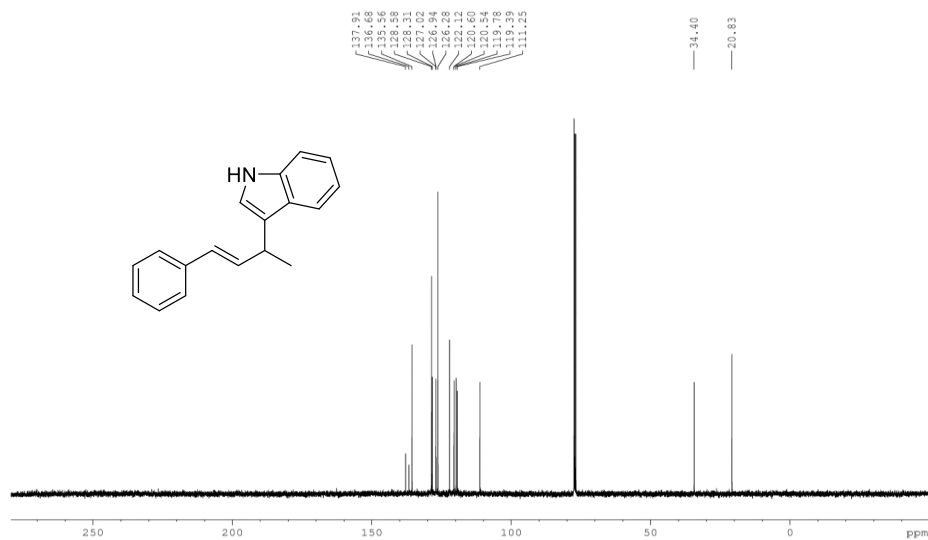
Compound **74b** ^{1}H NMR (600 MHz, C$_6$D$_6$)
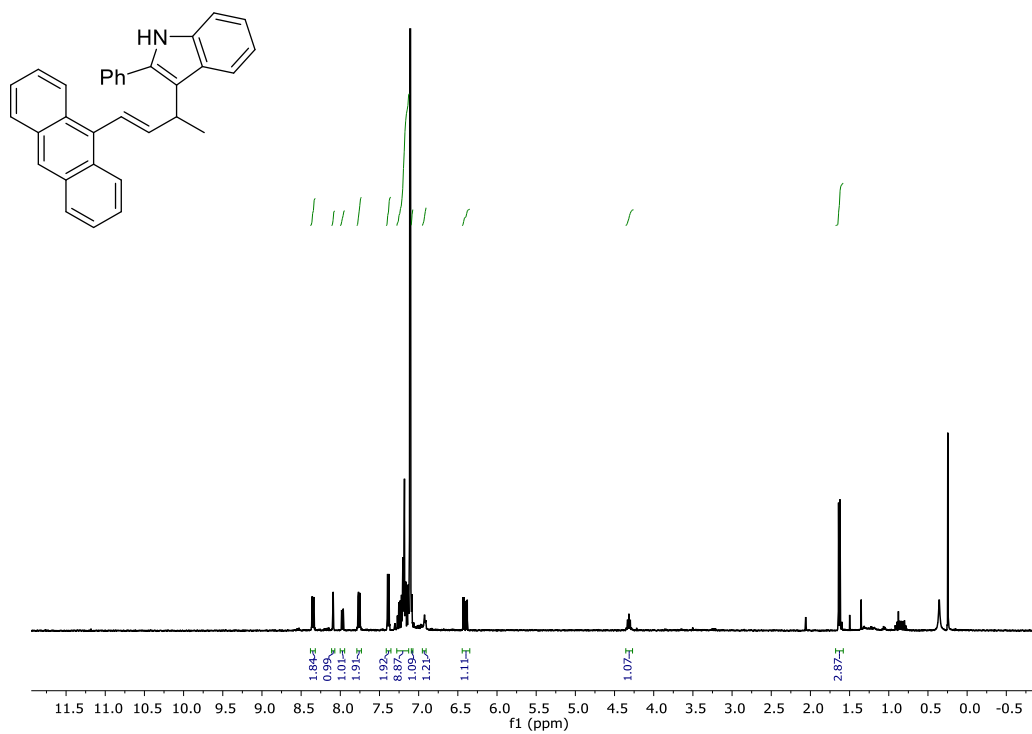
Compound **74b** ^{13}C NMR (100 MHz, CDCl$_3$)
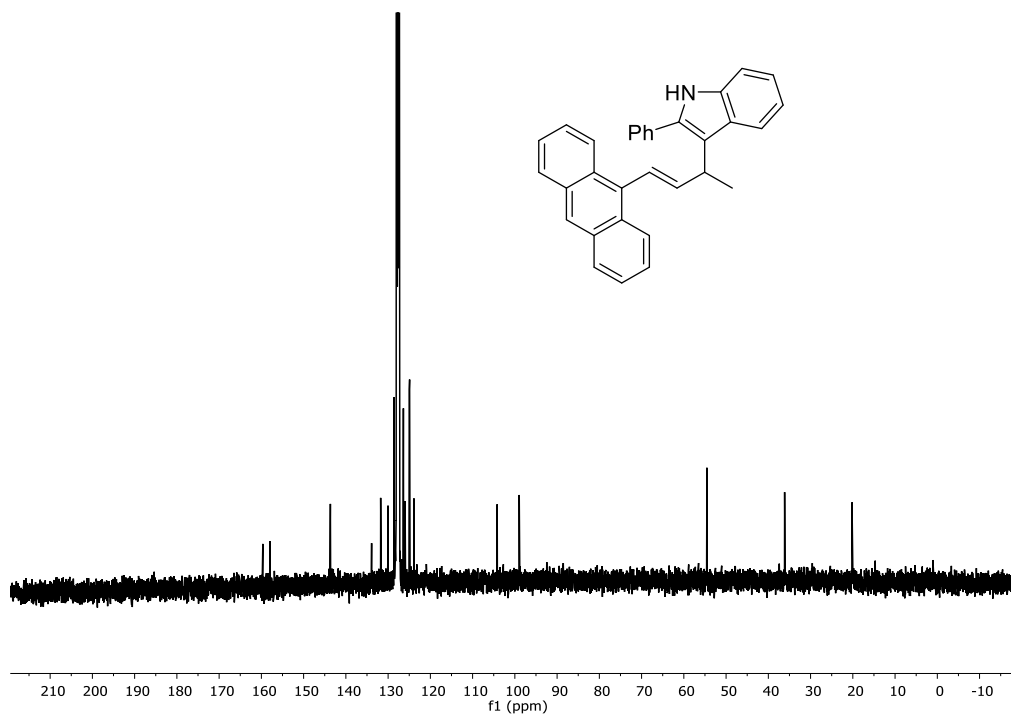
Compound **74c** ^{1}H NMR (400 MHz, CDCl$_3$)
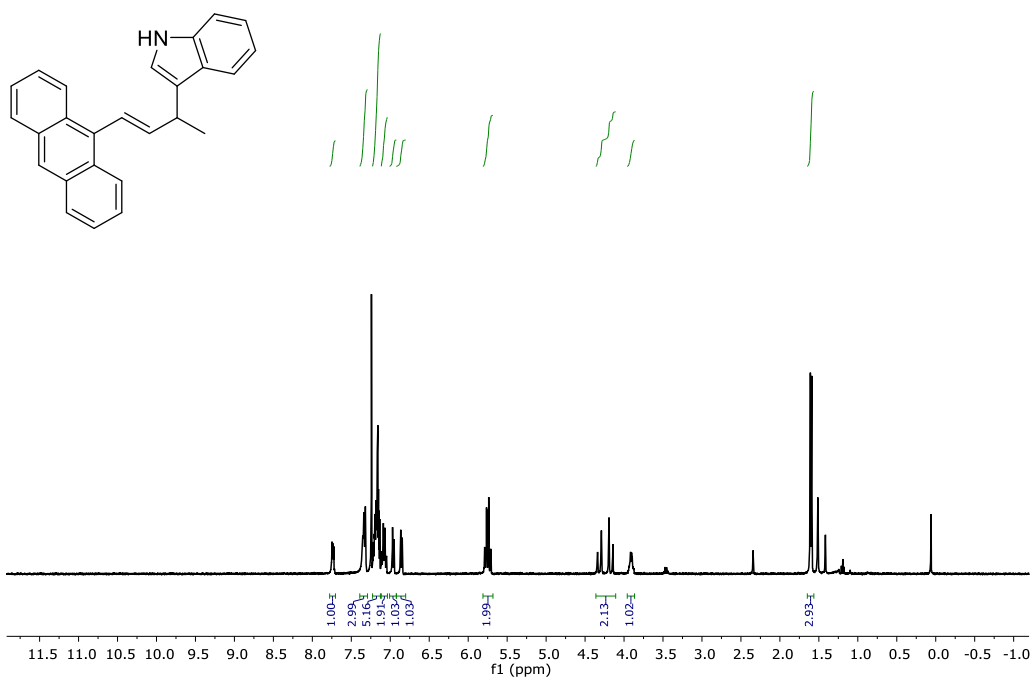
Compound **74c** ^{13}C NMR (100 MHz, CDCl$_3$)

Compound **74d** ^{1}H NMR (400 MHz, CDCl$_3$)
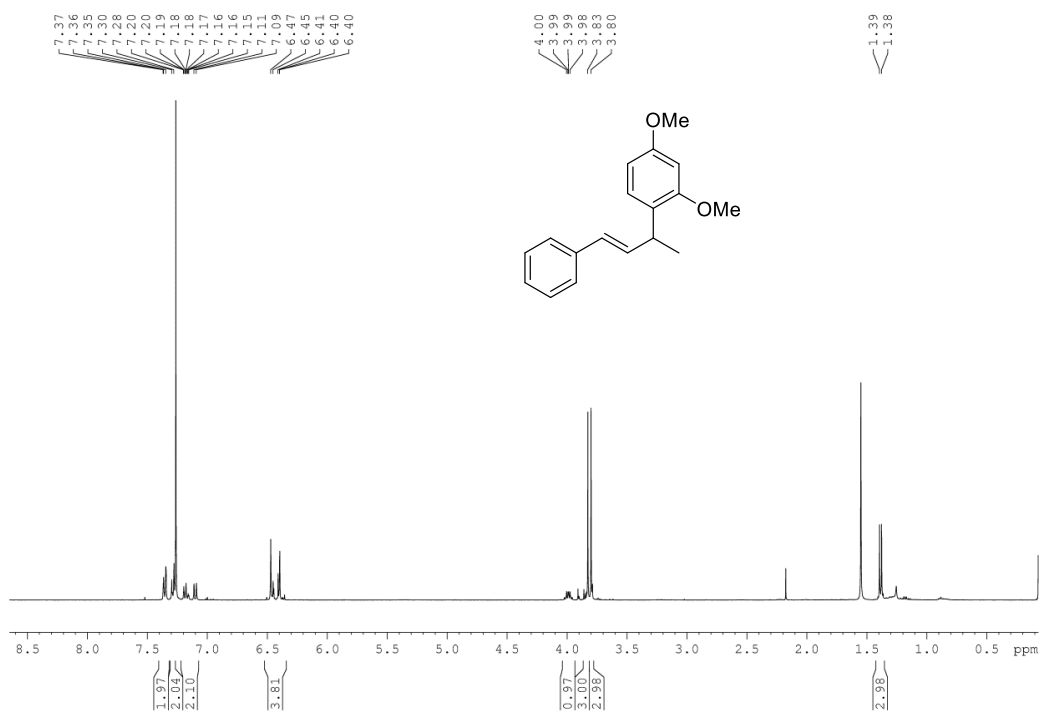
Compound **74d** ^{13}C NMR (100 MHz, CDCl$_3$)
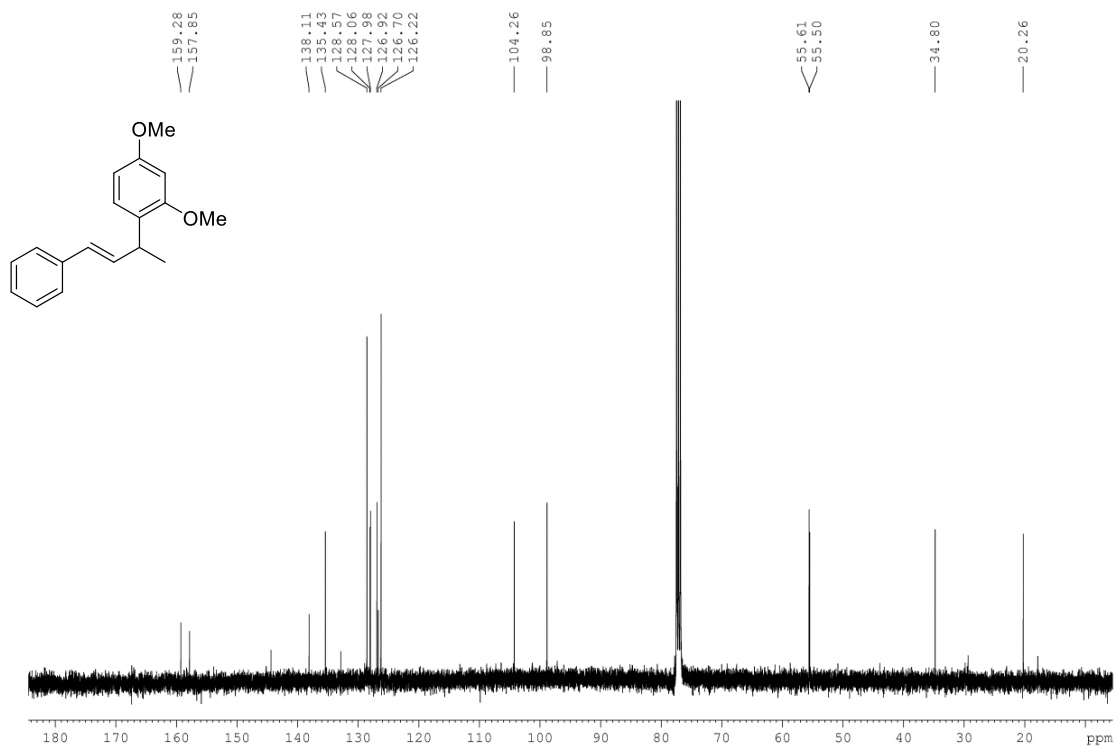
Compound **74e** ^{1}H NMR (400 MHz, CDCl$_3$)
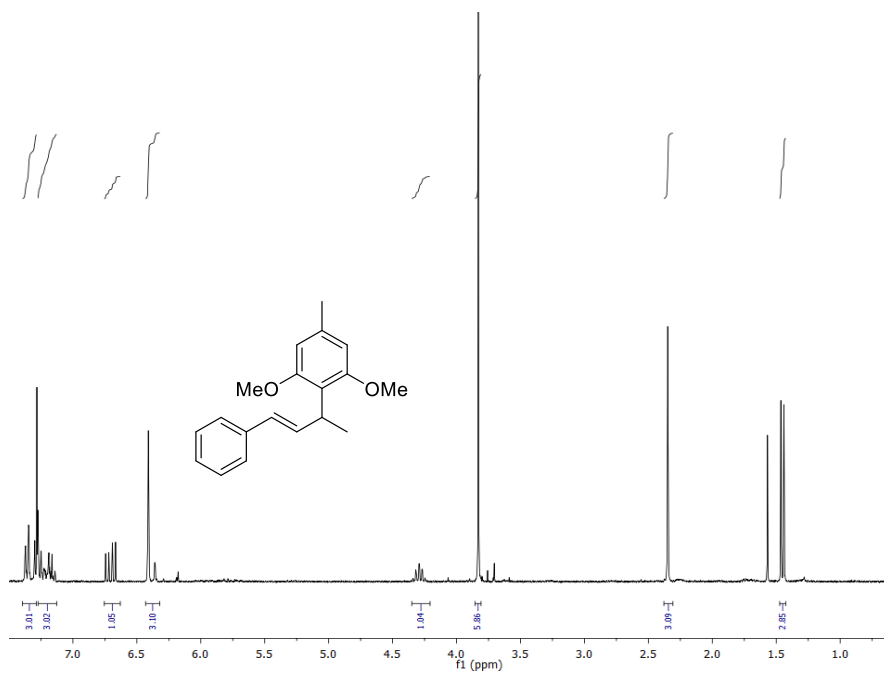
Compound **74e** ^{13}C NMR (100 MHz, CDCl$_3$)
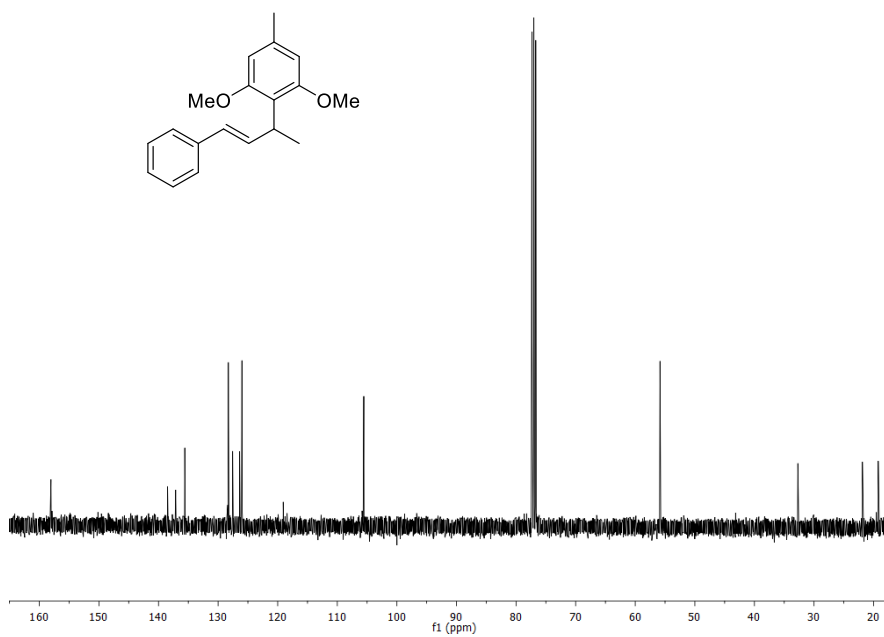
Compound **74f** ^{1}H NMR (400 MHz, CDCl$_3$) (mixture of 4- and 2- regioisomers):
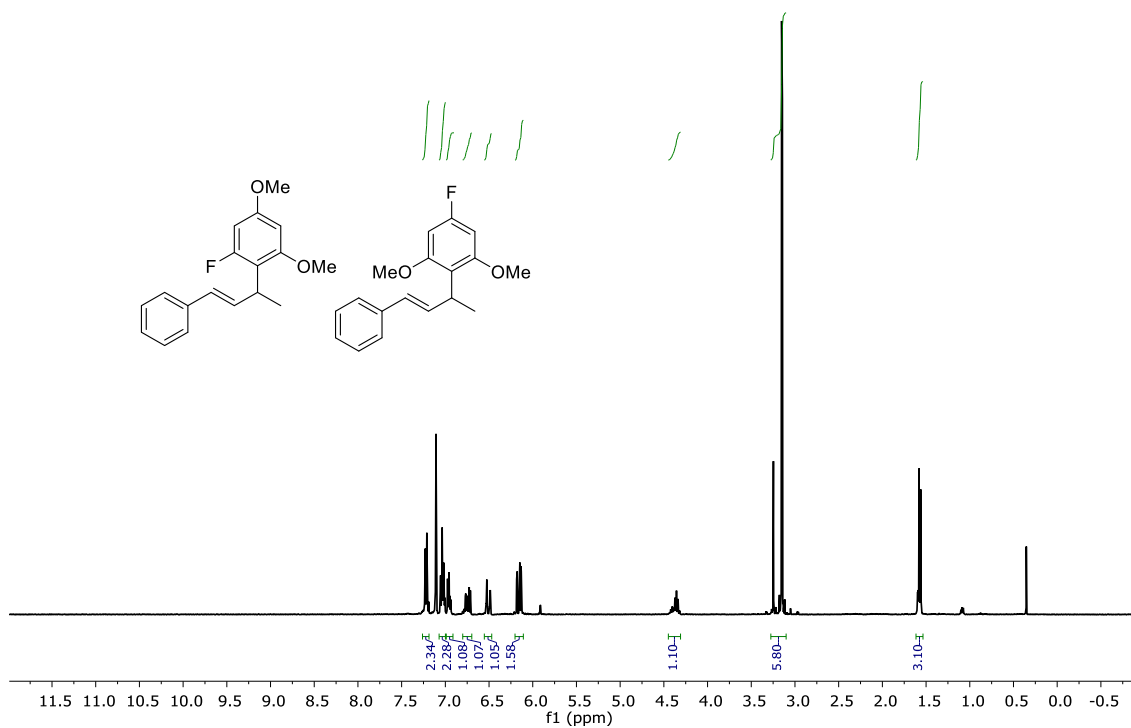
Compound **74g** ^{1}H NMR (400 MHz, C$_6$D$_6$)
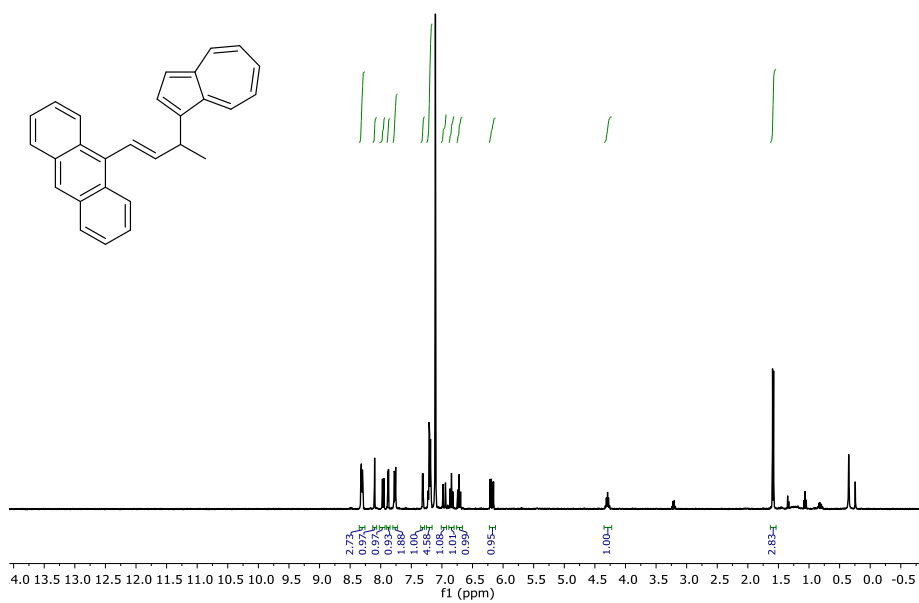
Compound **74g** ^{13}C NMR (100 MHz, CDCl$_3$)
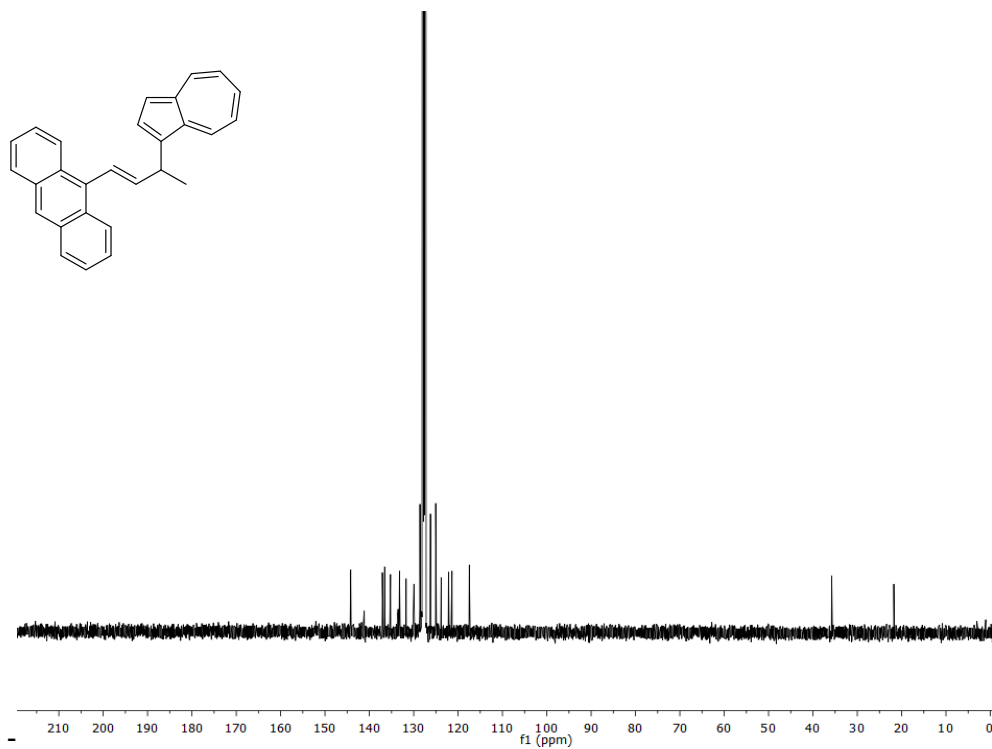
Compound **74h** ^{1}H NMR (400 MHz, C$_6$D$_6$)
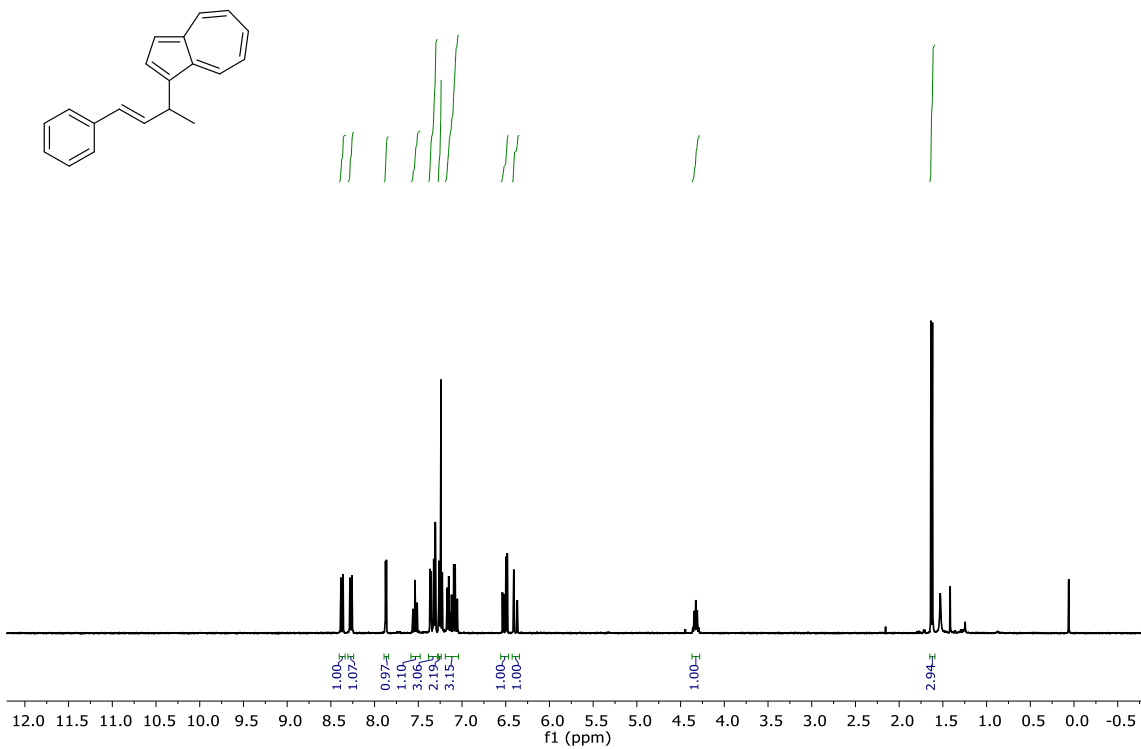
Compound **74h** ^{13}C NMR (100 MHz, CDCl$_3$)
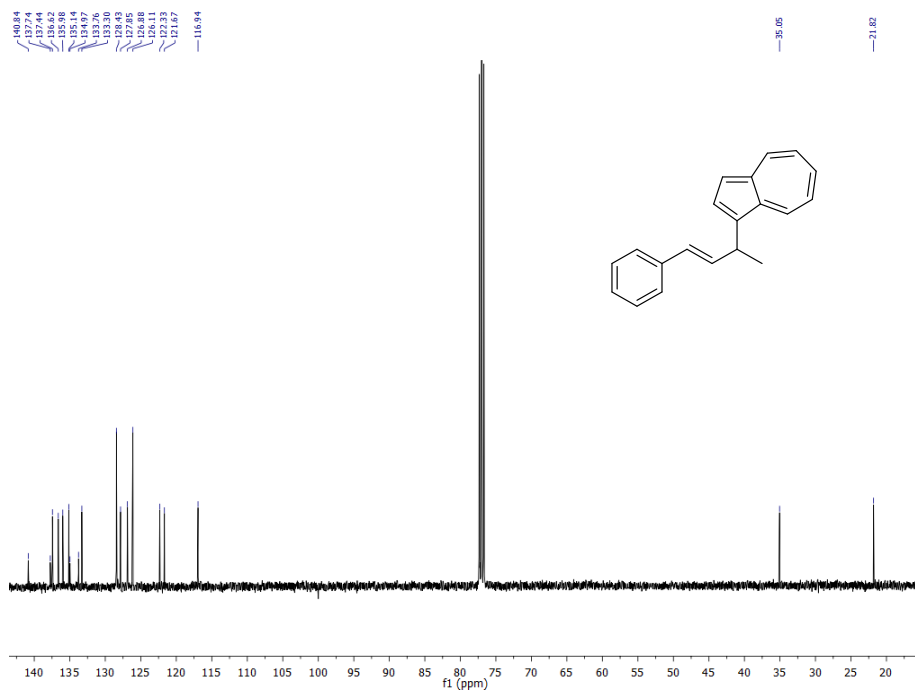
Compound **74i** ^{1}H NMR (400 MHz, C$_6$D$_6$)
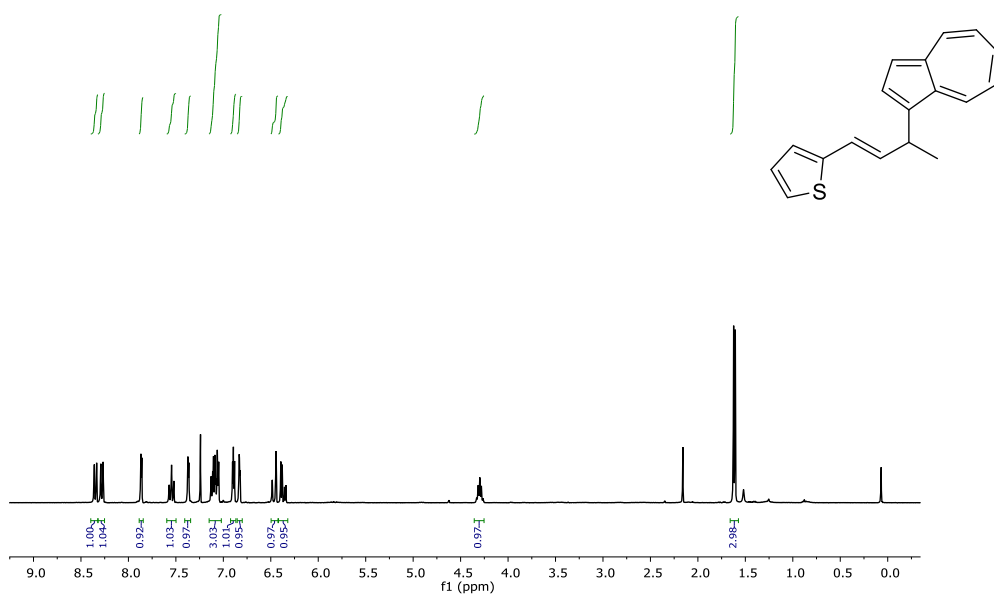
Compound **74h** ^{13}C NMR (101 MHz, CDCl$_3$)
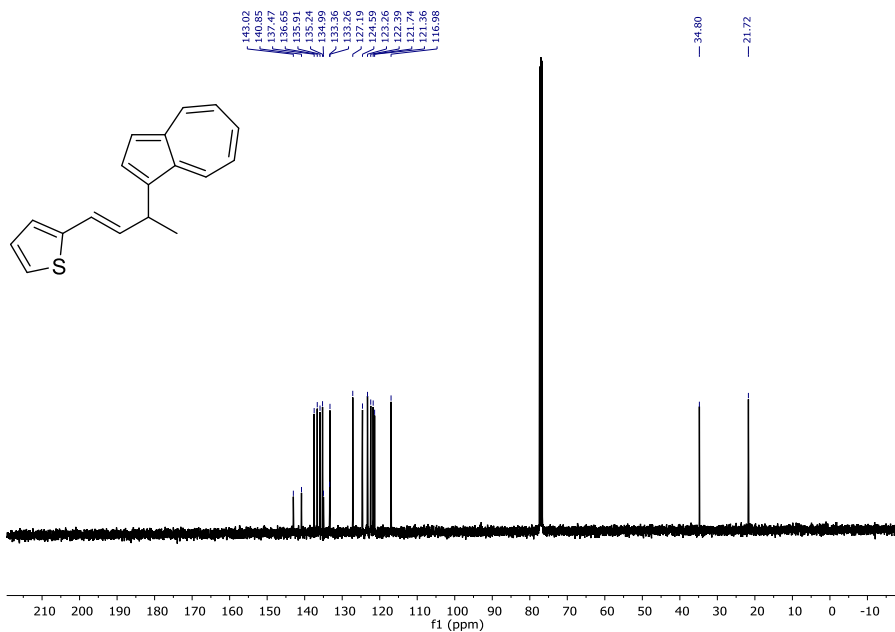
Compound **132** ^{1}H NMR (400 MHz, CDCl${}_3$)
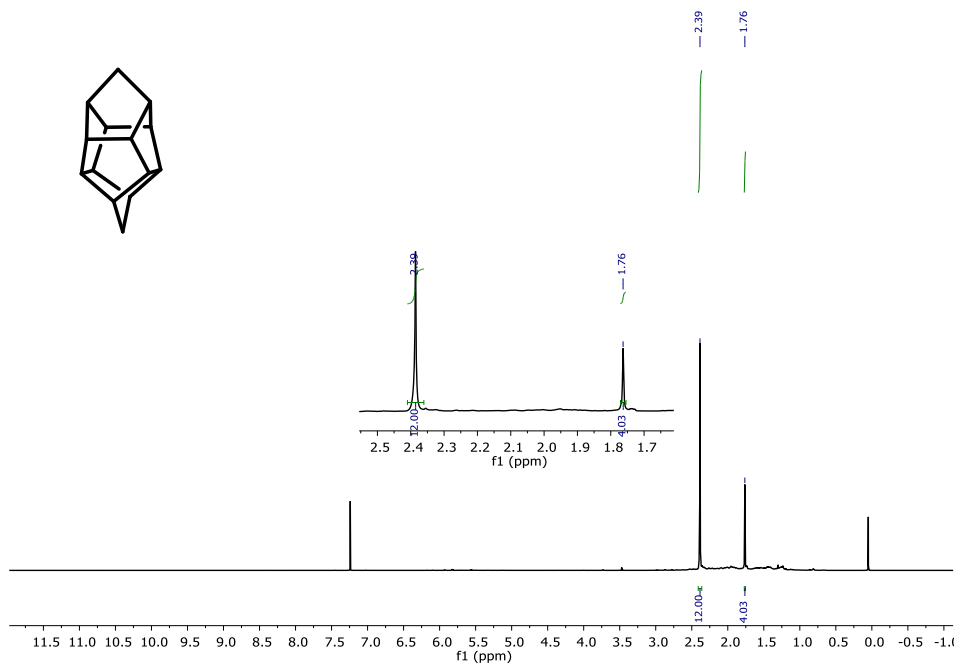
Compound 132 ^{13}C NMR (100 MHz, CDCl${}_3$)
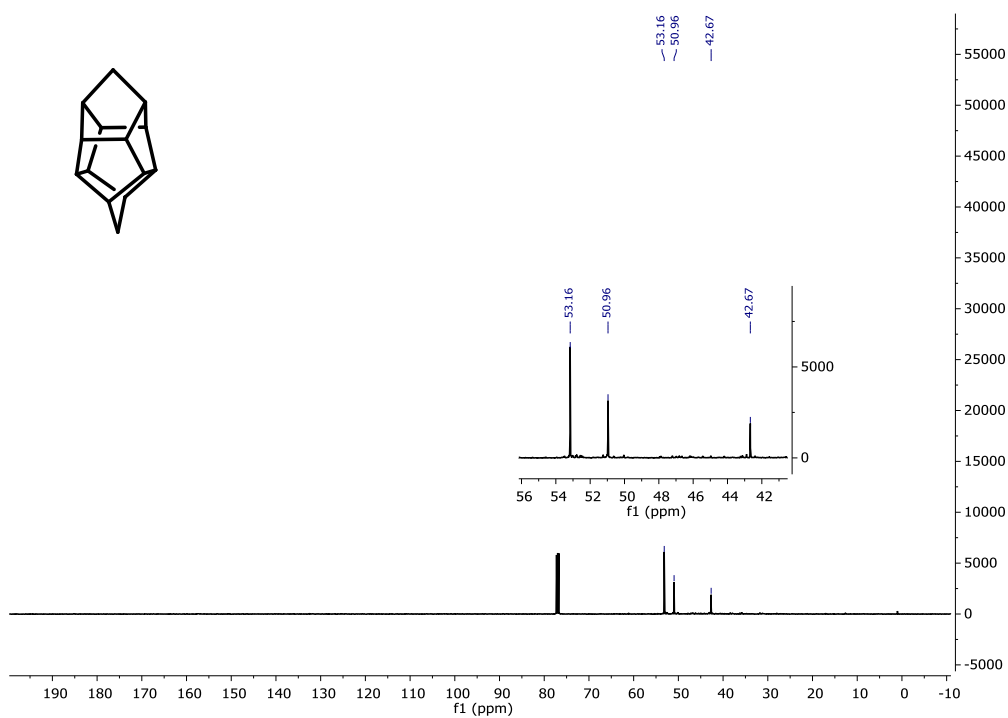
Compound **132** ^{13}C APT NMR (100 MHz, CDCl$_3$)
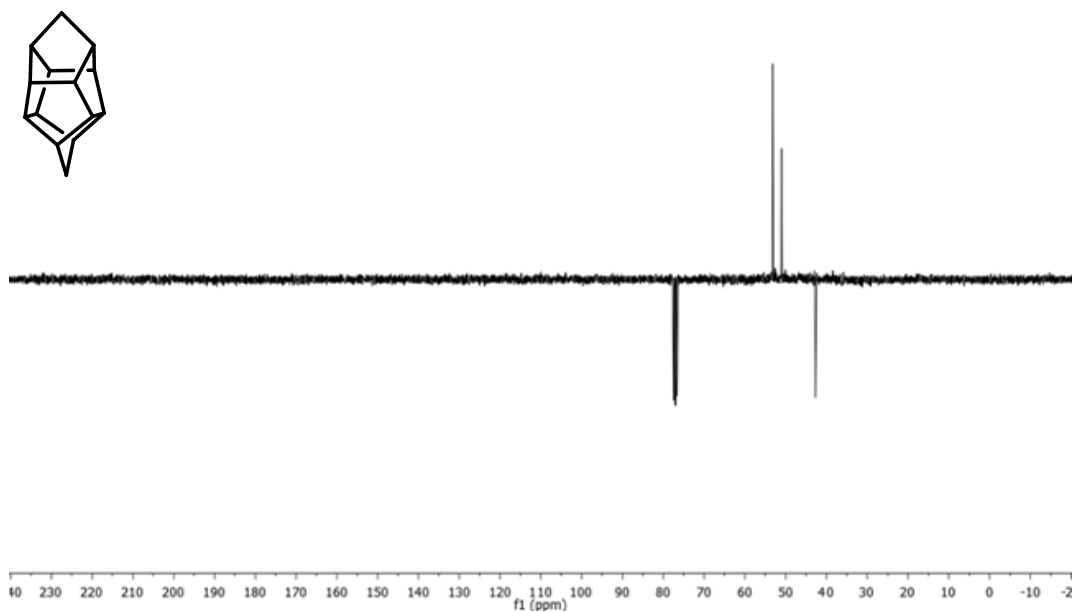
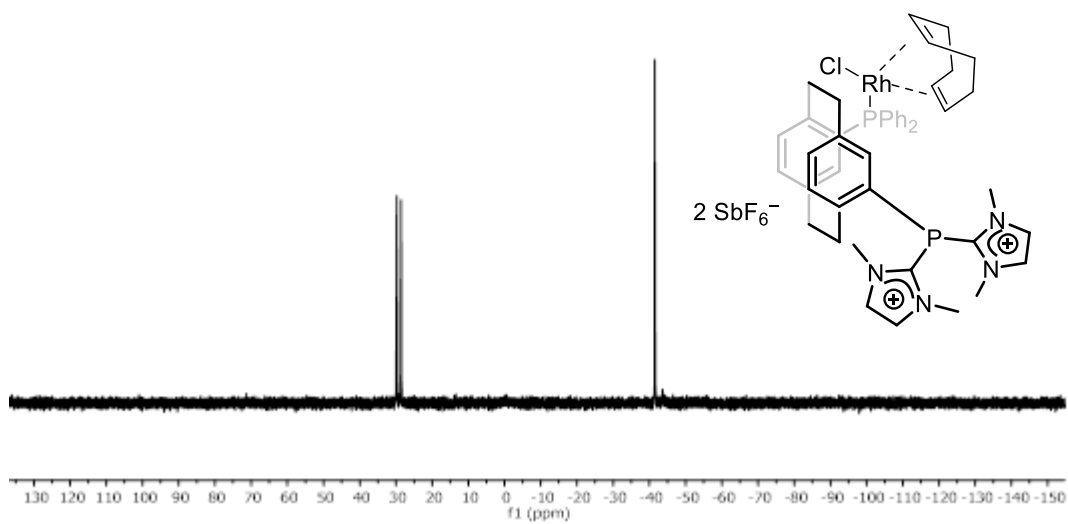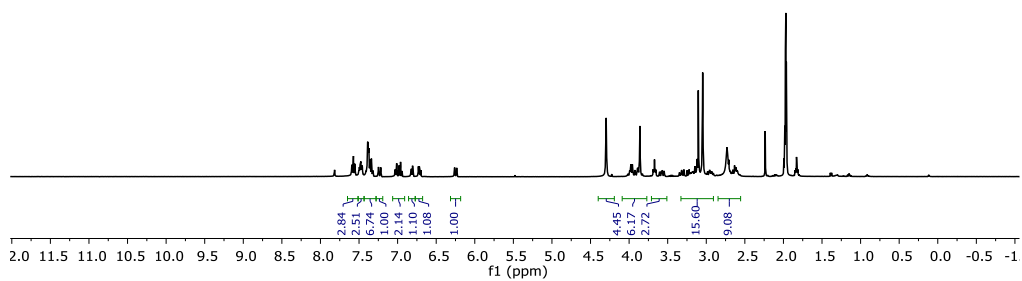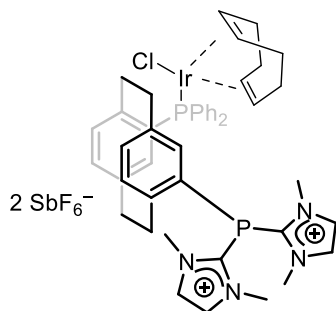Compound **142** ^{1}H NMR (400 MHz, CDCl$_3$)
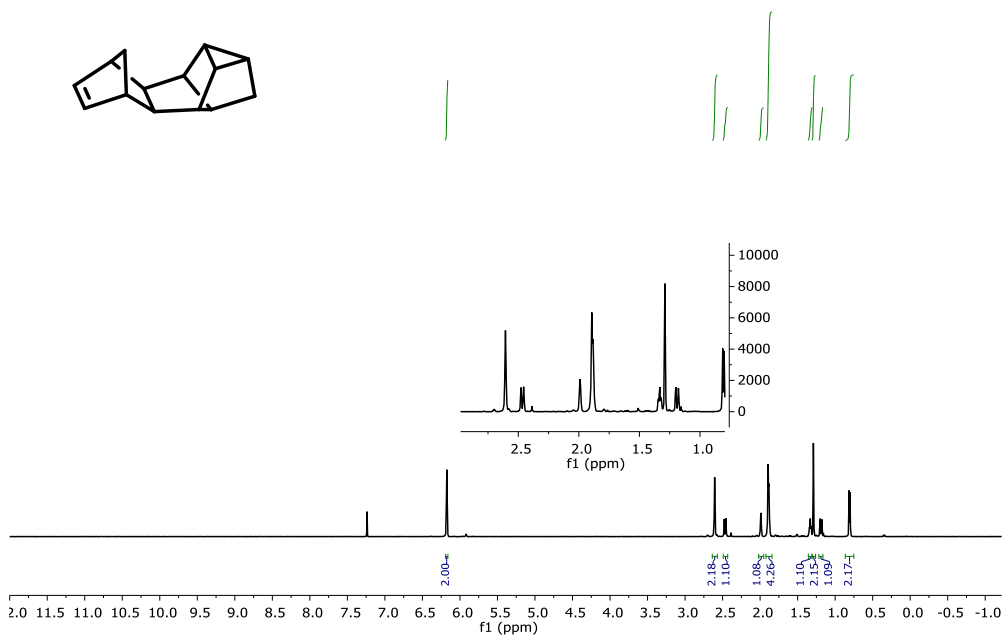
Compound **142** ^{13}C NMR (126 MHz, CDCl$_3$)
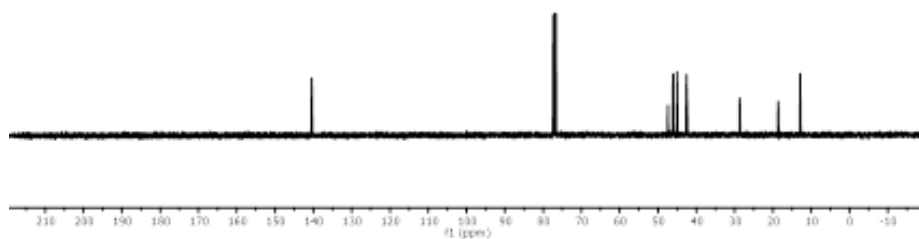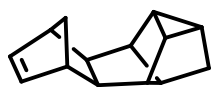
Compound **146** ^{1}H NMR (400 MHz, CDCl$_3$)
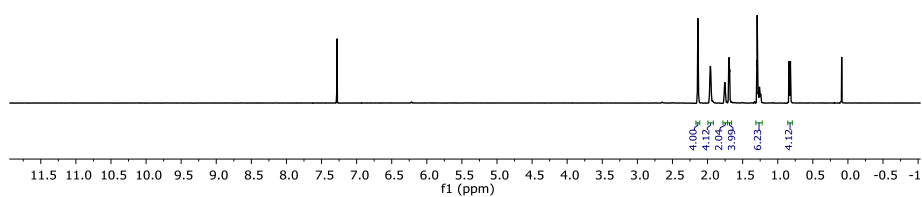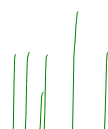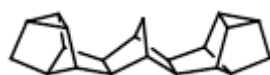
Compound **146** ^{13}C NMR (100 MHz, CDCl$_3$)
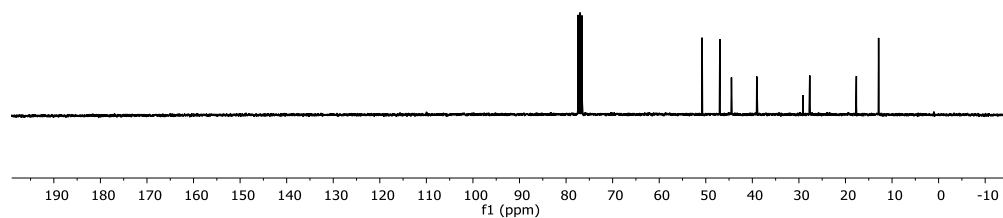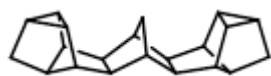
Compound **146** ^{13}C APT NMR (100 MHz, CDCl$_3$)
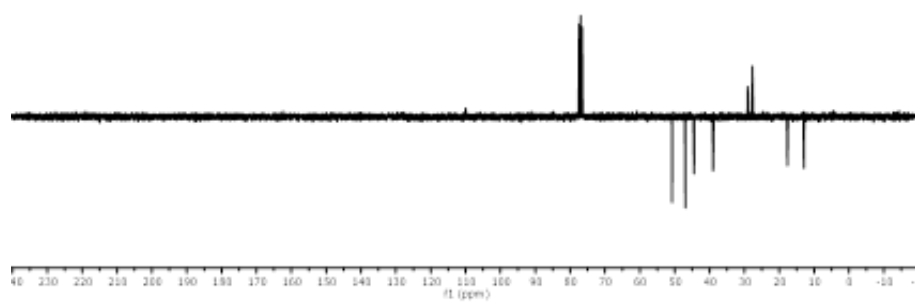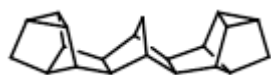
Compound **153a** ^{1}H NMR (400 MHz, CD$_2$Cl$_2$)
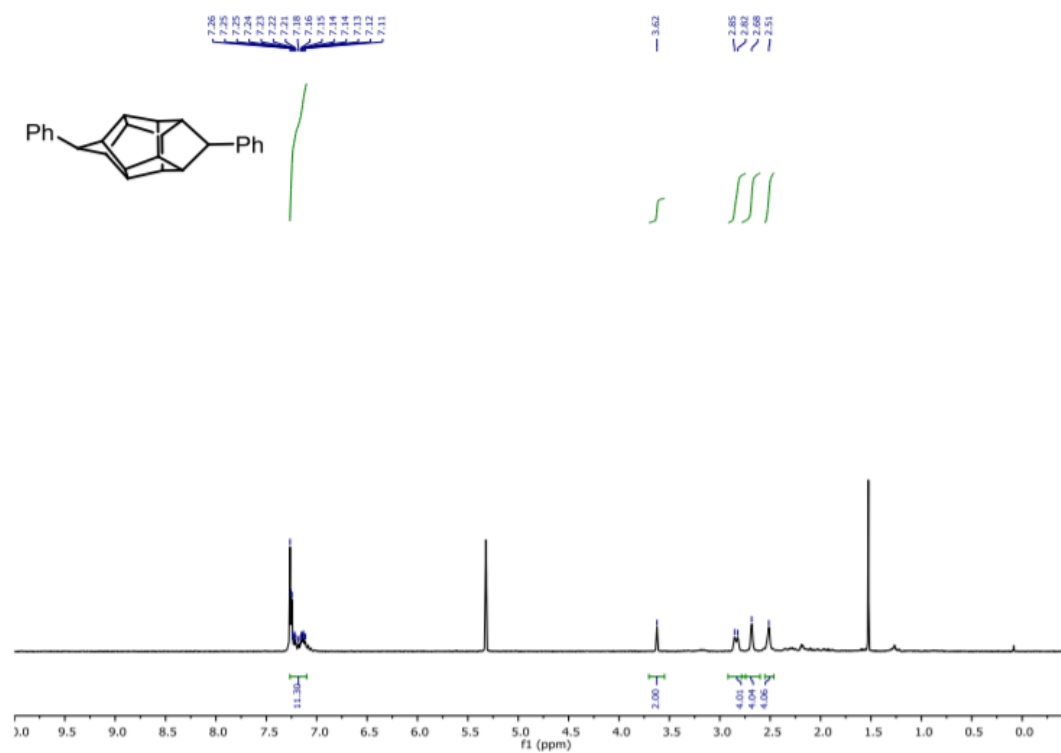
Compound **153a** ^{13}C NMR (100 MHz, CDCl$_3$)
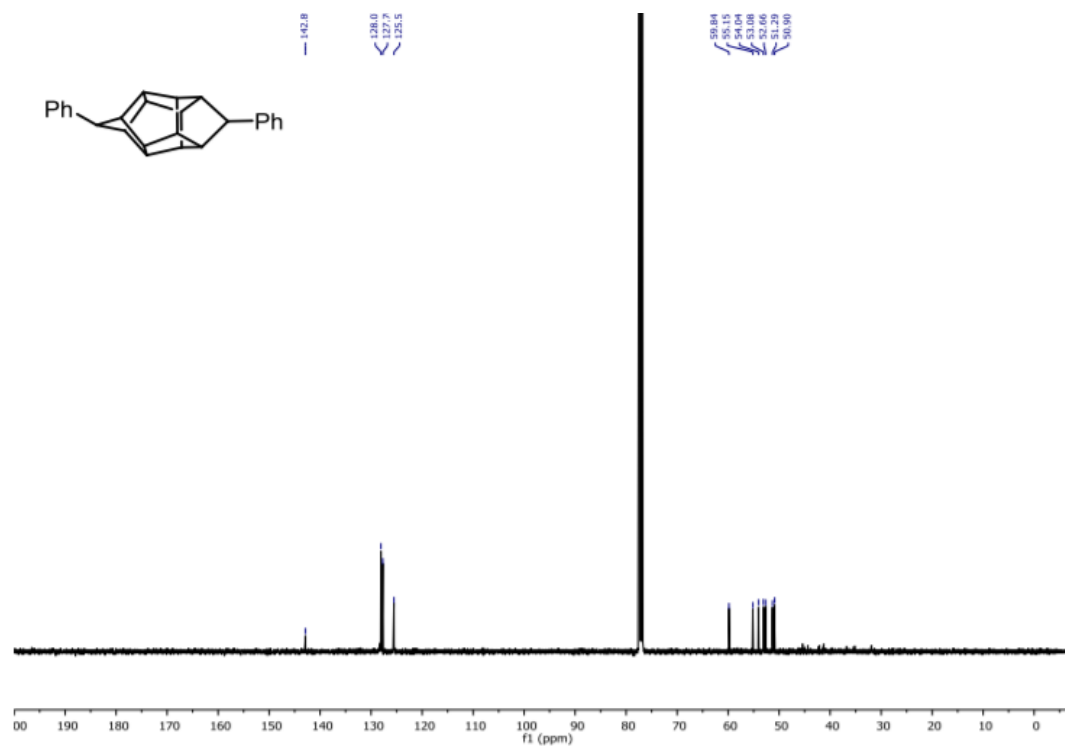
Compound **153b** ^{1}H NMR (400 MHz, CDCl$_3$)
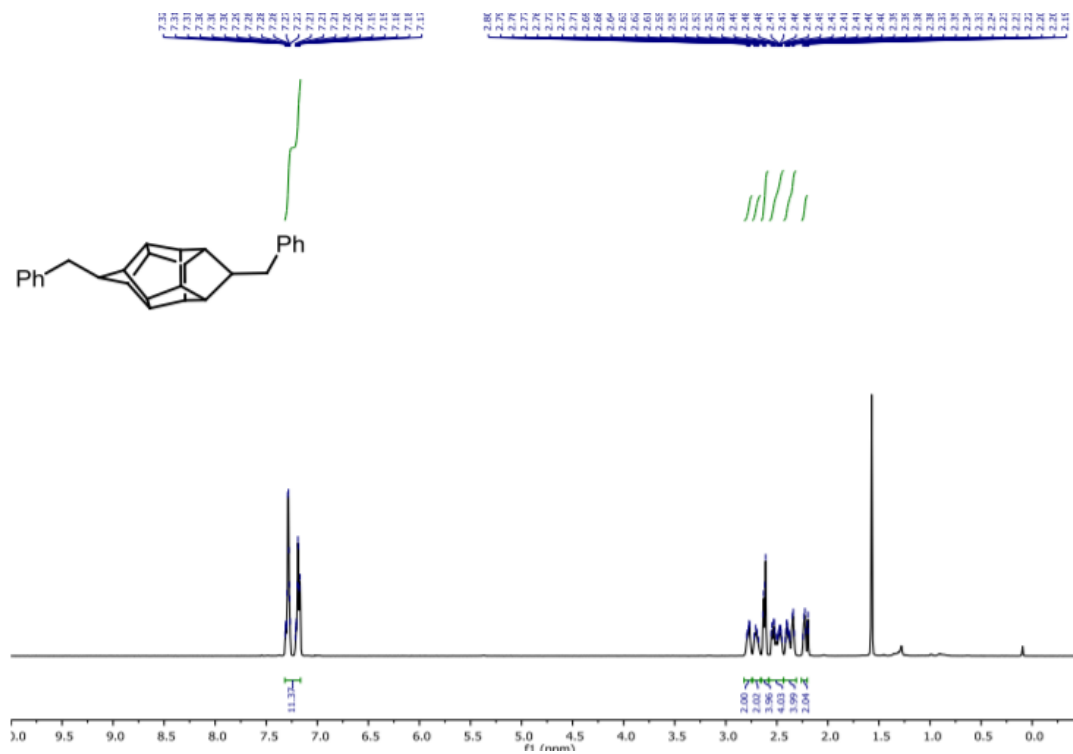
Compound **153b** ^{13}C NMR (100 MHz, CDCl$_3$)
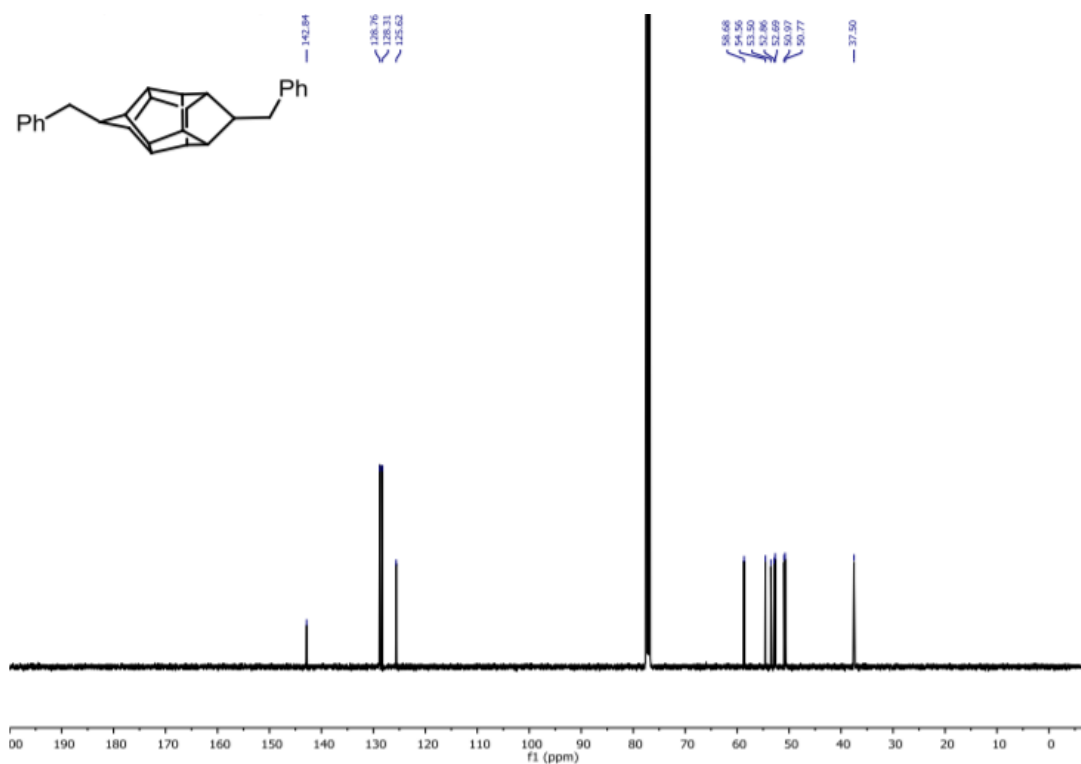
Compound **153c** ^{1}H NMR (400 MHz, CDCl$_3$)
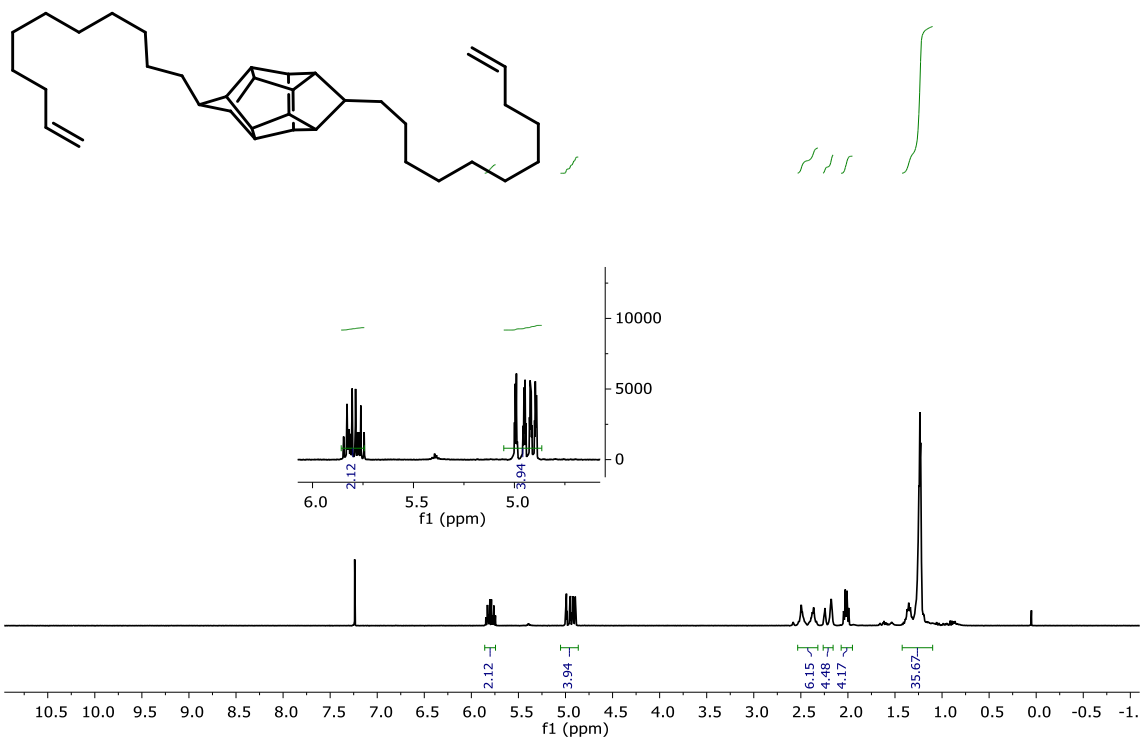
Compound **153c** ^{13}C NMR (100 MHz, CDCl$_3$)
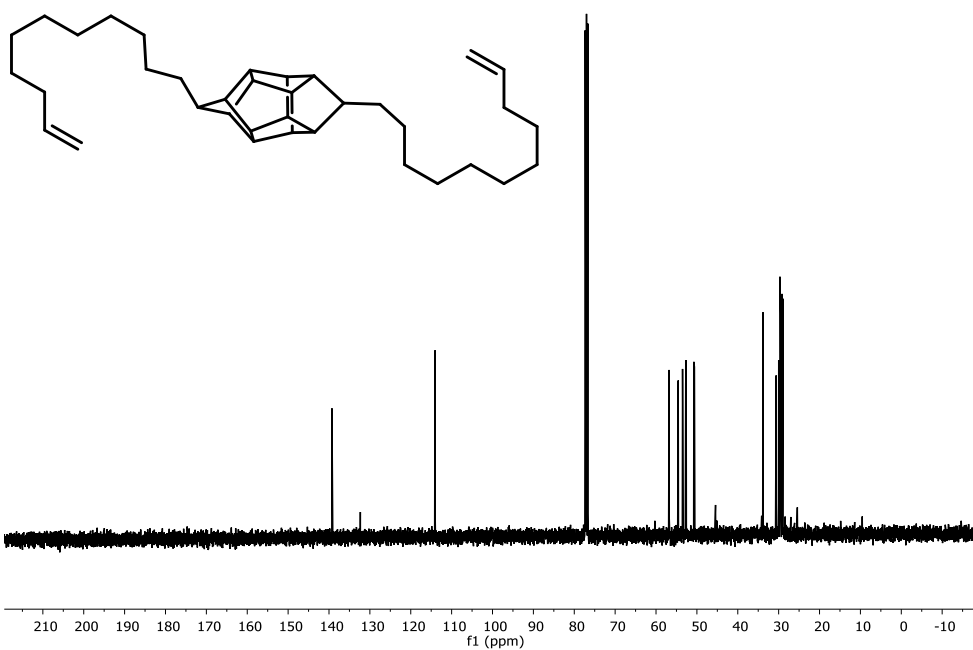
Compound **153d** ^{1}H NMR (400 MHz, CDCl$_3$)
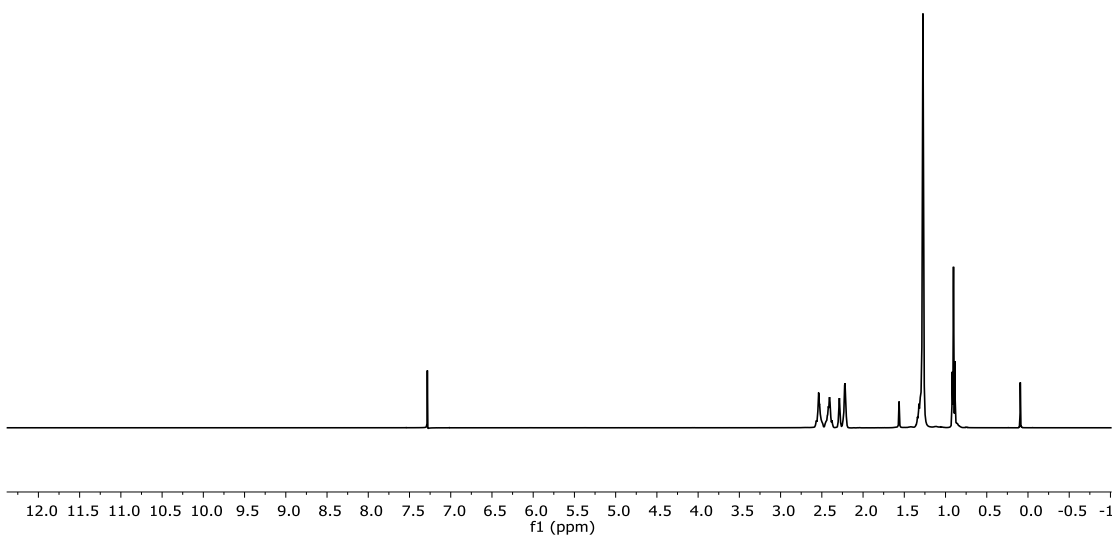
Compound **153d** ^{13}C NMR (100 MHz, CDCl$_3$)
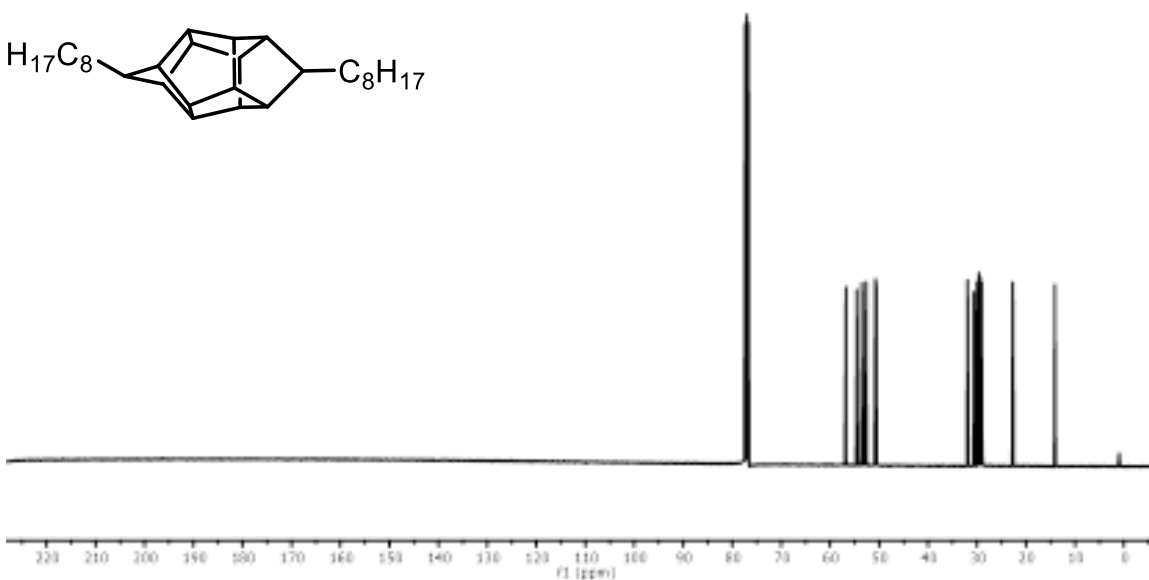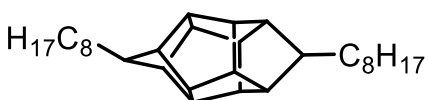
Compound **153e** ^{1}H NMR (400 MHz, CDCl₃)
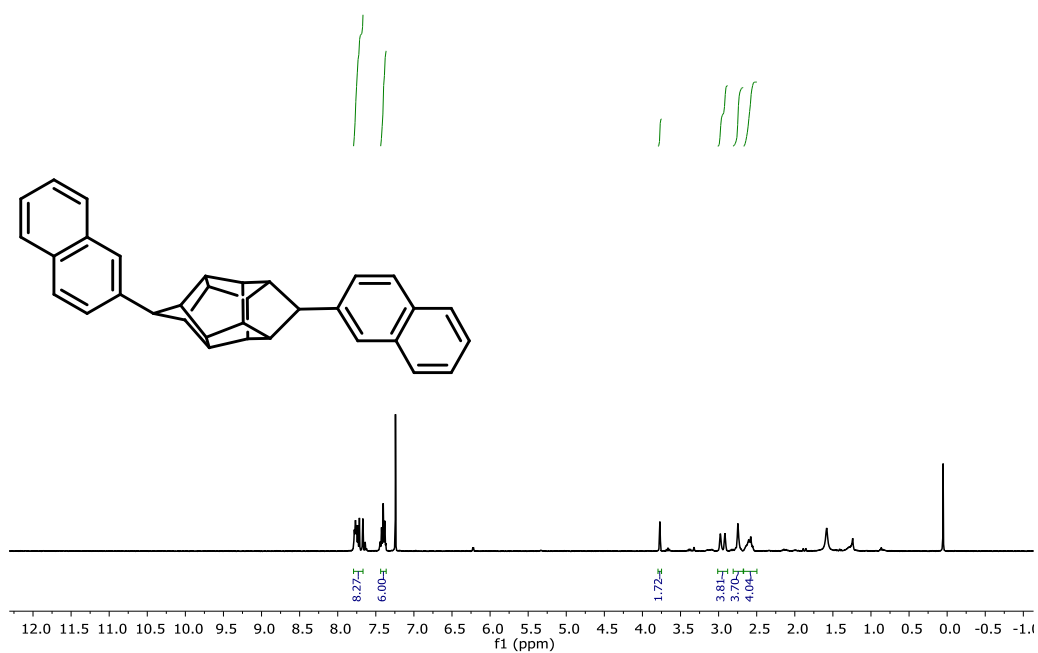
Compound **153e** ^{13}C NMR (100 MHz, CDCl₃)
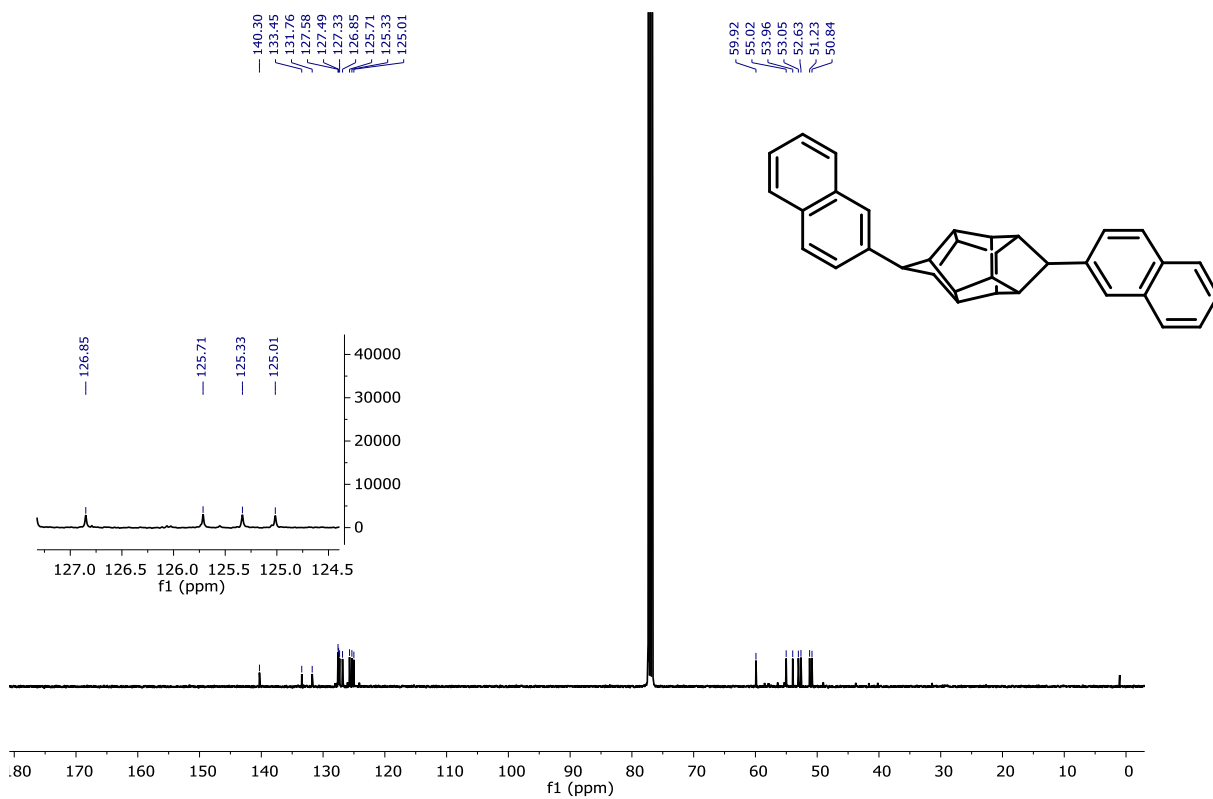
Compound **153j** ^{1}H NMR (400 MHz, CDCl$_3$)
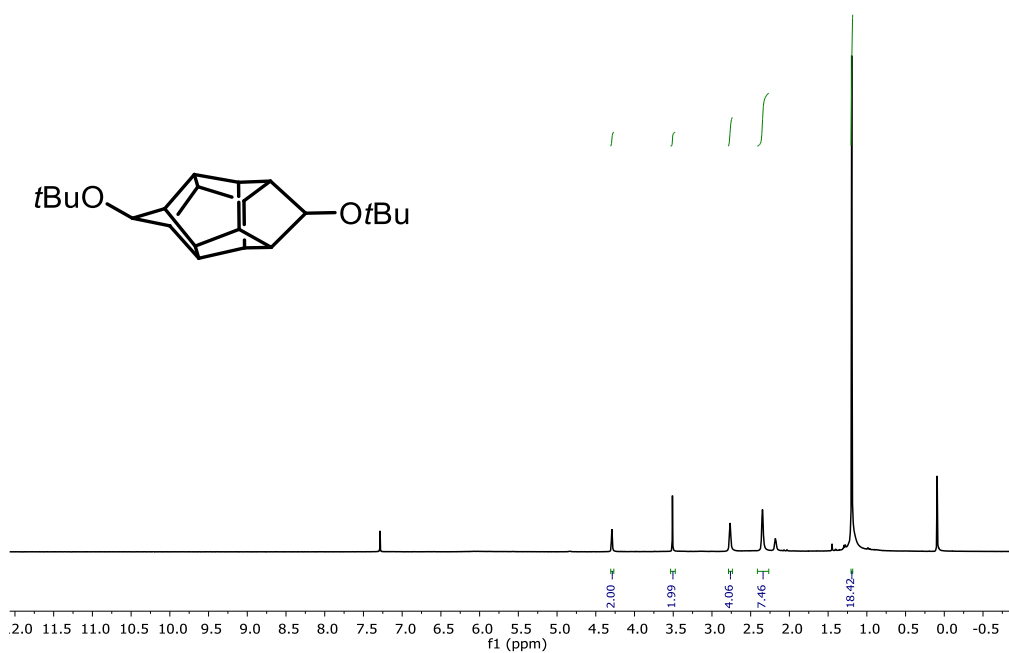
Compound **153j** ^{13}C NMR (100 MHz, CDCl$_3$)
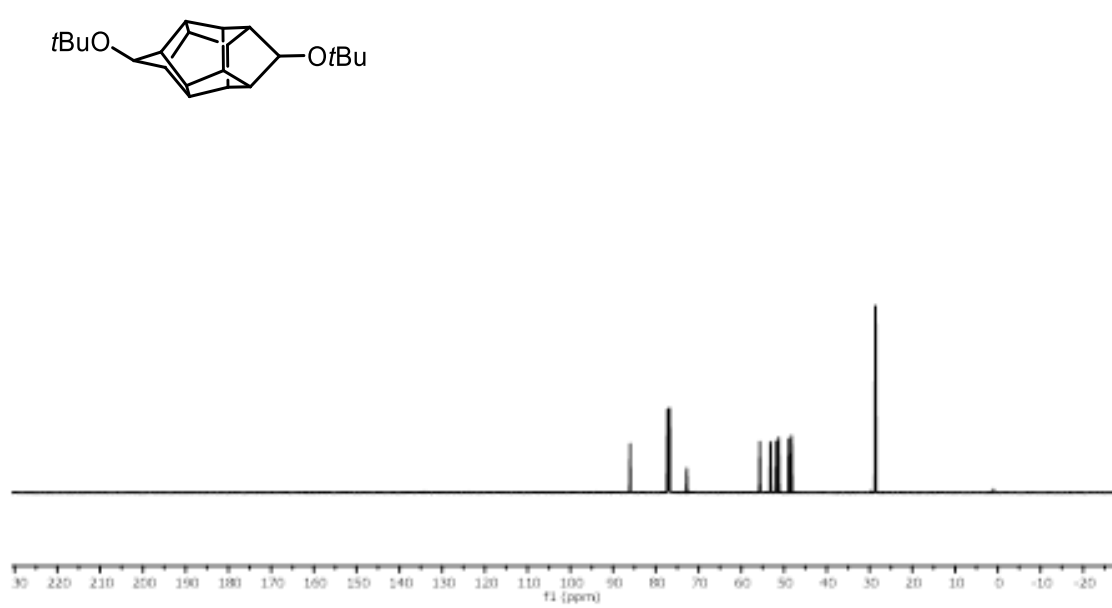
Compound **155** ¹H NMR (400 MHz, CDCl₃)
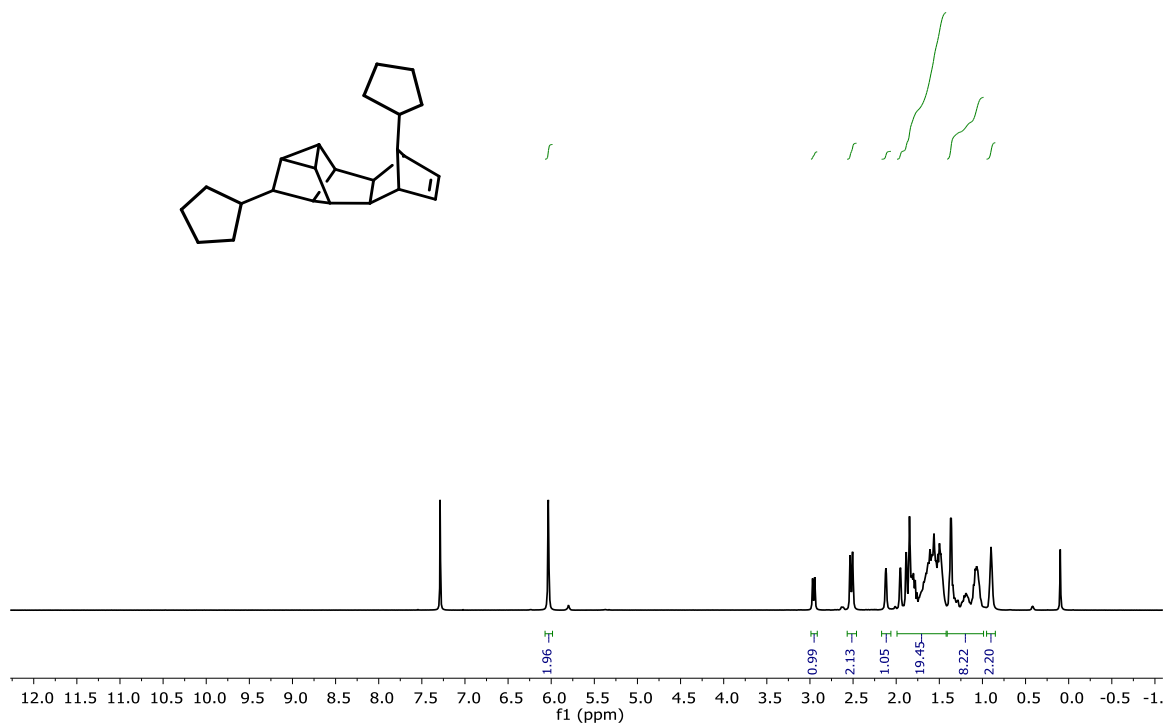
Compound **155** ¹³C NMR (100 MHz, CDCl₃)
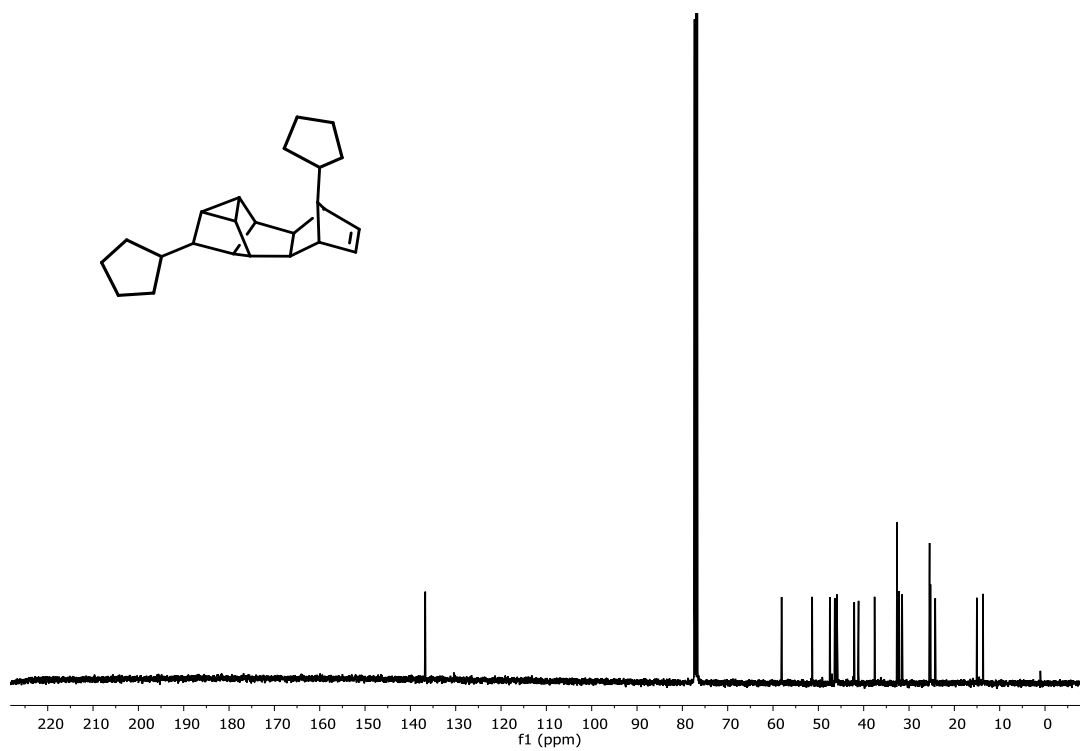
Compound **162** ^{1}H NMR (400 MHz, CD$_3$CN)
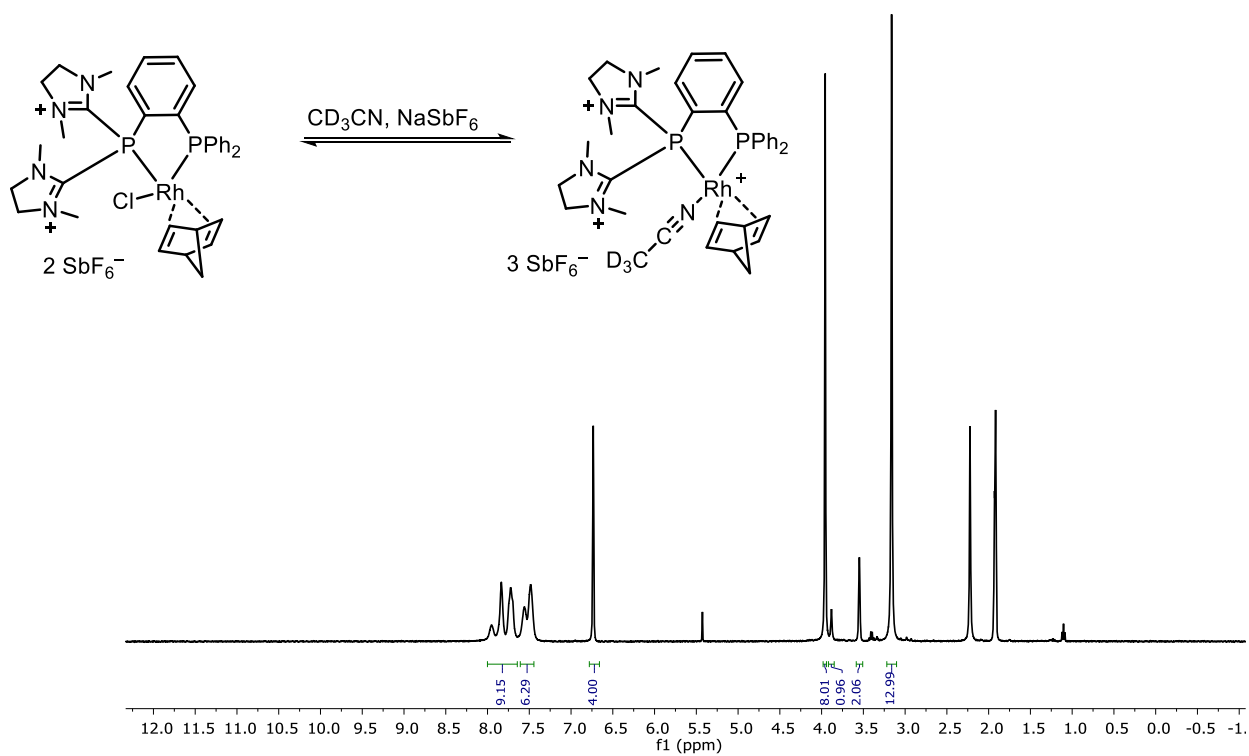
Compound **162** ^{31}P NMR (162 MHz, CD$_3$CN)
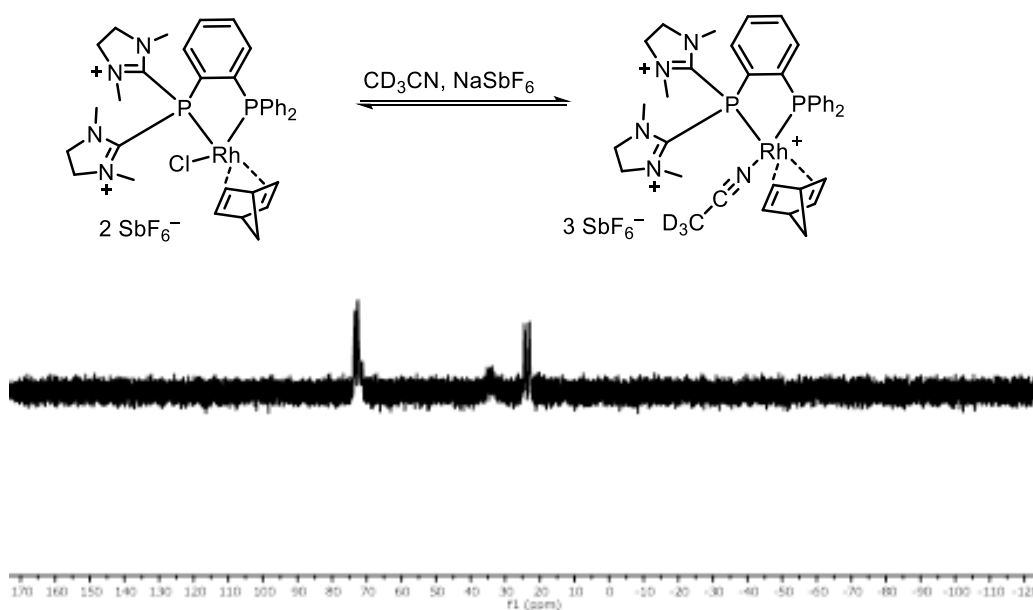
Compound **162** ^{13}C NMR (101 MHz, CD$_3$CN)
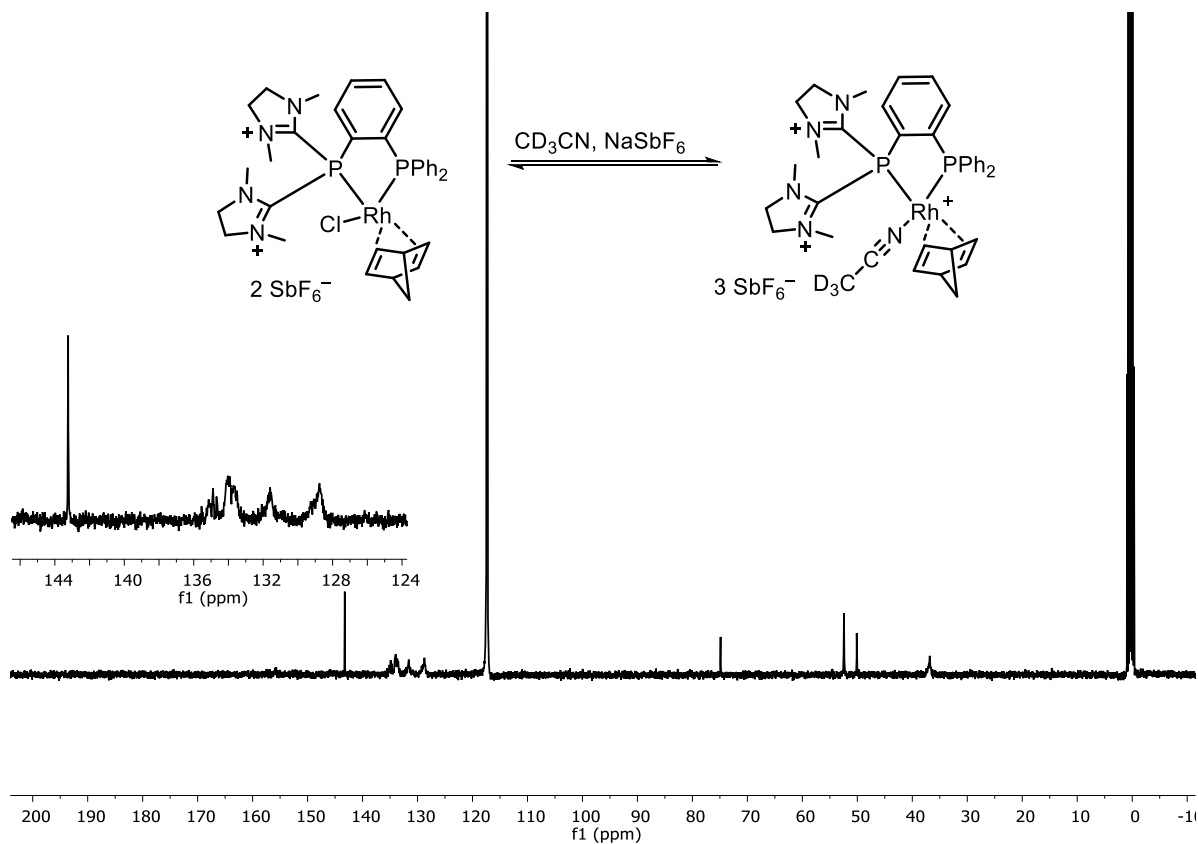
Compound **167** ^{1}H NMR (400 MHz, CDCl$_3$)
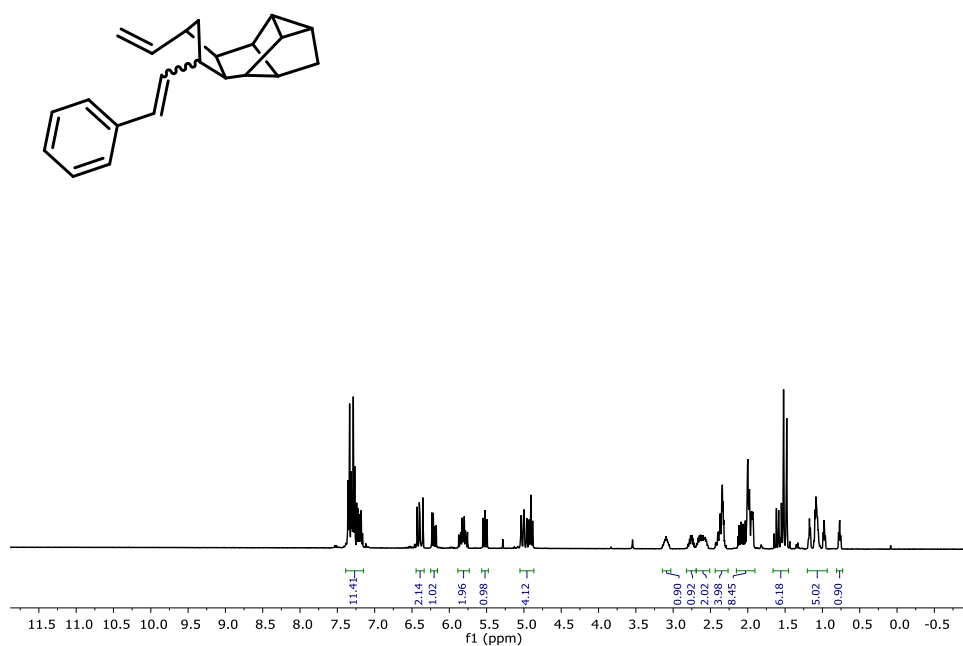
Compound **167** ^{13}C NMR (100 MHz, CDCl$_3$)
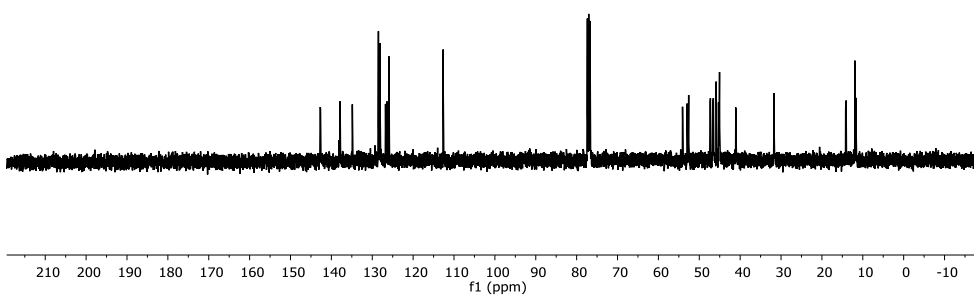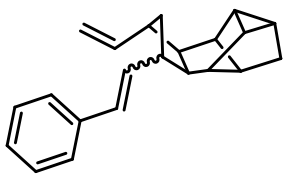
Compound **168** ^{1}H NMR (400 MHz, CDCl$_3$)
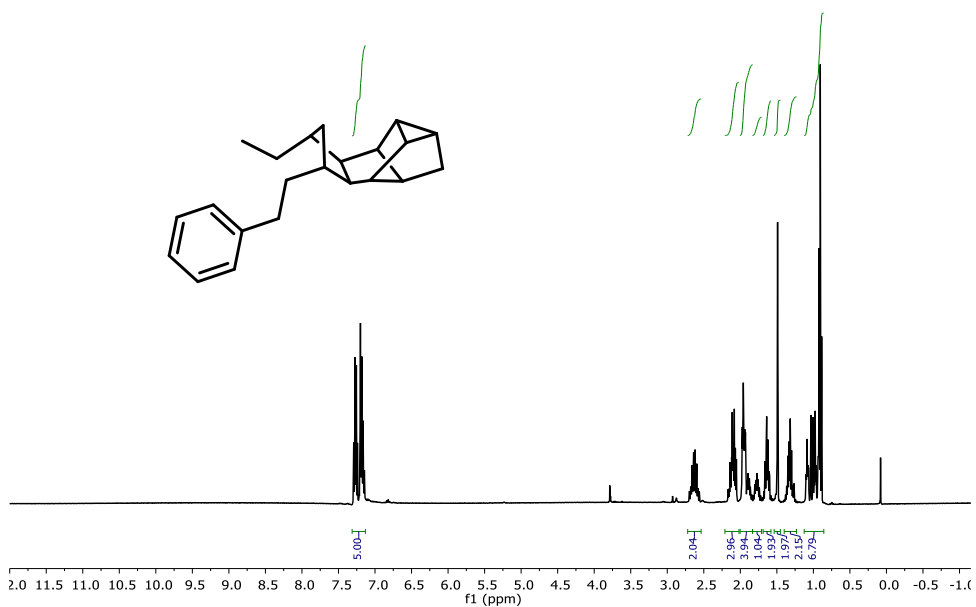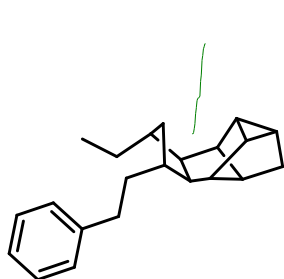
Compound **168** ^{13}C NMR (100 MHz, CDCl$_3$)
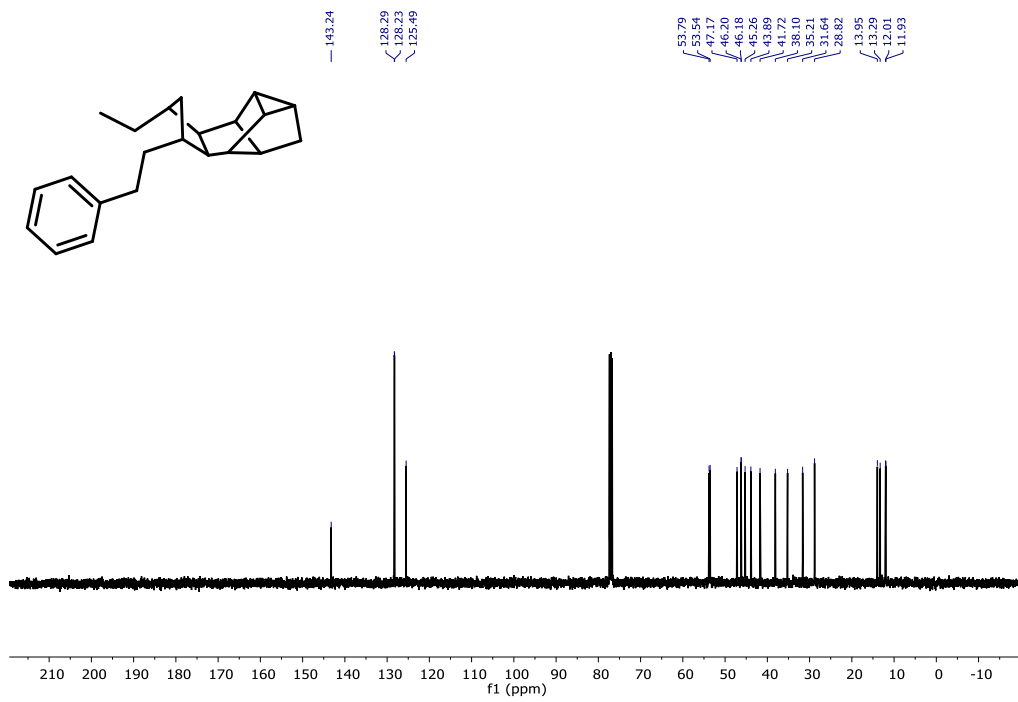
Compound **163** ^{1}H NMR (400 MHz, CDCl$_3$)
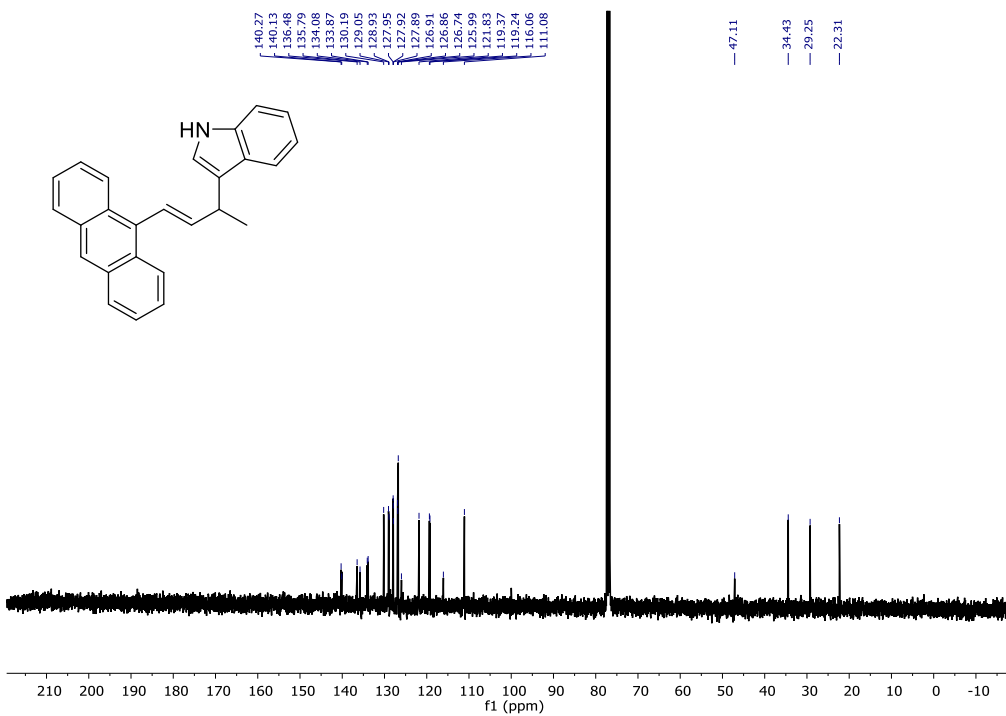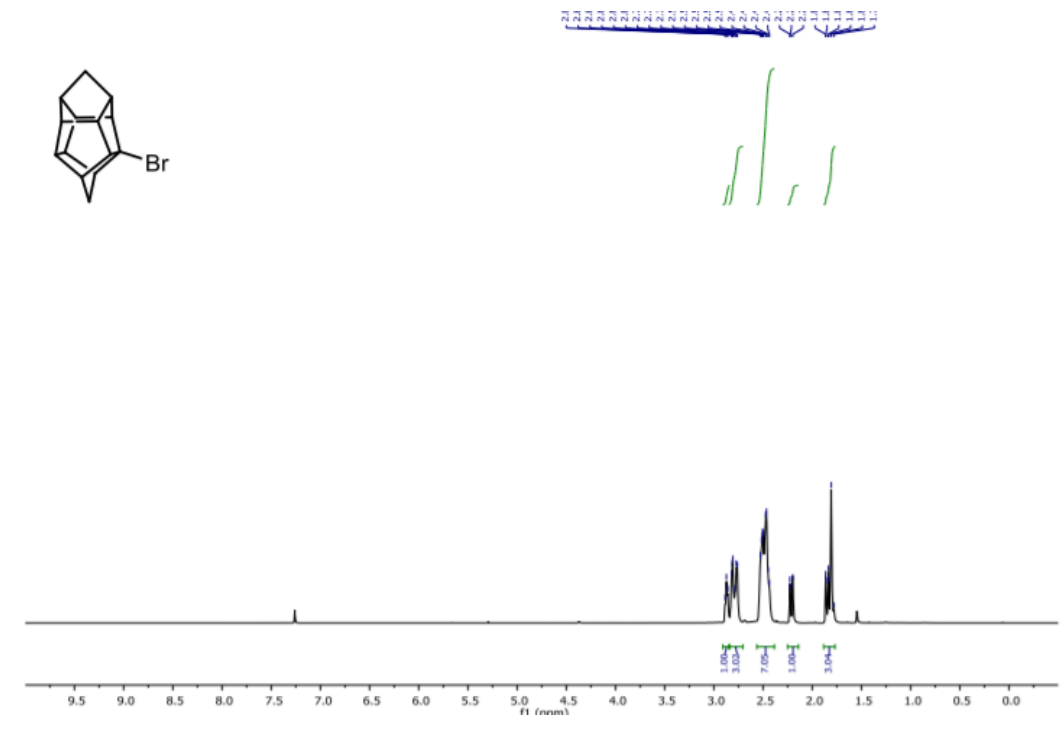
Compound **163** ^{13}C NMR (101 MHz, CDCl$_3$)
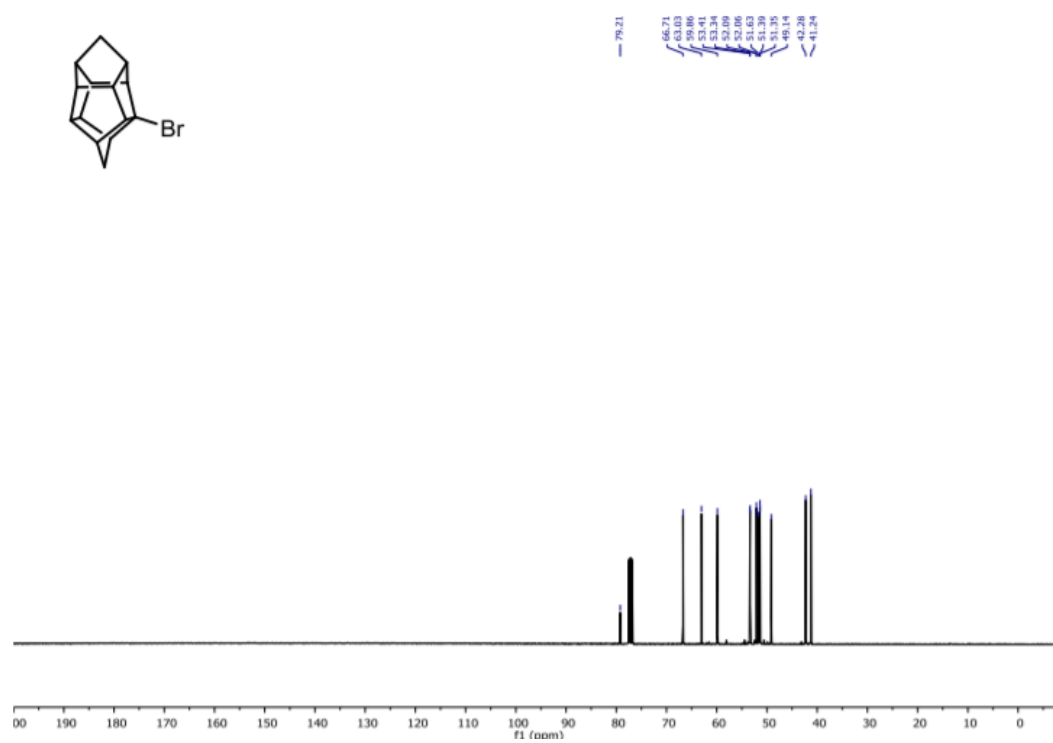
Compound **164** ^{1}H NMR (300 MHz, C$_6$D$_6$)
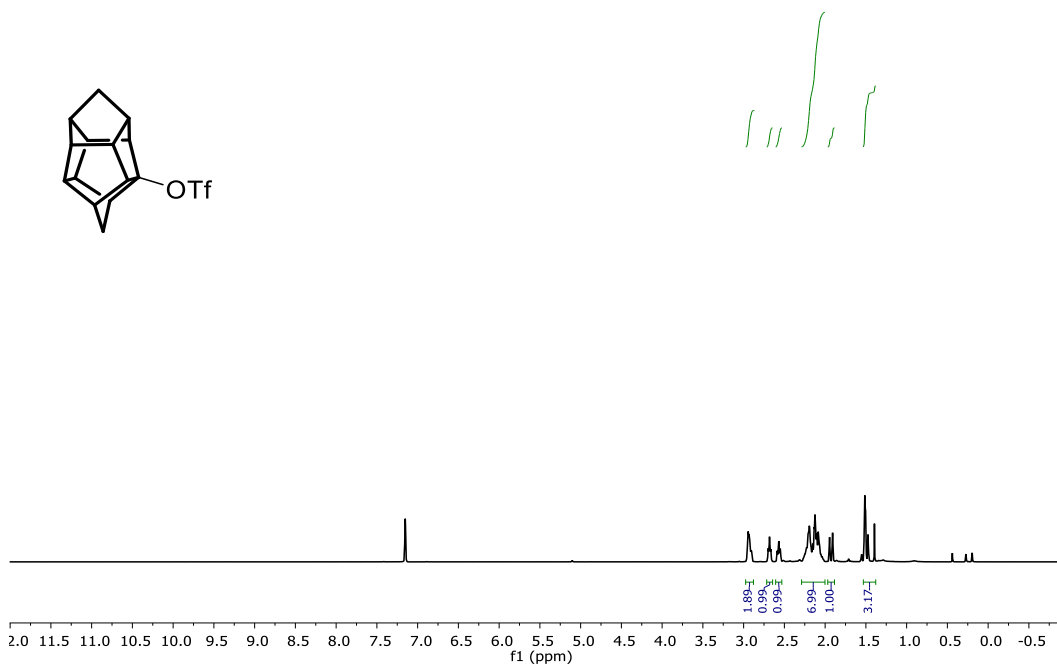
Compound **164** ^{19}F NMR (282 MHz, C$_6$D$_6$)
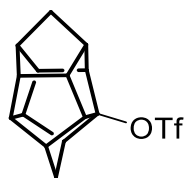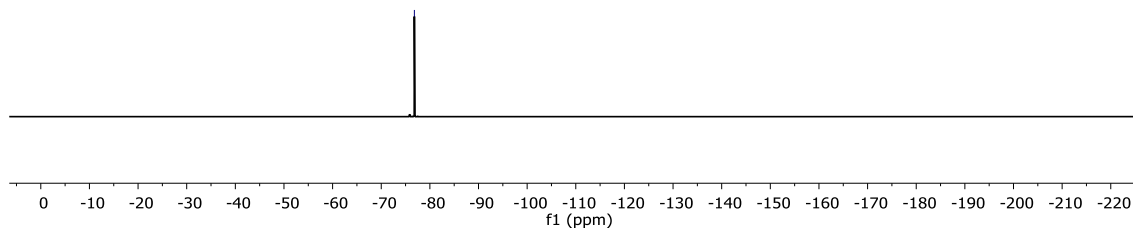
Compound **164** ^{13}C NMR (100 MHz, C$_6$D$_6$)
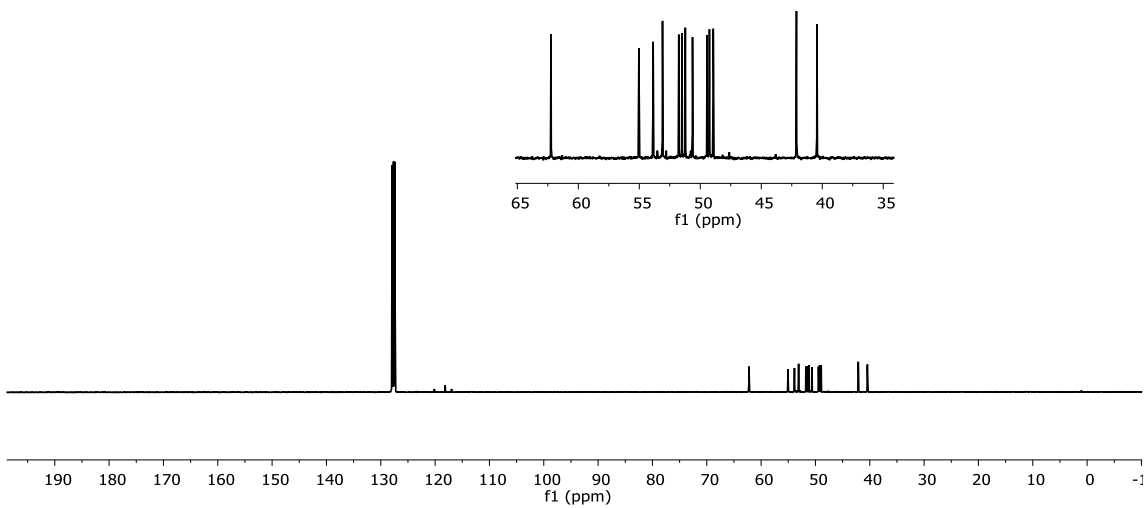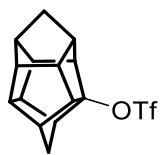
Compound **165** ^{1}H NMR (300 MHz, C$_6$D$_6$)
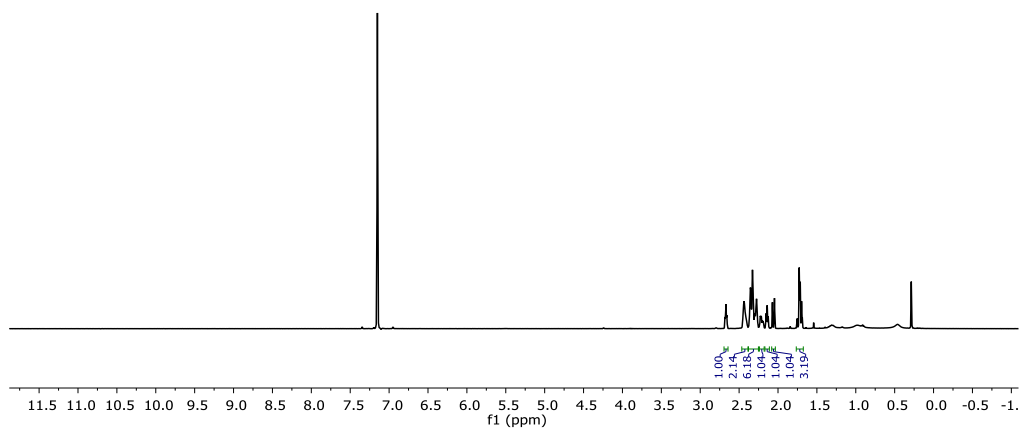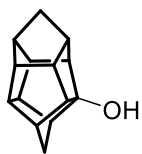
Compound **165** ^{13}C NMR (101 MHz, C$_6$D$_6$)
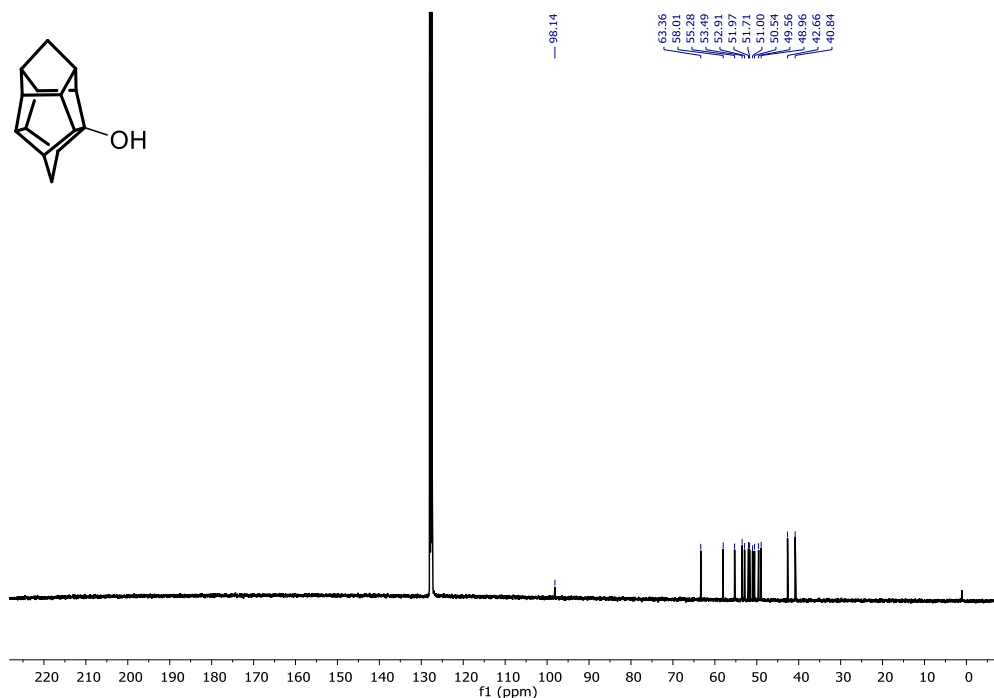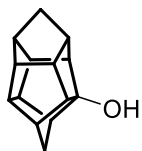
Compound **166** ^{1}H NMR (400 MHz, CDCl$_3$)
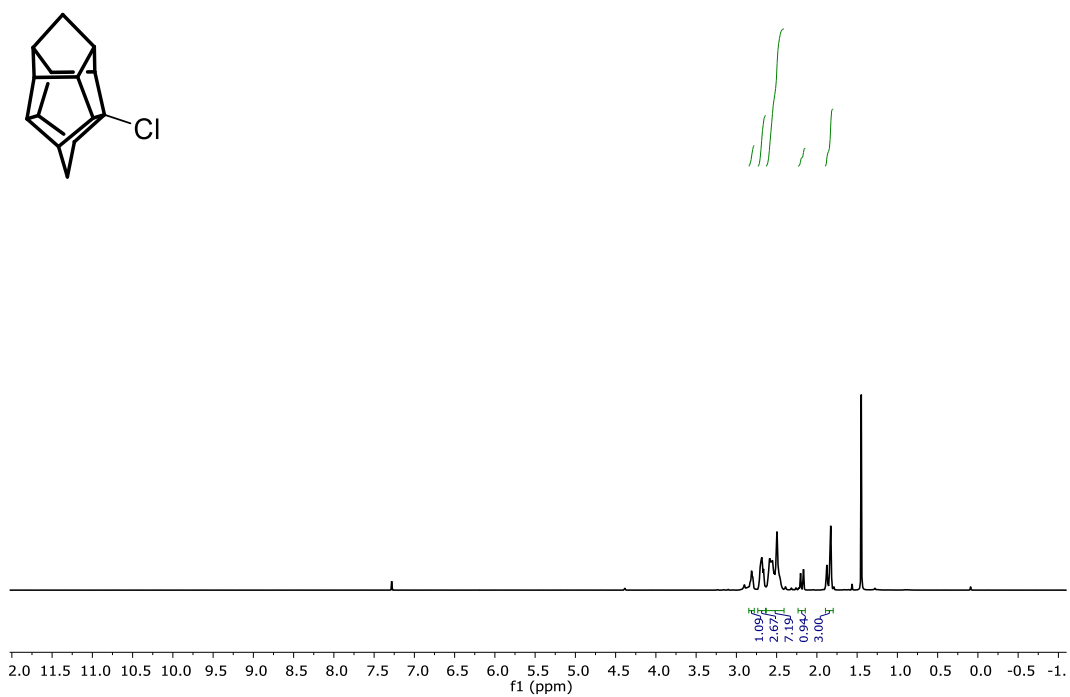
Compound **166** ^{13}C NMR (101 MHz, CDCl$_3$)
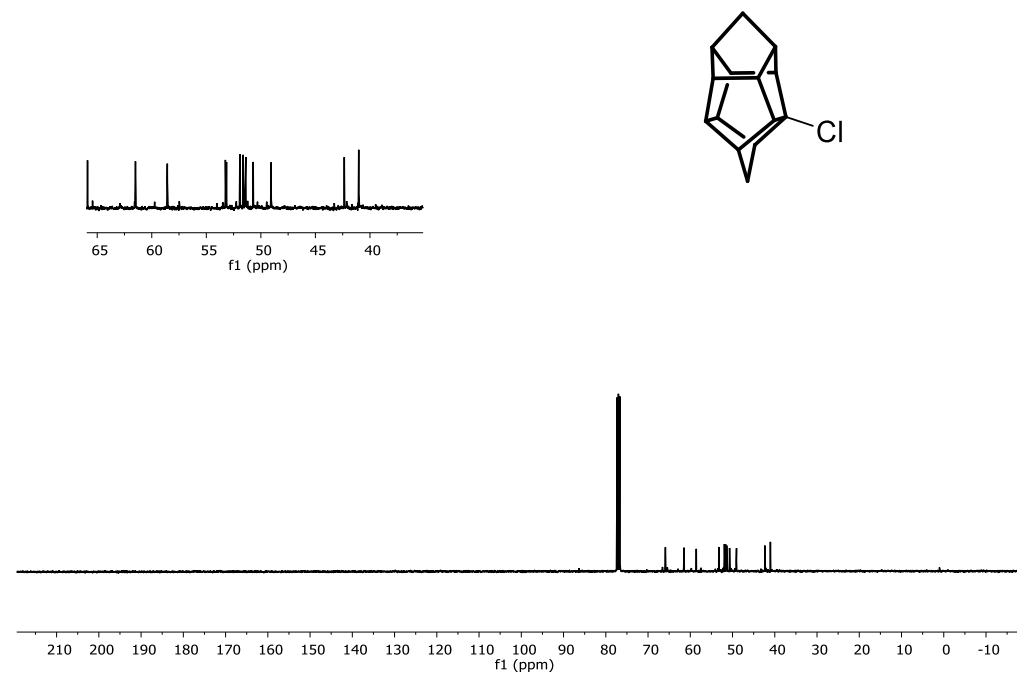
8.1.4 Solid state structures
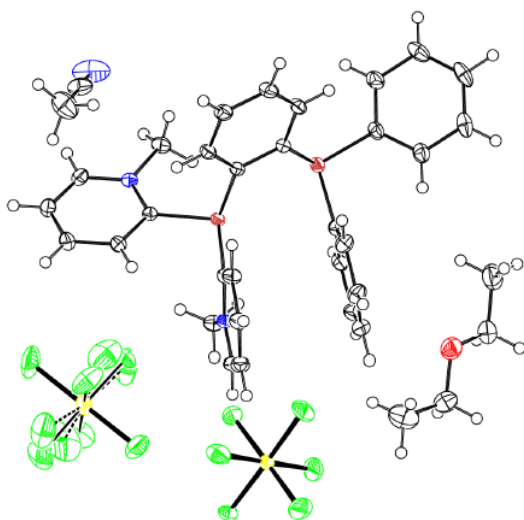
Table 11. Crystal Data and structure refinement of compound 97.

Identification code	mo_0103_CG_0m
Empirical formula	$C_{36}H_{41}F_{12}N_3OP_2Sb_2$
Formula weight	1065.16
Temperature/K	99.99
Crystal system	monoclinic
Space group	$P2_1/c$
a/Å	17.1817(4)
b/Å	9.9336(2)
c/Å	24.7294(6)
α/°	90
β/°	97.4180(10)

γ/°	90
Volume/Å^3	4185.39(16)
Z	4
ρ_{calc}g/cm^3	1.690
μ/mm^{-1}	1.454
F(000)	2104.0
Crystal size/mm^3	0.421 × 0.22 × 0.152
Radiation	MoKα (λ = 0.71073)
2Θ range for data collection/°	4.424 to 59.184
Index ranges	-23 ≤ h ≤ 23, -13 ≤ k ≤ 13, -34 ≤ l ≤ 34
Reflections collected	68188
Independent reflections	11716 [R_{int} = 0.0209, R_{sigma} = 0.0150]
Data/restraints/parameters	11716/0/547
Goodness-of-fit on F^2	1.106
Final R indexes [I>=2σ (I)]	R_1 = 0.0256, wR_2 = 0.0628
Final R indexes [all data]	R_1 = 0.0267, wR_2 = 0.0634
Largest diff. peak/hole / e Å^{-3}	2.07/-1.33
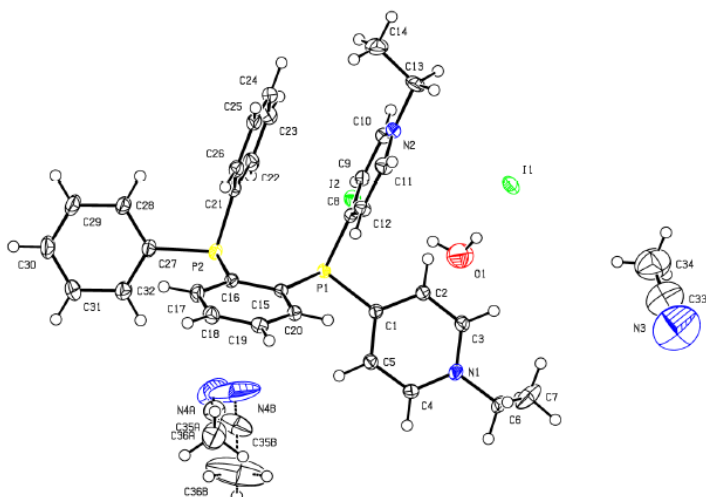
Table 12. Crystal Data and structure refinement of compound 98.

Identification code	mo_0148_CG_0m
Empirical formula	$C_{36}H_{40}I_2N_4OP_2$
Formula weight	860.46
Temperature/K	100.0
Crystal system	monoclinic
Space group	$P2_1/n$
a/Å	17.1396(11)
b/Å	8.7304(7)
c/Å	25.7395(14)
α/°	90
β/°	98.040(2)
γ/°	90

Volume/Å^3	3813.7(4)
Z	4
ρ_{calc}g/cm^3	1.499
μ/mm^{-1}	1.765
F(000)	1712.0
Crystal size/mm^3	0.272 × 0.051 × 0.051
Radiation	MoKα (λ = 0.71073)
2Θ range for data collection/°	4.932 to 61.082
Index ranges	-22 ≤ h ≤ 24, -12 ≤ k ≤ 12, -36 ≤ l ≤ 36
Reflections collected	69603
Independent reflections	11666 [R_{int} = 0.0334, R_{sigma} = 0.0230]
Data/restraints/parameters	11666/18/442
Goodness-of-fit on F^2	1.053
Final R indexes [I>=2σ (I)]	R_1 = 0.0271, wR_2 = 0.0619
Final R indexes [all data]	R_1 = 0.0337, wR_2 = 0.0651
Largest diff. peak/hole / e Å^{-3}	0.95/-1.08
((Please make the marked in yellow letters in other Tables in italic as well))	
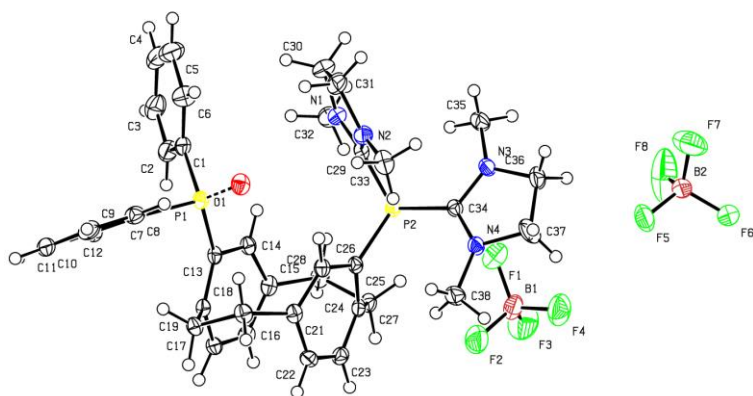
Table 13. Crystal Data and structure refinement of compound 103.

Identification code	Pbca
Empirical formula	$C_{38}H_{44}B_2F_8N_4O_{0.4}P_2$
Formula weight	798.77
Temperature/K	100.02
Crystal system	orthorhombic
Space group	Pbca
a/Å	15.1449(13)
b/Å	12.8865(9)
c/Å	38.447(3)
α/°	90
β/°	90
γ/°	90
Volume/Å^3	7503.4(10)

Z	8
ρ_{calc}g/cm^3	1.414
μ/mm^{-1}	0.192
F(000)	3322.0
Crystal size/mm^3	0.194 × 0.178 × 0.042
Radiation	MoKα (λ = 0.71073)
2Θ range for data collection/°	5.02 to 54.23
Index ranges	-19 ≤ h ≤ 19, -16 ≤ k ≤ 16, -49 ≤ l ≤ 49
Reflections collected	69415
Independent reflections	8270 [R_{int} = 0.0447, R_{sigma} = 0.0258]
Data/restraints/parameters	8270/0/501
Goodness-of-fit on F^2	1.134
Final R indexes [I>=2σ (I)]	R_1 = 0.0566, wR_2 = 0.1269
Final R indexes [all data]	R_1 = 0.0678, wR_2 = 0.1319
Largest diff. peak/hole / e Å^{-3}	0.81/-0.55
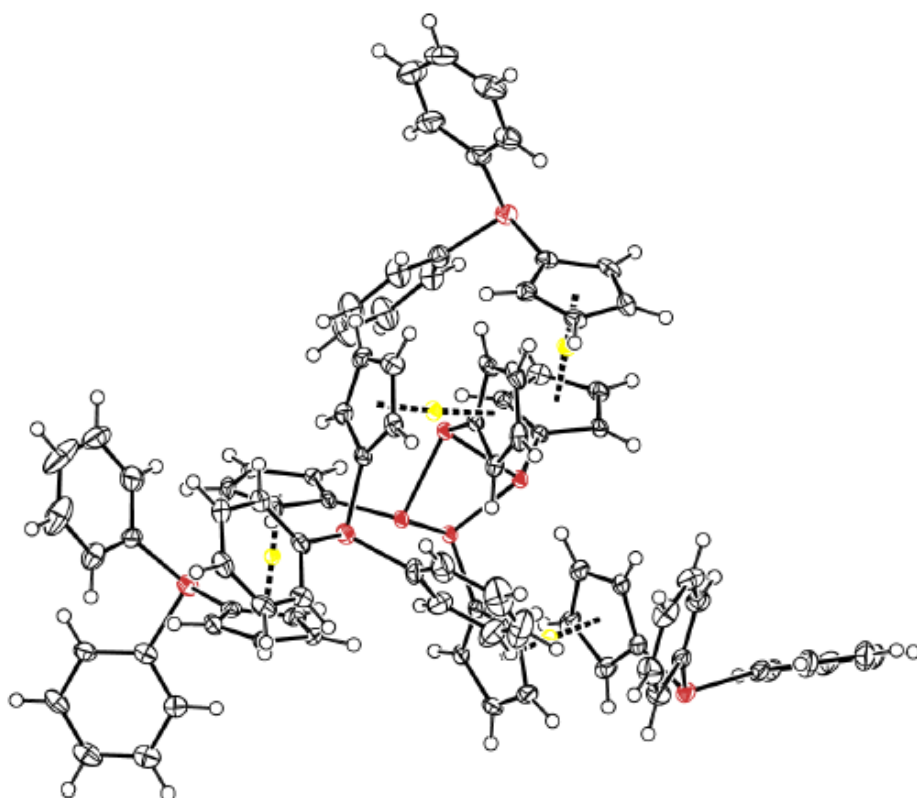
Table 14. Crystal Data and structure refinement of compound 108.

Identification code	Pca21
Empirical formula	$C_{88}H_{72}Fe_4P_8$
Formula weight	1600.61
Temperature/K	99.96
Crystal system	orthorhombic
Space group	$Pca2_1$
a/Å	22.506(2)
b/Å	11.4901(12)
c/Å	28.314(2)

α/°	90
β/°	90
γ/°	90
Volume/Å^3	7321.9(13)
Z	4
ρ_{calc}g/cm^3	1.452
μ/mm^{-1}	1.000
F(000)	3296.0
Crystal size/mm^3	0.143 × 0.113 × 0.054
Radiation	MoKα (λ = 0.71073)
2Θ range for data collection/°	4.566 to 59.172
Index ranges	-31 ≤ h ≤ 31, -15 ≤ k ≤ 15, -39 ≤ l ≤ 39
Reflections collected	119390
Independent reflections	20507 [R_{int} = 0.0430, R_{sigma} = 0.0345]
Data/restraints/parameters	20507/1/902
Goodness-of-fit on F^2	1.027
Final R indexes [I>=2σ (I)]	R_1 = 0.0377, wR_2 = 0.0847
Final R indexes [all data]	R_1 = 0.0439, wR_2 = 0.0877
Largest diff. peak/hole / e Å^{-3}	1.73/-0.41

Flack parameter	0.000(3)
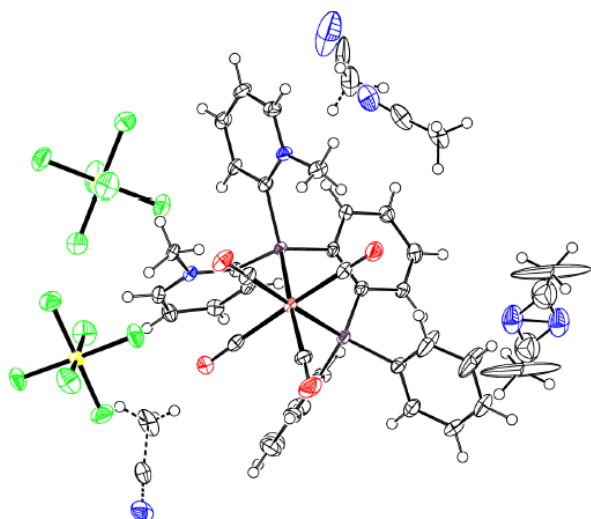
Table 15. Crystal Data and structure refinement of compound 112.

Identification code	mo_0166_CG_0m_4
Empirical formula	$C_{38}H_{34}F_{12}MoN_4O_4P_2Sb_2$
Formula weight	1240.07
Temperature/K	100.02
Crystal system	triclinic
Space group	*P*-1
a/Å	9.2818(15)
b/Å	12.207(2)
c/Å	20.587(3)
α/°	82.662(6)
β/°	82.046(4)
γ/°	88.310(5)

Volume/Å^3	2291.0(6)
Z	2
ρ_{calc}g/cm^3	1.798
μ/mm^{-1}	1.601
F(000)	1208.0
Crystal size/mm^3	0.271 × 0.101 × 0.096
Radiation	MoKα (λ = 0.71073)
2Θ range for data collection/°	4.432 to 57.468
Index ranges	-12 ≤ h ≤ 12, -16 ≤ k ≤ 16, 0 ≤ l ≤ 27
Reflections collected	11517
Independent reflections	11517 [R_{int} = ?, R_{sigma} = 0.0277]
Data/restraints/parameters	11517/15/621
Goodness-of-fit on F^2	1.146
Final R indexes [I>=2σ (I)]	R_1 = 0.0421, wR_2 = 0.1228
Final R indexes [all data]	R_1 = 0.0452, wR_2 = 0.1248
Largest diff. peak/hole / e Å^{-3}	2.29/-1.86
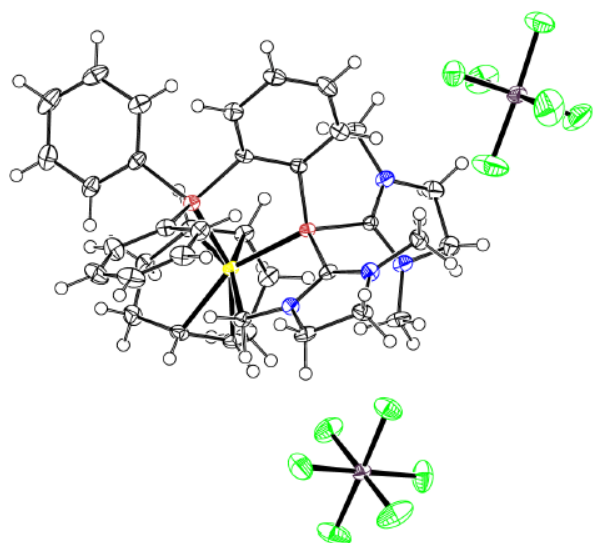
Table 16. Crystal Data and structure refinement of compound 122.

Identification code	mo_0050_CG_0m
Empirical formula	$C_{36}H_{45}F_{12}IrN_4P_2Sb_2$
Formula weight	1259.40
Temperature/K	100.01
Crystal system	triclinic
Space group	*P*-1
a/Å	10.2241(7)
b/Å	14.1523(10)
c/Å	14.7915(9)
α/°	94.986(2)
β/°	100.036(2)
γ/°	103.582(2)

Volume/Å^3	2030.2(2)
Z	2
ρ_{calc}g/cm^3	2.060
μ/mm^{-1}	4.758
F(000)	1212.0
Crystal size/mm^3	0.315 × 0.146 × 0.102
Radiation	MoKα (λ = 0.71073)
2Θ range for data collection/°	4.478 to 59.996
Index ranges	-14 ≤ h ≤ 14, -19 ≤ k ≤ 19, -20 ≤ l ≤ 20
Reflections collected	90890
Independent reflections	11839 [R_{int} = 0.0441, R_{sigma} = 0.0266]
Data/restraints/parameters	11839/0/517
Goodness-of-fit on F^2	1.213
Final R indexes [I>=2σ (I)]	R_1 = 0.0368, wR_2 = 0.0761
Final R indexes [all data]	R_1 = 0.0465, wR_2 = 0.0832
Largest diff. peak/hole / e Å^{-3}	3.88/-2.33
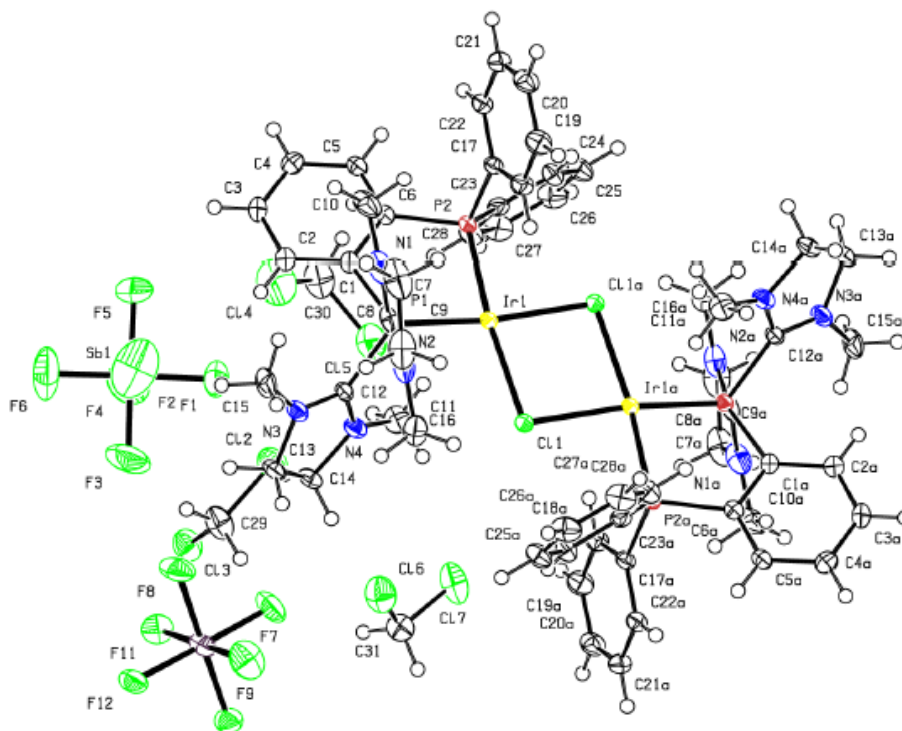
Table 17. Crystal Data and structure refinement of compound 124.

Identification code	mo_0071_CG_0m
Empirical formula	$C_{31}H_{40}Cl_7F_{12}IrN_4P_2Sb_2$
Formula weight	1442.46
Temperature/K	99.99
Crystal system	monoclinic
Space group	$P2_1/n$
a/Å	13.2775(6)
b/Å	13.0737(6)
c/Å	26.3722(10)
α/°	90

β/°	92.2920(10)
γ/°	90
Volume/Å^3	4574.2(3)
Z	4
ρ_{calc}g/cm^3	2.095
μ/mm^{-1}	4.633
F(000)	2760.0
Crystal size/mm^3	0.489 × 0.177 × 0.132
Radiation	MoKα (λ = 0.71073)
2Θ range for data collection/°	4.374 to 59.364
Index ranges	-18 ≤ h ≤ 18, -18 ≤ k ≤ 18, -36 ≤ l ≤ 36
Reflections collected	212279
Independent reflections	12921 [R_{int} = 0.0450, R_{sigma} = 0.0184]
Data/restraints/parameters	12921/0/536
Goodness-of-fit on F^2	1.122
Final R indexes [I>=2σ (I)]	R_1 = 0.0481, wR_2 = 0.1286
Final R indexes [all data]	R_1 = 0.0567, wR_2 = 0.1375
Largest diff. peak/hole / e Å^{-3}	4.02/-1.75
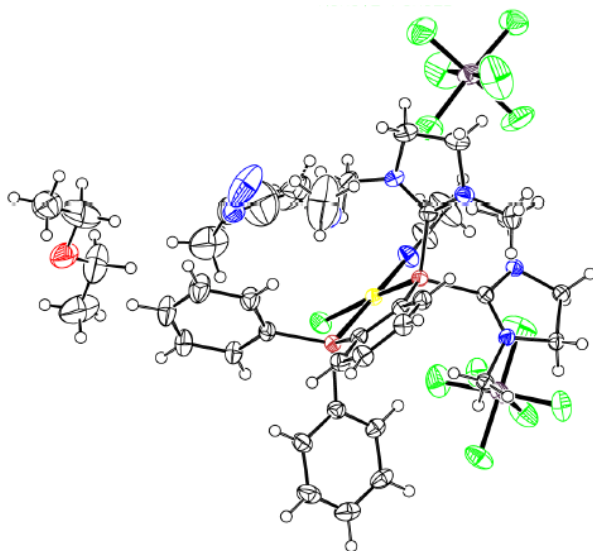
Table 18. Crystal Data and structure refinement of compound 125

Identification code	0368_CG_0m_4
Empirical formula	$C_{36}H_{48}ClF_{12}IrN_7O_{0.5}P_2Sb_2$
Formula weight	1347.90
Temperature/K	99.99
Crystal system	monoclinic
Space group	$P2_1/c$
a/Å	17.5401(15)
b/Å	15.8048(10)
c/Å	17.9433(15)
α/°	90
β/°	111.298(2)

$\gamma/°$	90
Volume/Å^3	4634.5(6)
Z	4
ρ_{calc}g/cm^3	1.932
μ/mm^{-1}	4.234
F(000)	2604.0
Crystal size/mm^3	0.231 × 0.214 × 0.083
Radiation	MoKα (λ = 0.71073)
2Θ range for data collection/°	4.818 to 65.256
Index ranges	-26 ≤ h ≤ 24, 0 ≤ k ≤ 23, 0 ≤ l ≤ 27
Reflections collected	17158
Independent reflections	17158 [R_{int} = **?,** R_{sigma} = 0.0421]
Data/restraints/parameters	17158/63/608
Goodness-of-fit on F^2	1.046
Final R indexes [I>=2σ (I)]	R_1 = 0.0365, wR_2 = 0.0992
Final R indexes [all data]	R_1 = 0.0402, wR_2 = 0.1029
Largest diff. peak/hole / e Å^{-3}	2.33/-2.03
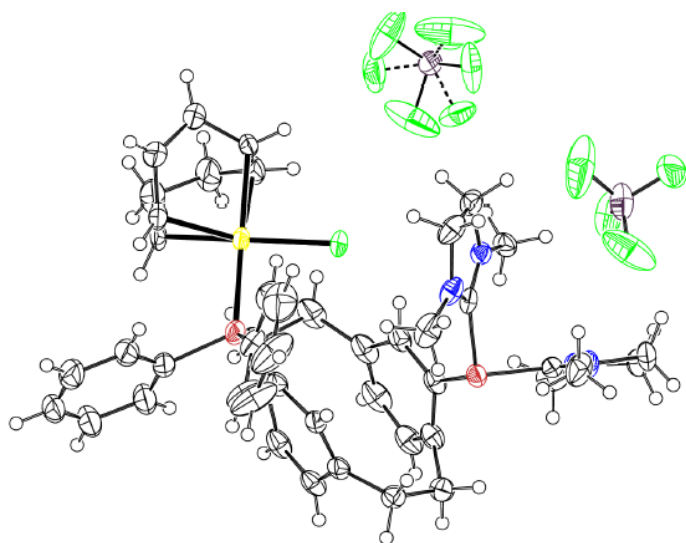
Table 19. Crystal Data and structure refinement of compound 127.

Identification code	P21c
Empirical formula	$C_{48.5}H_{54}B_2Cl_6F_8IrN_4P_2$
Formula weight	1333.41
Temperature/K	99.99
Crystal system	monoclinic
Space group	$P2_1/c$
a/Å	25.239(2)
b/Å	13.7444(13)
c/Å	15.8005(11)
α/°	90
β/°	91.633(3)
γ/°	90

Volume/Å^3	5479.0(8)
Z	4
ρ_{calc}g/cm^3	1.617
μ/mm^{-1}	2.853
F(000)	2656.0
Crystal size/mm^3	0.442 × 0.271 × 0.072
Radiation	MoKα (λ = 0.71073)
2Θ range for data collection/°	4.382 to 59.33
Index ranges	-35 ≤ h ≤ 35, -19 ≤ k ≤ 19, -21 ≤ l ≤ 17
Reflections collected	91185
Independent reflections	15139 [R_{int} = 0.0346, R_{sigma} = 0.0255]
Data/restraints/parameters	15139/3/609
Goodness-of-fit on F^2	1.032
Final R indexes [I>=2σ (I)]	R_1 = 0.0412, wR_2 = 0.0903
Final R indexes [all data]	R_1 = 0.0492, wR_2 = 0.0945
Largest diff. peak/hole / e Å^{-3}	2.52/-2.61
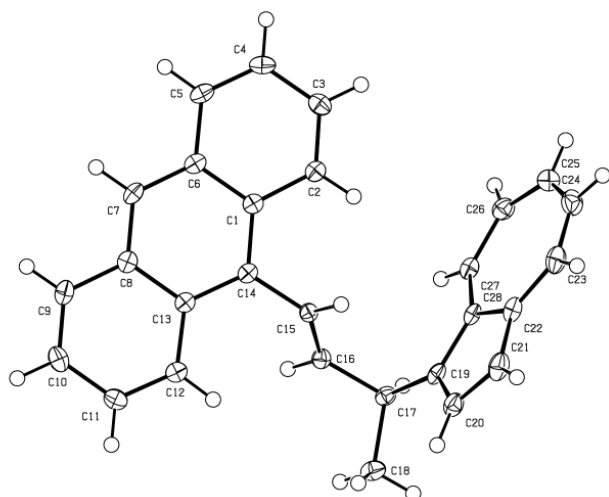
Table 20. Crystal Data and structure refinement of compound 74g.

Identification code	ja7b01441_si_008
Empirical formula	$C_{28}H_{22}$
Formula weight	358.45
Temperature/K	100
Crystal system	monoclinic
Space group	$C2/c$
a/Å	27.455(2)
b/Å	8.9353(7)
c/Å	19.0572(14)
α/°	90
β/°	125.169(2)

γ/°	90
Volume/Å^3	3821.7(5)
Z	8
ρ_{calc}g/cm^3	1.246
μ/mm^{-1}	0.530
F(000)	1520.0
Crystal size/mm^3	0.412 × 0.177 × 0.086
Radiation	Cu-Kα (λ = 1.54178)
2Θ range for data collection/°	7.878 to 135.47
Index ranges	-32 ≤ h ≤ 32, -10 ≤ k ≤ 10, -22 ≤ l ≤ 22
Reflections collected	62737
Independent reflections	3282 [R_{int} = 0.0282, R_{sigma} = 0.0101]
Data/restraints/parameters	3282/0/254
Goodness-of-fit on F^2	1.034
Final R indexes [I>=2σ (I)]	R_1 = 0.0371, wR_2 = 0.0975
Final R indexes [all data]	R_1 = 0.0383, wR_2 = 0.0986
Largest diff. peak/hole / e Å^{-3}	0.16/-0.21
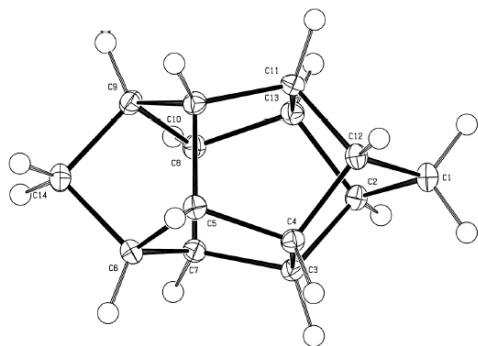
Table 21. Crystal Data and structure refinement of compound 132.

Identification code	0722_CG_0m
Empirical formula	$C_{14}H_{16}$
Formula weight	184.27
Temperature/K	100.03
Crystal system	monoclinic
Space group	$P2_1/c$
a/Å	8.5612(4)
b/Å	7.5856(3)
c/Å	13.9790(7)
α/°	90
β/°	92.364(2)
γ/°	90
Volume/Å³	907.05(7)
Z	4

$\rho_{calc}g/cm^3$	1.349
μ/mm^{-1}	0.075
F(000)	400.0
Crystal size/mm^3	0.331 × 0.272 × 0.142
Radiation	MoKα (λ = 0.71073)
2Θ range for data collection/°	4.762 to 61.046
Index ranges	-12 ≤ h ≤ 12, -10 ≤ k ≤ 10, -19 ≤ l ≤ 19
Reflections collected	28144
Independent reflections	2764 [R_{int} = 0.0259, R_{sigma} = 0.0112]
Data/restraints/parameters	2764/0/191
Goodness-of-fit on F^2	1.060
Final R indexes [I>=2σ (I)]	R_1 = 0.0361, wR_2 = 0.0973
Final R indexes [all data]	R_1 = 0.0375, wR_2 = 0.0987
Largest diff. peak/hole / e Å^{-3}	0.38/-0.19
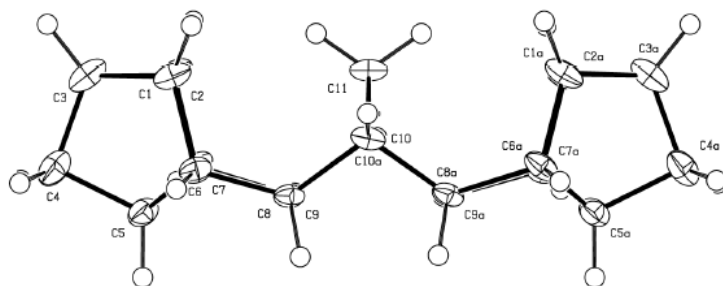
Table 22. Crystal Data and structure refinement of compound 146.

Identification code	mo_0261_CG_0m
Empirical formula	$C_{21}H_{24}$
Formula weight	276.40
Temperature/K	99.99
Crystal system	monoclinic
Space group	$C2/c$
a/Å	11.196(2)
b/Å	6.0291(10)
c/Å	21.415(4)
α/°	90
β/°	101.081(6)
γ/°	90
Volume/Å^3	1418.6(5)
Z	4

$\rho_{calc}g/cm^3$	1.294
μ/mm^{-1}	0.072
F(000)	600.0
Crystal size/mm^3	0.348 × 0.284 × 0.028
Radiation	MoKα (λ = 0.71073)
2Θ range for data collection/°	7.418 to 63.018
Index ranges	-12 $\leq$ h $\leq$ 16, -8 $\leq$ k $\leq$ 8, -31 $\leq$ l $\leq$ 31
Reflections collected	11857
Independent reflections	2372 [R_{int} = 0.0248, R_{sigma} = 0.0240]
Data/restraints/parameters	2372/0/96
Goodness-of-fit on F^2	1.045
Final R indexes [I>=2σ (I)]	R_1 = 0.0402, wR_2 = 0.1109
Final R indexes [all data]	R_1 = 0.0463, wR_2 = 0.1159
Largest diff. peak/hole / e Å^{-3}	0.33/-0.20
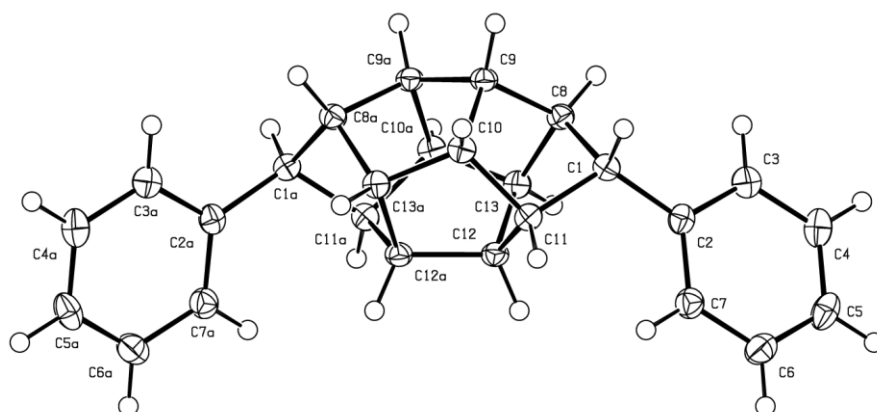
Table 23. Crystal Data and structure refinement of compound 153a.

Identification code	Fdd2
Empirical formula	$C_{26}H_{24}$
Formula weight	336.45
Temperature/K	100.0
Crystal system	orthorhombic
Space group	*F*dd2
a/Å	10.7615(5)
b/Å	48.479(2)
c/Å	6.5309(3)
α/°	90
β/°	90
γ/°	90
Volume/Å³	3407.2(3)

Z	8
ρ_{calc}g/cm^3	1.312
μ/mm^{-1}	0.553
F(000)	1440.0
Crystal size/mm^3	0.463 × 0.186 × 0.016
Radiation	CuKα (λ = 1.54178)
2Θ range for data collection/°	7.294 to 148.69
Index ranges	-13 ≤ h ≤ 10, -60 ≤ k ≤ 59, -8 ≤ l ≤ 8
Reflections collected	7177
Independent reflections	1697 [R_{int} = 0.0474, R_{sigma} = 0.0331]
Data/restraints/parameters	1697/1/118
Goodness-of-fit on F^2	1.068
Final R indexes [I>=2σ (I)]	R_1 = 0.0331, wR_2 = 0.0874
Final R indexes [all data]	R_1 = 0.0335, wR_2 = 0.0876
Largest diff. peak/hole / e Å^{-3}	0.25/-0.20
Flack parameter	-0.3(8)
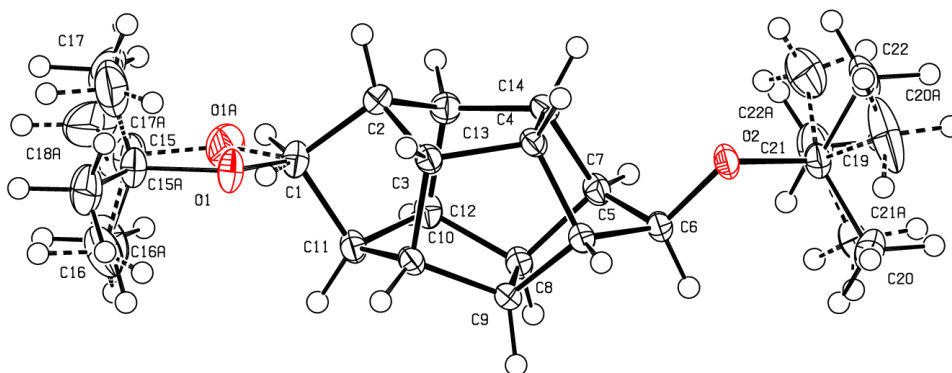
Table 24. Crystal Data and structure refinement of compound 153j.

Identification code	mo_0347_CG_0m
Empirical formula	$C_{22}H_{32}O_2$
Formula weight	328.47
Temperature/K	149.89
Crystal system	triclinic
Space group	*P*-1
a/Å	6.2141(3)
b/Å	11.0472(7)
c/Å	14.1117(8)
α/°	106.291(2)
β/°	91.935(2)
γ/°	97.467(2)
Volume/Å³	919.45(9)

Z	2
ρ_{calc} g/cm^3	1.186
μ/mm^{-1}	0.074
F(000)	360.0
Crystal size/mm^3	0.4 × 0.2 × 0.2
Radiation	MoKα (λ = 0.71073)
2Θ range for data collection/°	5.56 to 65.244
Index ranges	-9 ≤ h ≤ 8, -16 ≤ k ≤ 16, -19 ≤ l ≤ 21
Reflections collected	16256
Independent reflections	6654 [R_{int} = 0.0199, R_{sigma} = 0.0258]
Data/restraints/parameters	6654/405/290
Goodness-of-fit on F^2	1.041
Final R indexes [I>=2σ (I)]	R_1 = 0.0447, wR_2 = 0.1199
Final R indexes [all data]	R_1 = 0.0489, wR_2 = 0.1233
Largest diff. peak/hole / e Å^{-3}	0.43/-0.21
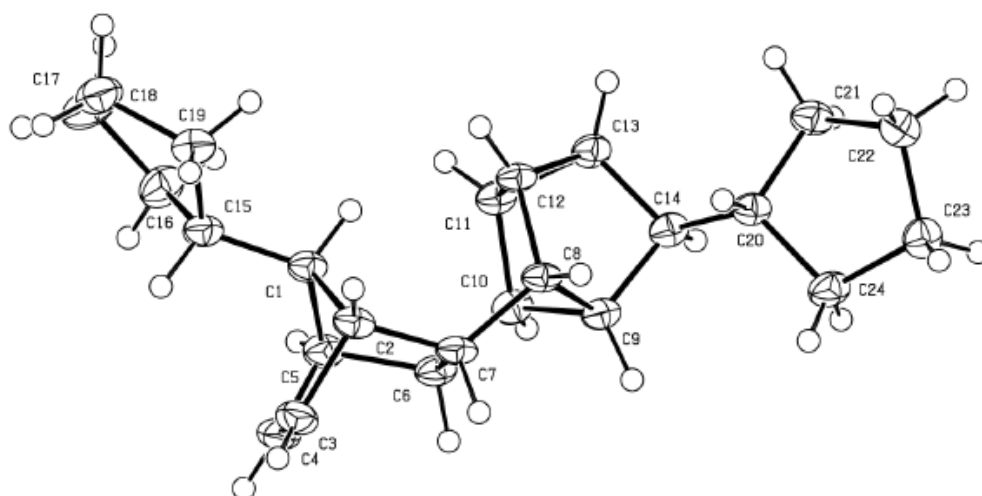
Table 25. Crystal Data and structure refinement of compound 154*.

Identification code	mo_0288_CG_0m
Empirical formula	$C_{24}H_{32}$
Formula weight	320.49
Temperature/K	100.01
Crystal system	monoclinic
Space group	$P2_1/c$
a/Å	6.199(2)
b/Å	10.325(3)
c/Å	27.838(11)
α/°	90
β/°	95.540(19)
γ/°	90

Volume/Å^3	1773.3(10)
Z	4
ρ_{calc}g/cm^3	1.200
μ/mm^{-1}	0.067
F(000)	704.0
Crystal size/mm^3	0.623 × 0.139 × 0.008
Radiation	MoKα (λ = 0.71073)
2Θ range for data collection/°	4.92 to 61.2
Index ranges	-8 ≤ h ≤ 8, -14 ≤ k ≤ 12, -39 ≤ l ≤ 39
Reflections collected	15333
Independent reflections	5410 [R_{int} = 0.0398, R_{sigma} = 0.0522]
Data/restraints/parameters	5410/0/217
Goodness-of-fit on F^2	1.057
Final R indexes [I>=2σ (I)]	R_1 = 0.0630, wR_2 = 0.1529
Final R indexes [all data]	R_1 = 0.0830, wR_2 = 0.1638
Largest diff. peak/hole / e Å^{-3}	0.36/-0.25
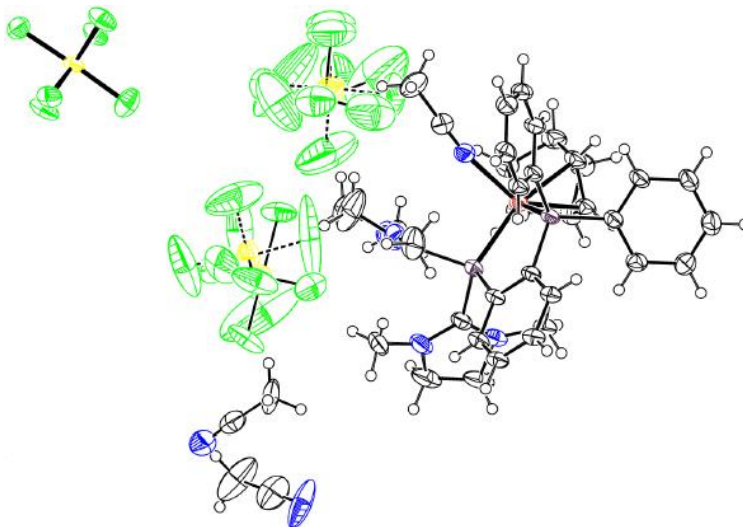
Table 26. Crystal Data and structure refinement of compound 162.

Identification code	mo_0253_CG_0m
Empirical formula	$C_{39}H_{48}F_{18}N_6P_2RhSb_3$
Formula weight	1472.93
Temperature/K	100.01
Crystal system	monoclinic
Space group	$P2_1/n$
a/Å	11.6446(5)
b/Å	30.2205(18)
c/Å	14.8547(8)
α/°	90
β/°	98.551(2)
γ/°	90

Volume/Å^3	5169.3(5)
Z	4
ρ_{calc} g/cm^3	1.893
μ/mm^{-1}	2.027
F(000)	2856.0
Crystal size/mm^3	0.368 × 0.199 × 0.052
Radiation	MoKα (λ = 0.71073)
2Θ range for data collection/°	4.37 to 68.82
Index ranges	-18 ≤ h ≤ 18, -48 ≤ k ≤ 47, -23 ≤ l ≤ 23
Reflections collected	153750
Independent reflections	21687 [R_{int} = 0.0249, R_{sigma} = 0.0153]
Data/restraints/parameters	21687/146/765
Goodness-of-fit on F^2	1.092
Final R indexes [I>=2σ (I)]	R_1 = 0.0540, wR_2 = 0.1424
Final R indexes [all data]	R_1 = 0.0594, wR_2 = 0.1460
Largest diff. peak/hole / e Å^{-3}	2.15/-2.34

9 Bibliography

References

(1) Choi, T.-L.; Grubbs, R. H. Controlled living ring-opening-metathesis polymerization by a fast-initiating ruthenium catalyst. *Angew. Chem., Int. Ed. Engl.* **2003**, *42* (15), 1743–1746. DOI: 10.1002/anie.200250632.

(2) Védrine, J. Heterogeneous Catalysis on Metal Oxides. *Catalysts* **2017**, *7* (11), 341. DOI: 10.3390/catal7110341.

(3) Hartwig, J. F. *Organotransition metal chemistry*:*From bonding to catalysis*; University Science Books, 2010.

(4) Li, H.; Johansson Seechurn, C. C. C.; Colacot, T. J. Development of Preformed Pd Catalysts for Cross-Coupling Reactions, Beyond the 2010 Nobel Prize. *ACS Catal.* **2012**, *2* (6), 1147–1164. DOI: 10.1021/cs300082f.

(5) Beller, M.; Renken, A.; van Santen, R. A., Eds. *Catalysis*:*From principles to applications*; Wiley-VCH-Verlag GmbH & Co. KGaA, 2012.

(6) Chadwick, J. C. *Homogeneous Catalysts*:*Activity - Stability - Deactivation*, 1st ed.; John Wiley & Sons Incorporated, 2011.

(7) Lawrance, G. A. *Introduction to Coordination Chemistry*; John Wiley & Sons, Ltd, 2010. DOI: 10.1002/9780470687123.

(8) Arnold, P. L.; Casely, I. J. F-block N-heterocyclic carbene complexes. *Chem. Rev.* **2009**, *109* (8), 3599–3611. DOI: 10.1021/cr8005203.

(9) Birkholz, M.-N.; Freixa, Z.; van Leeuwen, P. W. N. M. Bite angle effects of diphosphines in C-C and C-X bond forming cross coupling reactions. *Chem. Soc. Rev.* **2009**, *38* (4), 1099–1118. DOI: 10.1039/b806211k.

(10) η (eta or hapto) in inorganic nomenclature. In *IUPAC Compendium of Chemical Terminology*; Nič, M., Jirát, J., Košata, B., Jenkins, A., McNaught, A., Eds.; IUPAC, 2009. DOI: 10.1351/goldbook.H01881.

(11) Huttner, G.; Lange, S.; Fischer, E. O. Molecular Structure of Bis(hexamethylbenzene)-ruthenium(0). *Angew. Chem. Int. Ed. Engl.* **1971**, *10* (8), 556–557. DOI: 10.1002/anie.197105561.

(12) Noyori, R.; Ohkuma, T.; Kitamura, M.; Takaya, H.; Sayo, N.; Kumobayashi, H.; Akutagawa, S. Asymmetric hydrogenation of .beta.-keto carboxylic esters. A practical, purely chemical access to .beta.-hydroxy esters in high enantiomeric purity. *J. Am. Chem. Soc.* **1987**, *109* (19), 5856–5858. DOI: 10.1021/ja00253a051.

(13) Franke, R.; Selent, D.; Börner, A. Applied hydroformylation. *Chem. Rev.* **2012**, *112* (11), 5675–5732. DOI: 10.1021/cr3001803.

(14) Johansson Seechurn, C. C. C.; Kitching, M. O.; Colacot, T. J.; Snieckus, V. Palladium-catalyzed cross-coupling: a historical contextual perspective to the 2010 Nobel Prize. *Angew. Chem., Int. Ed. Engl.* **2012**, *51* (21), 5062–5085. DOI: 10.1002/anie.201107017.

(15) Arndtsen, B. A.; Bergman, R. G.; Mobley, T. A.; Peterson, T. H. Selective Intermolecular Carbon-Hydrogen Bond Activation by Synthetic Metal Complexes in Homogeneous Solution. *Acc. Chem. Res.* **1995**, *28* (3), 154–162. DOI: 10.1021/ar00051a009.

(16) Grela, K. *Olefin Metathesis*:*Theory and Practice*; Wiley, 2014. DOI: 10.1002/9781118711613.

(17) Meakin, P.; Jesson, J. P.; Tolman, C. A. Nature of chlorotris(triphenylphosphine)rhodium in solution and its reaction with hydrogen. *J. Am. Chem. Soc.* **1972**, *94* (9), 3240–3242. DOI: 10.1021/ja00764a061.

(18) Biffis, A.; Centomo, P.; Del Zotto, A.; Zecca, M. Pd Metal Catalysts for Cross-Couplings and Related Reactions in the 21st Century: A Critical Review. *Chem. Rev.* **2018**, *118* (4), 2249–2295. DOI: 10.1021/acs.chemrev.7b00443.

(19) Sir Geoffrey Wilkinson 1921–1996 IN MEMORIAM. *Inorg. Chem.* **1996**, *35* (26), 7463–7464. DOI: 10.1021/ic961299i.

(20) Nguyen, S. T.; Johnson, L. K.; Grubbs, R. H.; Ziller, J. W. Ring-opening metathesis polymerization (ROMP) of norbornene by a Group VIII carbene complex in protic media. *J. Am. Chem. Soc.* **1992**, *114* (10), 3974–3975. DOI: 10.1021/ja00036a053.

(21) Schwab, P.; France, M. B.; Ziller, J. W.; Grubbs, R. H. A Series of Well-Defined Metathesis Catalysts–Synthesis of[RuCl2(⬜CHR ′)(PR3)2] and Its Reactions. *Angew. Chem. Int. Ed. Engl.* **1995**, *34* (18), 2039–2041. DOI: 10.1002/anie.199520391.

(22) Scholl, M.; Ding, S.; Lee, C. W.; Grubbs, R. H. Synthesis and activity of a new generation of ruthenium-based olefin metathesis catalysts coordinated with 1,3-dimesityl-4,5-dihydroimidazol-2-ylidene ligands. *Org. Lett.* **1999**, *1* (6), 953–956. DOI: 10.1021/ol990909q.

(23) Love, J. A.; Morgan, J. P.; Trnka, T. M.; Grubbs, R. H. A Practical and Highly Active Ruthenium-Based Catalyst that Effects the Cross Metathesis of Acrylonitrile. *Angew. Chem. Int. Ed.* **2002**, *41* (21), 4035–4037. DOI: 10.1002/1521-3773(20021104)41:21<4035:AID-ANIE4035>3.0.CO;2-I.

(24) Casey, C. P. 2005 Nobel Prize in Chemistry. Development of the Olefin Metathesis Method in Organic Synthesis. *J. Chem. Educ.* **2006**, *83* (2), 192. DOI: 10.1021/ed083p192.

(25) Fürstner, A. From understanding to prediction: gold- and platinum-based π-acid catalysis for target oriented synthesis. *Acc. Chem. Res.* **2014**, *47* (3), 925–938. DOI: 10.1021/ar4001789.

(26) Dorel, R.; Echavarren, A. M. Gold(I)-Catalyzed Activation of Alkynes for the Construction of Molecular Complexity. *Chem. Rev.* **2015**, *115* (17), 9028–9072. DOI: 10.1021/cr500691k.

(27) Fürstner, A.; Davies, P. W. Catalytic carbophilic activation: catalysis by platinum and gold pi acids. *Angew. Chem., Int. Ed. Engl.* **2007**, *46* (19), 3410–3449. DOI: 10.1002/anie.200604335.

(28) Shahzad, S. A.; Sajid, M. A.; Khan, Z. A.; Canseco-Gonzalez, D. Gold catalysis in organic transformations: A review. *Synth. Commun.* **2017**, *47* (8), 735–755. DOI: 10.1080/00397911.2017.1280508.

(29) Fürstner, A. Gold and platinum catalysis--a convenient tool for generating molecular complexity. *Chem. Soc. Rev.* **2009**, *38* (11), 3208–3221. DOI: 10.1039/b816696j.

(30) Wauters, I.; Debrouwer, W.; Stevens, C. V. Preparation of phosphines through C-P bond formation. *Beilstein J. Org. Chem.* **2014**, *10*, 1064–1096. DOI: 10.3762/bjoc.10.106.

(31) Miyaura, N.; Yamada, K.; Suzuki, A. A new stereospecific cross-coupling by the palladium-catalyzed reaction of 1-alkenylboranes with 1-alkenyl or 1-alkynyl halides. *Tetrahedron Lett.* **1979**, *20* (36), 3437–3440. DOI: 10.1016/S0040-4039(01)95429-2.

(32) Wolfe, J. P.; Singer, R. A.; Yang, B. H.; Buchwald, S. L. Highly Active Palladium Catalysts for Suzuki Coupling Reactions. *J. Am. Chem. Soc.* **1999**, *121* (41), 9550–9561. DOI: 10.1021/ja992130h.

(33) Martin, R.; Buchwald, S. L. Palladium-Catalyzed Suzuki-Miyaura Cross-coupling Reactions Employing Dialkylbiaryl Phosphine Ligands. *Acc. Chem. Res.* **2008**, *41* (11), 1461–1473. DOI: 10.1021/ar800036s.

(34) Kamer, P. C.; van Leeuwen, P. W.; Reek, J. N. Wide bite angle diphosphines: xantphos ligands in transition metal complexes and catalysis. *Acc. Chem. Res.* **2001**, *34* (11), 895–904. DOI: 10.1021/ar000060.

(35) Kürti, L.; Czakó, B. *Strategic applications of named reactions in organic synthesis*:*Background and detailed mechanisms ; 250 named reactions*, [Nachdr.]; Elsevier Acad. Press, 2009.

(36) Shimizu, H.; Nagasaki, I.; Matsumura, K.; Sayo, N.; Saito, T. Developments in asymmetric hydrogenation from an industrial perspective. *Acc. Chem. Res.* **2007**, *40* (12), 1385–1393. DOI: 10.1021/ar700101x.

(37) Rowlands, G. J. Planar Chiral Phosphines Derived from [2.2]Paracyclophane. *Isr. J. Chem.* **2012**, *52* (1-2), 60–75. DOI: 10.1002/ijch.201100098.

(38) Vineyard, B. D.; Knowles, W. S.; Sabacky, M. J.; Bachman, G. L.; Weinkauff, D. J. Asymmetric hydrogenation. Rhodium chiral bisphosphine catalyst. *J. Am. Chem. Soc.* **1977**, *99* (18), 5946–5952. DOI: 10.1021/ja00460a018.

(39) Jacobsen, E. N., Ed. *Comprehensive asymmetric catalysis*; Springer, 1999.

(40) Yang, J. Y.; Chen, S.; Dougherty, W. G.; Kassel, W. S.; Bullock, R. M.; DuBois, D. L.; Raugei, S.; Rousseau, R.; Dupuis, M.; Rakowski DuBois, M. Hydrogen oxidation catalysis by a nickel diphosphine complex with pendant tert-butyl amines. Chem. Commun. **2010**, *46* (45), 8618–8620. DOI: 10.1039/c0cc03246h.

(41) Beletskaya, I. P.; Nájera, C.; Yus, M. Stereodivergent Catalysis. *Chem. Rev.* **2018**, *118* (10), 5080–5200. DOI: 10.1021/acs.chemrev.7b00561.

(42) Tolman, C. A. Electron donor-acceptor properties of phosphorus ligands. Substituent additivity. *J. Am. Chem. Soc.* **1970**, *92* (10), 2953–2956. DOI: 10.1021/ja00713a006.

(43) Tolman, C. A. Steric effects of phosphorus ligands in organometallic chemistry and homogeneous catalysis. *Chem. Rev.* **1977**, *77* (3), 313–348. DOI: 10.1021/cr60307a002.

(44) Frisch, A. C.; Beller, M. Catalysts for cross-coupling reactions with non-activated alkyl halides. *Angew. Chem., Int. Ed. Engl.* **2005**, *44* (5), 674–688. DOI: 10.1002/anie.200461432.

(45) Farina, V.; Krishnan, B. Large rate accelerations in the stille reaction with tri-2-furylphosphine and triphenylarsine as palladium ligands: mechanistic and synthetic implications. *J. Am. Chem. Soc.* **1991**, *113* (25), 9585–9595. DOI: 10.1021/ja00025a025.

(46) Balaban, T. S.; Cossy, J.; Bellus, D.; Houben, J.; Weyl, T., Eds. *Science of synthesis*:*Houben-Weyl methods of molecular transformations*, Paper archive copy; Thieme, 2005.

(47) Tarselli, M. A.; Liu, A.; Gagné, M. R. Gold(I)-catalyzed intermolecular hydroarylation of allenes with nucleophilic arenes: scope and limitations. *Tetrahedron* **2009**, *65* (9), 1785–1789. DOI: 10.1016/j.tet.2008.10.110.

(48) Wang, Z. J.; Benitez, D.; Tkatchouk, E.; Goddard, W. A.; Toste, F. D. Mechanistic study of gold(I)-catalyzed intermolecular hydroamination of allenes. *J. Am. Chem. Soc.* **2010**, *132* (37), 13064–13071. DOI: 10.1021/ja105530q.

(49) Troev, K. D. *Polyphosphoesters*:*Chemistry and application*, 1st ed.; Elsevier insights; Elsevier, 2012.

(50) Herrmann, W. A.; Kohlpaintner, C. W.; Hanson, B. E.; Kang, X. Syntheses of Water-Soluble Phosphines and their Transition Metal Complexes. In *Inorganic*

syntheses; Darensbourg, M. Y., Ed.; Inorganic Syntheses; John Wiley & Sons, 1998; pp 8–25. DOI: 10.1002/9780470132630.ch2.

 (51) Amatore, C.; Blart, E.; Genet, J. P.; Jutand, A.; Lemaire-Audoire, S.; Savignac, M. New synthetic applications of water-soluble acetate Pd/TPPTS catalyst generated in Situ. evidence for a true Pd(0) species intermediate. *J. Org. Chem.* **1995**, *60* (21), 6829–6839. DOI: 10.1021/jo00126a037.

 (52) Cornils, B.; Fischer, R. W.; Kohlpaintner, C. Butanals. In *Ullmann's encyclopedia of industrial chemistry,* 6th, completely rev. ed.; Wiley-VCH, 2003. DOI: 10.1002/14356007.a04_447.

 (53) Smith, R. T.; Ungar, R. K.; Sanderson, L. J.; Baird, M. C. Rhodium complexes of the water-soluble phosphine Ph2PCH2CH2NMe3+. Their complexes with hydride, olefin, and carbon monoxide ligands. Their use as olefin hydrogenation and hydroformylation catalysts in aqueous solution and in aqueous/organic solvent two-phase systems, and adsorbed on a cation-exchange resin. *Organometallics* **1983**, *2* (9), 1138–1144. DOI: 10.1021/om50003a012.

 (54) Nagel, U.; Kinzel, E. Enantioselektive katalytische Hydrierung von α-(Acetylamino)-zimtsäure mit einem Rhodium-Phosphankomplex in wäßriger Lösung. *Chem. Ber.* **1986**, *119* (5), 1731–1733. DOI: 10.1002/cber.19861190525.

 (55) Błażewska, K. M.; Mathey, F.; Bellus, D.; Houben, J.; Weyl, T., Eds. *Science of synthesis*:*Houben-Weyl methods of molecular transformations*, Thieme, 2009.

 (56) Nicholls, L. D. M.; Alcarazo, M. Applications of α-Cationic Phosphines as Ancillary Ligands in Homogeneous Catalysis. *Chem. Lett.* **2019**, *48* (1), 1–13. DOI: 10.1246/cl.180810.

 (57) Johannsen, T.; Golz, C.; Alcarazo, M. α-Cationic Phospholes: Synthesis and Applications as Ancillary Ligands. *Angew. Chem., Int. Ed. Engl.* **2020**, *59* (50), 22779–22784. DOI: 10.1002/anie.202009303.

(58) Smith, D. C.; Klaman, A. L.; Cadoret, J.; Nolan, S. P. Synthetic and thermochemical studies of fluorinated tertiary phosphine ligands R2PRf [R=Cy, Ph, iPr; Rf=CH2CH2(CF2)5CF3] in an organoiron system. *Inorg. Chim. Acta* **2000**, *300-302*, 987–991. DOI: 10.1016/S0020-1693(99)00600-3.

(59) Haldón, E.; Kozma, Á.; Tinnermann, H.; Gu, L.; Goddard, R.; Alcarazo, M. Synthesis and reactivity of α-cationic phosphines: the effect of imidazolinium and amidinium substituents. *Dalton Trans.* **2016**, *45* (5), 1872–1876. DOI: 10.1039/c5dt02341f.

(60) V.Komarov, I.; Yu.Kornilov, M.; Tolmachev, A. A.; Yurchenko, A. A.; Rusanov, E. B.; Chernega, A. N. Tungsten pentacarbonyl as a potential protecting group for soft lewis base centres in alkylation of multifunctional molecules. *Tetrahedron* **1995**, *51* (41), 11271–11280. DOI: 10.1016/0040-4020(95)00689-6.

(61) Kuhn, N.; Fahl, J.; Bläser, D.; Boese, R. Synthese und Eigenschaften von [Ph2(Carb)P]AlCl4 (Carb = 2,3-Dihydro-1,3-diisopropyl-4,5-dimethylimidazol-2-yliden) - ein stabiler Carben-Komplex des dreiwertigen Phosphors [1]. *Z. Anorg. Allg. Chem.* **1999**, *625* (5), 729–734. DOI: 10.1002/(SICI)1521-3749(199905)625:5<729:AID-ZAAC729>3.0.CO;2-D.

(62) Azouri, M.; Andrieu, J.; Picquet, M.; Richard, P.; Hanquet, B.; Tkatchenko, I. Straightforward Synthesis of Donor-Stabilised Phosphenium Adducts from Imidazolium-2-carboxylate and Their Electronic Properties (Eur. J. Inorg. Chem. 31/2007). *Eur. J. Inorg. Chem.* **2007**, *2007* (31), 4853. DOI: 10.1002/ejic.200790080.

(63) Tinnermann, H.; Wille, C.; Alcarazo, M. Synthesis, structure, and applications of pyridiniophosphines. *Angew. Chem. Int. Ed. Engl.* **2014**, *53* (33), 8732–8736. DOI: 10.1002/anie.201401073.

(64) Petuškova, J.; Bruns, H.; Alcarazo, M. Cyclopropenylylidene-stabilized diaryl and dialkyl phosphenium cations: applications in homogeneous gold catalysis. *Angew. Chem. Int. Ed. Engl.* **2011**, *50* (16), 3799–3802. DOI: 10.1002/anie.201100338.

(65) Alcarazo, M. Synthesis, Structure, and Applications of α-Cationic Phosphines. *Acc. Chem. Res.* **2016**, *49* (9), 1797–1805. DOI: 10.1021/acs.accounts.6b00262.

(66) Azouri, M.; Andrieu, J.; Picquet, M.; Cattey, H. Synthesis of new cationic donor-stabilized phosphenium adducts and their unexpected P-substituent exchange reactions. *Inorg. Chem.* **2009**, *48* (3), 1236–1242. DOI: 10.1021/ic801870w.

(67) Carreras, J.; Gopakumar, G.; Gu, L.; Gu, L.; Gimeno, A.; Linowski, P.; Petuškova, J.; Thiel, W.; Alcarazo, M. Polycationic ligands in gold catalysis: synthesis and applications of extremely π-acidic catalysts. *J. Am. Chem. Soc.* **2013**, *135* (50), 18815–18823. DOI: 10.1021/ja411146x.

(68) Petuškova, J.; Patil, M.; Holle, S.; Lehmann, C. W.; Thiel, W.; Alcarazo, M. Synthesis, structure, and reactivity of carbene-stabilized phosphorus(III)-centered trications L3P3+. *J. Am. Chem. Soc.* **2011**, *133* (51), 20758–20760. DOI: 10.1021/ja210223s.

(69) Henne, F. D.; Dickschat, A. T.; Hennersdorf, F.; Feldmann, K.-O.; Weigand, J. J. Synthesis of Selected Cationic Pnictanes LnPnX3-n(n+) (L = Imidazolium-2-yl; Pn = P, As; n = 1-3) and Replacement Reactions with Pseudohalogens. *Inorg. Chem.* **2015**, *54* (14), 6849–6861. DOI: 10.1021/acs.inorgchem.5b00765.

(70) Diebolt, O.; Tricas, H.; Freixa, Z.; van Leeuwen, P. W. N. M. Strong π-Acceptor Ligands in Rhodium-Catalyzed Hydroformylation of Ethene and 1-Octene: Operando Catalysis. *ACS Catal.* **2013**, *3* (2), 128–137. DOI: 10.1021/cs300470u.

(71) Fan, B.-M.; Yang, Q.-j.; Hu, J.; Fan, C.-l.; Li, S.-f.; Yu, L.; Huang, C.; Tsang, W. W.; Kwong, F. Y. Asymmetric hydroalkynylation of norbornadienes promoted by chiral iridium catalysts. *Angew. Chem. Int. Ed.* **2012**, *51* (31), 7821–7824. DOI: 10.1002/anie.201203107.

(72) Clayden, J.; Greeves, N.; Warren, S. G. *Organic chemistry*, 2nd ed.; Oxford University Press, 2012.

(73) Yadav, J. S.; Deshpande, P. K.; Reddy, E. R. Preparation of 1,3-Dienes, its Application to the Synthesis of (Z,E)-9,11-Tetradecadienyl Acetate and (E,E)-10,12-Hexa-decadienal: Sex Pheromones of Cotton Pests. *Synth. Commun.* **1989**, *19* (1-2), 125–134. DOI: 10.1080/00397918908050960.

(74) Smith, M.; March, J. *March's advanced organic chemistry*:*Reactions, mechanisms, and structure*, Eighth edition; John Wiley & Sons, Inc, 2020.

(75) Wessig, P.; Müller, G. The dehydro-Diels-Alder reaction. *Chem. Rev.* **2008**, *108* (6), 2051–2063. DOI: 10.1021/cr0783986.

(76) Diels, O.; Alder, K. Synthesen in der hydroaromatischen Reihe. *Justus Liebigs Ann. Chem.* **1928**, *460* (1), 98–122. DOI: 10.1002/jlac.19284600106.

(77) Widenhoefer, R. A.; Han, X. Gold-Catalyzed Hydroamination of C–C Multiple Bonds. *Eur. J. Org. Chem.* **2006**, *2006* (20), 4555–4563. DOI: 10.1002/ejoc.200600399.

(78) Nakao, Y.; Kashihara, N.; Kanyiva, K. S.; Hiyama, T. Nickel-catalyzed alkenylation and alkylation of fluoroarenes via activation of C-H bond over C-F bond. *J. Am. Chem. Soc.* **2008**, *130* (48), 16170–16171. DOI: 10.1021/ja807258m.

(79) Goldfogel, M. J.; Roberts, C. C.; Meek, S. J. Intermolecular hydroamination of 1,3-dienes catalyzed by bis(phosphine)carbodicarbene-rhodium complexes. *J. Am. Chem. Soc.* **2014**, *136* (17), 6227–6230. DOI: 10.1021/ja502275w.

(80) Roberts, C. C.; Matías, D. M.; Goldfogel, M. J.; Meek, S. J. Lewis acid activation of carbodicarbene catalysts for Rh-catalyzed hydroarylation of dienes. *J. Am. Chem. Soc.* **2015**, *137* (20), 6488–6491. DOI: 10.1021/jacs.5b03510.

(81) Canac, Y.; Maaliki, C.; Abdellah, I.; Chauvin, R. Carbeniophosphanes and their carbon → phosphorus → metal ternary complexes. *New J. Chem.* **2012**, *36* (1), 17–27. DOI: 10.1039/C1NJ20808J.

(82) Genet, J.-P.; Ayad, T.; Ratovelomanana-Vidal, V. Electron-deficient diphosphines: the impact of DIFLUORPHOS in asymmetric catalysis. *Chem. Rev.* **2014**, *114* (5), 2824–2880. DOI: 10.1021/cr4003243.

(83) Bonnaventure, I.; Charette, A. B. Probing the importance of the hemilabile site of bis(phosphine) monoxide ligands in the copper-catalyzed addition of diethylzinc to N-phosphinoylimines: discovery of new effective chiral ligands. *J. Org. Chem.* **2008**, *73* (16), 6330–6340. DOI: 10.1021/jo800969x.

(84) Csákÿ, A. G.; Molina, M. T. 1,2-Bis(diphenylphosphino)benzene. In *Encyclopedia of reagents for organic synthesis*; Wiley, 1995; p 417. DOI: 10.1002/047084289X.rn01300.

(85) Moores, A. Atom Economy - Principles and Some Examples. In *Handbook of Green Chemistry*; Anastas, P. T., Ed.; Wiley VCH Imprint, 2013. DOI: 10.1002/9783527628698.hgc001.

(86) Sheldon, R. A. Atom efficiency and catalysis in organic synthesis. *Pure Appl. Chem.* **2000**, *72* (7), 1233–1246. DOI: 10.1351/pac200072071233.

(87) Trost, B. M. Atom Economy—A Challenge for Organic Synthesis: Homogeneous Catalysis Leads the Way. *Angew. Chem. Int. Ed. Engl.* **1995**, *34* (3), 259–281. DOI: 10.1002/anie.199502591.

(88) Shirakura, M.; Suginome, M. Nickel-catalyzed addition of C-H bonds of terminal alkynes to 1,3-dienes and styrenes. *J. Am. Chem. Soc.* **2008**, *130* (16), 5410–5411. DOI: 10.1021/ja800997j. Published Online: Apr. 2, 2008.

(89) Prelog, V.; Seiwerth, R. Über die Synthese des Adamantans. *Ber. Dtsch. Chem. Ges. A/B* **1941**, *74* (10), 1644–1648. DOI: 10.1002/cber.19410741004.

(90) Fort, R. C.; Schleyer, P. v. R. Adamantane: Consequences of the Diamondoid Structure. *Chem. Rev.* **1964**, *64* (3), 277–300. DOI: 10.1021/cr60229a004.

(91) R. Schleyer, P. von. A SIMPLE PREPARATION OF ADAMANTANE. *J. Am. Chem. Soc.* **1957**, *79* (12), 3292. DOI: 10.1021/ja01569a086.

(92) Zou, F.; Chen, H.; Fu, S.; Chen, S. Shape memory materials based on adamantane-containing polyurethanes. *RSC Adv.* **2018**, *8* (45), 25584–25591. DOI: 10.1039/c8ra05111a.

(93) Zhang, K.; Wang, L.; Liang, Y.; Yang, S.; Liang, J.; Cheng, F.; Chen, J. A thermally and electrochemically stable organic hole-transporting material with an adamantane central core and triarylamine moieties. *Synth. Met.* **2012**, *162* (5-6), 490–496. DOI: 10.1016/j.synthmet.2012.01.006.

(94) Kovalenko, A.; Yumusak, C.; Heinrichova, P.; Stritesky, S.; Fekete, L.; Vala, M.; Weiter, M.; Sariciftci, N. S.; Krajcovic, J. Adamantane substitutions: a path to high-performing, soluble, versatile and sustainable organic semiconducting materials. *J. Mater. Chem. C* **2017**, *5* (19), 4716–4723. DOI: 10.1039/C6TC05076J.

(95) Karlen, S. D.; Ortiz, R.; Chapman, O. L.; Garcia-Garibay, M. A. Effects of rotational symmetry order on the solid state dynamics of phenylene and diamantane rotators. *J. Am. Chem. Soc.* **2005**, *127* (18), 6554–6555. DOI: 10.1021/ja042512.

(96) Eaton, P. E.; Cole, T. W. The Cubane System. *J. Am. Chem. Soc.* **1964**, *86* (5), 962–964. DOI: 10.1021/ja01059a072.

(97) Katz, T. J.; Acton, N. Synthesis of prismane. *J. Am. Chem. Soc.* **1973**, *95* (8), 2738–2739. DOI: 10.1021/ja00789a084.

(98) Gund, T. M.; Osawa, E.; van Williams, Z.; Schleyer, P. V. R. Diamantane. I. Preparation of diamantane. Physical and spectral properties. *J. Org. Chem.* **1974**, *39* (20), 2979–2987. DOI: 10.1021/jo00934a009.

(99) Ternansky, R. J.; Balogh, D. W.; Paquette, L. A. Dodecahedrane. *J. Am. Chem. Soc.* **1982**, *104* (16), 4503–4504. DOI: 10.1021/ja00380a040.

(100) Lee, C.-H.; Liang, S.; Haumann, T.; Boese, R.; Meijere, A. de. p-[32.56]Octahedrane, the(CH)12 Hydrocarbon withD3d Symmetry. *Angew. Chem. Int. Ed. Engl.* **1993**, *32* (4), 559–561. DOI: 10.1002/anie.199305591.

(101) Bird, C. W.; Colinese, D. L.; Cookson, R. C.; Hudec, J.; Williams, R. O. Dimerization of bicycloheptadiene by metal carbonyls. *Tetrahedron Lett.* **1961**, *2* (11), 373–375. DOI: 10.1016/S0040-4039(01)91642-9.

(102) Mehta, G.; Padma, S. D2h-bishomohexaprismane ("garudane"). Design of the face-to-face 2 + 2 dimer of norbornadiene. *J. Am. Chem. Soc.* **1987**, *109* (23), 7230–7232. DOI: 10.1021/ja00257a076.

(103) Schrauzer, G. N.; Bastian, B. N.; Fosselius, G. A. π-Complex Multicenter Reactions Promoted by Binuclear Catalyst Systems. "Binor-S," a New Heptacyclotetradecane via Stereospecific Dimerization of Bicycloheptadiene. *J. Am. Chem. Soc.* **1966**, *88* (21), 4890–4894. DOI: 10.1021/ja00973a024.

(104) Aminov, R. I.; Khusnutdinov, R. I. A new method for the synthesis of diamantane by hydroisomerization of binor-S on treatment with sulfuric acid. *Beilstein J. Org. Chem.* **2020**, *16*, 2534–2539. DOI: 10.3762/bjoc.16.205.

(105) Acton, N.; Roth, R. J.; Katz, T. J.; Frank, J. K.; Maier, C. A.; Paul, I. C. Dimerization and trimerization of norbornadiene by soluble rhodium catalysts. *J. Am. Chem. Soc.* **1972**, *94* (15), 5446–5456. DOI: 10.1021/ja00770a048.

(106) Chow, T. J.; Chao, Y. S.; Liu, L. K. Molybdenum-mediated dimerization of norbornadiene and derivatives. *J. Am. Chem. Soc.* **1987**, *109* (3), 797–804. DOI: 10.1021/ja00237a026.

(107) Lim, H. N.; Dong, G. Catalytic Cage Formation via Controlled Dimerization of Norbornadienes: An Entry to Functionalized HCTDs (Heptacyclo6.6.0.0(2,6).0(3,13).0(4,11).0(5,9).0(10,14)tetradecanes). *Org. Lett.* **2016**, *18* (5), 1104–1107. DOI: 10.1021/acs.orglett.6b00207.

(108) Prosser-McCartha, C. M.; Hill, C. L. Direct selective acylation of an unactivated carbon-hydrogen bond in a caged hydrocarbon. Approach to systems for carbon-hydrogen bond functionalization that proceed catalytically and selectively at high substrate conversion. *J. Am. Chem. Soc.* **1990**, *112* (9), 3671–3673. DOI: 10.1021/ja00165a069.

(109) Marchand, A. P.; Wang, Y.; Alihodzic, S.; Barton, D. H.R. Oxidative functionalization of unactivated carbon-hydrogen bonds in heptacyclo[6.6.0.02,6.03,13.04,11.05,9.010,14]tetradecane (HCTD). *Tetrahedron* **1997**, *53* (4), 1257–1264. DOI: 10.1016/S0040-4020(96)01110-6.

(110) Marchand, A. P.; Alihodžić, S.; I. N. N. Namboothiri, a.; Ganguly, B. Photochemical Chlorocarbonylation of HCTD by Oxalyl Chloride. Carbocation-Mediated Rearrangement of HCTD Derivatives to Novel, Substituted Heptacyclopentadecanes. *J. Org. Chem.* **1998**, *63* (23), 8390–8396. DOI: 10.1021/jo981299v.

(111) Alcarazo, M.; Zieliński, A.; Marset, X.; Golz, C.; Wolf, L. M. Two - Step Synthesis of Heptacyclo[6.6.0.02,6.03,13.04,11.05,9.010,14] tetradecane from Norbornadiene: Mechanism of the Cage Assembly and Post - synthetic Functionalization. *Angew. Chem. Int. Ed.* **2020.** DOI: 10.1002/anie.202010766.

(112) Osborn, J. A.; Schrock, R. R. Coordinatively unsaturated cationic complexes of rhodium(I), iridium(I), palladium(II), and platinum(II). Generation, synthetic utility, and some catalytic studies. *J. Am. Chem. Soc.* **1971**, *93* (12), 3089–3091. DOI: 10.1021/ja00741a069.

(113) Gunawan, M. A.; Hierso, J.-C.; Poinsot, D.; Fokin, A. A.; Fokina, N. A.; Tkachenko, B. A.; Schreiner, P. R. Diamondoids: functionalization and subsequent applications of perfectly defined molecular cage hydrocarbons. *New J. Chem.* **2014**, *38* (1), 28–41. DOI: 10.1039/C3NJ00535F.

(114) Schreiner, P. R.; Lauenstein, O.; Kolomitsyn, I. V.; Nadi, S.; Fokin, A. A. Selective C-H Activation of Aliphatic Hydrocarbons under Phase-Transfer Conditions. *Angew.*

Chem., Int. Ed. Engl. **1998**, *37* (13-14), 1895–1897. DOI: 10.1002/(SICI)1521-3773(19980803)37:13/14<1895:AID-ANIE1895>3.0.CO;2-A.

(115) Michrowska, A.; Bujok, R.; Harutyunyan, S.; Sashuk, V.; Dolgonos, G.; Grela, K. Nitro-substituted Hoveyda-Grubbs ruthenium carbenes: enhancement of catalyst activity through electronic activation. *J. Am. Chem. Soc.* **2004**, *126* (30), 9318–9325. DOI: 10.1021/ja048794v.